SBUF

PROJEKTNR. 14030

Ground-borne vibration in end-bearing pile foundations

Numerical analyses and full-scale field tests

FREDDIE THELAND
KTH Royal Institute of Technology

2025-01-31

KTH VETENSKAP OCH KONST

SKANSKA

Doctoral Thesis in Civil and Architectural Engineering

Ground-borne vibration in end-bearing pile foundations

Numerical analyses and full-scale field tests

FREDDIE THELAND

KTH ROYAL INSTITUTE OF TECHNOLOGY

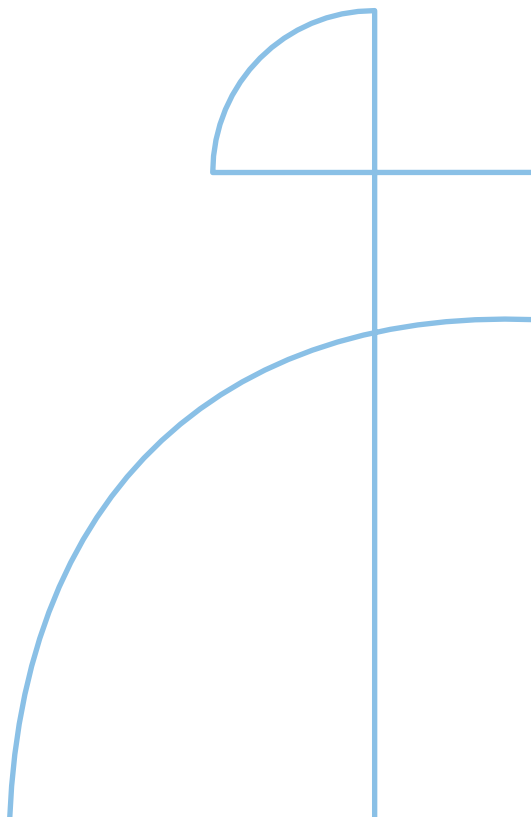

Ground-borne vibration in end-bearing pile foundations

Numerical analyses and full-scale field tests

FREDDIE THELAND

Academic Dissertation which, with due permission of the KTH Royal Institute of Technology, is submitted for public defence for the Degree of Doctor of Philosophy on Friday the 31st of January 2025, at 1:00 p.m. in B3, Brinellvägen 23, Stockholm.

Doctoral Thesis in Civil and Architectural Engineering
KTH Royal Institute of Technology
Stockholm, Sweden 2025

TRITA-ABE-DLT-2438
ISBN 978-91-8106-170-3

Printed by: Universitetsservice US-AB, Sweden 2025

Abstract

Ground-borne vibration originating from roads or railways is a growing concern in the design of buildings in urban areas. For soft cohesive soils, which are particularly susceptible to ground-borne vibration, pile foundations are often used. In shallow formations of soft soil on till and bedrock, which are conditions encountered in densely populated areas in Sweden, the piles are designed as end-bearing to transfer loads to the bedrock. The transmission of vibrations to a building is governed by the interaction between the soil and the foundation. It is therefore essential that the dynamic interaction between the foundation and the soil is taken into account when predicting vibrations in buildings at a design stage.

This thesis aims to increase the understanding of ground-borne vibration transmission to end-bearing pile foundations and investigate how it can be taken into account in vibration assessment for buildings yet to be constructed. The problem is addressed through experiments and numerical simulations. A set of full-scale field tests are performed at a site with clay on till and bedrock to validate model predictions. Vibration measurements are performed in three stages of construction of a pile foundation: (1) at the free ground surface, (2) on the top of four end-bearing concrete piles and (3) on the concrete pile cap joining the piles together. Numerical models are implemented to investigate the influence of pile and soil parameters. The results are subsequently used to develop a simple approximation factor that can be used for estimating the foundation response from vibrations at the ground surface.

The main scientific contributions of this work is the experimental validation of models for predicting ground-borne vibrations in an end-bearing pile foundation and an investigation of the influence of pile and soil properties on dynamic pile-soil interaction. The results show that the vertical vibration level of piles is considerably affected by the fixation of the pile tip and the relationship between the pile axial stiffness and the stiffness of the soil. It is found that, in contrast to floating piles, the vertical response of end-bearing piles subjected to an incident wave field can be significantly affected by pile-soil-pile interaction. The field tests show that, if the dynamic properties of the soil can be accurately determined, a numerical model can predict the dynamic vibration response of the pile foundation with reasonable accuracy. This provides confidence in the results obtained from numerical models, motivating their use for vibration assessment.

Keywords: Dynamic soil-structure interaction; Pile group; End-bearing pile; Pile-soil-pile interaction; Environmental vibration; Ground-borne vibration

Sammanfattning

Omgivningsvibrationer från tåg och biltrafik är ett växande problem vid dimensionering av byggnader i stadsmiljö. I lösa kohesionsjordar, som är särskilt känsliga för sådana vibrationer, används ofta pålar vid grundläggning. Vid jordförhållanden med relativt grunda formationer av lös jord på morän och berg, vilket är vanligt förekommande i tätbefolkade områden i Sverige, används ofta spetsburna pålar. Transmissionen av vibrationer från jorden till en byggnad beror på interaktionen mellan jorden och byggnadens grundläggning. Det är därför viktigt att ta hänsyn till den dynamiska interaktionen mellan jord och grundläggning då man avser förutsäga vibrationer i en byggnad i dimensioneringssyfte.

Syftet med denna avhandling är att öka kunskapen kring transmissionen av markburna vibrationer till spetsburna pålfundament samt att undersöka hur hänsyn kan tas till dess inverkan i vibrationsutredningar. Frågeställningen adresseras genom både experiment och numeriska analyser. Fältförsök i full skala har utförts på en plats med lerjord på morän och berg för att validera numeriska prediktionsmodeller. Vibrationsmätningar har utförts vid tre olika skeden vid installation av ett pålfundament: (1) på den fria markytan, (2) på fyra spetsburna betongpålar och (3) på pålfundamentet som sammanfogar pålarna vid markytan. Numeriska modeller har använts för att undersöka inverkan av parametrar för pålarna och jorden. Resultaten har därefter använts för att utveckla en approximativ reduktionsfaktor som appliceras på uppmätta vibrationer på markytan för att estimera vibrationer av spetsburna pålar.

Avhandlingen har resulterat i en validering av numeriska modellers användning för att förutsäga markburna vibrationer i spetsburna pålfundament samt en undersökning av hur pålarnas och jordens egenskaper påverkar den dynamiska interaktionen mellan spetsburna pålar och jord. Resultaten visar att överföringen av vertikala vibrationer från jorden till pålarna påverkas av förhållandet mellan jordens styvhet och pålens axialstyvhet. Resultaten visar även att interaktioner mellan pålar i en grupp påverkar den vertikala responsen orsakad av en dynamisk last på markytan. Fältförsöken visar att om jordens dynamiska egenskaper kan bestämmas med noggrannhet, ger prediktioner från numeriska modeller representativa resultat. Detta ökar tillförlitligheten till resultat erhållna från sådana numeriska modeller vilket motiverar deras användning vid vibrationsutredningar.

Nyckelord: Dynamisk jord-struktur-interaktion; Pålgrupp; Spetsburna pålar; Omgivningsvibrationer; Markinducerade vibrationer

Preface

I would like to express my gratitude towards my main supervisor Jean-Marc Battini for his guidance, support, encouragement and many suggestions during the research project. I would also like to thank my co-supervisors Geert Lombaert, Stijn François, Abbas Zageneh, Fanny Deckner, Costin Pacoste and Peter Blom for their support, encouragement, suggestions and many valuable discussions. A special thanks is also directed to Johan Spross for his review of the thesis.

I am very grateful to Andréas Andersson for suggesting the test site used for the experiments in this work and to his parents Ragnvald and René for granting access to the site and for their generous hospitality. I would also like to thank the Swedish Geotechnical Institute and Martin Holmén for providing the data from laboratory measurements on soil samples from the test site and for welcoming me for a site visit in Linköping. Thanks to all my friends and colleagues at the Department of Civil and Architectural Engineering for creating an open work environment and for making KTH an enjoyable place to work.

Last, but never least, I would like to thank my beloved wife Jennifer for her endless love and support, and our two wonderful sons Alfred and Ebbot for making our lives the big adventure that it is.

Östersund, December 2024

Freddie Theland

Funding Acknowledgement

The research presented in this doctoral thesis was conducted during 2018 to 2025 at the Department of Civil and Architectural Engineering, KTH Royal Institute of Technology, Sweden. The research was funded by the Swedish Building, Development and Research fund (SBUF) and the funding for experiments was received from Trafikverket, Vinnova and the Richertska research foundation. The financial support is gratefully acknowledged.

List of Publications

This doctoral thesis consists of five journal papers. Throughout the thesis, these are referred to by their Roman numerals:

Paper I: Theland, F., Lombaert, G., François, S., Pacoste, C., Deckner, F., Battini, J-M. Assessment of small-strain characteristics for vibration predictions in a Swedish clay deposit. *Soil Dynamics and Earthquake Engineering*, vol. 150, 106804, 2021.

Paper II: Theland, F., Lombaert, G., François, S., Pacoste, C., Deckner, F., Blom, P., Battini, J-M. Dynamic response of driven end-bearing piles and a pile group in soft clay: an experimental validation study. *Engineering Structures*, vol. 267, 114629, 2022.

Paper III: Theland, F., Lombaert, G., François, S., Zangeneh, A., Deckner, F., Battini, J-M. Measurements and predictions of vibration response of end-bearing pile group in soft clay due to vertical ground surface load. Submitted to *Engineering Structures*, October 2024.

Paper IV: Theland, F., Lombaert, G., François, S., Zangeneh, A., Deckner, F., Battini, J-M. Design procedure for estimating the vertical response of end-bearing piles from free field vibrations produced by a nearby surface load. Accepted for publication in *Structures*, December 2024.

Paper V: Theland, F., Lombaert, G., François, S., Zangeneh, A., Deckner, F., Battini, J-M. The influence of pile-soil-pile interaction on the vertical response of end-bearing pile groups in soil on bedrock subjected to a vertical load at the soil's surface. Submitted to *Transportation Geotechnics*, November 2024.

The papers were written by the first author whereas the co-authors contributed to the planning of the work and the reviewing of the papers. The numerical and experimental works presented in the papers were performed by the first author except for the bender element tests presented in Paper I which were performed by Martin Holmén at the Swedish Geotechnical Institute (SGI). The estimation of damping ratios from the measurement data provided by SGI was performed by the author of the thesis.

Other relevant contributions by the author to international conferences within the framework of the research project, that are not part of the thesis, include:

– Theland, F., Battini, J-M., Pacoste, C., Lombaert, G., François, S., Deckner, F. Soil-structure interaction of and end-bearing pile foundation: design of an experimental case study. *Proceedings of the International Conference on Structural Dynamics*, EURODYN, 2020, pp. 2846-2856.

– Theland, F., Pacoste, C., Deckner, F., Lombaert, G., François, S., Battini, J-M. The influence of near-surface soil layer resonance on vibrations in pile foundations. *Current Perspectives and New Directions in Mechanics, Modelling and Design of Structural Systems : Proceedings of the 8th International Conference on Structural Engineering, Mechanics and Computation*, 2022, pp. 84-89.

Contents

Chapter 1

Introduction

1.1 Background

Vibrations in the built environment arising from activities such as road or railway traffic, industrial manufacturing processes or construction may cause disturbance to residents or be disruptive to vibration sensitive equipment in nearby buildings. Issues related to ground-borne vibration from railways have received increasing attention worldwide in recent years due to development of new railway lines, increased axle loads and utilisation of previously unbuilt land in close proximity to existing tracks [27, 68]. A variety of different models have been developed for the prediction of ground-borne vibration to aid in the design and planning of new buildings and infrastructure, ranging from early stage scoping models [8, 12, 26, 69] to strategies for more detailed vibration assessment. Predictions can be based on site measurements and empirical relationships [42, 84], numerical models or a combination thereof [62, 74, 110].

The large variability of soil conditions encountered in different projects can have a considerable influence on ground-borne vibration [27]. The properties of the soil influence the excitation mechanisms at the source, the wave propagation in the soil [60, 67] and the soil-structure interaction governing the transmission into buildings [62]. Spatial variation of soil stratigraphy, limited knowledge of the dynamic soil properties and the existence of nearby structures can make it a challenging task to accurately model the problem. When designing a new building, vibrations from pre-existing sources can be measured on the soil prior to construction and used as a basis for predicting vibrations in the building. This eliminates the need for modelling the source and the propagation path, and can thus reduce model uncertainty. However, it requires that the vibrations measured in the soil can be related to the vibration in the planned building. This transmission depends on the properties of the soil, the foundation type, the building and the incident wave field produced by the vibration source. For this reason, measurements of the vibration transmission between the soil and the building foundation show large variations between different sites [111]. This makes statistical data disregarding the specific soil conditions and foundation type, typically used in empirical prediction models, associated with a high degree of uncertainty. An alternative to using such empirical data is to make use of a numerical model for predicting the

transmission of ground-borne vibration between the soil and the foundation. This approach takes into account the site specific soil conditions and the properties of the foundation. Moreover, considering only the interaction between the soil and the foundation, the influence of the specific building design can be treated separately. This can be used to better understand the dynamic interaction between the soil and the foundation and to develop simple methods for taking it into account for vibration assessment. This approach was considered by Sanitate [99] for surface foundations in the development of an analysis framework for base isolation of buildings subjected to ground-borne vibration. However, experimental validation of such an approach would be required to ascertain that accurate predictions can be made using information from site investigations.

Geological conditions of soft clay, silt or sand overlying a densely compacted till and crystalline bedrock are typically encountered in densely populated urban areas in Sweden. Such soil conditions are prone to high levels of ground-borne vibration [12, 42, 43, 46]. In these soils, driven end-bearing piles are commonly used for foundation design, where prefabricated concrete piles are predominantly used [10, 25]. End-bearing piles in soft soils have a significantly higher vertical stiffness than floating piles due to the contribution from the axial stiffness of the piles [86]. For this reason, the transmission of vertical vibrations to end-bearing pile foundations differ from the case of floating piles [4, 83].

Despite the large amount of research conducted on pile foundations related to applications in earthquake engineering, the vibration response of end-bearing pile foundations subjected to ground-borne vibration originating from sources at the ground surface has not been previously investigated. A better understanding of the interaction between the soil and the foundation under such conditions would aid in the development of methods for taking soil-pile interaction into account for vibration assessment. It could also help limiting the transmission of ground-borne vibration to a building through foundation design. This could lead to a higher degree of land utilisation in areas with soft soil on till and bedrock where ground-borne vibration might be a concern. In turn, this would contribute to a more sustainable development of urban environments, where both the needs for housing and transportation can be met without compromising the health of residents.

1.2 Aim and scope

The aim of this research is to improve the knowledge of how ground-borne vibration is transmitted to end-bearing pile foundations and investigate how that knowledge can be used for vibration assessment. Specific objectives of the research are to:

- Perform full-scale field measurements to validate numerical predictions of ground-borne vibration in soil, end-bearing piles and a pile group foundation.
- Evaluate how numerical and experimental data can be combined for predicting ground-borne vibration.

- Identify the factors that govern the dynamic response of end-bearing pile foundations subjected to loads at the ground surface.
- Develop simple methods to take into account the influence of dynamic soil-pile interaction that can be used for vibration assessment.

The results presented in this thesis may be of interest for a range of applications in the field of soil dynamics, but the focus of the research is on ground-borne vibration in buildings in the frequency range 1-80 Hz. This corresponds to the frequency range of building vibrations which is relevant for human comfort and vibration sensitive equipment [50].

1.3 Limitations

The following limitations of the research apply:

- In numerical simulations, the soil and the piles are assumed to be of linear elastic material. This is often a justified assumption for traffic induced ground-borne vibration, as the associated amplitude of shear strains in the soil is usually small [49].
- The soil is idealised as horizontally layered.
- The vibration source applied to the soil is in all cases, both numerically and experimentally, considered as a stationary vertical load applied at the ground surface. Excitation due to the stationary part of a train passage can in many cases be approximated as a series of point sources without any significant loss of accuracy [9, 62].
- The influence of a building is not considered and only the dynamic interaction between the foundation and the soil is studied.
- Only vertical piles are considered.
- Foundation caps of pile groups are assumed not to be in contact with the soil.

1.4 Scientific contributions

The research presented in this thesis has resulted in the following scientific contributions:

- Assessment of methods for determining the dynamic small-strain soil properties for a Swedish clay on till and bedrock.

- Identification of the influence of a dry layer of soil over saturated soil and bedrock on the vibration response at the ground surface due to a vertical surface load.
- Presentation of a comprehensive set of results from full-scale field tests of the dynamic response of a group of four end-bearing piles.
- Validation of linear elastic numerical models for predicting vibration responses of an end-bearing pile group foundation.
- Assessment of a hybrid prediction method used for combining a model with measurements taken at an earlier construction stage.
- Development of a design procedure for estimating the vibration response of end-bearing piles from measured free field vibrations.
- Analysis of the influence of pile-soil-pile interaction on the vertical response of end-bearing pile group foundations subjected to waves induced by a vertical load at the ground surface.

1.5 Outline of the thesis

This thesis consists of five scientific papers preceded by an introductory part. The introductory part is intended to provide the reader with the background, the theoretical foundation and the practical context of the performed research. The remainder of the thesis is organised as follows. Chapter 2 presents a framework used for the assessment of train-induced ground-borne vibration in buildings based on site measurements. The assessment of building vibrations from measurements of vibrations at the ground surface is discussed. Chapter 3 presents an overview of different methods for determining the dynamic small-strain soil properties required to model wave propagation in soil. Chapter 4 describes how the dynamic soil-structure interaction problem can be decomposed into separate parts and how that can be used to combine a numerical model with measurements performed prior to construction. Chapter 5 describes the numerical models used in the research work. Chapter 6 presents a summary of the research work. Chapter 7 discuss the results from the performed research. Chapter 8 presents the conclusions and suggestions for further research.

Chapter 2

Vibration assessment in the built environment

Ground-borne vibration in the built environment is subject to many sources of uncertainty. It is therefore often advisable to incorporate measurements for detailed vibration assessment. This chapter outlines a framework adopted in international standards for detailed vibration assessment of railway induced ground-borne vibration in buildings. It is described how the problem can be subdivided into separate source, propagation and receiver terms. This forms a basis for making predictions based on a combination of site measurements and correction factors obtained either empirically or from a numerical model.

2.1 Transmission of ground-borne vibration

The problem of ground-borne vibration can be decomposed into three components: the source, the propagation path and the receiver, as illustrated in fig. 2.1. The vibration response at a certain location in this system can be expressed as a function of each of these terms:

$$A(f) = \mathscr{A}\Big((S(f), P(f), R(f)\Big) \tag{2.1}$$

where $A(f)$ is the vibration response of interest as a function $\mathscr{A}$ of the source $S(f)$, propagation path $P(f)$ and receiver $R(f)$ terms which are evaluated at each cyclic frequency f. Equation (2.1) considers the inter-dependency between the three terms. Assuming that this cross-coupling between the three terms can be neglected, eq. (2.1) can instead be expressed as:

$$A(f) = S(f)P(f)R(f) \tag{2.2}$$

This simplified form is the foundation of empirical models for the prediction of ground-borne vibration arising from rail systems as proposed in the international standard ISO 14837-1 [48]. Equation (2.2) is strictly speaking not valid for moving loads due to the Doppler effect. However, it can provide a reasonable estimate for the quasi-stationary

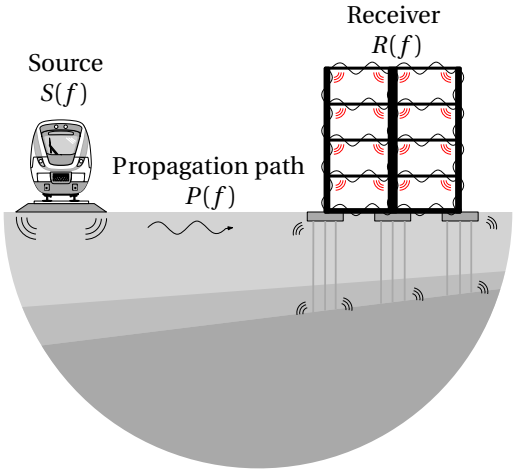

Figure 2.1: *Illustration of the three components involved in transmission of ground-borne vibration.*

response during a train passage if the train speed is relatively low compared to the wave speed of the soil [110].

The decomposition of the problem into these three different terms allows for combining measurements with empirical correction factors, or numerical simulation results, to make predictions for vibration assessment. In the case where a building is to be constructed close to existing sources of ground-borne vibration, only the transmission of vibrations into the building has to be predicted from vibration measurements at the site.

2.2 Assessment of ground-borne vibration based on site measurements

Several empirical models that follow the structure of eq. (2.2) have been developed for the prediction of ground-borne vibrations from railways. Examples include the methods developed by the Swiss Federal Railways (SBB) [63], Melke [81] for underground railways, Madshus et al. [74] based on measurement in Sweden and Norway and the US Federal Rail road Administration (FRA) and the Federal Transit Administration (FTA) [42, 93]. The framework for detailed vibration assessment proposed by FRA and FTA has been used in the scientific literature as a basis for the development of hybrid prediction procedures, which combine the use of measurements and numerical models [61, 62, 104, 110]. It has recently been used for the development of a prediction tool based on such hybrid procedures for estimating ground-borne vibration due to railway traffic [94]. The framework of the FRA/FTA method is briefly described herein as an example to demonstrate how ground-borne vibration in buildings can be estimated from site measurements.

Figure 2.2 presents an overview of the source, propagation and receiver measurement points which are considered in the following.

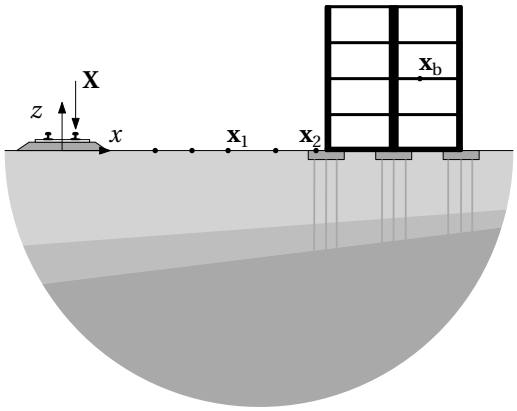

Figure 2.2: *Source and receiver points in the FRA procedure.*

The vibration level $L_v(\mathbf{x}_b)$ at a receiver location $\mathbf{x}_b$ within the building structure is the root mean square (RMS) velocity during the stationary part of a train passage expressed in decibels in one third octave bands. Equation (2.2) is thereby a sum instead of a product, of the source, propagation and receiver terms expressed in the same logarithmic basis:

$$L_v(\mathbf{x}_b) = L_F(\mathbf{X},\mathbf{x}_1) + \mathrm{TM}_L(\mathbf{X},\mathbf{x}_1) + C_b(\mathbf{x}_1,\mathbf{x}_b) \tag{2.3}$$

where $L_F(\mathbf{X},\mathbf{x}_1)$ is the equivalent force density of a line load representing the train, $\mathrm{TM}_L(\mathbf{X},\mathbf{x}_1)$ is the line source transfer mobility that characterises the transfer of vibrations from the source points $\mathbf{X}$ along the track to the receiver point $\mathbf{x}_1$ and $C_b(\mathbf{x}_1,\mathbf{x}_b)$ is a correction term relating the vibrations on the ground surface to the vibration in the building at location $\mathbf{x}_b$.

For the case where the railway is under operation, the vibration velocity response $L_v(\mathbf{x}_1)$ at the position $\mathbf{x}_1$ due to a train passage can be measured, replacing the force density and the line source transfer mobility:

$$L_v(\mathbf{x}_1) = L_F(\mathbf{X},\mathbf{x}_1) + \mathrm{TM}_L(\mathbf{X},\mathbf{x}_1) \tag{2.4}$$

The correction term between the vibrations measured on the soil in the position $\mathbf{x}_1$ and the vibration response at position $\mathbf{x}_b$ in the building can be split into two components [94]:

$$C_b(\mathbf{x}_1,\mathbf{x}_b) = C_{b2}(\mathbf{x}_1,\mathbf{x}_2) + C_{b3}(\mathbf{x}_2,\mathbf{x}_b) \tag{2.5}$$

where $C_{b2}(\mathbf{x}_1,\mathbf{x}_2)$ is the correction factor between the soil and the position $\mathbf{x}_2$ at the buildings foundation and $C_{b3}(\mathbf{x}_2,\mathbf{x}_b)$ is the correction factor between the foundation and the floors in the building, i.e. at position $\mathbf{x}_b$.

2.2.1 Empirical correction factors

Empirical correction factors have been established from statistical datasets based on site measurements. The datasets available in the literature are often broadly categorised in terms of building and foundation type. These correction factors are therefore associated with a large degree of uncertainty.

Figure 2.3 presents the correction factors $C_{b2}(\mathbf{x}_1, \mathbf{x}_2)$ proposed by the FRA/FTA which relate the vibrations on the ground surface to vibrations at the foundation level for different building types. The frequency range extends to 250 Hz for these curves as they are also applied for assessment of of re-radiated noise. For these curves, there are no data related to the specific soil conditions. The properties of the soil have been shown to have an important influence on ground-borne vibration in buildings [62].

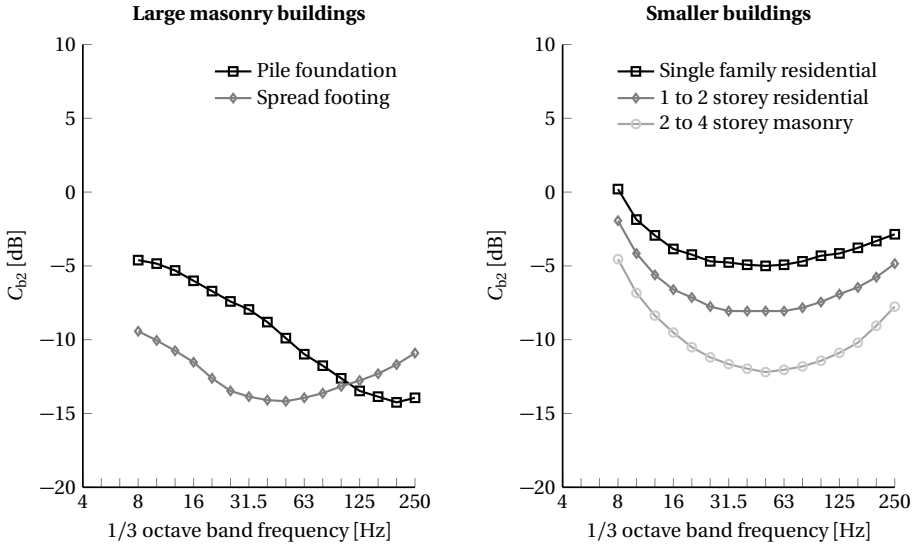

Figure 2.3: *Empirical values for the correction factor $C_{b2}(\mathbf{x}_1, \mathbf{x}_2)$ proposed by the FRA and FTA [42, 93].*

Reumers et al. [94] used the framework of the FRA/FTA procedure with correction factors obtained from the EU FP7 project RIVAS database instead [111]. Figure 2.4 presents an overview of average values for $C_{b2}(\mathbf{x}_1, \mathbf{x}_2)$ in one third octave band center frequencies for different soil conditions, obtained from the empirical data set. The curves are based on a statistical mean value and its corresponding 60% confidence interval, corresponding to one standard deviation of about ±5 dB [111]. Detailed information on the soil conditions and foundation types related to this data set is not available and the attribution to soil stiffness has been assigned based on results from numerical analyses. Measurements of train-induced vibrations at the site Furet in Sweden, for which the soil conditions correspond to the classification of soft soil, were found to follow the curve proposed for stiff soil up to about 50 Hz [111]. This shows

the uncertainty related to these correction terms and a standard deviation of ±5 dB for to each of the curves in fig. 2.4 was proposed in RIVAS [111].

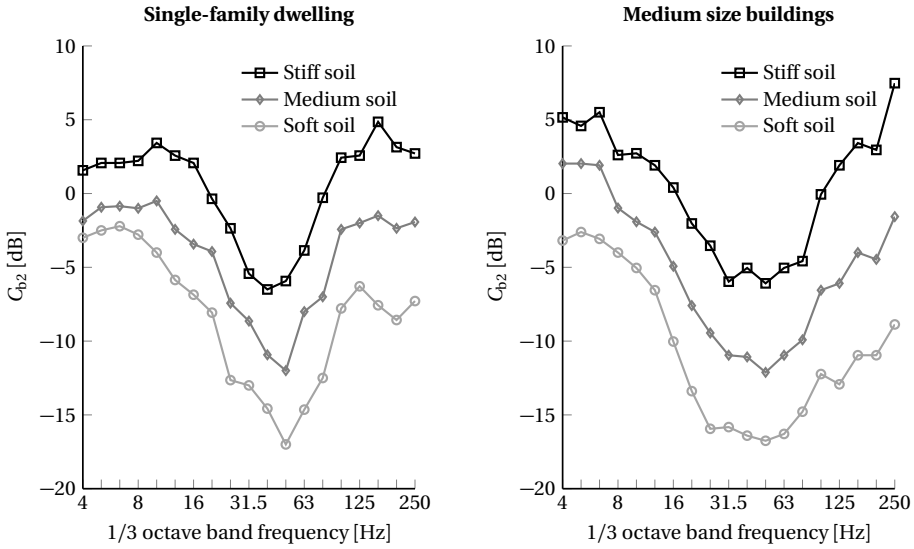

Figure 2.4: *Empirical values for the correction factor $C_{b2}(\mathbf{x}_1,\mathbf{x}_2)$ for single-family dwellings and medium size buildings, which are lower than four storeys, for different categories of soil conditions. The curves are average values from experimental results in the RIVAS database [111]. Adapted from Reumers et al. [94].*

To estimate the level of vibration of floors in a building, the FRA/FTA assigns the factor $C_{b3}(\mathbf{x}_2,\mathbf{x}_b)$ with an attenuation of $1-2$ dB/floor and an amplification of 6 dB in the range of fundamental floor resonances. The attenuation with increasing floor height has been shown to not be generally applicable [62, 116]. Figure 2.5 presents the empirical curves from the RIVAS project for the factor $C_{b3}(\mathbf{x}_2,\mathbf{x}_b)$. Two classifications of different building types are considered, one with wooden floors and one with concrete floors, with average floor resonance frequencies of 16 and 31.5 Hz, respectively. The differences between the amplification factors proposed by the FRA/FTA and the ones obtained in the RIVAS project are significant, more than 10 dB at resonance above the first floor. Comparing the empirical values for the different correction factors obtained from the FRA/FTA and the RIVAS project illustrates the degree of uncertainty associated with the assessment of ground-borne vibrations in buildings.

2.2.2 Predicting building vibrations from measurements before construction

The empirical correction factors are, for practical reasons, defined for the case when the building is present. Therefore, $C_{b2}(\mathbf{x}_1,\mathbf{x}_2)$ and $C_{b3}(\mathbf{x}_2,\mathbf{x}_s)$ are generally affected both

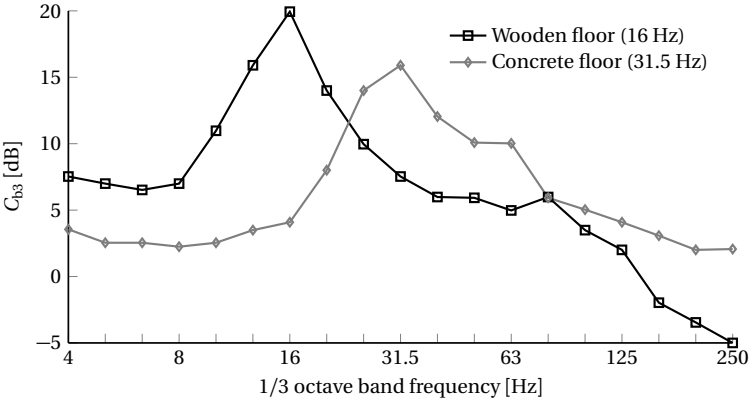

Figure 2.5: *Empirical values for the correction factor $C_{b3}(\mathbf{x}_1, \mathbf{x}_2)$ for wooden floors with an average floor resonance frequency of 16 Hz and concrete floors with an average floor resonance frequency of 31.5 Hz. The curves are average values from experimental results in the RIVAS database [111]. Adapted from Reumers et al. [94].*

by the properties of the building and the dynamic interaction between the foundation and the soil. Moreover, the presence of the building affects the vibrations in the soil, especially at locations close to the building. Therefore, correction factors established using measurements on ground surface prior to construction as reference differ from the ones obtained for a building which is already present [66]. For vibration assessment in the case were a building is to be constructed in close proximity to a railway, the use of existing empirical values might therefore not be appropriate. In that case, the corrections should instead be defined with respect to vibrations measured prior to construction, i.e. on the free ground surface at the location of the foundation or on the foundation before the building is erected [100]. It is further explained in chapter 4 how results obtained at different stages of construction can be combined.

2.2.3 Correction factors from numerical models

An alternative to using empirical curves is to use a numerical model for predicting the correction factors $C_{b2}(\mathbf{x}_1, \mathbf{x}_2)$ and $C_{b3}(\mathbf{x}_2, \mathbf{x}_s)$. As the correction factor $C_{b2}(\mathbf{x}_1, \mathbf{x}_2)$ is relative to the response in the soil at the point $\mathbf{x}_1$, only the relationship between the vibrations in the soil and in the building is required to be well represented. In this case, the vibrations at the free ground surface in the absence of the building can also be used as the reference value.

Chapter 3

Determination of dynamic small-strain soil properties

Mechanical models are commonly used for the analysis of ground-borne vibration under the assumption that the soil undergoes small deformations. This is often a justified assumption for ground-borne vibration induced by railway or road traffic, allowing to treat soil and bedrock as linear elastic materials. However, to model the soil, the associated small-strain soil properties are required. In practice, these properties are estimated from empirical correlations applied with index parameters obtained from conventional geotechnical tests, dynamic laboratory investigations or dynamic in situ measurements. This chapter presents an overview of the methods used in Paper I for estimating the dynamic small-strain soil properties required to perform predictions of wave propagation in soil.

3.1 Wave propagation in soil

Wave propagation in soil under small-strain deformation can be modelled using elastodynamic theory. The Cauchy equations of motion for a solid material reads:

$$\nabla \cdot \boldsymbol{\sigma} + \rho \mathbf{b} = \rho \ddot{\mathbf{u}} \tag{3.1}$$

where $\nabla = \{\partial/\partial x, \partial/\partial y, \partial/\partial z\}$ is a differential operator, $\boldsymbol{\sigma}$ is the stress tensor, ρ the material density, $\rho\mathbf{b}$ the body force per unit volume and $\mathbf{u}$ the displacement vector with $\ddot{\mathbf{u}}$ denoting its second material derivative with respect to time. For a linear elastic material, the constitutive relations can be written:

$$\boldsymbol{\sigma} = \mathsf{C} : \boldsymbol{\epsilon} \tag{3.2}$$

where C is the fourth-order elasticity tensor and $\boldsymbol{\epsilon}$ the strain tensor. The small strain tensor is related to the displacements by:

$$\boldsymbol{\epsilon} = \frac{1}{2}\Big((\nabla \mathbf{u})^T + \nabla \mathbf{u}\Big) \tag{3.3}$$

Taking eqs. (3.2) and (3.3) into consideration and assuming an isotropic material, eq. (3.1) can be rewritten as the Navier equations:

$$(\lambda+2G)\nabla\nabla\cdot\mathbf{u}-G\nabla\times\nabla\times\mathbf{u}+\rho\mathbf{b}=\rho\ddot{\mathbf{u}} \tag{3.4}$$

where the Lamé constant λ and the shear modulus G are related to the modulus of elasticity E and Poisson's ratio ν by:

$$\lambda=\frac{\nu E}{(1+\nu)(1-2\nu)},\quad G=\frac{E}{2(1+\nu)} \tag{3.5}$$

Adopting Helmholtz decomposition,

$$\mathbf{u}=\nabla\Phi+\nabla\times\boldsymbol{\Psi},\quad \nabla\cdot\boldsymbol{\Psi}=0, \tag{3.6}$$

with Φ a scalar wave potential and $\boldsymbol{\Psi}$ a divergence free vector field potential, eq. (3.4) can be rewritten as two uncoupled wave equations [1]:

$$(\lambda+2G)\nabla^2\Phi=\rho\ddot{\Phi} \tag{3.7}$$

$$G\nabla^2\boldsymbol{\Psi}=\rho\ddot{\boldsymbol{\Psi}} \tag{3.8}$$

In an infinite linear elastic, isotropic, homogeneous solid, two types of waves can exist. These waves consist of the dilatational wave (P-wave) and the shear wave (S-wave). The material wave speeds are related to the elastic material properties as obtained from eqs. (3.7) and (3.8) by:

$$C_\mathrm{p}=\sqrt{\frac{\lambda+2G}{\rho}} \tag{3.9}$$

$$C_\mathrm{s}=\sqrt{\frac{G}{\rho}} \tag{3.10}$$

For a solid that is not of infinite extent, boundary conditions and impedance mismatch at material interfaces cause reflection and refraction of waves and can lead to the existence of other types of waves, such as surface waves propagating along a traction free boundary.

Material damping in soil under small-strain loading is caused by dissipation of energy e.g. due to friction between soil particles. In the low frequency range, the small-strain damping in soils is almost rate independent [49]. For small damping ratios, hysteretic material damping can be taken into account in a linear formulation by adopting complex elastic moduli [95]:

$$(\lambda+2G)^*=(\lambda+2G)(1+\mathrm{i}2\beta_\mathrm{p}) \tag{3.11}$$

$$G^*=G(1+\mathrm{i}2\beta_\mathrm{s}) \tag{3.12}$$

where i is the imaginary unit, β_p and β_s are the damping ratios in volumetric and deviatoric deformation, respectively.

Water saturation of soft soils can influence the properties governing wave propagation. In general, a saturated soil acts as a two-phase poroelastic medium which can be modelled with Biot's theory [19]. However, in the frequency range of interest for ground-borne vibration in buildings, the wavelengths of the propagating waves are long compared to the pore structure in the soil. Therefore, the soil can be considered as an equivalent elastic solid medium without any significant loss of accuracy [102]. Assuming small-strain behaviour of the soil, the material properties of a soil layer can thereby be characterised in terms of its density ρ, the wave propagation speeds C_p and C_s, and their corresponding material damping ratios β_p and β_s.

It should, however, be recognized that due to the negligible compressibility of water compared to the matrix of soil particles in soft soils, the P-wave speed of such soils approaches the speed of sound in water $C_\mathrm{p} \approx 1500$ m/s when fully saturated [49]. This can lead to large contrasts in P-wave speed at the interface between saturated and not fully saturated soil, which may cause layer resonances of vertically propagating P-waves [102]. These resonances occur in a dry layer with thickness h_1 approximately at the frequencies where standing waves develop in a layer built in at its base:

$$f_{\mathrm{p},n} = (2n+1)\frac{C_\mathrm{p}}{4h_1}, \quad n = 0, 1, 2, \ldots \tag{3.13}$$

Such resonances exist also for S-waves for a layer of thickness h_2 built in at its base (but not due to the presence of the ground water table) and similarly occur at the frequencies:

$$f_{\mathrm{s},n} = (2n+1)\frac{C_\mathrm{s}}{4h_2}, \quad n = 0, 1, 2, \ldots \tag{3.14}$$

3.2 Investigation methods

The dynamic small-strain soil properties can have a large influence on the vibration response in the free field [27, 67], soil-structure interaction and the transmission of ground-borne vibration into buildings [62]. Prediction of ground-borne vibration using a model therefore generally requires an accurate representation of the soil. However, due to project restrictions and budget constraints, geotechnical or geophysical investigations are usually limited. It is therefore important to understand the advantages and the limitations of different methods for estimating the small-strain properties of the soil for vibration assessment purposes.

3.2.1 Empirical methods

Empirical correlations are useful to obtain estimates of the small-strain properties from information obtained from standard site investigations. A large variety of different empirical correlations have been presented in the literature for estimating the

small-strain shear modulus G_0 for different soil conditions. The following presentation is limited to empirical correlations for cohesive soils, mainly based on data from Scandinavian clays.

Larsson and Mulabdić [65] presented and evaluated empirical correlations for cohesive soils based on results from seismic cone penetration and cross-hole tests and recommended for high and medium-plastic clays the relation:

$$G_0 = \left(\frac{208}{I_\mathrm{p}} + 250\right) s_\mathrm{u} \tag{3.15}$$

where I_p is the plasticity index (in decimals) and s_u the undrained shear strength. For low-plastic clays and clayey gyttja, an alternative correlation based on the liquid limit w_L was suggested by [65]:

$$G_0 = 504 \frac{s_\mathrm{u}}{w_\mathrm{L}} \tag{3.16}$$

These relations are appropriate for Scandinavian clays, as the sites included in the database to establish the relation were located in Sweden and Norway. It should be noted that only s_u determined from dilatometer, corrected field vane or fall cone tests should be used for the presented relations.

The initial shear modulus can also be estimated from empirical correlations established for cone penetration tests with pore water pressure measurement (CPTu). Mayne and Rix [80] presented an empirical correlation between CPTu and the initial shear modulus for cohesive soils based on data from clays around the world, where the sites considered by Larsson and Mulabdić [65] constituted a significant part of the data set used as a basis for the correlation. The initial shear modulus can be estimated from:

$$G_0(z) = p_\mathrm{a} \frac{99.5}{e(z)^{1.13}} \left(\frac{q_\mathrm{t}(z)}{p_\mathrm{a}}\right)^{0.695} \tag{3.17}$$

where $q_\mathrm{t}(z)$ is the corrected cone tip resistance, z is the depth, $p_\mathrm{a} = 100$ kPa is a reference pressure and $e(z)$ is the void ratio as a function of depth. The advantages of using the CPTu data for estimating the initial shear modulus are the same as for the CPTu test in general, i.e. it provides a high resolution with depth and is based on in situ conditions. However, the method is applicable strictly only for cohesive soils and might yield inaccurate results if applied to intermediate layers of non-cohesive soil or mixed soils [49].

3.2.2 Seismic cone penetration test

The seismic cone penetration test is a dynamic test performed using a CPT probe equipped with motion sensors and follows the same principle as down-hole surveys [96]. The test is performed by hitting a pre-loaded beam at the ground surface with a hammer in the transverse direction, inducing S-waves propagating from the surface. The arrival of the S-waves are preferably measured at depth using two stations, allowing to determine the interval wave speed in the medium in between the positions of

the sensors. Using two stations rather than one eliminates the reliance on an accurate trigger, resulting in more accurate wave speed estimations [52].

The time delay in the arrival of S-waves is estimated from the two recorded signals. This can be achieved by visual inspection, the cross-over method using two signals of reverse polarity or cross-correlation in either the time or frequency domain [21, 96]. Cross-correlation methods have the advantage that the full waveforms are taken into account when computing the time shift between the signals and that they allow for automation, thereby removing user subjectivity [7, 16, 52]. The time domain cross-correlation between the receiver signals $a_1(t)$ and $a_2(t)$ and the estimated time shift Δt are given by:

$$c_{12}(t) = \int_{-\infty}^{\infty} a_1(\tau) a_2(\tau + t)\, \mathrm{d}\tau \tag{3.18}$$

$$\Delta t = \underset{t}{\operatorname{argmax}}\ c_{12}(t) \tag{3.19}$$

Assuming straight travel paths of the waves, as illustrated in fig. 3.1, and a horizontal offset x_s between the source and the receivers, the S-wave speed can be calculated as:

$$C_\mathrm{s}^\mathrm{SCPT} = \frac{r_{2k} - r_{1k}}{\Delta t_k} \tag{3.20}$$

where $r_{1k} = \sqrt{z_{1k}^2 + x_\mathrm{s}^2}$ and $r_{2k} = \sqrt{z_{2k}^2 + x_\mathrm{s}^2}$ denote the radial distance to receiver 1 and 2, respectively. Following Verachtert [108] and Areias and Van Impe [6] the shear

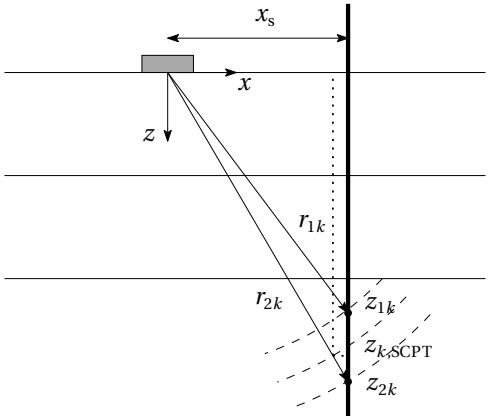

Figure 3.1: *Straight travel path model and interpreted investigation depth $z_{k,\mathrm{SCPT}}$ from the SCPT.*

wave speeds are attributed to the depth $z_{k,\mathrm{SCPT}}$ corresponding to the radial distance $(r_{1k} + r_{2k})/2$ between the source and the bottom receiver, i.e.:

$$z_{k,\mathrm{SCPT}} = \frac{z_{2k}(r_{1k} + r_{2k})}{2 r_{2k}} \tag{3.21}$$

The SCPT was extensively used in the investigations of Larsson and Mulabdić [65], where it was found that for Swedish clays, the shear strains in the upper part of the soil might exceed the limits for which the soil can be considered as elastic. Therefore, measurements in the upper part of profiles with soft soils should be carefully executed. Moreover, the estimations of wave speeds in the uppermost meters of the soil are less reliable due to the small effective spacing between the sensors in eq. (3.20) [5, 52].

3.2.3 Bender element tests

Bender elements can be mounted into devices for conventional laboratory testing such as oedometer, triaxial and direct simple shear to measure the S- and P-wave speeds of a soil specimen under different loading conditions [49]. The bender elements flex when supplied with an electric voltage and likewise produce a voltage when deformed. The piezoelectric benders are mounted to the testing equipment in the top cap and the bottom pedestal, allowing to determine the travel time over the interval to obtain the material wave speed. In addition, anisotropy may also be characterized by mounting elements in the perpendicular direction [91, 106].

The test is fast and considered to be a reliable method to determine the S- and P-wave speeds of samples. However, a general issue with laboratory investigations of small-strain properties is that they require high quality samples. The quality of the samples can have a significant effect on the estimated S-wave speed in Scandinavian clays [114]. Moreover, small specimens evaluated in the laboratory might not be representative for the in situ soil conditions over a larger area.

The evaluation of material damping with bender elements has been addressed only by a few authors [20, 22, 52]. The most accurate among the methods is the Hilbert transform method proposed by Cheng and Leong [22]. Their estimation results were shown to be within a relative error of 10% from numerical simulations and the results were validated against resonant column tests for an Ottawa sand. This method was used in Paper I to estimate material damping from P-wave signals from tests on samples in an oedometer provided by SGI [45].

3.2.4 Seismic refraction

Seismic refraction is a non-invasive geophysical method for groundwater exploration and sub-surface mapping of bedrock [64]. The method is based on the measurement of the dynamic surface response due to an impulse load applied at the ground surface. The loads are in practice generated by a hammer or small explosive loads. The P-wave is the fastest travelling wave and is thus the first to arrive at the receivers. The first arrival at each receiver is identified, and the arrival time and source-receiver offset data is used to estimate P-wave speeds and depth of soil layers from a model inversion. The model inversion is based on Snell's law and the assumption of a horizontally stratified soil profile where the P-wave speed is increasing with depth. Snell's law is given by:

$$\frac{C_{\mathrm{p}j}}{\sin\theta_j} = \frac{C_{\mathrm{p}j+1}}{\sin\theta_{j+1}} \tag{3.22}$$

where θ_j is the angle of the incident P-wave in layer j travelling with P-wave velocity $C_{\mathrm{p}j}$ and θ_{j+1} is the angle of the refracted P-wave in layer $j+1$ with corresponding P-wave velocity $C_{\mathrm{p}j+1}$. If the condition $C_{\mathrm{p}j+1} > C_{\mathrm{p}j}$ holds, the incident P-wave is critically refracted, travelling with a velocity $C_{\mathrm{p}j+1}$ along the boundary between layers j and $j+1$, whenever the incident angle equals $\theta_{j\mathrm{c}} = \arcsin(C_{\mathrm{p}j}/C_{\mathrm{p}j+1})$.

Figure 3.2 presents a schematic representation of a refraction test where each receiver represents the first arrival corresponding to each layer. At the first receiver, a direct

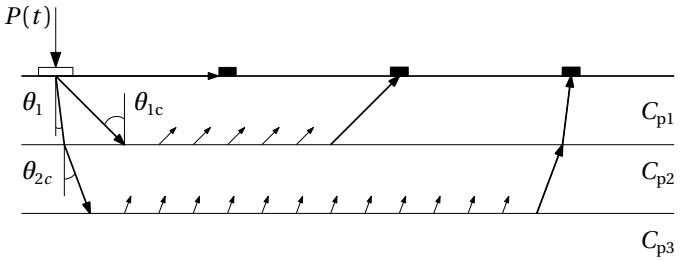

Figure 3.2: *Schematic illustration of a seismic refraction test.*

wave travelling in the upper layer arrives first. The first arrival at the second receiver is a wave that is critically refracted at an angle $\theta_{1\mathrm{c}}$ at the interface between the first and the second layer. The wave travels along the upper boundary of the second layer with the velocity $C_{\mathrm{p}2}$ and is refracted back towards the surface. The third ray is refracted at the interface between the first and the second layer with an angle θ_1, and is critically refracted at the interface between the second and third layer at an angle $\theta_{2\mathrm{c}}$, where it is refracted back towards the surface in a similar fashion. For a regular soil profile, where the stiffness is increasing with depth, the first arrivals at the closest receivers will correspond to direct waves in the uppermost layer and refracted waves will be the first to arrive at receivers positioned at larger distances.

The P-wave speeds $C_{\mathrm{p}j}$ of a layered soil can be obtained from the slopes and intersections of lines of a bilinear curve representing the first arrival times as a function of receiver distance, provided that the P-wave velocity increases with depth at the site, and can be calculated as:

$$C_{\mathrm{p}j} = \frac{r_{j+1} - r_j}{t_{\mathrm{p}j+1} - t_{\mathrm{p}j}} \tag{3.23}$$

where r_j is the source-receiver distance at the jth breakpoint of the bilinear curve and $t_{\mathrm{p}j}$ is the corresponding arrival time of the P-wave. The layer thickness h_j of layer j can then be calculated as [108]:

$$h_j = \frac{\tan\theta_{jj}}{2}\Big(C_{\mathrm{p}j+1}t_{\mathrm{p}j+1} - r_{j+1} - 2\sum_{i=1}^{j-1}\frac{h_i}{\tan\theta_{ij}}\Big) \tag{3.24}$$

with θ_{ij} defined by:

$$\theta_{ij} = \arcsin\left(\frac{C_{\mathrm{p}i}}{C_{\mathrm{p}j+1}}\right) \tag{3.25}$$

A limitation of the method is that when the condition of a regular soil profile, i.e. a strictly increasing P-wave speed with depth, is violated, any intermediate softer layer will undetectable. Moreover, when sharp stiffness contrasts are present, the wave refracted in an underlying much stiffer layer may reach all the receivers before the wave that is refracted in an intermediate layer, leaving it undetected.

3.2.5 Surface wave methods

At the stress-free boundary at the ground surface, not only P- and S-waves exist, but also surface waves. The surface waves develop as a consequence of the traction-free boundary condition and propagate along the surface. For a homogeneous halfspace, the surface wave (Rayleigh wave) travels with a constant speed C_{R} that is closely related to the S-wave speed of the soil and is approximately [1]:

$$C_{\mathrm{R}} \approx C_{\mathrm{s}} \frac{0.862 + 1.14\,\nu}{1+\nu} \tag{3.26}$$

Surface waves are subjected to a lower degree of geometrical attenuation than body waves, as they propagate along the surface rather than in the volume of soil. The amplitude of the soil displacements due to the surface wave decays exponentially with depth and the displacements diminish for depths larger than approximately two wavelengths. Figure 3.3 illustrates the influence of geometrical attenuation and the distribution of relative displacements for the P-wave, the S-wave and the Rayleigh wave for the motion induced in the soil from a vertically oscillating circular footing.

For harmonic loading, the Rayleigh wavelength is inversely proportional to the frequency:

$$\lambda_{\mathrm{R}} = \frac{C_{\mathrm{R}}}{f} \tag{3.27}$$

which means that, as the frequency increases, the penetration depth of the Rayleigh wave decreases.

Surface waves in layered soil

If layering or variation of the stiffness with depth is introduced in the soil, multiple modes of surface waves exist and they become dispersive, i.e. the wave speeds of the surface waves depend on the frequency. This can be represented by dispersion curves, which describe the variation of wave speeds with frequency. As the penetration depth of a surface wave is proportional to its wavelength, the dispersion curves contain

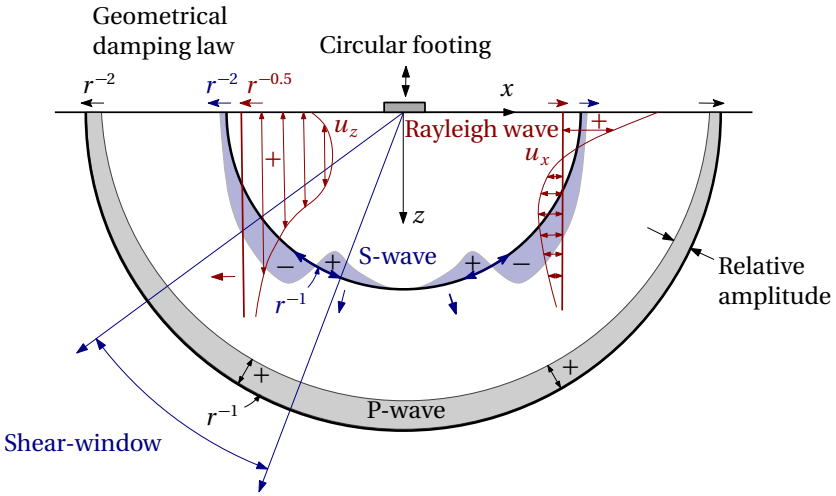

Figure 3.3: *Distribution of displacements from waves emanating from a rigid vertically oscillating circular footing on a homogeneous isotropic halfspace. Adapted from Woods [115].*

information about the material properties at depth in the soil profile, where longer wavelengths contain information of the deeper layers and shorter wavelengths of the more shallow soil [33]. This is the foundation for a class of methods to estimate the small-strain properties in soil from dynamic measurements performed at the ground surface referred to as Spectral Analysis of Surface Waves (SASW) or Multi Channel Analysis of Surface Waves (MASW). Assuming a horizontally stratified soil of linear elastic isotropic layers, theoretical dispersion curves can be obtained analytically in the frequency-wavenumber domain [44, 55, 107]. The direct stiffness method is used for this purpose in this thesis. This method is further described in chapter 5.

Surface wave measurements

Experimental dispersion curves are estimated from field measurements. There are two types of tests, the passive test which involves ambient sources of vibration and the active test which also involves excitation applied at the ground surface [33]. The experimental procedure for the active test is the same as in the seismic refraction test. An array of receivers are placed at the ground surface extending from the position where a dynamic load is applied. The responses are measured and transformed from the time to the frequency domain using discrete Fourier transform, and from the spatial to the wavenumber domain using appropriate integral transform techniques (e.g. [32, 89, 119]). In the frequency-wavenumber domain, dispersion curves are identified as distinct peaks in the spectrum [90]. The identified dispersion curves can subsequently be used to estimate the experimental attenuation curves of the surface waves from the spectral peaks using methods from structural dynamics [11, 109]. The attenuation curves describe the spatial attenuation related to material damping in the soil

as a function of frequency or wavelength.

Model inversion

The dynamic soil properties are estimated from a model inversion formulated as a multi-objective non-linear least squares problem, minimizing the misfit between the experimental and theoretical dispersion and attenuation curves in order to obtain the properties making up the soil profile. This problem suffers from non-uniqueness and the outcome of the inversion strongly depends on the initial number of layers and soil properties assumed. This is especially the case for soils with an irregular variation of stiffness with depth [108]. It is therefore beneficial to incorporate any information available of stratification and soil properties obtained from site investigations.

Surface measurement methods are non-invasive as they require measurements only on the surface of the soil. Due to the spatial distribution of the measurement points over a larger distance, the identified in situ properties take a larger body of soil into account than point wise investigation methods such as laboratory sampling or SCPT. However, as the methods are based on model inversions, they are sensitive to violations of the fundamental model assumptions such as lateral variations of the soil properties or inclined layers of soil or rock. In the case of small layer inclinations, an equivalent horizontally stratified model can still capture the propagation of surface waves at a site [108]. In that case, however, the properties of the layers do not necessarily reflect the true properties of the soil. Therefore, careful consideration should be taken when assessing the validity of an identified soil model when used for prediction purposes.

Chapter 4

Dynamic soil-structure interaction

The dynamic behaviour of a building is governed both by the mechanical properties of the structure and the soil-foundation system. The interaction between the soil and the foundation strongly depends on the relationship between the foundation geometry and the wavelengths in the soil. Therefore, the influence of soil-structure interaction on the dynamic response of a structure is generally frequency dependent. Pile group foundations are particularly sensitive to the loading frequency, due to the interaction between the piles through the soil. This chapter presents how the general problem of soil-structure interaction can be decomposed into equivalent excitation forces and frequency dependent stiffness and damping values at the soil-foundation or the foundation-structure boundary using a substructure formulation. This formulation of the problem provides a theoretical framework for analysing the influence of dynamic interaction between foundations and soil and for combining experimental data with numerical models to predict ground-borne vibration in buildings.

4.1 Substructure analysis

The dynamic soil-structure interaction problem consists of a structure in contact with a deformable soil with loads applied to the soil, to the structure or both. Figure 4.1 presents an overview of the general problem. The most straightforward way to model this problem is to take all the components involved into account. In many cases, this can become computationally prohibitive and the complexity of the problem can make it difficult to generalise results. In a more practical context, this high degree of complexity also makes it difficult to accurately perform vibration assessment, as modelling errors are introduced due to the often limited information about the soil conditions.

In order to separate the influence of soil-structure interaction on the dynamic behaviour of the structure from the excitation applied to the structure through wave loading of the building foundation, the problem can be formulated adopting a substructure approach. This approach has been presented in different forms in the literature for dynamic soil-structure interaction problems. It has also been extensively used for computational and experimental applications in structural dynamics [28].

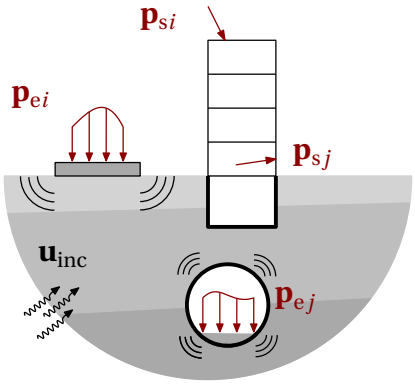

Figure 4.1: *The general dynamic soil-structure interaction problem.*

The formulation presented here is based on the one presented by Kausel et al. [56].

Assuming linearity and a discretised geometry, the full problem corresponding to the case in fig. 4.1 can be formulated in the frequency domain as:

$$\mathbf{Z}_t\mathbf{u}_t(\omega) = \mathbf{p}_t(\omega) \tag{4.1}$$

where $\mathbf{u}_t(\omega)$ is the vector of displacements and $\mathbf{p}_t(\omega)$ is the vector of external forces, which are both functions of the circular frequency ω. The impedance matrix in eq. (4.1) is defined as:

$$\mathbf{Z}_t = \mathbf{K}_t + i\omega\mathbf{C}_t - \omega^2\mathbf{M}_t \tag{4.2}$$

where $\mathbf{K}_t$ is the stiffness matrix, $\mathbf{C}_t$ the damping matrix and $\mathbf{M}_t$ the mass matrix. If only the response within the building structure is of interest, this problem can be reformulated into an equivalent problem reduced to the domain of the structure.

With reference to fig. 4.2, the soil-structure problem can be decomposed by fulfilling compatibility and equilibrium conditions at the boundary between the structure and exterior soil domains $\Omega_s \cap \Omega_e$ through continuity of displacements $\mathbf{u}_b$ and equilibrium of tractions $\mathbf{p}_b$ along this boundary. A source in the exterior soil domain is here considered in terms of the force vector $\mathbf{p}_e$. Decomposing eq. (4.1) according to fig. 4.2, the system for the free body structure can be expressed as:

$$\begin{Bmatrix} \mathbf{Z}_{ss} & \mathbf{Z}_{sb} \\ \mathbf{Z}_{bs} & \mathbf{Z}_{bb} \end{Bmatrix} \begin{Bmatrix} \mathbf{u}_s \\ \mathbf{u}_b \end{Bmatrix} = \begin{Bmatrix} \mathbf{p}_s \\ \mathbf{p}_b \end{Bmatrix} \tag{4.3}$$

where the subscript s indicates the degrees of freedom associated with the structure and the subscript b the structures contribution to the degrees of freedom at the soil-structure boundary. The subsoil can be expressed in a similar way as:

$$\begin{Bmatrix} \mathbf{Z}_{ff} & \mathbf{Z}_{fe} \\ \mathbf{Z}_{ef} & \mathbf{Z}_{ee} \end{Bmatrix} \begin{Bmatrix} \mathbf{u}_b \\ \mathbf{u}_e \end{Bmatrix} = \begin{Bmatrix} -\mathbf{p}_b \\ \mathbf{p}_e \end{Bmatrix} \tag{4.4}$$

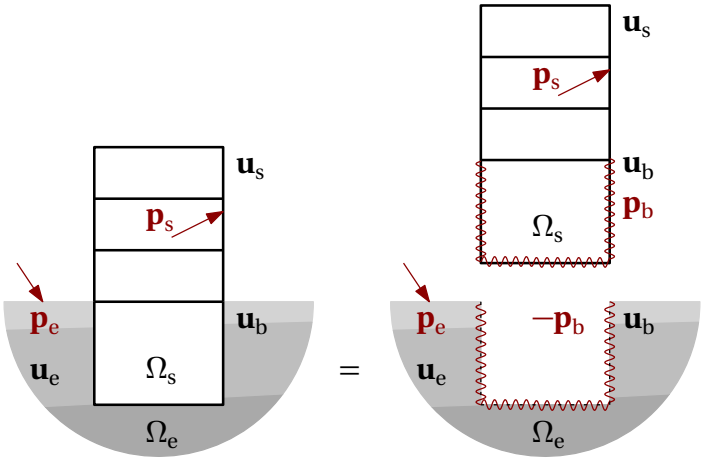

Figure 4.2: *Decomposition of the dynamic soil-structure interaction problem.*

where the subscript f denotes the subsoil contribution at the degrees of freedom of the soil-structure boundary and the subscript e denotes the degrees of freedom in the exterior soil domain Ω_e. A similar decomposition as in fig. 4.2 yields for the subsoil in fig. 4.3:

$$\begin{Bmatrix} \mathbf{Z}_{ff} & \mathbf{Z}_{fe} \\ \mathbf{Z}_{ef} & \mathbf{Z}_{ee} \end{Bmatrix} \begin{Bmatrix} \mathbf{u}_b^* \\ \mathbf{u}_e^* \end{Bmatrix} = \begin{Bmatrix} -\mathbf{p}_b^* \\ \mathbf{p}_e \end{Bmatrix} \tag{4.5}$$

where the displacements $\mathbf{u}_b^*$ and tractions $\mathbf{p}_b^*$ differ from the ones in eqs. (4.3) and (4.4). Figure 4.3 illustrates the corresponding situation under free field conditions.

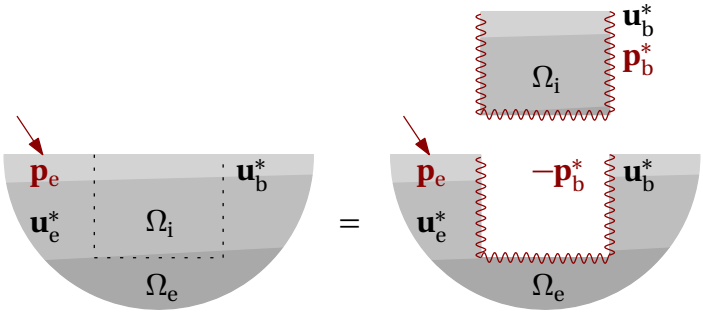

Figure 4.3: *Decomposition of free field soil excavation.*

The subsoil systems and the excitation forces $\mathbf{p}_e$ in eqs. (4.4) and (4.5) are identical. Taking the difference between the two subsoil systems, the excitation forces are eliminated and by condensation of the subsoil impedance matrix as $\mathbf{Z} = \mathbf{Z}_{ff} - \mathbf{Z}_{fe}\mathbf{Z}_{ee}^{-1}\mathbf{Z}_{ef}$, the tractions at the soil-structure boundary can be expressed as:

$$\mathbf{p}_b = -\mathbf{Z}\mathbf{u}_b + \mathbf{Z}\mathbf{u}_b^* + \mathbf{p}_b^* \tag{4.6}$$

Introducing eq. (4.6) into eq. (4.4) yields the general substructure formulation:

$$\begin{Bmatrix} \mathbf{Z}_{ss} & \mathbf{Z}_{sb} \\ \mathbf{Z}_{bs} & \mathbf{Z}_{bb}+\mathbf{Z} \end{Bmatrix} \begin{Bmatrix} \mathbf{u}_s \\ \mathbf{u}_b \end{Bmatrix} = \begin{Bmatrix} \mathbf{p}_s \\ \mathbf{Z}\mathbf{u}_b^* + \mathbf{p}_b^* \end{Bmatrix} \tag{4.7}$$

This formulation of the problem shows that:

1. The influence of soil-structure interaction for the case where loads are applied to the structure is entirely captured by the condensed soil impedance matrix $\mathbf{Z}$.
2. The excitation provided through the soil can be obtained from the free field problem, i.e. before erection of the structure, provided that the free field displacements $\mathbf{u}_b^*$ and tractions $\mathbf{p}_b^*$ can be obtained.

This formulation is general and makes no assumptions about the exterior soil domain Ω_e nor the boundary $\Omega_s \cap \Omega_e$. The domain Ω_e may contain any number of structures and different excitation mechanisms, as long as this is consistently regarded in the determination of $\mathbf{Z}$, $\mathbf{u}_b^*$ and $\mathbf{p}_b^*$. Therefore, it also applies for the case where the reference solution of eq. (4.5) consists of a soil-foundation system [112]. For such a system, $\mathbf{u}_b^*$ contains the displacements in the contact points between the structure and the foundation, $\mathbf{Z}$ the impedances of the foundation and $\mathbf{p}_b^* = \mathbf{0}$ at the free foundation contact points when the structure is not present.

If only the excitation $\mathbf{u}_b^*$ through the soil is considered and $\mathbf{p}_s = \mathbf{0}$, the contact point displacements for the case where the structure is connected to the foundation can be obtained by condensation of eq. (4.7) as:

$$\mathbf{u}_b = \left(\mathbf{Z}_s + \mathbf{Z}\right)^{-1} \mathbf{Z}\mathbf{u}_b^* \tag{4.8}$$

with $\mathbf{Z}_s = \mathbf{Z}_{bb} - \mathbf{Z}_{bs}\mathbf{Z}_{ss}^{-1}\mathbf{Z}_{sb}$. Equation (4.8) corresponds to the formulation expressed in terms of mobilities for applications in acoustics by Mondot and Petersson [82] and used by Ropars [97] for modelling ground-borne vibration in buildings.

Equations (4.7) and (4.8) provide a framework for combining numerical models with measurements performed on the foundation level, eliminating the need for modelling the soil-foundation system [34]. Such hybrid predictions are attractive for problems related to ground-borne vibration in urban environments, as it may be very difficult to fully characterise the soil conditions, the influence of nearby structures and all external sources at a site. This technique is applied in Paper III with experimental data obtained for an end-bearing pile group foundation.

For applications related to prediction of ground-borne vibration in new buildings, it is of particular interest to estimate the foundation response $\mathbf{u}_b^*$ from free field vibrations, as they can be measured in situ prior to any construction activities. The estimation of the vertical responses of end-bearing pile foundations from free field vibrations is the subject of Paper IV.

4.2 Impedances of rigid foundations

The framework presented in the previous section generally requires determination of $\mathbf{Z}$, $\mathbf{u}_\mathrm{b}^*$ and $\mathbf{p}_\mathrm{b}^*$, which for a deformable material are distributed over the entire boundary between the domain of interest Ω_s and the exterior domain Ω_e. For foundations that can be idealised as rigid, the number of degrees of freedom can be reduced to three translations and three rotations, such that $\mathbf{Z} \in \mathbb{C}^{6\times6}$, $\mathbf{u}_\mathrm{b}^* \in \mathbb{C}^{6\times1}$ and $\mathbf{p}_\mathrm{b}^* = \mathbf{0}$, with $\mathbb{C}$ denoting the complex set. The components of the impedance matrix can then be obtained from the response due to imposed displacements of the foundation reference node:

$$Z_{kl}(\omega) = \frac{p_k(\omega)}{u_l(\omega)}, \;\; u_{m\neq l} = 0 \tag{4.9}$$

where p_k is the force in degree of freedom k and u_l is the displacement in degree of freedom l. It is often not feasible to obtain experimental impedances directly, as the displacements in the inactive degrees of freedom usually cannot be restricted. Frequency response functions in terms of receptances are instead considered:

$$R_{kl}(\omega) = \frac{u_l(\omega)}{p_k(\omega)}, \;\; p_{m\neq k} = 0 \tag{4.10}$$

as the condition of zero external force applied to all non-active degrees of freedom is often easier to fulfil. The displacements $u_l(\omega)$ are difficult to measure directly and are therefore usually obtained from the corresponding accelerations $a_l(\omega)$ by integration performed in the frequency domain:

$$u_l(\omega) = (\mathrm{i}\omega)^{-2} a_l(\omega) \tag{4.11}$$

The impedance matrix can then be obtained as the inverse of the receptance matrix:

$$\mathbf{Z} = \mathbf{R}^{-1} \tag{4.12}$$

The values in the impedance matrix are complex, and for a massless foundation, the real and imaginary parts of eq. (4.9) can be interpreted as stiffness and damping terms, respectively:

$$Z_{kl}(\omega) = k_{kl}(\omega) + \mathrm{i}\omega c_{kl}(\omega) \tag{4.13}$$

where $k_{kl}(\omega)$ is the frequency dependent stiffness of the foundation and c_{kl} is the equivalent viscous damping coefficient. It should be noted that if several foundation elements are considered to be rigid contact points, the impedance matrix $\mathbf{Z}$ includes coupling terms between these foundation elements and $\mathbf{u}_\mathrm{b}^*$ has to be obtained for the case where all foundation elements are included.

The imaginary part of a foundation's impedance can be attributed to two different types of damping mechanisms [38]. When the displacement of the foundation causes wave propagation in the soil, energy is radiated away from the foundation. This is referred to as geometrical or radiation damping and is often the principal source of

foundation damping. However, this source of damping is only present for frequencies that initiate wave propagation. For soil on bedrock, no such radiation damping is present for frequencies below the cut-off frequencies for wave propagation for the associated mode of deformation. The other source of damping is due to the friction between soil particles which for small shear strains in the soil can be described by a hysteresis characterised by the material damping ratios for β_{p} and β_{s} as discussed in chapter 3. For typical material damping ratios in soil, this usually has only a small influence on the imaginary part of the foundation impedance compared to radiation damping.

4.3 Dynamic pile-soil interaction

The dynamic properties of a single pile installed in soil is governed by the material properties, geometry and orientation of the pile as well as the elastodynamic properties of the soil. In the lateral directions, piles are most sensitive to the soil properties closest to the surface [2, 37, 98]. This is due to the localised deformation of flexible piles when subjected to lateral excitation, where at a depth of 10-15 pile diameters, the stresses and displacements of the pile reduce to negligible proportions [37]. In the vertical direction, on the other hand, the pile impedance is influenced by the skin friction along the full length of the pile and the conditions at the pile end [2, 117].

For piles in soil over bedrock, the piles are also affected by layer resonances. The frequencies at which these resonances occur for vertical S-waves in a homogeneous stratum can be obtained from eq. (3.14). These frequencies act as cut-off frequencies for the onset of wave propagation in the soil, resulting in a reduction of the horizontal dynamic stiffness and an increased amount of radiation damping [37, 71]. In the vertical direction, the existence of radiation damping is instead governed by the cut-off frequency for the propagation of surface waves.

4.3.1 Pile-soil-pile interaction

When multiple closely spaced piles are joined together at the surface in a rigid foundation, pile-soil-pile interaction significantly influences the impedances of the foundation [85, 113]. This interaction between the piles leads to a strong dependence on frequency of the foundation impedances. The interaction is governed by the ratio between the pile-to-pile spacing and the wavelengths propagating in the soil [85].

For low frequencies, the interaction between piles through the soil causes additional displacements at each pile. Therefore, the group stiffness is less than the number of piles times the stiffness of a single pile. This is well known from static pile group analysis [92]. For frequencies associated with wavelengths in the soil which are close to twice the pile spacing, vertical motions of the piles induce displacements in the soil at the locations of the adjacent piles which instead is in the opposite direction to the forced motion of the pile. For pile groups with uniform pile spacing, this results in a

drastic increase in the vertical foundation impedance [29, 39, 40]. Similar mechanisms hold for the horizontal impedance of pile groups, where also longitudinal waves are involved in the interaction [77].

These interactions are most pronounced in homogeneous soil, where the waves emanating from the periphery of a stiff pile subjected to vertical excitation are of the same wavelength. Moreover, the phase differences between these waves are negligible over the length of the pile as the vertical motion of the pile is dominated by rigid body motion of the pile in the softer soil medium [78]. Non-homogeneous soils do not show as pronounced peaks in their vertical and rotational foundation impedances [2, 57, 85]. The same holds for end-bearing piles in homogeneous soil due to the considerable contribution to the vertical group stiffness from the axial stiffness of the piles [86]. Less pronounced dynamic interaction effects have also been found when the pile cap is embedded in the soil or when soil non-linearity is taken into account [30, 51]. In Paper II, the influence of such interactions through the soil is experimentally investigated and numerical predictions are validated for an end-bearing pile group foundation.

4.3.2 Response of pile foundations to an incident wave field

The response of pile foundations due to excitation provided by an incident wave field depends not only on the properties of the soil and the pile group but also on the character of the incident wave field. Significant research efforts have been dedicated to study the response of foundations subjected to vertically propagating and horizontally polarised S-waves, as it is of major interest for applications in earthquake engineering. Far less attention has been given to the response of pile foundations subjected to body waves of grazing incidence [79] or to surface waves, for which only floating piles in homogeneous soil have been considered [58, 75, 76]. For ground-borne vibration in the built environment were excitation is provided from vertical loads acting at the ground surface, the excitation of buildings is in most cases primarily due to surface waves. For floating piles subjected to surface waves in homogeneous soil, both the vertical and horizontal responses are similar to the free field response at low frequencies but are increasingly reduced as the wavelength becomes comparable to the size of the foundation [75]. The pile acts as a spatial filter over its length in a similar fashion as surface foundations do over the ground surface [72]. Similar effects as for surface foundations are also observed for pile group foundations, where interference occur due to phase differences in the excitation of the individual piles in the group. For floating pile groups in homogeneous soil subjected to surface waves, pile-soil-pile interaction has a negligible influence on the group response and can be disregarded [58, 76]. The influence of the end-bearing condition on the responses of piles and pile groups subjected to a vertical load at the ground surface is investigated in Papers III, IV and V.

Chapter 5

Numerical models for the analysis of ground-borne vibration

Modelling ground-borne vibration requires an accurate representation of the building, its foundation and the local soil conditions, but also that wave propagation through the soil is captured. For numerical methods that require discretisation of the geometry, this can become computationally prohibitive when the loads acting on the soil are located at a distance from the building so that the volume of soil between the source and the receiver has to be included in the model. This can be avoided by combining different models for the foundation and for the wave propagation through the soil. This chapter describes the numerical models used in the thesis for that purpose. A semi-analytical formulation for computing the displacements and tractions in a layered soil is presented. It is described how this model can be combined with finite element models to analyse pile foundations, allowing for an arbitrary distance between the source and the response points without increasing the computational demands.

5.1 Wave propagation in layered soil

Figure 5.1 illustrates a soil model consisting of an assembly of $N-1$ linear elastic, homogeneous, isotropic, horizontal layers of finite thickness on top of an elastic half-space. Analytical solutions for the displacements and tractions in arbitrary points of such a system does not exist in the temporal-spatial domain [54]. However, applying Fourier transformation from time to frequency and from the horizontal coordinates to horizontal wavenumbers, the response of such a system can be obtained analytically. This is the model which is used for estimating the small-strain properties of soil from vibration measurements performed at the ground surface discussed in section 3.2.5.

A variety of different methods have been developed for solving this problem [44, 55, 87, 107]. After obtaining the solutions in the frequency-wavenumber domain, the results can subsequently be transformed into the spatial domain by numerical integration. This semi-analytical solution avoids discretisation of the soil and can in many cases provide significant savings in computation time.

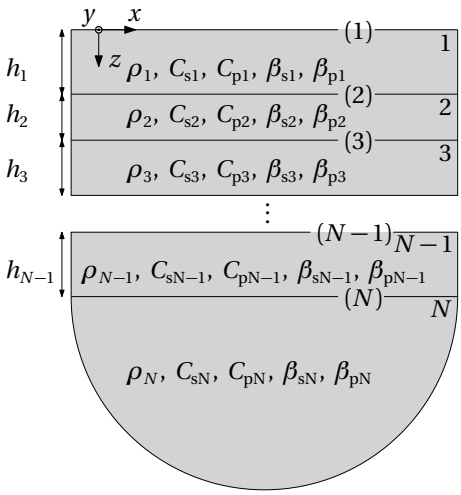

Figure 5.1: *A horizontally layered soil of linear (visco-)elastic material consisting of $N-1$ layers on a halfspace.*

5.1.1 The direct stiffness method

In this thesis, the direct stiffness method is used to solve problems related to wave propagation, using the Matlab toolbox EDT [103]. The principle of the method is here outlined. A more detailed description of the method is outside the scope of this thesis and can be found elsewhere (see e.g. [53, 54, 101]).

In the frequency-wavenumber domain, the equilibrium of a single layer illustrated in fig. 5.2 (a) can be expressed by:

$$\begin{Bmatrix} \tilde{\mathbf{K}}^{\mathrm{e}}_{11} & \tilde{\mathbf{K}}^{\mathrm{e}}_{12} \\ \tilde{\mathbf{K}}^{\mathrm{e}}_{21} & \tilde{\mathbf{K}}^{\mathrm{e}}_{22} \end{Bmatrix} \begin{Bmatrix} \tilde{\mathbf{u}}^{\mathrm{e}}_{1} \\ \tilde{\mathbf{u}}^{\mathrm{e}}_{2} \end{Bmatrix} = \begin{Bmatrix} \tilde{\mathbf{t}}^{\mathrm{e}}_{1} \\ \tilde{\mathbf{t}}^{\mathrm{e}}_{2} \end{Bmatrix} \tag{5.1}$$

where $\tilde{\mathbf{u}}^{\mathrm{e}}_{m}(k_x, k_y, \omega) = \{\tilde{u}_{xm}, \tilde{u}_{ym}, \mathrm{i}\tilde{u}_{zm}\}^{\mathrm{T}}$ is the modified displacement vector at interface m with the tilde denoting its representation in the frequency-wavenumber domain, (k_x, k_y) are the horizontal wavenumbers, $\tilde{\mathbf{t}}^{\mathrm{e}}_{m}(k_x, k_y, \omega) = \{\tilde{t}_{xm}, \tilde{t}_{ym}, \mathrm{i}\tilde{t}_{zm}\}^{\mathrm{T}}$ is the modified vector of tractions at the interface m and $\tilde{\mathbf{K}}^{\mathrm{e}}_{mn}$ are sub-matrices of the element stiffness matrix. The components associated with the vertical direction z are multiplied by the imaginary unit i in the modified system to obtain a symmetric stiffness matrix. Closed-form expressions for the layer and halfspace stiffness matrices can be derived from eq. (3.4) and are available in the literature [53].

The system of $N-1$ layers on a halfspace in fig. 5.1 can be constructed from these elements. Each layer is characterised by a stiffness matrix which depends on its thickness, material properties, the frequency and the horizontal wavenumbers. Assembly

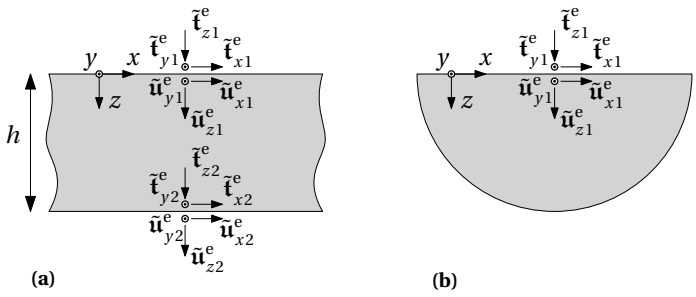

Figure 5.2: *The (a) layer and (b) halfspace elements in the freqeuncy-wavenumber domain.*

of the layers leads to a block-tridiagonal system of equations of the form:

$$\begin{Bmatrix} \tilde{\mathbf{K}}^1_{11} & \tilde{\mathbf{K}}^1_{12} & \mathbf{0} & \cdots & \mathbf{0} \\ \tilde{\mathbf{K}}^1_{21} & \tilde{\mathbf{K}}^1_{22}+\tilde{\mathbf{K}}^2_{11} & \tilde{\mathbf{K}}^2_{12} & \cdots & \mathbf{0} \\ \mathbf{0} & \tilde{\mathbf{K}}^2_{21} & \tilde{\mathbf{K}}^2_{22}+\tilde{\mathbf{K}}^3_{11} & \ddots & \vdots \\ \vdots & \vdots & \ddots & \ddots & \tilde{\mathbf{K}}^{N-1}_{12} \\ \mathbf{0} & \mathbf{0} & \cdots & \tilde{\mathbf{K}}^{N-1}_{21} & \tilde{\mathbf{K}}^{N-1}_{22}+\tilde{\mathbf{K}}_{\mathrm{hs}} \end{Bmatrix} \begin{Bmatrix} \tilde{\mathbf{u}}_1 \\ \tilde{\mathbf{u}}_2 \\ \tilde{\mathbf{u}}_3 \\ \vdots \\ \tilde{\mathbf{u}}_N \end{Bmatrix} = \begin{Bmatrix} \tilde{\mathbf{t}}_1 \\ \tilde{\mathbf{t}}_2 \\ \tilde{\mathbf{t}}_3 \\ \vdots \\ \tilde{\mathbf{t}}_N \end{Bmatrix} \tag{5.2}$$

where $\tilde{\mathbf{K}}_{\mathrm{hs}}$ is the stiffness matrix of the halfspace element, $\tilde{\mathbf{u}}_m$ collects the displacements and $\tilde{\mathbf{t}}_m$ the external tractions at the layer interface m.

Prescribing external tractions and solving eq. (5.2), the interface displacements $\tilde{\mathbf{u}}$ are obtained. The displacements and tractions on a horizontal plane at the elevation z within a layer can then be obtained from the layer interface displacements [101]:

$$\tilde{\mathbf{u}}(z) = \begin{Bmatrix} \tilde{\mathbf{N}}^{\mathrm{e}}_1(z) & \tilde{\mathbf{N}}^{\mathrm{e}}_2(z) \end{Bmatrix} \begin{Bmatrix} \tilde{\mathbf{u}}^{\mathrm{e}}_1 \\ \tilde{\mathbf{u}}^{\mathrm{e}}_2 \end{Bmatrix} \tag{5.3}$$

$$\tilde{\mathbf{t}}(z) = \begin{Bmatrix} \tilde{\mathbf{B}}^{\mathrm{e}}_1(z) & \tilde{\mathbf{B}}^{\mathrm{e}}_2(z) \end{Bmatrix} \begin{Bmatrix} \tilde{\mathbf{u}}^{\mathrm{e}}_1 \\ \tilde{\mathbf{u}}^{\mathrm{e}}_2 \end{Bmatrix} \tag{5.4}$$

where $\tilde{\mathbf{N}}^{\mathrm{e}}_1(z)$ and $\tilde{\mathbf{N}}^{\mathrm{e}}_2(z)$ contain shape functions for the displacements in the layer, and $\tilde{\mathbf{B}}^{\mathrm{e}}_1(z)$ and $\tilde{\mathbf{B}}^{\mathrm{e}}_2(z)$ the shape functions for the tractions on a horizontal plane in the layer.

To solve the three dimensional problem, the displacements, tractions and strains can be expressed in cylindrical coordinates, but then without the imaginary unit factor i applied to the vertical components. In that case, the stiffness matrix in eq. (5.2) and the shape functions in eqs. (5.3) and (5.4) are identical to the ones obtained for the case of plane strain [101]. Solving the problem in cylindrical coordinates has the computational advantage that the stiffness matrix only has to be assembled and inverted once for each radial wavenumber $k_r = \sqrt{k_x^2 + k_y^2}$. Kausel [54] showed that this can also be achieved for the general three dimensional problem expressed in a Cartesian frame of reference by rotation of the flexibility matrix for the plane strain (or cylindrical) problem.

The strain components $\tilde{\epsilon}_{xx}$, $\tilde{\epsilon}_{yy}$ and $\tilde{\epsilon}_{xy}$ at elevation m can in a Cartesian frame of reference be obtained from eq. (3.3) in the frequency-wavenumber domain as:

$$\tilde{\boldsymbol{\epsilon}}_m^{(xy)}(k_x,k_y,\omega)=\begin{Bmatrix}\tilde{\epsilon}_{xx}\\ \tilde{\epsilon}_{yy}\\ \tilde{\epsilon}_{xy}\end{Bmatrix}_m=\begin{Bmatrix}-\mathrm{i}k_x & 0 & 0\\ 0 & -\mathrm{i}k_y & 0\\ -\frac{1}{2}\mathrm{i}k_y & -\frac{1}{2}\mathrm{i}k_x & 0\end{Bmatrix}\begin{Bmatrix}\tilde{\mathrm{u}}_x\\ \tilde{\mathrm{u}}_y\\ \tilde{\mathrm{u}}_z\end{Bmatrix}_m \tag{5.5}$$

Multiplying the vertical components of the modified displacements and tractions with the imaginary unit $-\mathrm{i}$, the displacement and traction vectors $\tilde{\mathbf{u}}_m$ and $\tilde{\mathbf{t}}_m$ at elevation m in the frequency-wavenumber domain are obtained. The displacements, tractions and strains in the frequency-spatial domain can subsequently be obtained by the inverse Fourier transformations:

$$\mathbf{u}_m(x,y,\omega)=\left(\frac{1}{2\pi}\right)^2\int_{-\infty}^{\infty}\int_{-\infty}^{\infty}\tilde{\mathbf{u}}_m(k_x,k_y,\omega)\mathrm{e}^{-\mathrm{i}k_x x}\mathrm{e}^{-\mathrm{i}k_y y}\,\mathrm{d}k_x\mathrm{d}k_y \tag{5.6}$$

$$\mathbf{t}_m(x,y,\omega)=\left(\frac{1}{2\pi}\right)^2\int_{-\infty}^{\infty}\int_{-\infty}^{\infty}\tilde{\mathbf{t}}_m(k_x,k_y,\omega)\mathrm{e}^{-\mathrm{i}k_x x}\mathrm{e}^{-\mathrm{i}k_y y}\,\mathrm{d}k_x\mathrm{d}k_y \tag{5.7}$$

$$\boldsymbol{\epsilon}_m^{(xy)}(x,y,\omega)=\left(\frac{1}{2\pi}\right)^2\int_{-\infty}^{\infty}\int_{-\infty}^{\infty}\tilde{\boldsymbol{\epsilon}}_m^{(xy)}(k_x,k_y,\omega)\mathrm{e}^{-\mathrm{i}k_x x}\mathrm{e}^{-\mathrm{i}k_y y}\,\mathrm{d}k_x\mathrm{d}k_y \tag{5.8}$$

The full stress and strain tensors can then be calculated from the tractions $\mathbf{t}_m$ and the strains $\boldsymbol{\epsilon}_m^{(xy)}$ using the constitutive eq. (3.2) [101].

Equation (5.6) can alternatively be expressed as:

$$\mathbf{u}_m(x,y,\omega)=\left(\frac{1}{2\pi}\right)^2\int_{-\infty}^{\infty}\int_{-\infty}^{\infty}\tilde{\mathbf{G}}_{mn}\tilde{\mathbf{p}}_n\mathrm{e}^{-\mathrm{i}k_x x}\mathrm{e}^{-\mathrm{i}k_y y}\,\mathrm{d}k_x\mathrm{d}k_y \tag{5.9}$$

where $\tilde{\mathbf{G}}_{mn}$ is the flexibility submatrix, or the Green's functions, at elevation m due to a load applied at elevation n in the frequency-wavenumber domain and $\tilde{\mathbf{p}}_n$ is the corresponding unmodified load vector. The Green's functions in the frequency-spatial domain thereby correspond to the responses $\mathbf{u}_{l,m}(x,y,\omega)$ due to loads $\tilde{p}_{l,n}=\delta(z-z_n)$ applied in each direction $l=\{x,y,z\}$ in the frequency-wavenumber domain, where $\delta(\cdot)$ is the Dirac delta function.

5.2 Finite element modelling of soil-structure interaction

The finite element method is a versatile tool for modelling arbitrary geometries on bounded domains. However, modelling unbounded domains require special consideration of the conditions at the model boundary. In elastodynamics, wave reflections at the model boundary must be avoided to satisfy Sommerfeld's radiation condition, stating that waves propagating outwards in the unbounded domain should vanish at

infinity [1]. This requires either that a large enough soil domain is considered, which adds a large number of degrees of freedom to the model, or the use of absorbing boundary conditions attenuating any outgoing waves as they approach the boundary of the model. Different formulations for such boundaries exist, including methods that impose attenuation at the boundaries of the model [59, 73] or that apply artificial stretching of the spatial coordinates to simulate an extended (infinite) model domain [18]. A theoretically perfect wave absorber that combines both imposed attenuation and coordinate stretching is the perfectly matched layer (PML) [17].

5.2.1 Perfectly matched layers

The idea behind the PML is to artificially extend the spatial domain and impose strong attenuation such that no waves are reflected back into the domain of interest. In this thesis, the time-harmonic formulation proposed by Basu and Chopra [14] is adopted. Alternative formulations for time domain analysis are also available in the literature [13, 15, 31].

Figure 5.3 presents an illustration of the PML concept. In order to avoid any reflections

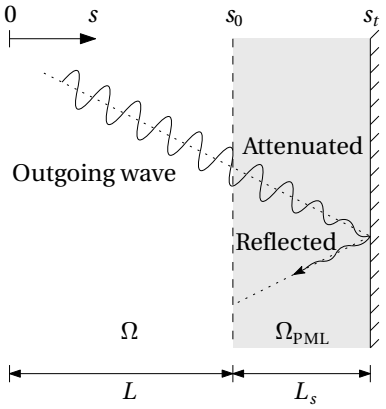

Figure 5.3: *PML domain Ω_{PML} enforcing attenuation of outgoing waves from the regular domain Ω.*

at the boundary $\Omega \cap \Omega_{\mathrm{PML}}$ between the regular and the PML domains, continuity is enforced by applying the following complex coordinate stretching:

$$s \rightarrow \hat{s} = s_0 + \int_{s_0}^{s_t} \psi_s(s)\, \mathrm{d}s \tag{5.10}$$

where s_0 denotes the coordinate on the boundary between the regular domain Ω and the PML domain Ω_{PML}, s_t the global coordinate of the outer boundary of the PML region in the direction s and $\psi_s(s) \in \mathbb{C}$ is the stretch function. This provides a "perfect match" at the boundary between the regular and the PML domains and therefore no reflections of impinging waves occur at this boundary if the two domains are of the

same material. This property is lost when approximation is introduced in terms of domain discretisation. However, the reflections that arise are small if the mesh size is kept small compared to the shortest wavelength considered.

The implementation of PMLs for linear elastic solids in a finite element context require a modification of the regular finite elements in terms of the globally defined stretch functions $\psi_{\mathrm{s}}(s)$. Basu and Chopra [14] proposed the stretch function:

$$\psi_{\mathrm{s}}(s) = 1 + \frac{\alpha_s^{\mathrm{e}}(s)}{b_0} - \mathrm{i}\frac{\alpha_s^{\mathrm{p}}(s)}{b_0} \tag{5.11}$$

where $b_0 = \omega L_s / C_{\mathrm{s}}$ is a dimensionless frequency and $\alpha_s^{\mathrm{e}}(s)$ and $\alpha_s^{\mathrm{p}}(s)$ define the attenuation profiles of the evanescent and propagating waves, respectively. One choice is to assign both attenuation functions as:

$$\alpha_s^j(s) = \begin{cases} 0 & 0 \le s \le s_0 \\ \alpha_{s0}^j \Big(\dfrac{s - s_0}{L_s} \Big)^q & s_0 \le s \le s_{\mathrm{t}} \end{cases} \tag{5.12}$$

with α_{s0}^j, $j = \{\mathrm{e}, \mathrm{p}\}$ user defined scaling parameters for the evanescent and propagating waves and q determining the sharpness of the attenuation profile.

The tuning of PML parameters is non-trivial as the absorption efficiency of the PML layers depend on the wave field, the mesh density and the PML layer thickness L_{s}. Moreover, as PMLs are non-physical entities, there is no intuition tied to physical phenomena to rely upon. Recommendations provided in the literature are mostly based on analyses of one-dimensional problems. Nevertheless, these guidelines provide a good starting point for analysis of three dimensional problems.

François et al. [36] showed that the real part that attenuates the evanescent waves, $\alpha_s^{\mathrm{e}}(s)$, both artificially stretches the thickness L_{s} of the PML layer and increases the apparent wavelength $\tilde{\lambda}$ inside the PML as:

$$\tilde{\lambda} = \frac{\lambda}{\mathrm{Re}(\psi_{\mathrm{s}})} \tag{5.13}$$

This imposes strict requirements on the mesh to resolve the response at higher frequencies for large values of $\alpha_{s0}^{\mathrm{e}}(s)$, as smaller wavelengths have to be resolved by the mesh. It should be noted that for a stretch function on the form of eq. (5.11), both the real and imaginary parts are down-scaled with the dimensionless frequency b_0, which partly counteracts this effect. Attenuation of the propagating waves is imposed by the parameter $\alpha_{s0}^{\mathrm{p}}(s)$. However, imposing strong attenuation also requires a dense mesh to obtain an accurate finite element solution, and a balance between attenuation and approximation error must be sought.

5.2.2 Wave propagation using a substructure formulation

The analysis of a soil-structure system is straightforward using absorbing boundary conditions such as PMLs, and can be directly modelled using a finite element formulation. However, when the source is located outside the building, the domain size

increases drastically with the distance between the source and the receiver, especially for three dimensional problems, as the continuum of soil has to be modelled. This can become computationally restrictive, especially for high frequencies in soft soil as the mesh requirements are related to the wavelengths in the soil.

Papadopoulos et al. [88] proposed a substructure formulation (see eq. (4.7)) to combine a separate source model for computing the incident wave field, with a finite element model with perfectly matched layers (FE-PML). If only the response in the vicinity of the foundation is of interest, the exterior soil domain Ω_e in fig. 5.4 can be modelled with PMLs, which both satisfy the Sommerfeld radiation condition and the impedance match at the boundary. Thereby, the condensed soil impedance matrix can be obtained from the impedance of the PML domain:

$$\mathbf{Z}^{\mathrm{PML}} = \left(\mathbf{Z}_{\mathrm{ff}} - \mathbf{Z}_{\mathrm{fe}}\mathbf{Z}_{\mathrm{ee}}^{-1}\mathbf{Z}_{\mathrm{ef}}\right)^{\mathrm{PML}} \tag{5.14}$$

where the subscript f denotes the degrees of freedom at the boundary $\mathrm{b} = \Omega_i \cap \Omega_e$ and e the degrees of freedom in the exterior PML domain. The equivalent tractions imposed

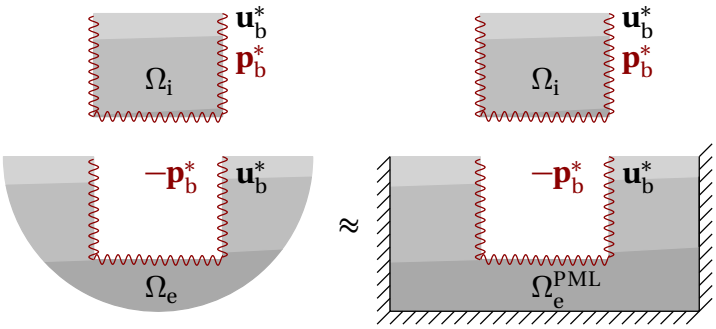

Figure 5.4: *Decomposition of the free field soil approximated as a truncated domain of perfectly matched layers.*

by the incident wave field obtained from the source model are subsequently obtained as:

$$\mathbf{p}_b = \mathbf{Z}^{\mathrm{PML}}\mathbf{u}_b^* + \mathbf{p}_b^* \tag{5.15}$$

where $\mathbf{u}_b^*$ and $\mathbf{p}_b^*$ are the displacements and tractions at the boundary of the excavated soil island in fig. 5.4, obtained from a separate source model.

The tractions $\mathbf{p}_b$ can subsequently be applied at the boundary b in the FE-PML model, where the (non-PML) domain of interest can be arbitrarily modified. For a specific load case, this means that eq. (5.15) only has to be computed once and different conditions within the domain of interest can be considered by only solving the FE-PML system of equations.

In Paper IV, this formulation is adopted in combination with the semi-analytical model outlined in section 5.1.1 for analysing the response of end-bearing pile groups due to vertical loads applied at the ground surface.

5.3 Pile model based on beam elements and Green's functions

Based on the availability of the Green's functions for a layered halfspace, as obtained from eq. (5.9), the dynamic analysis of pile foundations can be reduced to a system which is expressed in variables relating only to the piles [3]. Such a model is not only computationally efficient, but can be a useful tool for studying the influence of the coupling between the piles through the soil. The formulation of this model is presented here to explain its main features and is a summary of the more comprehensive description by Álamo [2].

5.3.1 Pile equations

Modelling the piles with beam elements in three dimensional space and assuming hysteretic material damping, the dynamic equilibrium equation for the piles reads:

$$\left(\mathbf{K}_\mathrm{p}(1+2\mathrm{i}\beta^*)-\omega^2\mathbf{M}_\mathrm{p}\right)\mathbf{u}_\mathrm{p}=\mathbf{p}_\mathrm{p} \tag{5.16}$$

where $\mathbf{K}_\mathrm{p}$ is the pile stiffness matrix, β^* the pile hystereic material damping ratio, $\mathbf{M}_\mathrm{p}$ is the pile mass matrix, $\mathbf{u}_\mathrm{p}$ are the pile displacements and $\mathbf{p}_\mathrm{p}$ contain the external forces acting on the piles. The mass matrix $\mathbf{M}_\mathrm{p}$ for the piles is obtained with an effective density obtained as the difference between the pile density and the density of the soil medium, as in the following, soil continuity is assumed to not be affected by the presence of the piles [3].

The piles are discretised by two noded beam elements with ten degrees of freedom, disregarding the torsional degrees of freedom of the piles. Figure 5.5 illustrates the definition of the pile element displacement degrees of freedom, nodal forces and the assumed linear distribution of pile-soil interaction tractions acting over each pile element.

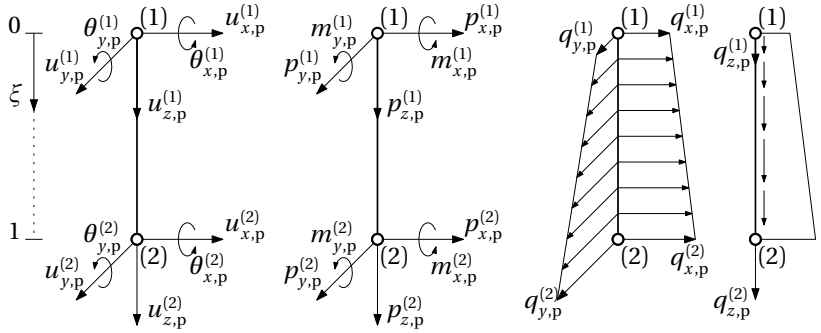

Figure 5.5: *Beams element definitions including the assumed linear distribution of pile-soil interaction tractions.*

The force vector in eq. (5.16) can be decomposed as:

$$\mathbf{p}_\mathrm{p} = \mathbf{p}_\mathrm{e} + \mathbf{p}_\mathrm{q} \tag{5.17}$$

where $\mathbf{p}_\mathrm{e}$ denotes the external force vector and $\mathbf{p}_\mathrm{q}$ the forces due to the pile-soil interaction tractions $\mathbf{q}_\mathrm{p}$ at the pile nodes. The element pile-soil interaction tractions in fig. 5.5 can be described in terms of the nodal values for each direction $l = x, y, z$ by:

$$q_{l,\mathrm{p}}(\xi) = \varphi_1(\xi) q_{l,\mathrm{p}}^{(1)} + \varphi_2(\xi) q_{l,\mathrm{p}}^{(2)} \tag{5.18}$$

with the linear shape functions:

$$\varphi_1(\xi) = 1 - \xi \tag{5.19}$$

$$\varphi_2(\xi) = \xi \tag{5.20}$$

Using eq. (5.18) and the shape functions for the beam element displacements and rotations, the equivalent nodal forces for the distributed tractions over the element can be related to the nodal interaction tractions and may be expressed by:

$$\mathbf{p}_\mathrm{q} = \mathbf{Q}\mathbf{q}_\mathrm{p} \tag{5.21}$$

where $\mathbf{Q}$ is the a global matrix that transforms the nodal values for the pile-soil interaction tractions to equivalent nodal forces. Introducing eqs. (5.17) and (5.21) in eq. (5.16) the dynamic equilibrium of the piles can be written:

$$\left(\mathbf{K}_\mathrm{p}(1 + 2\mathrm{i}\beta^*) - \omega^2 \mathbf{M}_\mathrm{p}\right)\mathbf{u}_\mathrm{p} - \mathbf{Q}\mathbf{q}_\mathrm{p} = \mathbf{p}_\mathrm{e} \tag{5.22}$$

It should be noted that the equivalent nodal moments induced by the distributed translational tractions over the pile are related to the translational nodal tractions $\mathbf{q}_\mathrm{p}$ through the matrix $\mathbf{Q}$. This way, the influence of the pile bending stiffness is taken into account.

5.3.2 Soil equations

In the soil, the piles are considered as the line loads $\mathbf{q}_\mathrm{s}$. Adopting the reciprocity theorem for elastodynamics, and initially assuming that no body loads are present in the soil, the soil displacements $\mathbf{u}_\mathrm{s}^\kappa$ in a collocation point κ can be related to the loads applied along the lines Γ_p in the soil, corresponding to the pile elements, as:

$$\mathbf{u}_\mathrm{s}^\kappa = \int_{\Gamma_\mathrm{p}} \mathbf{g}^* \mathbf{q}_\mathrm{s} \, \mathrm{d}\Gamma_\mathrm{p} \tag{5.23}$$

where $\mathbf{g}^*$ is a second order tensor containing the displacement Green's functions for a layered halfspace, i.e. the translational responses at the point κ due to a point load applied in each one of the three Cartesian directions along Γ_p.

Considering the discretisation of the piles, eq. (5.23) can be obtained as the superposition of the contribution over each line corresponding to a beam element Γ_l. Assuming

the same linear shape functions for the load distributions over the lines Γ_l as for the beam elements, eq. (5.23) can be evaluated as:

$$\mathbf{u}_{\mathrm{s}}^{\kappa} = \sum_{l=1}^{N_l} \int_{\Gamma_l} \mathbf{g}^{*} \left(\varphi_1 \mathbf{q}_{l,\mathrm{s}}^{(1)} + \varphi_2 \mathbf{q}_{l,\mathrm{s}}^{(2)} \right) \mathrm{d}\Gamma_l \tag{5.24}$$

This equation is expressed in terms of the nodal values of $\mathbf{q}_{\mathrm{s}}$ and can thus be expressed as the linear system:

$$\mathbf{u}_{\mathrm{s}}^{\kappa} = \mathbf{G}^{\kappa} \mathbf{q}_{\mathrm{s}} \tag{5.25}$$

where $\mathbf{G}^{\kappa}$ is a soil influence matrix that relates the interaction tractions in the soil $\mathbf{q}_{\mathrm{s}}$ to the displacements at the collocation point κ and is obtained from the assembly of the elemental ones for each element l:

$$\mathbf{G}_l^{\kappa} = \left\{ \int_{\Gamma_l} \mathbf{g}^{*} \varphi_1 \, \mathrm{d}\Gamma_l \qquad \int_{\Gamma_l} \mathbf{g}^{*} \varphi_2 \, \mathrm{d}\Gamma_l \right\} \tag{5.26}$$

As the Green's functions are not available in closed form in the frequency-spatial domain, but obtained through numerical integration, the integrals in eq. (5.26) are evaluated numerically using Gaussian quadrature. Finally, applying eq. (5.25) to all pile nodes, a system of equations relating the pile-soil interaction tractions to the soil displacements $\mathbf{u}_{\mathrm{s}}$ at the locations of the pile nodes is obtained:

$$\mathbf{u}_{\mathrm{s}} = \mathbf{G} \mathbf{q}_{\mathrm{s}} \tag{5.27}$$

5.3.3 Incident loading

The displacement field in the soil described by eq. (5.27) is due to the scattering caused by the interaction tractions over the lines in the soil corresponding to the positions of the piles. As the system is linear, the total wave field in the soil can be expressed as the superposition of this scattered field and some arbitrary incident wave field $\mathbf{u}_{\mathrm{inc}}$. It follows that eq. (5.27) can be written as:

$$\mathbf{u}_{\mathrm{s}} = \mathbf{G} \mathbf{q}_{\mathrm{s}} + \mathbf{u}_{\mathrm{inc}} \tag{5.28}$$

This also holds for points in the soil other than the positions of the piles. In that case, the matrix $\mathbf{G}$ is replaced with an influence matrix where the collocation points instead correspond to the observation points in the soil. This way, the total wave field in the soil can be obtained in post-processing.

5.3.4 Pile-soil coupling

The pile and soil equations are coupled by imposing the compatibility and equilibrium conditions:

$$\mathbf{u}_{\mathrm{p}} = \mathbf{u}_{\mathrm{s}} \tag{5.29}$$

$$\mathbf{q}_{\mathrm{p}} = -\mathbf{q}_{\mathrm{s}} \tag{5.30}$$

and combining eqs. (5.22) and (5.28). This leads to the following system of equations:

$$\begin{Bmatrix} \mathbf{Z}_\mathrm{p} & -\mathbf{Q} \\ \boldsymbol{\Upsilon} & \mathbf{G} \end{Bmatrix} \begin{Bmatrix} \mathbf{u}_\mathrm{p} \\ \mathbf{q}_\mathrm{p} \end{Bmatrix} = \begin{Bmatrix} \mathbf{p}_\mathrm{e} \\ \mathbf{u}_\mathrm{inc} \end{Bmatrix} \tag{5.31}$$

where $\mathbf{Z}_\mathrm{p} = \mathbf{K}_\mathrm{p}(1+2\mathrm{i}\beta^*) - \omega^2\mathbf{M}_\mathrm{p}$ is the pile impedance matrix and $\boldsymbol{\Upsilon}$, in the case of vertical piles, is a selection matrix for the translational degrees of freedom of the displacement vector $\mathbf{u}_\mathrm{p}$. Constraint equations can subsequently be added to this system to rigidly connect the piles at the surface so as to model at rigid pile cap. This system is exclusively written in terms of pile variables and thereby requires no discretisation of the soil. The interaction between the piles through the soil is governed by the corresponding coupling terms in the fully populated soil influence matrix $\mathbf{G}$. This is used to study the influence of pile-soil-pile interaction on the vertical response of end-bearing piles in Paper V.

Chapter 6

Summary of research work

To meet the aims of the thesis, the research work performed is divided into two categories. The first category is focused on the validation of numerical models for the prediction of the dynamic behaviour of an end-bearing pile foundation in soft clay. Papers I, II and III address this through a series of controlled full-scale field tests conducted at a designated test site in a soft clay soil on till and bedrock. Paper I addresses the site characterisation for the purpose of vibration prediction in soil. Paper II considers the dynamic responses of piles installed at the site when subjected to external loads applied to the foundation. Paper III then addresses the response of the pile foundation when subjected to vertical loads applied at the ground surface. The second category of the research is focused on investigating how the end-condition influence the transmission of vibrations to pile foundations using numerical simulations. Paper IV develops a simple procedure to estimate the vertical response of end-bearing piles from free field vibrations. Paper V proceeds with investigating how the end-condition affects the interaction between the piles through the soil with respect the their vertical response. This chapter provides an overview of the experimental research work and a brief summary of each one of the papers appended to this thesis.

6.1 Overview of the experimental research work

Figure 6.1 presents an overview of the test site used for conducting the experiments with the location of the pile group indicated. The test site is located in an uncultivated field where no other construction activities were conducted during the time of the experiments. The dynamic measurements of vibrations at the ground surface were in Paper I primarily considered along the line corresponding to section A–A in fig. 6.1. The point wise investigations were performed at the position where the pile group is installed and between the two small concrete foundations.

Figure 6.2 presents an overview of three experiments conducted at different stages of construction of the pile group foundation. In Paper II, the load cases corresponding to the forces P_1 in stages 2 and 3 in fig. 6.2 were considered. In stage 2, the loads were successively applied to each one of the piles to characterise the interaction between

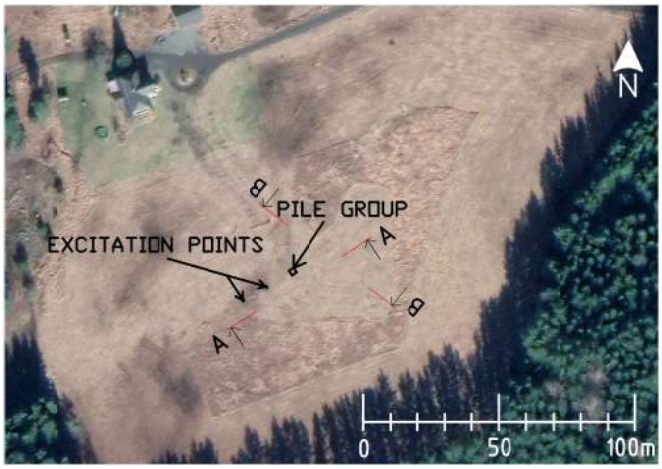

(a)

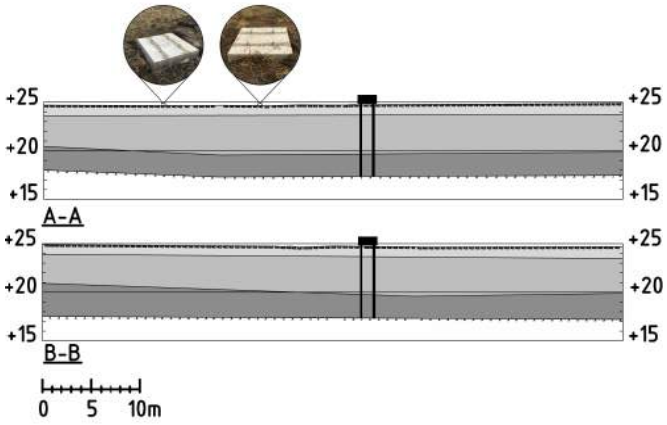

(b)

Figure 6.1: *Overview of the test site with (a) an aerial photo with the positions of the excitation points and the pile foundation indicated [41] and (b) interpreted sections from soil investigations with dry crust clay (light gray), clay (gray) and till (dark gray) layers indicated.*

the piles through the soil. For these tests, the instrumented impact hammer in fig. 6.3 was used.

In Paper III, all three stages were considered with the force P_2 applied to the two small concrete foundations indicated in fig. 6.1. The force P_2 was applied using the electro-dynamic shaker in fig. 6.3 mounted on each one of the two small concrete foundations. In addition, the results in stage 2 applying both load cases P_1 and P_2 were combined to predict the responses of the pile group in stage 3.

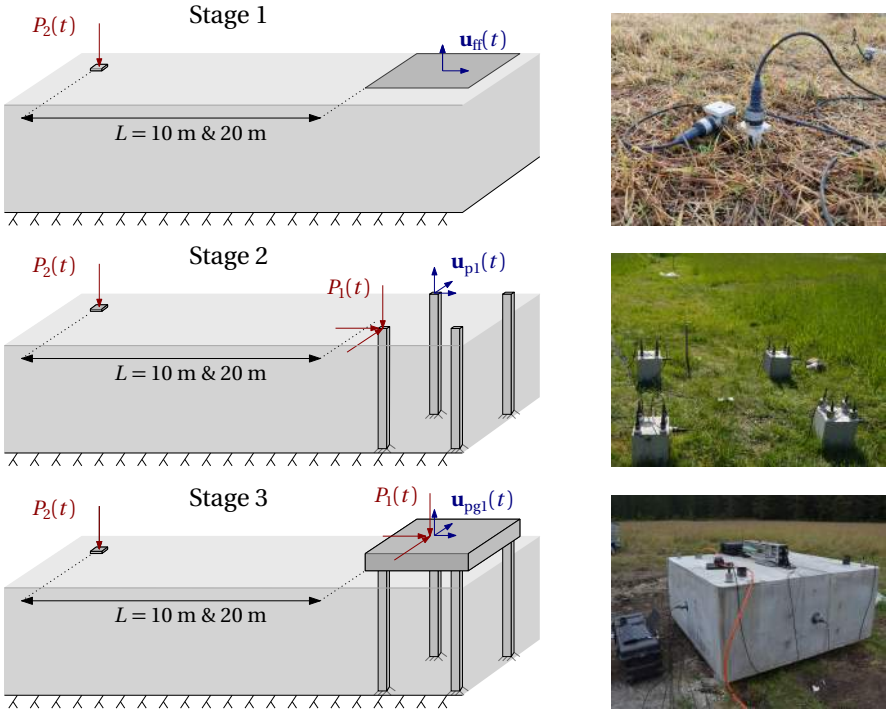

Figure 6.2: *Schematic overview of the measurements performed for the three stages of construction of the pile group with the corresponding instrumentation at the site.*

(a) **(b)**

Figure 6.3: *Dynamic excitation instruments (a) Wölfel BD.05 electrodynamic inertial shaker mounted on one of the small concrete foundations and (b) Dytran 5803 A instrumented impact hammer.*

6.2 Summary of the papers

Paper I

Assessment of small-strain characteristics for vibration predictions in a Swedish clay deposit.

Freddie Theland, Geert Lombaert, Stijn François, Costin Pacoste, Fanny Deckner and Jean-Marc Battini

Soil Dynamics and Earthquake Engineering, 2021, vol. 150, 106804.

Modelling wave propagation in soil requires knowledge of the small-strain soil properties and the soil stratigraphy. However, in most cases limited resources are available for dedicated site investigation. This paper presents the results from an extensive site investigation of the dynamic small-strain properties of a clay soil on till and bedrock. Results obtained from empirical relations, laboratory tests and in situ measurements with the methods described in chapter 3 were compared and synthesised into a layered soil model. The value of information obtained from the tests for modelling wave propagation in the soil was investigated by comparing vibrations at the ground surface obtained from the semi-analytical model presented in section 5.1.1 to measurements performed at the site. It was found that P-waves refracted along the bedrock surface can have a considerable contribution to the vibration response at the ground surface and that amplification can occur in the soil situated above the ground water table.

The highlights from this paper are:

- Results from different investigation methods were used to establish a layered dynamic soil model of a shallow clay deposit.
- S-wave speeds from empirical and seismic methods were in good agreement.
- Resonance of the top soil layer due to refracted P-waves was found to significantly contribute to the surface response.
- Seasonal variations affected the vibrations related to the properties of the top soil layer.

Only the surface wave measurements were able to provide estimates of the properties in the top soil layer, that allowed reproducing the resonant response observed from the measurements. The estimates of material damping in the clay obtained from the laboratory samples were on the other hand found to be most representative for calculating the vibration response in the soil.

Paper II

Dynamic response of driven end-bearing piles and a pile group in soft clay: an experimental validation study.

Freddie Theland, Geert Lombaert, Stijn François, Costin Pacoste, Fanny Deckner, Peter Blom and Jean-Marc Battini

Engineering Structures, 2022, vol. 267, 114629.

Dynamic interaction between piles and soil can have a considerable influence on the dynamic characteristics of pile foundations (see chapter 4). This paper presents measurement data from full-scale field tests on the dynamic response of end-bearing piles subjected to external dynamic loads. The piles were installed at the site considered in Paper I and experiments were conducted before and after casting of the concrete pile cap. The measurement results were compared to predictions from a numerical FE-PML model based solely on the information provided from the site investigations in Paper I. The results verified the influence of dynamic pile-soil-pile interaction on the vertical responses predicted by the numerical model. It was also found that the horizontal responses of individual piles were affected by the different conditions in the topmost soil when measured at different occasions.

The highlights from this paper are:

- Experimental impedances were retrieved for end-bearing piles and a pile group.
- Pile-soil-pile interaction was experimentally characterised before and after casting of a concrete pile cap.
- Predictions obtained from a linear elastic numerical model were in close agreement with measurements on the pile cap.

It should be noted that point-impedances were considered in this paper that were not obtained from the inverted receptance matrix (see section 4.2). This study is, to the best of this authors knowledge, the first to provide experimental evidence of vertical dynamic stiffening caused by pile-soil-pile interaction.

Corrections:

1. *Equations (2) and (3) in the paper refer to the case of forces aligned with the coordinate axes, which was adopted in post-processing. This does not correspond to the illustration in fig. 6 and the signs in the equations should therefore be reversed.*
2. *Both experimental and numerical results in fig. 15 (b) are of the wrong sign due to an error in the generation of the plots.*

None of these errors affect the conclusions of the paper.

Paper III

Measurements and predictions of vibration response of end-bearing pile group in soft clay due to vertical ground surface load.

Freddie Theland, Geert Lombaert, Stijn François, Abbas Zangeneh, Fanny Deckner and Jean-Marc Battini

Submitted to *Engineering Structures*, October 2024.

In this paper, predictions of vibrations in an end-bearing pile foundation using a numerical model are validated from full-scale field tests conducted on the pile foundation considered in Paper II. The predictions are assessed for all three stages of construction described in section 6.1. Hybrid predictions using the methods described in section 4.1 were also considered, where the vibrations of the pile cap were predicted from the ones measured in the prior construction stage on the free pile tops, the pile responses due to local excitation considered in Paper II and a model of the pile cap. A fairly good agreement between the measurements and the numerical predictions was found, especially in the vertical direction. Using the hybrid method, the accuracy of the predictions improved for the horizontal and rotational directions and was similar for the vertical direction.

The highlights from this paper are:

- Full-scale field tests were performed in three stages of construction of a pile group.
- Numerical predictions of vibrations due to loads at the ground surface were validated.
- A hybrid prediction method combining numerical and experimental data was evaluated.
- Measurements of vibration responses were related to free field responses measured prior to construction.

The results also indicated that, in the vertical direction, pile-soil-pile interaction has an important influence on the group response.

Paper IV

Design procedure for estimating the vertical response of end-bearing piles from free field vibrations produced by a nearby surface load.

Freddie Theland, Geert Lombaert, Stijn François, Abbas Zangeneh, Fanny Deckner and Jean-Marc Battini

Submitted to *Structures*, August 2024.

Methods for vibration assessment in buildings can, as outlined in chapter 2, be based on measurements of vibrations on the free surface of the soil. For deep foundations such as piles, dynamic interaction between the piles and the soil not only affects the impedance of the foundation but has also a strong influence on the vibration transmission through the foundation. This paper presented the development of a procedure that can be used in a design stage to estimate the vertical response of end-bearing pile foundations from free field vibrations caused by a load acting at the ground surface. Numerical simulations of pile foundations were considered using the numerical modelling strategy presented in section 5.2 and a system of dimensionless parameters was established to obtain general relations that can be used in design. The vertical responses of end-bearing piles in soil over rigid bedrock were compared to floating piles in the same soil to illustrate the influence of the end-condition. It was shown that the vertical response of end-bearing piles strongly depends on the relationship between their axial stiffness and the stiffness of the soil.

The highlights from this paper are:

- Development of a procedure to estimate the vertical response of end-bearing piles from free field vibrations.
- A simple equation to compute an interaction factor from the pile slenderness and the pile-soil stiffness ratio was proposed.
- Limitations regarding pile axial resonances and guided P-waves were considered.
- The vertical group response of square 2×2 pile groups was shown to be bounded by the single pile response.

It was also indicated that pile-soil-pile interaction influence the vertical response of end-bearing pile groups to a greater extent compared to the case of floating pile groups in the same soil. This was further investigated in Paper V.

Paper V

The influence of pile-soil-pile interaction on the vertical response of end-bearing pile groups in soil on bedrock subjected to a vertical load at the ground surface.

Freddie Theland, Geert Lombaert, Stijn François, Abbas Zangeneh, Fanny Deckner and Jean-Marc Battini

Submitted to *Transportation Geotechnics*, November 2024.

Papers III and IV indicated that, in contrast to floating piles in homogeneous soil, the vertical response of end-bearing pile groups subjected to loads acting at the ground surface can be considerably affected by pile-soil-pile interaction. This paper used the numerical model described in section 5.3 to investigate how pile-soil-pile interaction influence the vertical response of end-bearing pile groups. The relationship between the incident wave field and the scattered wave field from a single pile was used to illustrate the interaction between piles at different relative positions. It was found that up to a certain frequency, which is mainly governed by the S-wavelength in the soil and the pile spacing, interaction between the piles reduces the vertical group response. For higher frequencies, it was found that the interaction between the piles which are aligned in the transverse direction with respect to the horizontal propagation direction of the incident wave field, instead causes amplification of the group response.

The highlights from this paper are:

- Pile-soil-pile interaction considerably affects the vertical response of end-bearing pile groups.
- Interaction reduces the group response up to a certain frequency which mainly depends on the pile spacing and the S-wavelength in the soil.
- Interaction between piles aligned in the direction transverse to the propagation direction of the incident wave field may cause amplification of the group response.
- Stronger interaction effects were found for piles which have a higher axial stiffness.

It was also shown that by reducing the pile spacing in the direction transverse to the incident wave field, the group response is further reduced for lower frequencies, as the amplifying effects thereby are shifted to higher frequencies.

Chapter 7

Discussion

The research performed in this thesis has focused on the dynamic behaviour of end-bearing pile foundations subjected to ground-borne vibration. This chapter presents a general discussion of the results with a focus on the validation of prediction models for ground-borne vibration in end-bearing pile foundations and on the influence of the end-bearing condition on the dynamic interaction between piles and soil.

7.1 Predicting ground-borne vibration

Predicting ground-borne vibration in buildings involves several components: the source of excitation, the wave propagation in the soil, the dynamic soil-foundation interaction and the interaction between the foundation and the building. All of these components are potential sources of epistemic uncertainty. In practice, the knowledge of the dynamic small-strain soil properties and their spatial distribution is always limited, and predictions therefore has to be made based on a discrete set of observations.

The transmission of vibrations from the soil to a building can be characterised by the dynamic response of its foundation (see section 4.1). For deep foundations such as piles, this requires that the incident wave field in the soil, induced by the dynamic excitation, is accurately represented over the depth of the foundation. This may be challenging to predict, especially for cases where the stratigraphy is irregular (i.e. not horizontally layered) and where large contrasts in stiffness between layers are present, such as between soil and bedrock. These are conditions that can considerably affect the wave propagation in the soil [23]. Moreover, soil heterogeneity can also have a significant influence on the incident wave field produced by loads applied at the ground surface [88].

In light of the considerable degree of uncertainty related to such problems, the experiments performed in this research project have been focused on only investigating the dynamic characteristics of the soil-foundation system. Using a reproducible source that can be measured and considering only the response of the foundation, errors related to modelling the source of excitation or a building are eliminated.

7.1.1 Validation of numerical models

The purpose of the experiments performed in Papers II and III was to validate the use of numerical models for predicting ground-borne vibration in an end-bearing pile foundation based on the information provided from the site investigations performed in Paper I. The three problems addressed in Papers I, II and III each impose different requirements on the model. Predicting the free field response at the surface of the soil requires only a model of the soil. As noted in section 3.2.5, the inverse problem that is solved to estimate the dynamic small-strain soil properties from vibrations measured at the surface is non-unique. This means that a horizontally layered soil model may be able to produce a representative vibration response at the surface of the soil, even if the model does not reflect the true material properties of the soil. An example is when layers of soil are inclined. In that case, a representative horizontally layered soil model can be fitted to the data, but the properties in model do not necessarily correspond to the true properties of the soil [108]. This is the reason for the slightly different value of the S-wave speed of the fourth layer considered in Paper I compared to the one used in Papers II and III. In Paper I a longer distance was covered and the point of excitation was in a position where the layer of till was situated at a more shallow depth. For the tests performed in the vicinity of the pile foundation, on the other hand, the soil was almost horizontally layered and results from the point wise SCPT tests taken at the positions of the excitation points and the pile group were therefore considered as more representative. For the models of the pile foundation, an accurate representation of the soil where the foundation is installed is more important, at least up to a depth equal to the pile length, as the interaction between the foundation and the soil influence the dynamic response of the foundation.

Apart from the model inversion used for the soil investigations, model updating has not been considered in this research to better fit the results from the measurements. Updating of model parameters based on measurements may be a useful strategy to identify appropriate values for certain problems, e.g. identifying stiffness and damping properties of certain connections in structures. However, as for the inverse problem solved for estimating the dynamic soil properties, model updating generally suffers from non-uniqueness as the optimisation problem is rarely convex. This means that the parameters of the fitted model do not necessarily correspond to their true values. Moreover, soil conditions are site specific and ad hoc modification of models is often not a feasible option in practice. Instead, predictions have to rely on the information available from site investigations. For this reason, the numerical predictions which are compared to the measurements in Papers II and III are based on the information available from the site investigations. This provides an example of the predictive capability of a numerical model for this type of problem.

Despite the detailed site investigations, the predictions of the vibrations of the pile foundation in Papers II and III are subject to uncertainties regarding the properties of the soil, the stratigraphy, soil heterogeneity and pile-soil contact conditions. Therefore, model error is inevitable and an agreement between predictions and measurements comparable to results for problems in e.g. bridge dynamics should not expected. The dynamic behaviour of the pile group foundation in the vertical direction is most accurately predicted both in Paper II and Paper III. However, these are results only for a single study and measurements from other sites with similar, but not identical, conditions would be required to establish a general level of prediction accuracy that can be expected. Nevertheless, the results provide confidence in the ability of the models to describe the dynamic behaviour of this foundation type, especially in the vertical direction, and justifies their use for further analysis to generalise the results using simulations. This is further discussed in section 7.2.

7.1.2 Combining measurements with models

In urban environments, the existence of nearby buildings and infrastructure will also influence the wave field in the soil due to wave scattering. Such effects are very difficult to capture through modelling due to the high degree of added complexity and that information related to existing structures might not always be publicly available. In such a situation, it might be preferred to base predictions on measurements conducted directly at the site. This way, the site specific conditions are implicitly taken into account and the uncertainty related to modelling the source and the propagation path are eliminated altogether. In this context, the approach addressed in Paper III based on combining a model with vibration measurements on the completed foundation using a substructure formulation (see section 4.1) can be of particular value. This approach requires no information regarding the properties of the soil, the location of the source or the different types of waves involved in the excitation. It also takes into account the potential influence of source-receiver interaction. However, it requires that measurements are performed when the foundation has already been constructed.

It is not always possible to perform measurements during construction and even less so to alter the foundation design at this stage. Relating vibrations measured in the free field to the vibration of a foundation is therefore a strategy better suited for estimating vibration levels at a design stage. A distinction should be made between empirical correction factors established from measurements on existing buildings (see section 2.2.1) and approaches where the influence of the foundation and the building are treated separately. Using the latter approach, simplified models for predicting ground-borne vibration in buildings from free field vibrations have been developed in the literature for surface foundations [8, 24, 70, 99]. The advantage of this approach is that it allows for taking into account the influence of the local soil conditions, the type of incident loading and the type of foundation in estimating the vibrations of the foundation from measured free field vibrations. Using a numerical model, this can of course also be achieved by using a full model of the soil, the foundation and the building by adopting an empirical frame work as described in chapter 2. However, by decomposing the problem into separate components, approximate relations can be established to provide tools that are more suitable for design calculations.

7.2 The influence of the end-bearing condition

In earthquake engineering, the horizontal, rocking and torsional excitation of foundations due to incident wave fields originating from deep, distant sources is of primary interest. For this reason, the dynamic vertical response of foundations due to seismic excitation has received far less attention in the literature on soil dynamics. On the contrary, for ground-borne vibrations in mid and low-rise buildings, the vertical vibrations of floors are often of primary concern [42]. In those cases, the excitation is mainly provided from axial wave propagation in the columns that translate into bending waves in the floors. Conversely, bending of the columns mainly translate into axial waves in the floors. Therefore, the vertical response of the foundation is in many cases used as input in simplified models for estimating ground-borne vibration in buildings, see e.g. [8, 66, 118]. This highlights the importance of the vertical component of the foundation response for the prediction of ground-borne vibration in a building. For buildings on shallow foundations, some authors suggest using the vertical free field response as input and to consider dynamic soil-structure interaction only through the foundation impedance [8, 70]. For pile foundations, such an assumption can lead to substantial prediction errors

[47]. In the light of the results presented in Paper IV, this is most certainly the case for end-bearing piles. Neglecting the influence of dynamic pile-soil interaction on the excitation would overestimate the vertical vibration response in the building, especially since end-bearing pile foundations are much stiffer and provide less radiation damping in the vertical direction compared to floating pile foundations [86]. In this context, it should be stressed that, in general, design choices to reduce ground-borne vibration should not be based solely on the vibration response of the foundation. It should instead be based on the resulting vibration response in the building, which is also affected by the dynamic interaction between the building and the foundation.

For foundation systems consisting of e.g. several footings or pile foundations, the vibration response is generally influenced by the interaction between different foundation elements when excited by an incident wave field. For surface foundations, the influence of these interactions can in some cases be neglected or be taken into account in an average sense [24, 99]. For floating piles in homogeneous soil, the interaction between different piles through the soil when subjected to an incident wave field is also of minor importance and can in most cases be disregarded [58, 76]. It was found in Papers III and IV that this is not the case for end-bearing piles, and was therefore further analysed in Paper V. This has several implications for different applications related to predictions of ground-borne vibration. The vertical vibration of a pile that is positioned behind a number of neighbour piles with respect to the direction of the incident wave field can be substantially reduced compared to the solitary single pile (see Papers III and V). Therefore, vibration measurements on a single end-bearing pile that is used as a reference, e.g. for model validation or as input for analysis of building vibrations, should be carefully selected if other piles are present at the site so that vibration levels are not underestimated.

In Paper IV, it was shown that the vertical vibration of a single pile can be used as a conservative estimate for the vibration response of square 2×2 pile groups. It should be emphasised that this considers the whole foundation, including both the influence of phase differences in the excitation of the piles and pile-soil-pile interaction. As presented in Paper V, this does not strictly hold for piles that are aligned transverse to the direction of the incident wave field and are all thereby excited in phase. Generally, the coupling of the vertical degrees of freedom between end-bearing piles through the soil should therefore be taken into account. This makes simplified modelling of end-bearing pile foundations more involved. Further research is required to better understand the interaction through the soil between different foundation elements in larger foundation systems and to propose methods for taking it into account in an approximate way. In this context, the results presented in Paper V may be used as a starting point.

Chapter 8

Conclusions and suggestions for further research

The research presented in this thesis focused on characterising the vibration transmission through end-bearing pile foundations and investigating how it can be taken into account in the context of vibration assessment for new buildings in environments where ground-borne vibration may be an concern. The research has been performed partly through full-scale field tests on a designated test site to validate the use of numerical models and partly by numerical analyses of idealised systems similar to those validated through the experiments to investigate the general influence of dynamic interaction between soil and pile foundations on the transmission of ground-borne vibration. This chapter presents the main conclusions from the work and some suggestions for directions of further research.

8.1 Conclusions

The principal findings of the research presented in this thesis are here listed.

- The vibration characteristics of an end-bearing pile foundation were predicted with fairly good accuracy using a linear elastic numerical model and the dynamic small-strain soil properties obtained from site investigations. The vertical impedance and vibrations due to loads at the ground surface for a pile group were particularly well predicted.
- The vibration response of the pile foundation was also well predicted from measurements of individual pile vibration responses and impedances when combined with a model using a substructure formulation. This hybrid modelling approach does not require knowledge of neither the incident wave field nor the properties of the soil and can be applied in practice for design verification at an intermediate construction stage.
- For saturated soft soils on stiff bedrock, guided and critically refracted P-waves were found to have a significant contribution to the vibration response at the ground surface. These waves travel at a considerably higher speed than the surface waves and are therefore subjected to less material damping for a given frequency and attenuate more slowly with distance. It was also found that the response at the ground surface to these

waves can be amplified by a shallow dry layer of soil at its natural frequency for vertically propagating P-waves.

- The vertical response of end-bearing piles was found to be more sensitive to guided P-wave compared to surface waves, with respect to the response measured at the ground surface.
- The vertical response of end-bearing piles in soil on bedrock due to loads at the ground surface were found to be strongly influenced by the relationship between the piles' axial stiffness and the stiffness of the soil.
- A simple procedure for estimating the vertical response of end-bearing piles from measured free field vibrations was proposed.
- Pile-soil-pile interaction was found to have an important influence on the vertical response of end-bearing piles subjected to an incident wave field produced by a vertical load at the ground surface. The interaction can either reduce or amplify the group response, depending on the pile spacing and wavelengths in the soil. This is in contrast to floating piles in homogeneous soil for which pile-soil-pile interaction has a negligible influence.

8.2 Further research directions

8.2.1 Column-floor building models for assessment of ground-borne vibration

The research presented in this thesis mainly focus on the transmission properties of foundation elements, with an emphasis on vertical vibrations. However, as described in chapter 4, the dynamic response of a building subjected to ground-borne vibration is not only governed by the response of the foundation, but the combined effect of the foundation response and the dynamic interaction between the foundation and the building.

Buildings are complicated structures of large scale, and it is therefore desirable to develop simple methods to describe the their general behaviour. Models based on vertical foundation impedance and one dimensional transfer matrices that consider axial wave propagation through columns and propagation of bending waves in connecting slabs have been proposed for estimating train induced vibration in buildings [8]. This method has been experimentally validated and show acceptable accuracy for the case when the building is present [105, 118]. Li et al. [66] also combined the column model and a Bayesian Neural Network to predict the input from free field vibrations measured prior to construction, highlighting the importance of taking into account the influence of the foundation on the input provided to the model.

It is suggested that further research is aimed at combining such simple models with foundation impedances and correction factors (such as the ones presented in Paper IV) for developing a design analysis framework for vibration prediction based on measured free field vibrations at the location where the foundation is to be constructed. This would provide a simple, yet site specific and physics based, way for estimating building vibrations as opposed to approaches based on currently available empirical correction factors.

8.2.2 Ground-borne vibration in buildings with a basement

In many cases, soil is excavated to build an underground basement level where the foundation is constructed. When piles are used for such a foundation, the foundation interacts with the soil not only through the piles but also through the walls of the basement level which are in contact with the soil. This affects both the foundation impedance and the excitation of the foundation due to an incident wave field [35]. The transmission of vibrations to buildings with such foundations could be investigated through numerical simulations using e.g. the FE-PML formulation described in section 5.2, which allows for an arbitrary foundation geometry modelled with finite elements while retaining computational efficiency by computing the incident wave field from a separate source model. This would allow to better understand how the foundation design influences the vibration transmission to buildings and may produce recommendations for how to take it into account for vibration assessment.

8.2.3 Hybrid predictions at intermediate construction stages

The results obtained in Paper III by combining measurements from an intermediate construction stage with a model using a substructure formulation, show that such intermediate measurements can be valuable for design verification with regard to ground-borne vibration. It is therefore of interest to evaluate the use of such methods for larger foundation systems and whole buildings. Measurements performed at intermediate construction stages, e.g. when the foundation elements are in place, can be used to assess whether vibration mitigation measures may be required. This could in a first step be evaluated by numerical modelling, which may lead to recommendations regarding appropriate model simplifications that can be adopted to reduce complexity for practical application. A real case study can then be considered for validating the use of the method by tracking the changes in vibration characteristics between different construction stages. This could, apart from validating the method itself, also lead to a better understanding of the vibration transmission between a building and its foundation.

Bibliography

[1] Achenbach, J. *Wave propagation in elastic solids*. Elsevier, 1975.

[2] Álamo, G. M. *Dynamic response of piled structures. Implementation of a model based on the integral formulation of the problem and the use of a fundamental solution for the layered half space*. PhD thesis, Universidad de Las Palmas de Gran Canaria, 2018.

[3] Álamo, G. M., Martínez-Castro, A. E., Padrón, L. A., Aznárez, J. J., Gallego, R., and Maeso, O. Efficient numerical model for the computation of impedance functions of inclined pile groups in layered soils. *Engineering Structures*, 126:379–390, 2016. ISSN 0141-0296. DOI:10.1016/j.engstruct.2016.07.047.

[4] Anoyatis, G., Di Laora, R., and Mylonakis, G. Axial kinematic response of end-bearing piles to P waves. *International Journal for Numerical and Analytical Methods in Geomechanics*, 37(17):2877–2896, 2013. DOI:10.1002/nag.2166.

[5] Areias, L. Method to reduce variability of S-wave profiles in seismic cone penetration tests. In *International Conferences on Recent Advances in Geotechnical Earthquake Engineering and Soil Dynamics*, 2010.

[6] Areias, L. and Van Impe, F. W. Effect of travel path in the SCPT test method. In *GeoShanghai International Conference 2006*, pages 236–242, 2006.

[7] Areias, L. and Van Impe, W. *Interpretation of SCPT Data Using Cross-over and Cross-Correlation Methods*, pages 110–116. Springer Berlin Heidelberg, Berlin, Heidelberg, 2004. ISBN 978-3-540-39918-6.

[8] Auersch, L. Simple and fast prediction of train-induced track forces, ground and building vibrations. *Railway Engineering Science*, 28(3):232–250, 2020. DOI:10.1007/s40534-020-00218-7.

[9] Auersch, L. Site-specific amplitude-distance laws, wave velocities, damping, and transfer functions of the soil from hammer impacts and application to railway-induced ground vibration: Similarities and mid-frequency differences. *Journal of Vibration Engineering & Technologies*, 11(6):2671–2687, Sep 2023. ISSN 2523-3939. DOI:10.1007/s42417-023-01095-0.

[10] Axelsson, G. Design of piles - Swedish practice. In *ISSMGE - ETC 3 International Symposium on Design of Piles in Europe*, Leuven, Belgium, April 2016.

[11] Badsar, S., Schevenels, M., Haegeman, W., and Degrande, G. Determination of the material damping ratio in the soil from SASW tests using the half-power bandwidth method. *Geophysical Journal International*, 182(3):1493–1508, 2010. DOI:10.1111/j.1365-246X.2010.04690.x.

[12] Bahrekazemi, M. *Train-induced ground vibration and its prediction*. PhD thesis, KTH Royal Institute of Technology, 2004.

[13] Basu, U. Explicit finite element perfectly matched layer for transient three-dimensional elastic waves. *International Journal for Numerical Methods in Engineering*, 77(2):151–176, 2009. DOI:10.1002/nme.2397.

[14] Basu, U. and Chopra, A. K. Perfectly matched layers for time-harmonic elastodynamics of unbounded domains: theory and finite-element implementation. *Computer Methods in Applied Mechanics and Engineering*, 192(11):1337 – 1375, 2003. ISSN 0045-7825. DOI: 10.1016/S0045-7825(02)00642-4.

[15] Basu, U. and Chopra, A. K. Perfectly matched layers for transient elastodynamics of unbounded domains. *International Journal for Numerical Methods in Engineering*, 59 (8):1039–1074, 2004. DOI:10.1002/nme.896.

[16] Baziw, E. J. Derivation of seismic cone interval velocities utilizing forward modeling and the downhill simplex method. *Canadian Geotechnical Journal*, 39(5):1181–1192, 2002. DOI:10.1139/t02-061.

[17] Berenger, J.-P. A perfectly matched layer for the absorption of electromagnetic waves. *Journal of Computational Physics*, 114(2):185 – 200, 1994. ISSN 0021-9991. DOI:10.1006/jcph.1994.1159.

[18] Bettess, P. Infinite elements. *International Journal for Numerical Methods in Engineering*, 11(1):53–64, 1977. DOI:10.1002/nme.1620110107.

[19] Biot, M. A. Theory of propagation of elastic waves in a fluid-saturated porous solid. i. low-frequency range. *The Journal of the Acoustical Society of America*, 28(2):168–178, 1956. DOI:10.1121/1.1908239.

[20] Brocanelli, D. and Rinaldi, V. Measurement of low-strain material damping and wave velocity with bender elements in the frequency domain. *Canadian Geotechnical Journal*, 35(6):1032–1040, 1998. DOI:10.1139/t98-058.

[21] Campanella, R. G. and Stewart, W. P. Seismic cone analysis using digital signal processing for dynamic site characterization. *Canadian Geotechnical Journal*, 29(3):477–486, 1992. DOI:10.1139/t92-052.

[22] Cheng, Z. and Leong, E. Determination of damping ratios for soils using bender element tests. *Soil Dynamics and Earthquake Engineering*, 111:8 – 13, 2018. ISSN 0267-7261. DOI: 10.1016/j.soildyn.2018.04.016.

[23] Chouw, N., Le, R., and Schmid, G. Propagation of vibration in a soil layer over bedrock. *Engineering Analysis with Boundary Elements*, 8(3):125–131, 1991. ISSN 0955-7997. DOI: 10.1016/0955-7997(91)90021-K.

[24] Colaço, A., Barbosa, D., and Alves Costa, P. Hybrid soil-structure interaction approach for the assessment of vibrations in buildings due to railway traffic. *Transportation Geotechnics*, 32:100691, 2022. ISSN 2214-3912. DOI:10.1016/j.trgeo.2021.100691.

[25] Comission on Pile Research. Pile statistics for Sweden 2023, 2024.

[26] Connolly, D., Kouroussis, G., Giannopoulos, A., Verlinden, O., Woodward, P., and Forde, M. Assessment of railway vibrations using an efficient scoping model. *Soil Dynamics and Earthquake Engineering*, 58:37 – 47, 2014. ISSN 0267-7261. DOI:10.1016/j.soildyn.2013.12.003.

[27] Connolly, D., Alves Costa, P., Kouroussis, G., Galvin, P., Woodward, P., and Laghrouche, O. Large scale international testing of railway ground vibrations across europe. *Soil Dynamics and Earthquake Engineering*, 71:1 – 12, 2015. ISSN 0267-7261. DOI:10.1016/j.soildyn.2015.01.001.

[28] de Klerk, D., Rixen, D. J., and Voormeeren, S. N. General framework for dynamic substructuring: History, review and classification of techniques. *AIAA Journal*, 46(5):1169–1181, 2008. DOI:10.2514/1.33274.

[29] Dobry, R. and Gazetas, G. Simple method for dynamic stiffness and damping of floating pile groups. *Géotechnique*, 38(4):557–574, 1988. DOI:10.1680/geot.1988.38.4.557.

[30] Emani, P. and Maheshwari, B. Dynamic impedances of pile groups with embedded caps in homogeneous elastic soils using cifecm. *Soil Dynamics and Earthquake Engineering*, 29(6):963 – 973, 2009. ISSN 0267-7261. DOI:10.1016/j.soildyn.2008.11.003.

[31] Fathi, A., Poursartip, B., and Kallivokas, L. F. Time-domain hybrid formulations for wave simulations in three-dimensional pml-truncated heterogeneous media. *International Journal for Numerical Methods in Engineering*, 101(3):165–198, 2015.

[32] Forbriger, T. Inversion of shallow-seismic wavefields: I. Wavefield transformation. *Geophysical Journal International*, 153(3):719–734, 06 2003. ISSN 0956-540X. DOI: 10.1046/j.1365-246X.2003.01929.x.

[33] Foti, S., Hollender, F., Garofalo, F., Albarello, D., Asten, M., Bard, P.-Y., Comina, C., Cornou, C., Cox, B., Di Giulio, G., Forbriger, T., Hayashi, K., Lunedei, E., Martin, A., Mercerat, D., Ohrnberger, M., Poggi, V., Renalier, F., Sicilia, D., and Socco, V. Guidelines for the good practice of surface wave analysis: a product of the InterPACIFIC project. *Bulletin of Earthquake Engineering*, 16:2367–2420, 2018.

[34] François, S., Schevenels, M., Lombaert, G., and Degrande, G. Numerical modeling and in situ vibration measurements during the design and construction of low vibration floors at the corelab 1b research facility. In *Proceedings of ISMA 2014, International Conference on Noise and Vibration Engineering, Leuven, Belgium*, 2014.

[35] François, S., Pyl, L., Masoumi, H., and Degrande, G. The influence of dynamic soil-structure interaction on traffic induced vibrations in buildings. *Soil Dynamics and Earthquake Engineering*, 27(7):655–674, 2007. ISSN 0267-7261. DOI:10.1016/j.soildyn.2006.11.008.

[36] François, S., Schevenels, M., Lombaert, G., and Degrande, G. A two-and-a-half-dimensional displacement-based PML for elastodynamic wave propagation. *International Journal for Numerical Methods in Engineering*, 90(7):819–837, 2011. DOI: 10.1002/nme.3344.

[37] Gazetas, G. Seismic response of end-bearing single piles. *International Journal of Soil Dynamics and Earthquake Engineering*, 3(2):82 – 93, 1984. ISSN 0261-7277. DOI:10.1016/0261-7277(84)90003-2.

[38] Gazetas, G. Formulas and charts for impedances of surface and embedded foundations. *Journal of Geotechnical Engineering*, 117(9):1363–1381, 1991. DOI:10.1061/(ASCE)0733-9410(1991)117:9(1363).

[39] Gazetas, G. and Makris, N. Dynamic pile-soil-pile interaction. part I: Analysis of axial vibration. *Earthquake Engineering & Structural Dynamics*, 20(2):115–132, 1991. DOI:10.1002/eqe.4290200203.

[40] Gazetas, G., Fan, K., and Kaynia, A. Dynamic response of pile groups with different configurations. *Soil Dynamics and Earthquake Engineering*, 12(4):239 – 257, 1993. ISSN 0267-7261. DOI:10.1016/0267-7261(93)90061-U.

[41] Google Earth Pro V.7.3.3.7786. Brottby, Sweden, March 19, 2020. 59°35'24.3"N 18°10'26.0"W, Eye alt 383 m. Maxar Technologies 2020. http://www.earth.google.com [September 21, 2020].

[42] Hanson, C. E., Ross, J. C., and Towers, D. A. High-speed ground transportation noise and vibration impact assessment. Technical Report DOT/FRA/ORD-12/15, Federal Railroad Administration, 2012.

[43] Harris Miller Miller & Hanson Inc. Summary of European high-speed rail noise and vibration measurements. Report No. 293630-2, U.S. Federal Railroad Administration (FRA), 1996.

[44] Haskell, N. A. The dispersion of surface waves on multilayered media. *Bulletin of the Seismological Society of America*, 43(1):17–34, 01 1953. ISSN 0037-1106.

[45] Holmén, M. Laboratorierapport dnr 1.1-1904-0267, Statens geotekniska institut (SGI), 2020.

[46] Hunaidi, O. and Tremblay, M. Traffic-induced building vibrations in Montréal. *Canadian Journal of Civil Engineering*, 24(5):736–753, 1997. DOI:10.1139/l97-023.

[47] Hussein, M., Hunt, H., Kuo, K., Costa, P. A., and Barbosa, J. The use of sub-modelling technique to calculate vibration in buildings from underground railways. *Proceedings of the Institution of Mechanical Engineers, Part F: Journal of Rail and Rapid Transit*, 229 (3):303–314, 2015. DOI:10.1177/0954409713511449.

[48] ISO 14837-1:2005. Mechanical vibration – Ground-borne noise and vibration arising from rail systems – Part 1: General guidance, International Organization for Standardization, July 2005.

[49] ISO 14837-32:2015. Mechanical vibration – Ground-borne noise and vibration arising from rail systems – Part 32: Measurement of dynamic properties of the ground, International Organization for Standardization, 2015.

[50] ISO 2631-2:2003. Mechanical vibration and shock – Evaluation of human exposure to whole-body vibration – Part 2: Vibration in buildings (1 Hz to 80 Hz), International Organization for Standardization, Apr. 2003.

[51] Kanellopoulos, K. and Gazetas, G. Vertical static and dynamic pile-to-pile interaction in non-linear soil. *Géotechnique*, 70(5):432–447, 2020. DOI:10.1680/jgeot.18.P.303.

[52] Karl, L., Haegeman, W., Degrande, G., and Dooms, D. Determination of the material damping ratio with the bender element test. *Journal of Geotechnical and Geoenvironmental Engineering*, 134(12):1743–1756, 2008. DOI:10.1061/(ASCE)1090-0241(2008)134:12(1743).

[53] Kausel, E. *Fundamental Solutions in Elastodynamics: A Compendium*. Cambridge University Press, 2006.

[54] Kausel, E. Generalized stiffness matrix method for layered soils. *Soil Dynamics and Earthquake Engineering*, 115:663–672, 2018. ISSN 0267-7261. DOI:10.1016/j.soildyn.2018.09.003.

[55] Kausel, E. and Roësset, J. M. Stiffness matrices for layered soils. *Bulletin of the seismological Society of America*, 71(6):1743–1761, 1981.

[56] Kausel, E., Whitman, R. V., Morray, J. P., and Elsabee, F. The spring method for embedded foundations. *Nuclear Engineering and Design*, 48(2):377–392, 1978. ISSN 0029-5493. DOI:10.1016/0029-5493(78)90085-7.

[57] Kaynia, A. M. and Kausel, E. Dynamics of piles and pile groups in layered soil media. *Soil Dynamics and Earthquake Engineering*, 10(8):386 – 401, 1991. ISSN 0267-7261. DOI:10.1016/0267-7261(91)90053-3.

[58] Kaynia, A. M. and Novak, M. Response of pile foundations to rayleigh waves and obliquely incident body waves. *Earthquake Engineering & Structural Dynamics*, 21(4):303–318, 1992. DOI:10.1002/eqe.4290210403.

[59] Kouroussis, G., Verlinden, O., and Conti, C. Finite-dynamic model for infinite media: Corrected solution of viscous boundary efficiency. *Journal of Engineering Mechanics*, 137(7):509–511, 2011. DOI:10.1061/(ASCE)EM.1943-7889.0000250.

[60] Kouroussis, G., Conti, C., and Verlinden, O. Investigating the influence of soil properties on railway traffic vibration using a numerical model. *Vehicle System Dynamics*, 51(3):421–442, 2013. DOI:10.1080/00423114.2012.734627.

[61] Kuo, K., Verbraken, H., Degrande, G., and Lombaert, G. Hybrid predictions of railway induced ground vibration using a combination of experimental measurements and numerical modelling. *Journal of Sound and Vibration*, 373:263–284, 2016. ISSN 0022-460X. DOI:10.1016/j.jsv.2016.03.007.

[62] Kuo, K., Papadopoulos, M., Lombaert, G., and Degrande, G. The coupling loss of a building subject to railway induced vibrations: Numerical modelling and experimental measurements. *Journal of Sound and Vibration*, 442:459 – 481, 2019. ISSN 0022-460X. DOI:10.1016/j.jsv.2018.10.048.

[63] Kuppelwieser, H. and Ziegler, A. A tool for predicting vibration and structure-borne noise immissions caused by railways. *Journal of Sound and Vibration*, 193(1):261–267, 1996. ISSN 0022-460X. DOI:10.1006/jsvi.1996.0266.

[64] Lankston, R. W. *High-Resolution Refraction Seismic Data Acquisition and Interpretation*, pages 45–74. 1990.

[65] Larsson, R. and Mulabdić, M. Shear moduli in scandinavian clays. measurement of initial shear modulus with seismic cones. empirical correlations for the initial shear modulus in clay. Report 40, Swedish Geotechnical Institute, 1991.

[66] Li, X., Chen, Y., Zou, C., Wu, J., Shen, Z., and Chen, Y. Building coupling loss measurement and prediction due to train-induced vertical vibrations. *Soil Dynamics and Earthquake Engineering*, 164:107644, 2023. ISSN 0267-7261. DOI:10.1016/j.soildyn.2022.107644.

[67] Lombaert, G., Degrande, G., and Clouteau, D. The influence of the soil stratification on free field traffic-induced vibrations. *Archive of Applied Mechanics*, 71:661–678, 2001. DOI:10.1007/s004190100174.

[68] Lombaert, G., Degrande, G., François, S., and Thompson, D. J. Ground-borne vibration due to railway traffic: A review of excitation mechanisms, prediction methods and mitigation measures. In *Noise and Vibration Mitigation for Rail Transportation Systems*, pages 253–287, Berlin, Heidelberg, 2015. Springer Berlin Heidelberg.

[69] López-Mendoza, D., Romero, A., Connolly, D., and Galvín, P. Scoping assessment of building vibration induced by railway traffic. *Soil Dynamics and Earthquake Engineering*, 93: 147 – 161, 2017. ISSN 0267-7261. DOI:10.1016/j.soildyn.2016.12.008.

[70] López-Mendoza, D., Connolly, D., Romero, A., Kouroussis, G., and Galvín, P. A transfer function method to predict building vibration and its application to railway defects. *Construction and Building Materials*, 232:117217, 2020. ISSN 0950-0618. DOI:10.1016/j.conbuildmat.2019.117217.

[71] Luan, L., Zheng, C., Kouretzis, G., Ding, X., and Poulos, H. A new dynamic interaction factor for the analysis of pile groups subjected to vertical dynamic loads. *Acta Geotechnica*, 15, 2020. DOI:10.1007/s11440-020-00989-7.

[72] Luco, J. E. and Wong, H. L. Dynamic response of rectangular foundations for Rayleigh wave excitation. In *Proc. 6th World Conf. on Earthquake Eng.*, volume 2, pages 1542–1548, 1977.

[73] Lysmer, J. and Kuhlemeyer, R. L. Finite dynamic model for infinite media. *Journal of the Engineering Mechanics Division*, 95(4):859–878, 1969.

[74] Madshus, C., Bessason, B., and Hårvik, L. Prediction model for low frequency vibration from high speed railways on soft ground. *Journal of Sound and Vibration*, 193(1):195 – 203, 1996. ISSN 0022-460X. DOI:10.1006/jsvi.1996.0259.

[75] Makris, N. Soil-pile interaction during the passage of rayleigh waves: An analytical solution. *Earthquake Engineering & Structural Dynamics*, 23(2):153–167, 1994. DOI: 10.1002/eqe.4290230204.

[76] Makris, N. and Badoni, D. Seismic response of pile groups under oblique-shear and Rayleigh waves. *Earthquake Engineering & Structural Dynamics*, 24(4):517–532, 1995. DOI:10.1002/eqe.4290240405.

[77] Makris, N. and Gazetas, G. Dynamic pile-soil-pile interaction. part II: Lateral and seismic response. *Earthquake Engineering & Structural Dynamics*, 21(2):145–162, 1992. DOI: 10.1002/eqe.4290210204.

[78] Makris, N. and Gazetas, G. Displacement phase differences in a harmonically oscillating pile. *Géotechnique*, 43(1):135–150, 1993. DOI:10.1680/geot.1993.43.1.135.

[79] Mamoon, S. M. and Ahmad, S. Seismic response of piles to obliquely incident SH, SV, and P waves. *Journal of Geotechnical Engineering*, 116(2):186–204, 1990. DOI:10.1061/(ASCE)0733-9410(1990)116:2(186).

[80] Mayne, P. W. and Rix, G. J. $G_{\max}-q_c$ relationships for clays. *Geotechnical Testing Journal*, 16:54–60, 03 1993. DOI:10.1520/GTJ10267J.

[81] Melke, J. Noise and vibration from underground railway lines: Proposals for a prediction procedure. *Journal of Sound and Vibration*, 120(2):391–406, 1988. ISSN 0022-460X. DOI: 10.1016/0022-460X(88)90451-8.

[82] Mondot, J. and Petersson, B. Characterization of structure-borne sound sources: The source descriptor and the coupling function. *Journal of Sound and Vibration*, 114(3): 507–518, 1987. ISSN 0022-460X. DOI:10.1016/S0022-460X(87)80020-2.

[83] Mylonakis, G. and Gazetas, G. Kinematic pile response to vertical P-wave seismic excitation. *Journal of Geotechnical and Geoenvironmental Engineering*, 128(10):860–867, 2002. DOI:10.1061/(ASCE)1090-0241(2002)128:10(860).

[84] Nelson, J. and Saurenman, H. Prediction procedure for rail transportation groundborne noise and vibration. *Transportation Research Record*, (1143):26–35, 1987.

[85] Nogami, T. Dynamic group effect in axial responses of grouped piles. *Journal of Geotechnical Engineering*, 109(2):228–243, 1983. DOI:10.1061/(ASCE)0733-9410(1983) 109:2(228).

[86] Padrón, L., Aznárez, J., Maeso, O., and Saitoh, M. Impedance functions of end-bearing inclined piles. *Soil Dynamics and Earthquake Engineering*, 38:97 – 108, 2012. ISSN 0267-7261. DOI:10.1016/j.soildyn.2012.01.010.

[87] Pak, R. Y. S. and Guzina, B. B. Three-dimensional Green's functions for a multilayered half-space in displacement potentials. *Journal of Engineering Mechanics*, 128(4):449–461, 2002. DOI:10.1061/(ASCE)0733-9399(2002)128:4(449).

[88] Papadopoulos, M., François, S., Degrande, G., and Lombaert, G. The influence of uncertain local subsoil conditions on the response of buildings to ground vibration. *Journal of Sound and Vibration*, 418:200–220, 2018. DOI:10.1016/j.jsv.2017.12.021.

[89] Park, C. B., Miller, R. D., and Xia, J. *Imaging dispersion curves of surface waves on multichannel record*, pages 1377–1380. 1998.

[90] Park, C. B., Miller, R. D., and Xia, J. Multichannel analysis of surface waves. *GEOPHYSICS*, 64(3):800–808, 1999. DOI:10.1190/1.1444590.

[91] Pennington, D., Nash, D., and Lings, M. Horizontally mounted bender elements for measuring anisotropic shear moduli in triaxial clay specimens. *Geotechnical Testing Journal*, 24(2):133–144, 2001. DOI:10.1520/GTJ11333J.

[92] Poulos, H. G. Analysis of the settlement of pile groups. *Géotechnique*, 18(4):449–471, 1968. DOI:10.1680/geot.1968.18.4.449.

[93] Quagliata, A., Ahearn, M., Boeker, E., Roof, C., Volpe, J. A., Meister, L., and Singleton, H. Transit noise and vibration impact assessment. Technical Report 0123, Federal Transit Administration, 2018.

[94] Reumers, P., Degrande, G., Lombaert, G., Thompson, D. J., Ntotsios, E., Bouvet, P., Nélain, B., and Nuber, A. Integration of a hybrid vibration prediction model for railways into noise mapping software: methodology, assumptions and demonstration. *Railway Engineering Science*, 2024. DOI:10.1007/s40534-024-00346-4.

[95] Rizzo, F. J. and Shippy, D. J. An application of the correspondence principle of linear viscoelasticity theory. *SIAM Journal on Applied Mathematics*, 21(2):321–330, 1971. DOI: 10.1137/0121034.

[96] Robertson, P. K., Campanella, R. G., Gillespie, D., and Rice, A. Seismic Cpt to measure in situ shear wave velocity. *Journal of Geotechnical Engineering*, 112(8):791–803, 1986. DOI:10.1061/(ASCE)0733-9410(1986)112:8(791).

[97] Ropars, P. *Modélisation des vibrations d'origine ferroviaire transmises aux bâtiments par le sol*. PhD thesis, Université Paris-Est, 2011.

[98] Rovithis, E., Mylonakis, G., and Pitilakis, K. Dynamic stiffness and kinematic response of single piles in inhomogeneous soil. *Bulletin of Earthquake Engineering*, 11, 2013. DOI:10.1007/s10518-013-9473-0.

[99] Sanitate, G. *A performance-based design framework for base-isolated buildings against ground-borne vibration*. PhD thesis, 2020.

[100] Sanitate, G. and Talbot, J. Foundation vibration and the added-building effect: Experimental evidence from a ground-borne vibration measurement campaign. *Journal of Sound and Vibration*, 544:117390, 2023. ISSN 0022-460X. DOI:10.1016/j.jsv.2022.117390.

[101] Schevenels, M. *The impact of uncertain dynamic soil characteristics on the prediction of ground vibrations*. PhD thesis, KU Leuven, 2007.

[102] Schevenels, M., Degrande, G., and Lombaert, G. The influence of the depth of the ground water table on free field road traffic-induced vibrations. *International Journal for Numerical and Analytical Methods in Geomechanics*, 28(5):395–419, 2004. DOI: 10.1002/nag.342.

[103] Schevenels, M., Stijn François, and Degrande, G. EDT: An ElastoDynamics Toolbox for MATLAB. *Computers & Geosciences*, 35(8):1752 – 1754, 2009. ISSN 0098-3004. DOI: 10.1016/j.cageo.2008.10.012.

[104] Tao, Z.-Y., Wang, Y.-M., He, W., and Luo, Y.-K. Identification of line-source transfer mobility and force density by ground acceleration measurements. *Environmental Science and Pollution Research*, 30(19):54498–54510, 2023. DOI:10.1007/s11356-023-26242-8.

[105] Tao, Z.-Y., Zou, C., Yang, G.-R., and Wang, Y.-M. A semi-analytical method for predicting train-induced vibrations considering train-track-soil and soil-pile-building dynamic interactions. *Soil Dynamics and Earthquake Engineering*, 167:107822, 2023. ISSN 0267-7261. DOI:10.1016/j.soildyn.2023.107822.

[106] Teng, F.-C., Ou, C.-Y., and Hsieh, P.-G. Measurements and numerical simulations of inherent stiffness anisotropy in soft taipei clay. *Journal of Geotechnical and Geoenvironmental Engineering*, 140(1):237–250, 2014. DOI:10.1061/(ASCE)GT.1943-5606.0001010.

[107] Thomson, W. T. Transmission of elastic waves through a stratified solid medium. *Journal of Applied Physics*, 21(2):89–93, 1950. DOI:10.1063/1.1699629.

[108] Verachtert, R. *Deterministic and probabilistic determination of dynamic soil characteristics*. PhD thesis, KU Leuven, Department of Civil Engineering, 2017.

[109] Verachtert, R., Lombaert, G., and Degrande, G. Multimodal determination of Rayleigh dispersion and attenuation curves using the circle fit method. *Geophysical Journal International*, 212(3):2143–2158, 12 2018. ISSN 0956-540X. DOI:10.1093/gji/ggx523.

[110] Verbraken, H. *Prediction of railway induced vibration by means of numerical, empirical, and hybrid methods*. PhD thesis, KU Leuven, Department of Civil Engineering, 2013.

[111] Villot, M., Guigou, C., Jean, P., and Picard, N. Procedures to predict exposure in buildings and estimate annoyance. Deliverable D 1.6, RIVAS project SCP0-GA-2010-265754, 2012.

[112] Wolf, J. P. *Dynamic Soil-Structure Interaction*. Prentice-Hall, 1985. ISBN 0-13-221565-9.

[113] Wolf, J. P. and von Arx, G. A. Impedance function of a group of vertical piles. In *Proceedings of ASCE Geotechnical Engineering Specialty Conference*, pages 1024–1041, Pasadena, California, 1978.

[114] Wood, T. *On the Small Strain Stiffness of Some Scandinavian Soft Clays and Impact on Deep Excavations*. PhD thesis, Chalmers University of Technology, 2016.

[115] Woods, R. D. Screening of surface wave in soils. *Journal of the Soil Mechanics and Foundations Division*, 94(4):951–979, 1968. DOI:10.1061/JSFEAQ.0001180.

[116] Xia, H., Chen, J., Wei, P., Xia, C., De Roeck, G., and Degrande, G. Experimental investigation of railway train-induced vibrations of surrounding ground and a nearby multi-story building. *Earthquake Engineering and Engineering Vibration*, 8(1):137–148, 2009. DOI: 10.1007/s11803-009-8101-0.

[117] Zheng, C., Gan, S., Kouretzis, G., Ding, X., and Luan, L. Vertical vibration of a large diameter pile partially-embedded in poroelastic soil. *Soil Dynamics and Earthquake Engineering*, 139:106211, 2020. ISSN 0267-7261. DOI:10.1016/j.soildyn.2020.106211.

[118] Zou, C., Moore, J. A., Sanayei, M., and Wang, Y. Impedance model for estimating train-induced building vibrations. *Engineering Structures*, 172:739–750, 2018. ISSN 0141-0296. DOI:10.1016/j.engstruct.2018.06.032.

[119] Zywicki, D. J. and Rix, G. J. Mitigation of near-field effects for seismic surface wave velocity estimation with cylindrical beamformers. *Journal of Geotechnical and Geoenvironmental Engineering*, 131(8):970–977, 2005. DOI:10.1061/(ASCE)1090-0241(2005)131:8(970).

Paper I

Soil Dynamics and Earthquake Engineering 150 (2021) 106804

Contents lists available at ScienceDirect

Soil Dynamics and Earthquake Engineering

journal homepage: www.elsevier.com/locate/soildyn

Assessment of small-strain characteristics for vibration predictions in a Swedish clay deposit

Freddie Theland [a,*], Geert Lombaert [b], Stijn François [b], Costin Pacoste [a,d], Fanny Deckner [c], Jean-Marc Battini [a]

[a] Division of Structural Engineering and Bridges, KTH Royal Institute of Technology, Brinellvägen 23, 100 44, Stockholm, Sweden
[b] Department of Civil Engineering, KU Leuven, Kasteelpark Arenberg 40, 3001, Leuven, Belgium
[c] GeoMind KB, Hesselmans Torg 5, 131 54, Nacka, Sweden
[d] ELU Konsult AB, Valhallavägen 117, 115 31. Stockholm, Sweden

ARTICLE INFO

Keywords:
Environmental vibration
Dynamic soil properties
Clay
Surface waves
Topsoil

ABSTRACT

Environmental vibrations induced by human activities such as traffic, construction or industrial manufacturing can cause disturbance among residents or to vibration sensitive equipment in buildings. In Sweden, geological formations of soft clay overlying a stiff bedrock are soil conditions prone to ground vibrations that are encountered both in urban areas and along parts of the national railway network. This paper presents an extensive investigation of the small-strain soil properties for the prediction of environmental ground vibrations in a shallow clay where the bedrock is situated at 7.5 m depth. The small-strain properties are estimated using available empirical correlations, bender elements, seismic cone penetration tests, seismic refraction and inversion of surface wave dispersion and attenuation curves. The results are synthesised into a dynamic layered soil model which is validated by measurements at the soil's surface at source-receiver distances up to 90 m in the frequency range 1–80 Hz. Analyses of uncertainties in the estimated values of wave speeds and material damping are performed by model investigations, indicating that surface wave tests overestimate the damping compared to bender element tests. The properties of the topmost unsaturated part of the soil is found to have a significant influence on the response at large distances, caused by critically refracted P-waves resonating in the top layer.

1. Introduction

Human activities such as construction, industrial manufacturing processes or traffic on roads and railway can give rise to vibrations spreading to its surroundings through the soil. In the built environment, buildings located in the vicinity of vibration sources might experience excessive vibration levels, potentially leading to disruption in the operation of vibration sensitive equipment or discomfort for residents. For the assessment of ground borne vibrations in buildings, numerical or empirical models can be applied to predict building vibration levels prior to construction. The mechanical soil properties and the stratification at a site have a significant influence on the amplitude and frequency content of the dynamic response of the soil [1,2]. Therefore, numerical models require an estimation of these parameters while some empirical models directly make use of the free field surface responses at the prospective site [3,4].

Ground borne vibration emanating from railways is an important societal concern that is receiving an increasing amount of attention globally [5]. A number of studies have been focused on the validation of models to predict railway induced ground vibrations in the free field. In these studies, small-strain soil properties and layered soil models are obtained either from non-invasive geophysical methods, covering large volumes of soil, or in situ wave speed measurements taken at discrete points or over a smaller distance. Lombaert et al. [6] performed a validation of a numerical model for the prediction of railway induced vibrations in the free field. The validation study was performed in steps, separating the estimation of small-strain soil properties and the measurements of the track-free field responses and train passages, allowing to assess the propagation of errors in the prediction model. The results emphasized the large influence of the soil properties on the predicted free-field responses. Kouroussis et al. [7] validated a finite element model to compute the free field response in the time domain due to the passing of high speed trains. The layering of the soil at the site was shown to have a large influence on the frequency content of the

* Corresponding author.
E-mail address: freddie.theland@byv.kth.se (F. Theland).

https://doi.org/10.1016/j.soildyn.2021.106804
Received 23 November 2020; Received in revised form 27 April 2021; Accepted 30 April 2021
Available online 5 August 2021

predicted response. Connolly et al. [8] analysed ground borne vibration levels from measurement records at seventeen different sites along European railways. An assessment of the influence of train type, train speed and site conditions on the vibrations levels was undertaken. The site specific soil conditions were found to be the most influential aspect affecting the levels of ground borne vibration. In particular, the differences in vibration levels tended to increase with the distance from the track. These observations highlight the importance of correctly accounting for the soil conditions when constructing models to perform predictions of ground borne vibrations, especially with an increasing distance from the source.

Along the national railway tracks and in densely populated urban areas in Sweden, geological formations of soft clay deposits overlying till and a stiff bedrock are encountered. These type of soil conditions have been found to be prone to ground borne vibration problems [4,9,10]. The small-strain properties of Swedish clay soils have been studied extensively using laboratory measurements and seismic methods. Empirical relations have been established to determine the initial shear modulus for geotechnical engineering applications [11–13]. An extensive investigation of small-strain soil properties was performed in Ledsgård along the West-coast line between Göteborg and Malmö in Sweden, due to the exceptionally high amplitude of vibrations encountered at the railway track [14–16]. The properties were determined in the deep marine clay from both laboratory, invasive and non-invasive in situ measurements. Measured track and free field responses at frequencies below 5 Hz due to train passages could be numerically reconstructed using the identified soil properties [17,18].

Determination of the small-strain properties in Swedish clays has so far mainly been focused on the use for either track response or static small-strain deformation analyses. The analysis of environmental vibrations requires a representation of the soil that is able to predict the dynamic response at significant source-receiver distances. For practical applications project restrictions and budget constraints can limit the extent of site investigations available to estimate the small-strain properties. Therefore, it is important to understand the ability of different investigation methods to acquire the necessary information to perform accurate predictions with a dynamic soil model.

This paper presents an extensive geotechnical and geophysical site characterization of a Swedish clay deposit in the Stockholm area. The objectives of this paper are to investigate the ability to represent a clay deposit with a shallow bedrock by a linear elastic layered soil model for the prediction of environmental ground vibrations by synthesis of small-strain properties obtained from various site investigation methods and to compare their performance in acquiring the necessary properties.

The soil conditions at the site constitute a representative example of post-glacial clays encountered in Sweden, allowing extension of the presented conclusions to sites where similar conditions are encountered.

The small-strain properties of the soil are determined by empirical relations, invasive wave speed measurements and non-invasive geophysical investigation methods. The results are compared and a synthesis of the information provided by the investigations is made to establish a representative soil model. Parametric uncertainties in the estimated soil properties are identified their influence on the computed free field responses is investigated by numerical simulations and compared to measurements at different source-receiver offsets. Finally, response measurements at the soil's surface acquired during different seasons are presented to assess the influence of seasonal variations on the soil's dynamic response.

The outline of the paper is as follows. Section 2 presents the layout and general soil conditions of the site where the investigations are performed. Section 3 presents the results obtained from a geotechnical site investigation and an overview of the methods used to estimate the small-strain properties from both in situ tests and laboratory samples. Section 4 presents the setup and data processing of two measurement campaigns where frequency response functions are estimated along the soil's surface. These are used for model validation and non-invasive estimation of small-strain properties by seismic refraction and spectral analysis of surface waves (SASW) by inversion of dispersion and attenuation curves. In section 5, the small-strain properties obtained from different investigation methods are presented, compared and synthesised into a representative soil model. Section 6 presents a validation of the soil model and an analysis of the influence of remaining uncertainties on the soil properties on the predicted responses. Section 7 addresses the influence of seasonal variation on the soil's response. Finally, section 8 presents the conclusions of the paper.

2. Test site

The test site is located in Brottby, 40 km north of Stockholm, Sweden. The site is an agricultural field that has not been cultivated for more than ten years prior to the site investigations. The site is intended as a test site for experimental investigations on the small-strain dynamic behaviour of end-bearing pile foundations. It was chosen because of its particular stratification, with a soft clay underlain by till and bedrock, representative for soil conditions prone to high amplitudes of ground borne vibration, the potential to represent the soil with a layered soil model over the area of interest and that unlimited access to the site could be granted. As the site is located in a remote location, a minimum of outside disturbances is present during testing. Moreover, a designated site makes the placement of stationary reference points possible, allowing to compare measurements performed at different occasions to assess the influence of seasonal variations.

Fig. 1 presents an aerial view together with the locations of the performed site investigations.

Fig. 2 presents geological information of the soil deposits and the soil depth to bedrock [20]. The geological information gives an overview of the topography of the underlying bedrock at the site, suggesting that the field is positioned along a fracture zone in the bedrock, overlain by layers of till and clay. The site investigations are concentrated over an area in the center of the field where the estimated soil depth is 5–10 m, as presented in Fig. 1.

3. Invasive site investigations

3.1. Overview of site investigations

The positions where the invasive tests have been performed are presented in Fig. 1.

Penetration tests over the investigation area were performed to establish an interpretation of the stratigraphy on the site and in situ wave speeds were measured by SCPT. Samples of the clay were analysed in the laboratory, providing geotechnical parameters to perform empirical predictions of the small-strain soil properties, as well as estimates of wave speeds and material damping ratios from bender element tests.

3.2. Soil topography and stratification

In points P7–P12, weight soundings were performed to provide an overview of the general variation of the stratigraphy on the site. The weight sounding penetrates the softer soil layers, but cannot penetrate the stiffer non-cohesive soil. In P8 and P13, CPTU was performed in the clay giving an indirect interpretation of the layering at the site. In addition, disturbed samples were taken in points P11 and P13 to determine the soil types of the profile by visual inspection. Three plastic groundwater pipes of 76 mm diameter were installed down to the non-cohesive soil with a consecutive 1 m spacing in points P15–P17. Apart from measuring the ground water pressure levels, these sounding wells are also used to install multiple sensors in the soil for geophyscial tests. However, after pre-drilling the holes down to the bedrock, the pipes could not be pushed down further than 0.8 m into the non-cohesive soil due to collapse of the pre-drilled holes, preventing reliable cross- or

Point	Tests
P7	Ws
P8	Ws,SCPT,CPTU
P9	Ws
P10	Ws
P11	Ws,Scr
P12	Ws
P13	Scr,SCPT,CPTU,PS
P14	MWD
P15	MWD,Gwp
P16	MWD,Gwp
P17	MWD,Gwp
P18	MWD
P19	MWD

Fig. 1. Aerial photograph [19] of the test site with the geotechnical investigation points P7–P19 and measurement lines ML1 and ML2 along which dynamic measurements are performed due to applied hammer impacts (×) superimposed. Tests performed at each point are listed in the accompanying table as weight soundings (Ws), screw samples (Scr), measurement while drilling (MWD), installation of ground water pipes (Gwp), piston samples (PS), seismic cone penetration test (SCPT) and cone penetration test with measurement of pore water pressure (CPTU).

down-hole measurements. Soil/rock probing was performed in points P18 and P19 to determine the depth to the bedrock. The test is commonly used in Sweden and is internationally referred to as measuring while drilling (MWD) described in the international standard ISO 22476-15 [21,22]. During the drilling, driving force, resistance, penetration speed, engine pressure, hammer pressure and flushing pressure are registered versus the penetration depth. This allows interpretation of layering of soils not penetrable by the CPT probe, identification of inclusions such as boulders and quality assessment of the bedrock. In point P14 pre-drilling was initiated for installation of a ground water pipe, but came to an early stop at a depth of 4 m, indicating the presence of a boulder or a local variation of the bedrock topography.

The collective information acquired from the in situ tests results in an interpreted soil profile presented in Fig. 3, illustrated in the sections A–A and B–B with reference to Fig. 1. The soil consists of layers of dry-crust clay, saturated clay and till on top of a stiff bedrock.

3.3. Seismic cone penetration tests

Two seismic cone penetration tests (SCPT) and regular CPTU tests were performed in the points P8 and P13. The spacing of the triaxial accelerometers installed in the CPT probe was 1 m. Each test was performed by hitting ribbed plates pre-loaded by the drill rig, presented in Fig. 4. The tests were performed with a depth interval of 0.5 m and in each test 10 hits were applied in two perpendicular directions in the front and the back of the rig. The wave speeds are estimated based on the difference in arrival time between the receivers calculated using time domain cross-correlation and assuming a straight travel path from the center of the plates to the receivers.

Each measurement is assigned a representative depth $z_{SCPT} = z_2(r_1 + r_2)/2r_2$, where z_j and r_j are the probe depth and radial distance from the source point for sensor j, respectively [23].

3.4. Laboratory tests

In P13, two sets of piston samples were collected for laboratory analysis at the levels 1–4 m in the clay. High quality samples were obtained using a category A method according to ISO 22475–1:2006 [24]. Table 1 presents the classification of the soil collected in the piston samples of the clay, made by visual inspection in the laboratory in accordance with international standards [25,26].

Laboratory investigations of the soil included determination of the soil's density ρ, the water content w, the liquid and plastic limits w_L and w_P yielding the plasticity index I_p, the sensitivity of the clay S_t, the undrained shear strength τ_{fu} determined from both triaxial and fall-cone tests and the over-consolidation ratio (OCR) obtained from oedometer tests with a constant rate of strain (CRS). The sensitivity, the plastic limit and the OCR could not be determined for the 1 m level consisting of dry-crust clay, possibly due to disturbance of the tested sample. The soil

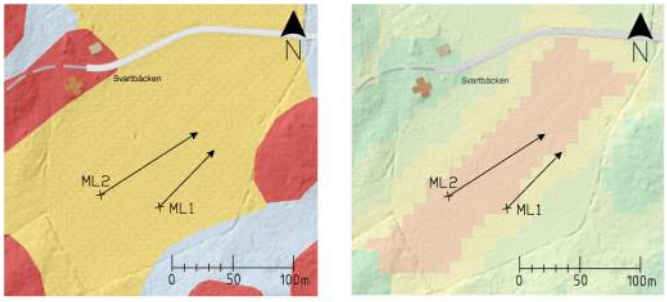

Fig. 2. Geological maps of (a) soil types at the site with colors indicating post-glacial clay (yellow), till (blue) and bedrock (red), and (b) soil depth with colors corresponding to an estimated soil depth of 5–10 m (red), 3–5 m (yellow) and depths less than 1 m (green) [20]. The measurement lines ML1 and ML2 are superimposed for reference. (For interpretation of the references to color in this figure legend, the reader is referred to the Web version of this article.)

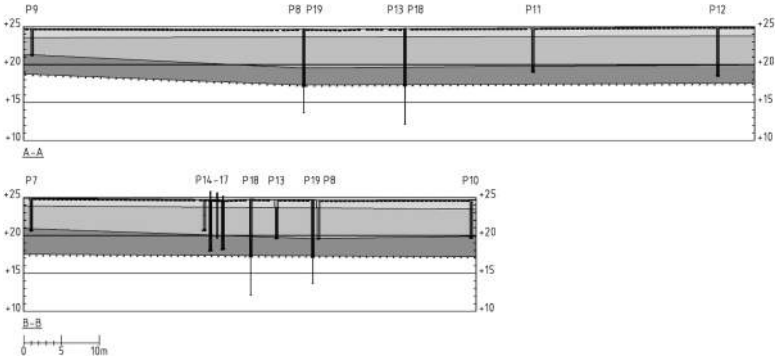

Fig. 3. Interpreted sections of the soil defined in Fig. 1 based on the information from the geotechnical site investigations. The investigation depth at each point is indicated and the interpreted layering of the soil is illustrated in shading as a dry-crust clay (top layer), soft clay (second layer) and till (third layer) on top of bedrock.

Fig. 4. Seismic cone penetration test equipment with two pre-loaded L-shaped plates, SCPT probe and a sledge hammer connected to the DAQ to trigger recording.

Table 1
Classification of the soil made by visual inspection according to ISO 14688–2:2017 [26].

Depth [m]	Soil classification
1	Sand infused slightly rusty brown **dry-crust clay**
2	Gray homogeneous **clay**
3	Sand infused lightly varved brown-gray **clay**
4	Lightly varved brown-gray **clay** with thin layers of silt
5	Sandy **gravel**

properties obtained from the laboratory measurements of the clay are presented in Table 2.

The triaxial apparatus and the oedometer housing were equipped with bender elements, allowing to perform measurements of the dilatational (P) and shear (S) wave speeds in the clay samples. The influence of anisotropy of the clay on the S-wave speed was investigated by performing measurements in both the axial and radial directions of the samples, corresponding to the vertical and horizontal in situ directions, respectively. The wave speed measurements in the axial direction were performed in a triaxial apparatus whereas the measurements of the wave speeds in the radial direction were performed in the oedometer using a radially oriented sample taken from the original piston sample by punching with the equipment presented in Fig. 5a, allowing to perform the analysis on standard size samples. The tests were performed with the samples re-loaded to in situ stresses.

The determination of wave speeds was limited to tests on two samples, one axially and one horizontally orientated, for samples collected at different levels. However, at the 2 m level the agreement between the wave speeds estimated from the two setups was evaluated by mounting an axially orientated sample in the oedometer. Table 3 presents a comparison of the results, indicating the consistency between the estimates obtained in oedometer and triaxial testing. Moreover, the axial wave speeds are compared to the radial ones at the in situ stress levels.

The results from the tests in the two perpendicular directions of the samples are presented in Table 4, indicating a structural anisotropy of the clay that varies with depth. However, for a horizontally stratified soil with vertical transverse isotropy (VTI), only the SH waves are affected by the S-wave speed anisotropy, while the P-SV waves are unaffected [28]. The anisotropy of the S-wave speeds is therefore disregarded in the remainder of this paper.

The material damping in the clay samples is estimated from the response signals generated from an axial excitation used to measure the P-wave speeds, applied as a single period of a sine at a frequency of 200 kHz. The damping is obtained using the Hilbert transform method recently introduced for material damping estimation from bender element tests by Cheng and Leong [29].

3.5. Empirical correlations

In literature, empirical correlations have been established for determining the initial shear modulus G_0 from index parameters used in geotechnical engineering. The international standard ISO 14837–32:2015 [30] gives an overview of methods for the evaluation of small-strain properties in soil, and lists the following two empirical

Table 2
Geotechnical parameters obtained from laboratory measurements on the clay piston samples from Brottby.

Depth	ρ	w	w_L	w_P	I_p	S_t	τ_{fu}^{triax}	τ_{fu}^{fc*}	OCR
[m]	[kg/m^3]	[%]	[%]	[%]	[%]	[−]	[kPa]	[kPa]	[−]
1	1880	31.8	59	–	–	–	54.4	>134.4	5**
2	1570	78.2	64	30	34	6	19.6	41.8	2.6
3	1720	53.6	49	20	29	15	19.2	16.0	1.9
4	1780	47.2	43	19	24	18	23.1	15.0	1.9

* Corrected with respect to the liquid limit according to Ref. [27].
** Estimated from CPT correlations.

Fig. 5. Laboratory preparation of (a) horizontal clay samples and (b) bender elements mounted in an oedometer housing.

Table 3
Comparison of measured S-wave speeds in samples collected at 2 m depth orientated in the axial and radial directions in triaxial and oedometer testing under different stress states.

Axial stress	$C_{s,a}$		$C_{s,r}$
	Triax	Oedometer	Oedometer
[kPa]	[m/s]	[m/s]	[m/s]
21.9		86.7	93.0
25.5	84.4	86.0	
27.9		86.5	93.6
54.0	88.9	89.0	

methods for the estimation of the initial shear modulus in cohesive soils.

The first method was established for Scandinavian clays by Larsson and Mulabdić [12]. The empirical relation is given by:

$$G_0 = \left(\frac{208}{I_p} + 250\right)\tau_{fu} \tag{1}$$

and is based on the plasticity index I_p (in decimals) and the undrained shear strength τ_{fu}. It should be noted that eq. (1) is restricted to the use of the undrained shear strength determined from a test that gives compatible results with the ones used for establishing the relation. The present relation is based on direct simple shear, dilatometer, corrected field vane and fall-cone tests [12].

In the second method, the initial shear modulus is estimated from empirical correlations established for CPT data. For cohesive soils, the initial shear modulus is estimated from [31]:

$$G_0(z) = p_a \frac{99.5}{e(z)^{1.13}} \left(\frac{q_t(z)}{p_a}\right)^{0.695} \tag{2}$$

where $p_a = 100$ kPa is a reference pressure, $e(z)$ is the void ratio as a function of the depth z and $q_t(z)$ is the corrected cone tip resistance. The correlation is based on data from a variety of different cohesive soils around the world, but predominantly on sites of soft Swedish clay with wave speeds determined from SCPT data [31]. The advantages of using the CPT data for estimating the initial shear modulus are the same as for the test in general, i.e. it provides a high resolution with depth and is based on in situ conditions. However, eq. (2) requires not only the results from the CPT, but also the variation of the void ratio with depth. At the present site, due to the full saturation of the clay below the dry crust, the void ratio can be estimated from:

$$e(z) = \frac{\rho(z)}{\rho_w(1 + 1/w(z)) - \rho(z)} \tag{3}$$

where ρ_w is the density of water, $\rho(z)$ is the soil density as a function of the depth z and $w(z)$ is the water content. As only point wise information is available of the clay density and water content, constant values of ρ and w obtained from Table 2 are assumed over each 1 m interval. The variation of the estimated S-wave speed with depth is subsequently

Table 4
Axial and radial effective stresses and S-wave speeds measured from triaxial test (axial) and oedometer test (radial) using bender elements.

Depth	σ'_a	σ'_r	$C_{s,a}$	$C_{s,r}$
[m]	[kPa]	[kPa]	[m/s]	[m/s]
1	59.0	46.0	139.0	162.4
2	25.5	21.9	84.4	93.0
3	32.3	24.0	89.4	85.9
4	40.0	26.0	95.1	86.7

calculated as:

$$C_s(z) = \sqrt{\frac{G_0(z)}{\rho(z)}} \tag{4}$$

4. Non-invasive site investigations

In addition to the invasive geotechnical tests by penetration of the soil, two active vibration measurements were performed along the measurement lines ML1 and ML2 in Fig. 1. The measurements along ML1 were conducted in the spring of 2019, while the measurements along ML2 were conducted in the autumn of the same year. The tests were performed by applying an impact force on the surface of the soil with an instrumented sledge hammer at the positions (×) indicated in Fig. 1 and measuring the vertical acceleration responses along the lines extending from the excitation points.

4.1. Setup

The impact is generated at the soil's surface by hitting a 400 × 400 × 80 mm aluminium plate with an instrumented hammer of model Dytran 5803A IEPE with a mass of 5.5 kg, presented in Fig. 6a. The accelerations are measured by means of 30 uniaxial seismic accelerometers of models Colibrys SF1500S (ML1), PCB 393A01 and PCB 393B31 (ML2). The accelerometers are mounted on 300 mm long aluminium pickets with a cruciform cross section, measuring the response in the vertical direction. Fig. 6b presents an accelerometer mounted on a picket. The picket is designed to minimize soil-structure interaction effects in the frequency range of interest [32,33].

The measurements are performed in multiple setups, where the sensors are consecutively moved 0.5 m between each setup, achieving a sensor spacing along the measurement lines of $\Delta r = 0.5$ m.

The number of setups was 12 for ML1 using 10 accelerometers and 6 for ML2 using 30 accelerometers.

The first sensor is offset 0.5 m from the excitation point and the lengths of the measurement lines ML1 and ML2 are 60 and 90 m, respectively. In each setup, 80–100 impacts and the corresponding acceleration responses have been recorded for processing, to ensure a high confidence in the measured responses at the farthest receiver.

4.2. Post-processing

In order to suppress noise in the measurement data occurring due to ambient or distant external vibration sources, the average frequency response function $\widehat{H}_{ij}(\omega)$ between the free field acceleration channel i at distance r and the hammer force channel j is computed as a function of the circular frequency ω, using the H_1 estimator [34]:

$$\widehat{H}_{ij}(\omega) = \frac{\widehat{S}_{ij}(\omega)}{\widehat{S}_{jj}(\omega)} \tag{5}$$

with the average cross power spectral density between channels i and j defined as:

$$\widehat{S}_{ij}(\omega) = \frac{1}{N}\sum_{k=1}^{N} x_i^k(\omega) x_j^{k*}(\omega) \tag{6}$$

where N is the number of events, $x_i^k(\omega)$ is the Fourier transform of the time signal acquired for event k for channel i and $x_j^{k*}(\omega)$ is the complex conjugate of the transformed signal acquired for channel j.

The frequency response function estimate $\widehat{H}_{ij}(\omega)$ is based upon multiple observations, and can therefore be considered as a stochastic variable with a standard deviation $\widehat{\sigma}_{|H_{ij}|}(\omega)$. The relative statistical errors $\widehat{\sigma}_{|H_{ij}|}(\omega)/|H_{ij}(\omega)|$, or coefficient of variation (COV), on the estimated transfer function $\widehat{H}_{ij}(\omega)$ is given by [35]:

$$\mathrm{COV}_{ij} = \sqrt{\frac{1-\gamma_{ij}^2(\omega)}{2N\gamma_{ij}^2(\omega)}} \tag{7}$$

$$\gamma_{ij}^2(\omega) = \frac{\widehat{S}_{ij}(\omega)\widehat{S}_{ij}^*(\omega)}{\widehat{S}_{ii}(\omega)\widehat{S}_{jj}^*(\omega)} \tag{8}$$

where $\gamma_{ij}(\omega)$ is the coherence between channels i and j. Fig. 7 presents the estimated acceleration frequency response functions, or accelerances, as a function of distance for the two test setups along ML1 and ML2, along with the corresponding coefficient of variation. A low variation is found in the frequency band between 8 and 60 Hz that significantly contributes to the response at a given offset. As the source-receiver distance increases, the higher frequency waves are attenuated due to material damping leading to a lower signal to noise ratio and eventually no response is measurable for the highest frequencies considered, leading to a high variation in the estimates.

The estimated accelerances are transformed from the frequency-spatial domain to the frequency-wavenumber domain by applying the transformation [36]:

$$\widetilde{H}(k_r,\omega) = \frac{1}{2}\int_0^{\infty} \widehat{H}(r,\omega) H_0^{(1)}(k,r) r \, \mathrm{d}r \tag{9}$$

where $\widehat{H}(r,\omega)$ are the estimated frequency response functions as a function of the radial distance r from the source point, k_r is the radial

(a) (b)

Fig. 6. Experimental setup of (a) excitation point foundation and (b) accelerometer mounting.

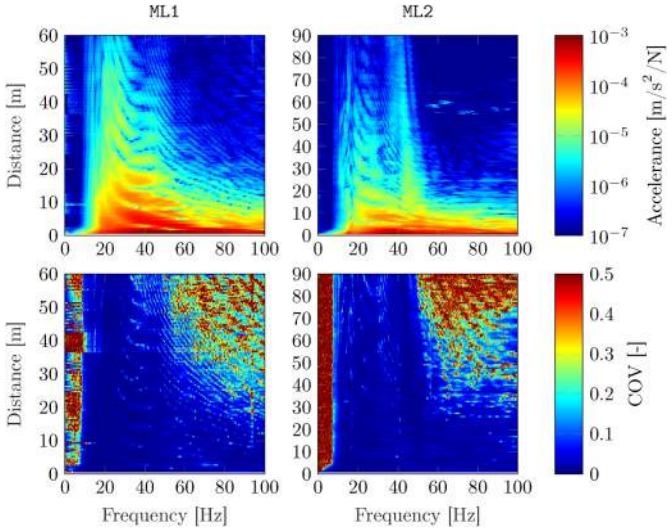

Fig. 7. Estimated accelerances and corresponding coefficients of variation for tests along measurement lines ML1 and ML2.

wave number and $H_0^{(1)}$ is the zero-th order Hankel function of the first kind. This transformation accounts for the cylindrical nature of the wave field when decomposing it into its plane wave components, and considers that the wave field consists solely of outing waves.

The integral of eq. (9) is numerically evaluated with a sampling of Δr corresponding to the distance in between the receivers and the integral is truncated at the array length. The evaluation of the integral is performed by the means of a generalized Filon quadrature scheme implemented in the Matlab toolbox EDT [37,38]. The resulting spectra are presented in Fig. 8 in terms of phase speed $C_r = \omega/k_r$ and frequency responses normalized for each frequency line.

4.3. Model inversion

The experimental measurements are subsequently post-processed to estimate the P- and S-wave speeds in the soil. The P-wave speeds are first estimated from a seismic refraction analysis based on the first arrival times at the receivers. The P- and S-wave speed, soil layer thickness and material damping ratios are subsequently obtained from a model inversion of the refraction, dispersion and attenuation curves. The dispersion curves of the surface waves are identified as peaks in the frequency-wavenumber spectra [39]. Surface waves attenuate due to both radiation and material damping. Material damping of surface waves results in a spatial decay of the surface waves proportional to $\exp(-A_n(\omega)r)$, where $A_n(\omega)$ is the attenuation coefficient of the associated surface wave mode n. The attenuation coefficients of the surface waves can be determined from the width of the peaks corresponding to the estimated dispersion curves. The half-power bandwidth and the circle fit method have been proposed as methods for estimating the attenuation coefficient from multiple dispersion curves [40,41]. Due to the presence of multiple dominant modes contributing to the response, apparent dispersion curves are determined by peak-picking in the frequency-phase speed spectra in Fig. 8 up to 60 and 46 Hz for ML1 and ML2, respectively. The attenuation curves are subsequently estimated using the half-power bandwidth method [40].

The theoretical dispersion and attenuation curves are obtained from the Green's functions for a horizontally layered soil on top of a halfspace computed using the direct stiffness method [42], which is a re-formulation of the Thomson-Haskell transfer matrix method [43,44]. The same soil model is used in section 6 to compute the free-field surface response. This is achieved by a Hankel transform of the Green's function from the frequency-wavenumber domain to the frequency-spatial domain which is implemented in the Matlab toolbox EDT [38]. The

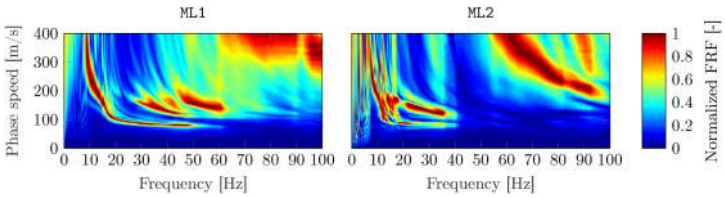

Fig. 8. Dispersion images normalized along each frequency line to the maximum value, for the tests along measurement lines ML1 and ML2.

assumption of a horizontally layered soil is justified based on the stratigraphy estimated from the soil investigations in Fig. 3, even if a small inclination of the layers is present [45].

The inverse problem is formulated as a non-linear least squares problem and is solved using a trust-region-reflective algorithm implemented in MATLAB [46], which is a local search method. Thereby, the problem suffers from non-uniqueness and the outcome strongly depends on the initial soil profile assumed. This is especially the case for soils that have an irregular variation of stiffness with depth [45]. Therefore, the initial soil profile is assigned considering the information available from the site investigations, including the stratification and the density of the clay. The densities of the till and bedrock were assumed as 2200 and 2700 kg/m^2, respectively. The initial S-wave speeds are heuristically obtained from the fundamental dispersion curve, relating the S-wave speed to the surface wave speed by $C_R = 1.1C_s$ and the representative depth as $z = \lambda_R/2.5$, with C_R and λ_R the surface wave speed and wavelength, respectively [47]. Due to the differences in the experimental dispersion curves, the soil properties of the profile obtained from the inversion along ML1 are used as an initial guess for the inversion along ML2, where the depth of the clay is adapted to be consistent with the observations made from the site investigations. Fig. 9 presents a comparison between the experimental dispersion and attenuation curves and the ones obtained from the inversion.

As the surface wave measurements cover a large portion of the soil, there is an inherent averaging over the distance covered by the measurement line. This can lead to differences between the identified profile from a model inversion and physical observations, as the inversion produces a horizontally layered soil model along the measurement line. Moreover, as the estimated profile is constructed by a discrete number of layers, averaging can occur over physical layer boundaries, especially when the stiffness contrast is low between the materials.

5. Synthesis of investigation results

Fig. 10 compares the S-wave speeds obtained from the empirical correlations with the ones obtained from the bender element, SCPT and SASW tests. The estimates from the CPT correlation agree closely with the results from the bender element tests and are also consistent with the SCPT results. Moreover, the variation in stiffness of the layers between 1 and 2 m predicted by both SASW tests are captured.

The empirical correlation of eq. (1) overestimates the S-wave speed in the upper 2 m of the soil but agrees with the other tests for the 3 and 4 m levels. Larsson and Mulabdić [12] noted that in comparison with SCPT results in Swedish clay, empirical relations tended to over-predict the initial shear modulus in the uppermost soil layers. For the present site, the estimated shear strengths obtained from the fall-cone and triaxial tests show large differences in the upper 2 m of the soil. In fact, employing the results obtained from the triaxial tests at the 1 and 2 m level yield, despite not being the basis for the empirical correlation, a better estimation of the S-wave speeds in line with the other tests. However, at the deeper levels the opposite holds demonstrating the significant influence of the chosen method to determine the shear strength on the estimated wave speeds.

For P13, a large scatter in the SCPT estimates obtained from the two setups is found in the upper 1.5 m of the soil. Generally, the upper part of a soil profile is not accurately estimated in the SCPT due to the small effective spacing of the sensors, even for synthetic signals [48]. Moreover, large amplitude impacts at the surface can induce shear strains in clays that are outside the range where the soil can be considered linear, violating the assumed test conditions [12]. Therefore, the results from the SCPT in the uppermost 1.5 m of the soil are considered less reliable.

It should be noted that none of the invasive methods to estimate the material wave speeds provide information of the top 1 m of the soil or the underlying till and bedrock. This is due to the practical limitations of the methods. Undisturbed samples were not practically attainable in the uppermost meter of the soil and the sampling is only applicable for the clay, as is the CPT and SCPT. In contrast, the surface wave methods provide estimates in the regions not covered by the invasive tests. The results indicate a significantly lower S-wave speed in the upper 0.8 m compared to the underlying layer, and provide estimates of the wave speeds in the till and the bedrock. Along ML1, a stiffer layer is estimated to be located closer to the surface than along ML2, agreeing with the observations made from the geotechnical site investigations, cf. Figs. 3 and 10. This emphasises the importance of considering the propagation path of interest for determining the soil properties by model inversion, as the stratification and layer depths affect the character of the wave propagation in the soil. However, the discrepancy between the estimated S-wave speeds in the till is large and should not be considered as the true material property, but rather as an effective value describing the wave propagation along the measurement line. The depth to bedrock is overestimated by the SASW test along ML2 compared to the physical observations. This is caused by the computed dispersion curve becoming insensitive to the position of the bedrock in the optimization problem.

Fig. 11 presents the P-wave speeds estimated from the two SASW and from the laboratory bender element tests.

The SASW tests estimate the P-wave speed in the upper meter of the soil to be significantly lower than the underlying soil, especially for the test along ML2. As the clay becomes saturated, the P-wave speed approaches the speed of sound in water and the Poisson's ratio becomes close to 0.5. It was observed during the site investigations that the clay is saturated at approximately 1 m below the surface. This is supported by the results from the bender element tests, indicating a P-wave speed in the clay of approximately 1200 m/s. The lower values obtained from the model inversions at depths below 2 m are therefore considered as inaccurate.

The material damping ratios estimated from the two model inversions agree closely, where the material damping ratios in volumetric (β_p) and deviatoric deformation (β_s) are assumed to be equal. The damping ratios β_p in the clay estimated from the P-wave bender element tests at the 2, 3 and 4 m depths are consistent with each other and

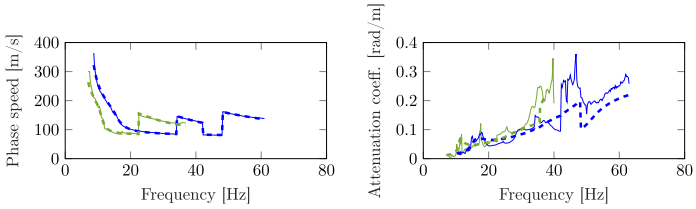

Fig. 9. Comparison of experimental (solid lines) and model (dashed lines) (a) dispersion and (b) attenuation curves for ML1 (blue) and ML2 (green). (For interpretation of the references to color in this figure legend, the reader is referred to the Web version of this article.)

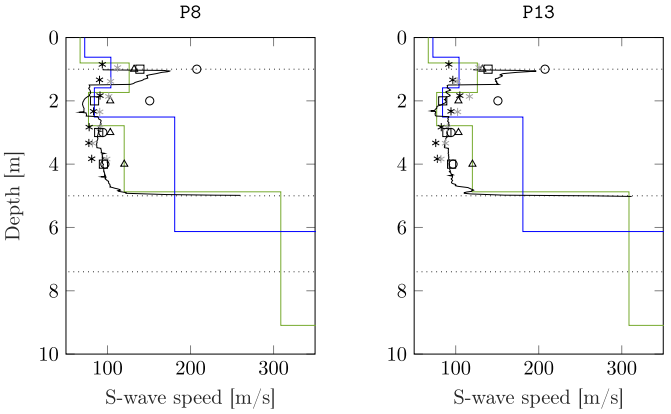

Fig. 10. S-wave speeds in points P8 and P13 estimated from empirical CPT correlation (black line) and SCPT (*) by hammer blows in the front (gray) and back (black) of the drill rig and observed layer boundaries (dotted lines). Estimates from SASW along ML1 (blue line) and ML2 (green line), empirical relation based on the shear strength from fall cone (○) and triaxial tests (△), and bender element laboratory tests in the vertical direction (□) obtained from samples taken at P13 are included for comparison. (For interpretation of the references to color in this figure legend, the reader is referred to the Web version of this article.)

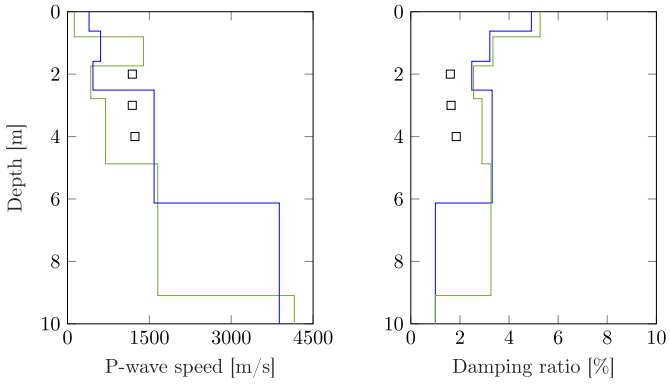

Fig. 11. P-wave speeds and material damping ratios estimated from SASW test along ML1 (blue line), ML2 (green line) and from bender element P-wave measurements estimated with the Hilbert transform method (□). (For interpretation of the references to color in this figure legend, the reader is referred to the Web version of this article.)

present lower values of the material damping compared to the ones obtained from the SASW tests. To accurately account for material damping becomes increasingly important with source-receiver distance, and is therefore especially relevant for predictions at significant distances with respect to the wavelengths of the propagating waves.

As the points P8 and P13 where the point wise investigations are performed are positioned along ML2, and the estimated profile obtained from the SASW test is in good agreement with the site observations, a representative layered soil model is assembled by synthesis of the estimated material parameters along ML2. Table 5 presents a summary of the soil properties synthesised from the tests. The P-wave speed of the top layer is inconsistently estimated from the two SASW tests carried out in different seasons and the difference in the estimated material damping ratios in the clay is significant. The influence of these material properties and seasonal variations on the surface response is therefore investigated next.

Table 5
Small-strain soil properties estimated for the soil profile along ML2 synthesised from the investigations.

Layer	Depth [m]	h [m]	C_s [m/s]	C_p [m/s]	β_s [−]	β_p [−]	ρ [kg/m^3]
1	0.80	0.80	67	125	0.053	0.053	1880
2	1.73	0.93	126	1200	0.017	0.017	1570
3	2.78	1.05	77	1200	0.017	0.017	1720
4	4.87	2.09	120	1200	0.017	0.017	1780
5	7.4	2.53	309	1654	0.033	0.033	2200
6	∞	∞	2236	4156	0.010	0.010	2700

6. Validation and physical interpretation

The synthesised model is validated against the measured frequency response functions along ML2. The comparison is made in terms of velocities and mobilities, where the mobilities are obtained from the

accelerance by divsion with iω.

To facilitate a comparison in the time domain, the computed and measured mobilities are subjected to an artificial band-limited impact load of similar character as employed in the measurements. The time- and frequency domain representations of the load are presented in Fig. 12.

6.1. Properties of the top soil layer

The estimated depths and S-wave speeds of the top soil layer are consistently estimated in the two SASW tests. However, the estimated P-wave speed differs substantially between the measurements. The influence on the computed response is therefore investigated by considering the P-wave speed of the first layer in Table 5 equal to the value C_{p1} = 395 m/s estimated from the SASW test along ML1.

Fig. 13 presents a comparison between experimental and computed mobilities, and time domain responses due to the impact load along ML2 at 30, 50, 70 and 90 m distance from the source.

The increased P-wave speed results only in slight differences for frequencies below 30 Hz at larger distances, while the responses predicted by the synthesised soil model at frequencies between 30 and 50 Hz are almost entirely absent. The time domain representation illustrates that this frequency content is related to the first arriving group of waves, which is also validated by the responses obtained from the measurement data. Fig. 7 in section 4.2 shows the measured accelerances along ML2. It presents a consistent peak in this frequency band showing, with a higher spatial resolution, a slow attenuation with distance and how this response is almost unaffected by wave interference at distances larger than 40 m.

Fig. 14 presents a comparison of the numerical and experimental mobility-frequency-phase speed spectra along ML2.

The synthesised soil model captures the relatively large contribution of dispersion curves with phase speeds higher than 1000 m/s at frequencies above 30 Hz in the spectrum obtained from the measurements. Assuming a higher P-wave speed in the top layer results, on the other hand, in a spectrum without this dispersion curve. The cut-off frequency of the dispersion curve associated with the P-wave speed of the first layer observed in Fig. 14 coincides with the resonance frequency of the fundamental eigenmode for vertically propagating P-waves of the top soil layer built in at its base $f_1 = C_{p1}/(4h_1) = 39$ Hz, with C_{p1} and h_1 the P-wave speed and thickness of the first layer, respectively. This is due to the high P-wave speed contrast between the top layer and the underlying ones. Moreover, Fig. 14 provides an indication of the wave speeds associated with the resonant response of the top layer. Higher frequency surface waves are generally attenuated more rapidly with distance compared to lower frequency waves due to material damping, as the effective attenuation is inversely proportional to the wavelength. However, the surface response observed above 30 Hz is not caused by a classical surface wave, but is a resonant response of the top layer due to P-waves refracted back towards the surface. P-waves that are critically refracted along the underlying layers travel at significantly higher speeds, and therefore with longer wavelengths, explaining the slow attenuation with distance in this frequency range. This phenomenon is further analysed in section 6.4.

To provide an overview of the topmost soil layer's influence on the attenuation with distance, the mobilities are represented in one-third-octave band spectra. Fig. 15 presents a comparison between sensors spaced by 5 m between 30 and 90 m source-receiver offset along the measurement line ML2, corresponding to distances longer than three wavelengths of the surface waves. Comparing Fig. 15a–c, it is evident that the slow attenuation with distance for the bands with center frequencies 31.5 and 40 Hz is only captured by the model where the top layer is present.

6.2. Elastic versus rigid bedrock

As the critically refracted body waves are amplified whenever the resonant frequency of the top layer falls within the frequency range of interest, considering the elasticity of the bedrock becomes important. As the bedrock is very stiff, a common assumption in modelling situations is to consider the bedrock as a rigid stratum. Fig. 16 presents a comparison of the responses computed at a 90 m source-receiver offset assuming the bedrock as an elastic halfspace and as rigid.

The response is identical at the lower frequencies associated with the surface waves. However, due to the lack of a bottom interface where waves are critically refracted, a substantially lower response is observed for higher frequencies when assuming the bedrock as a rigid stratum, demonstrating that this assumption cannot be motivated under the investigated soil conditions whenever larger source-receiver distances are of interest.

6.3. Material damping in the clay

The bender element tests are conducted on a very small specimen of the soil and at a much higher frequency than the range of interest, while the SASW tests yield estimates of the material damping based on data obtained over a larger body of soil and in situ conditions, but are sensitive to non-uniqueness. Therefore, the estimated values are uncertain and their influence on the predicted responses is investigated. Figs. 17 and 18 present a comparison between the measurements and the computed responses at the center and endpoints of ML1 and ML2, assuming the material damping in the clay according to the results from the bender elements test and the SASW inversions.

The model predictions assuming a material damping in the clay derived from the bender element tests yield more accurate predictions of amplitudes of the surface waves along both measurement lines, while the higher frequency content related to the refracted P-waves is less affected. These results suggest that reasonable estimates of damping values in homogeneous clays for performing vibration predictions can be obtained from bender element tests performed on standard size samples. However, further research is needed to confirm this conclusion.

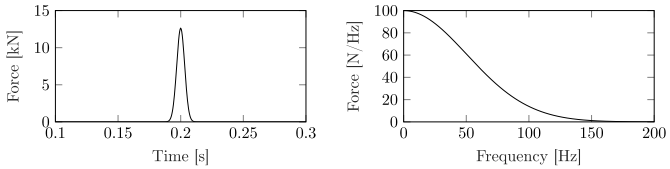

Fig. 12. Time-shifted Gaussian distribution applied as artificial impact load, (a) time and (b) frequency domain representation.

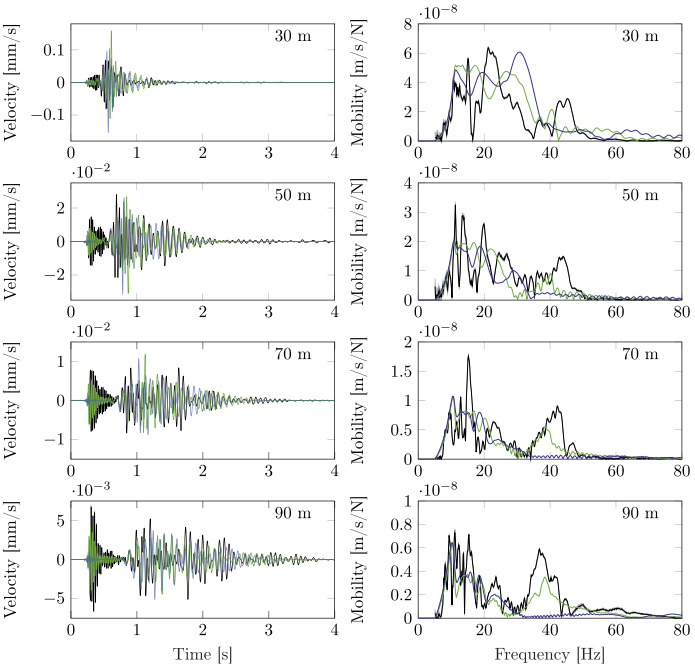

Fig. 13. Comparison of experimental and model results of time domain velocity responses due to a simulated impact (left) and mobilities (right) at 30, 50, 70 and 90 m from the source point along ML2. Responses are obtained from measurements (black) with 95% confidence bounds indicated, the synthesised soil model (green) and a soil model with an increased top layer P-wave speed (blue). (For interpretation of the references to color in this figure legend, the reader is referred to the Web version of this article.)

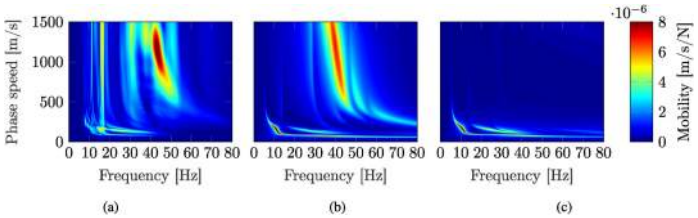

Fig. 14. Comparison of mobility-frequency-phase speed spectra along ML2 obtained from (a) measurements, (b) soil model with $C_{p1} = 125$ m/s and (c) soil model with $C_{p1} = 395$ m/s.

6.4. Sensitivity analysis of soil layer properties

Sections 6.1 and 6.2 compared the measured and computed surface responses and demonstrated the influence of the elastic properties of the dry top layer and the bedrock on the predicted response at the site. Schevenels et al. [49] showed that the layering introduced by the presence of the groundwater table in an otherwise homogeneous soil results in the existence of wave reflections, critically refracted waves and standing P-waves in the dry layer that influence the surface response. At the test site investigated in this paper, a large amplification is observed for the frequencies where standing P-waves develop in the dry layer due to the existence of a shallow bedrock with significantly higher material wave speeds than the soil.

In the following, the influence of soil layer thicknesses and the bedrock stiffness on the surface response is addressed to demonstrate the relevance of the observed phenomenon for sites with similar soil conditions. The soil profile identified for the test site is aimed at representing as closely as possible the dynamic behaviour of the soil. However, to facilitate understanding of the system, a simplified three layer model is considered to more clearly highlight the influence of the layering. Table 6 presents the soil properties assumed for the three layer soil model under consideration.

Four cases of parameter variations are considered to demonstrate the influence on the computed mobilities at a 90 m source-receiver offset. In order to avoid confounding, material damping ratios of all layers are set equal. In all cases where the P-wave speed is altered, Poisson's ratio is kept constant and the S-wave speed is changed accordingly.

First, the thickness of the top soil layer is investigated. Fig. 19a presents the effect of increasing only the thickness of the top layer, demonstrating the direct influence it has on the response with peaks

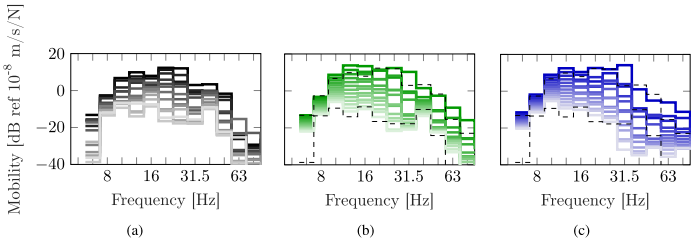

Fig. 15. One-third-octave band spectra for 13 equidistant points between 30 and 90 m source-receiver offset (dark to light) obtained from (a) measurements along ML2, (b) the synthesised soil model and (c) the soil model assuming $C_{p1} = 395$ m/s. The envelope of the measurements is superimposed on the simulation results for comparison (black dashed lines).

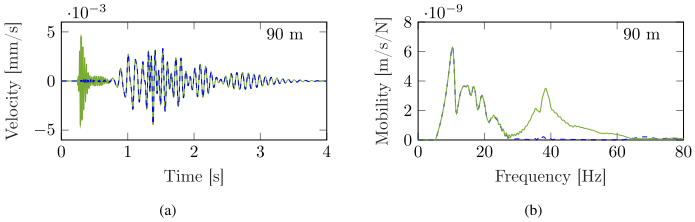

Fig. 16. Comparison of simulated (a) time domain velocity responses due to an impact load and (b) mobilities at 90 m from the source point assuming the bedrock as elastic (green) and as rigid (blue). (For interpretation of the references to color in this figure legend, the reader is referred to the Web version of this article.)

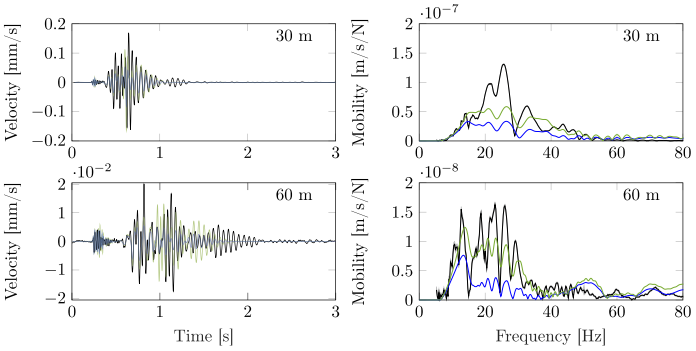

Fig. 17. Comparison of experimental and model results of time domain velocity responses due to a simulated impact (left) and mobilities (right) at the center and endpoint of ML1. Responses are obtained from measurements (black) with 95% confidence bounds indicated, a soil model assuming damping values in the clay obtained from bender element tests (green) and from the SASW inversions (blue). (For interpretation of the references to color in this figure legend, the reader is referred to the Web version of this article.)

corresponding to the resonance frequencies of a layer built in at its base $f_n = C_{p1}/4h_1(2n-1)$. Fig. 19b shows the influence of the same variation of layer thickness but with a constant resonance frequency of the top layer by adjustment of the P-wave speed. In contrast to Fig. 19a, the resonance peaks occur at the same frequency but present different amplitudes. This is due to the increase of the mass in the top layer with an increasing layer thickness, causing a reduction in amplitude of the layer resonance.

Second, the influence of increasing the depth of the saturated clay layer is illustrated in Fig. 20a, showing that as the layer thickness increases the resonance in the top layer remains present and no significant decrease of magnitude is observed for the considered depths and source-receiver distance. Third, Fig. 20b shows the influence of the bedrock wave speed. When the P-wave speed of the bedrock is equal to that of the saturated soil, the resonance peak diminishes. On the other hand, when refraction in the bedrock is possible the response of the top layer is significant, demonstrating the contribution from refracted waves to the total response in this frequency range.

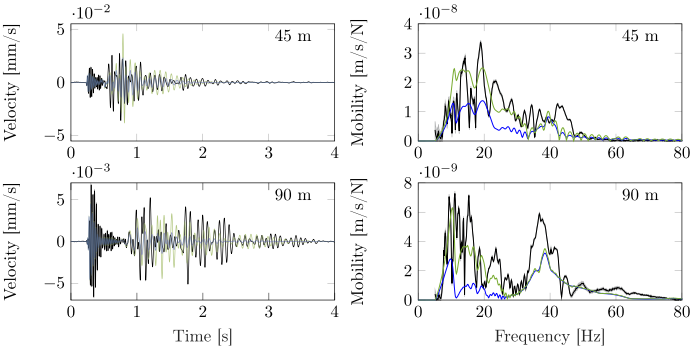

Fig. 18. Comparison of experimental and model results of time domain velocity responses due to a simulated impact (left) and mobilities (right) at the center and endpoint of ML2. Responses are obtained from measurements (black) with 95% confidence bounds indicated, the synthesised soil model (green) and a soil model assuming damping values from the SASW inversions (blue). (For interpretation of the references to color in this figure legend, the reader is referred to the Web version of this article.)

Table 6
Small-strain soil properties of a simplified three layer model used for sensitivity analysis.

Layer	h	C_s	C_p	β_s	β_p	ρ
	[m]	[m/s]	[m/s]	[−]	[−]	[kg/m^3]
1	0.80	70	125	0.03	0.03	1700
2	7	90	1200	0.03	0.03	1700
3	∞	2000	3600	0.03	0.03	2700

7. Seasonal variations

In the measurements, the response associated with the uppermost soil layer is not as pronounced along ML1 as along ML2, and the SASW along ML1 leads to a higher estimated P-wave speed than along ML2. It is here noted that the tests were performed along ML1 in the spring under dry conditions and along ML2 in the autumn under wet conditions with a higher moisture content in the soil at the surface. This leads to the hypothesis that seasonal variations affect the mechanical properties, and therefore the dynamic response, of the soil. Additional measurements have been performed at the site at different occasions and during different seasons. The temperature was not below 0 °C and there was no freezing of the soil at any of the occasions. Fig. 21 presents the response at point P10 due to a load applied at P8, with reference to Fig. 1 in section 2. The excitation was applied to a 0.5 × 0.5 × 0.2 m cast-in place concrete foundation and the sensor mount was left in place in between the measurements. The response at lower frequencies is unaltered in between the measurements, while for frequencies above 20 Hz, a

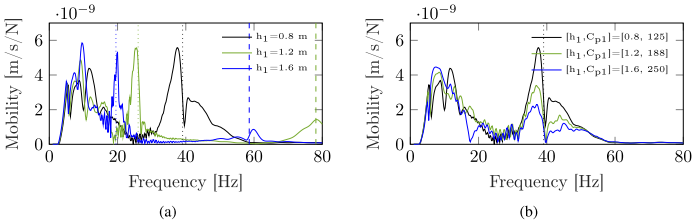

Fig. 19. Mobilities at the soil's surface at 90 m source-receiver distance assuming (a) different values of the top layer thickness and (b) adjusting the P-wave speed accordingly to obtain the same layer resonance frequency. The first (vertical dotted lines) and second (vertical dashed lines) layer resonance frequencies of a layer built in at it's base are indicated.

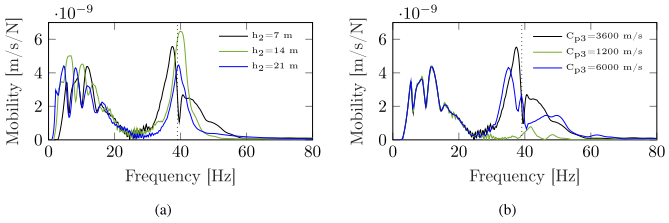

Fig. 20. Mobilities at the soil's surface at 90 m source-receiver distance assuming (a) different depths of the saturated clay and (b) different P-wave speeds of the elastic bedrock. The first layer resonance frequency (vertical dotted line) of a layer built in at it's base is indicated.

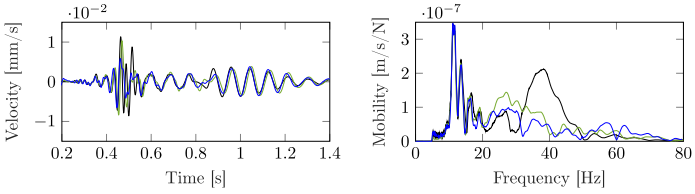

Fig. 21. Measurements performed in November (black), June (dark gray) and September (light gray) between points P8 and P10 presented as (a) time domain velocity responses due to an impact load and (b) mobilities.

difference in the response is observed between all three measurements. These observations show that seasonal variations change the dynamic response of the soil in this frequency range, associated with the resonance of the top layer treated in section 6.1 and more shallow penetration depths of the surface waves. Possible explanations for the observed variations are the moisture in the top part of the soil, closing micro fissures in the dry crust, and variation of the depth to where the clay becomes fully saturated. The ground water level was measured in the underlying non-cohesive soil at the time of each measurement, with reference to the ground surface. The ground water level varied from 1.75 m in November to 0.65 and 0.85 in June and September, respectively. As the depth to the saturated clay governs the resonance frequency of the top layer, the depth to the saturated clay is a possible explanation for the observed variations.

8. Conclusion

This paper presents an extensive site characterization of a Swedish clay deposit by geotechnical and seismic measurements to estimate material wave speeds and material damping in the soil for the prediction of environmental vibrations using a layered soil model. The soil conditions at the test site consist of a shallow soft clay underlain by till and a stiff bedrock. The stratigraphical layout over the area of investigation is estimated based on geotechnical site investigations whereas the soil is characterised from laboratory analyses of piston samples. Estimation of the wave speeds in the soil are obtained from empirical relations, bender element measurements in the vertical and horizontal directions, SCPT and two active surface wave measurements. The surface wave measurements are used to perform refraction analyses and model inversions of dispersion and attenuation curves (SASW), allowing to estimate layer thicknesses, material wave speeds and damping ratios.

The S-wave speeds estimated in the clay by SASW, SCPT, CPT empirical correlations and bender element tests are consistent while the empirical relation based on the shear strength derived from the fall-cone test and the plasticity index overestimates the wave speeds in the upper 2 m of the soil. CPT correlations provide satisfactory estimates for the S-wave speed in the clay under the studied conditions, and yield the most accurate estimation of S-wave speeds in the soil whenever dynamic measurements are unavailable. The material damping ratios of the soil are estimated from two SASW tests yielding consistent results, and from the free vibration of samples excited in axial motion using bender elements, yielding lower values for the saturated clay. It is demonstrated that the material damping measured in the laboratory leads to a closer agreement between predicted and measured responses for the identified soil profile.

Only the surface wave measurements are able to provide estimates of the wave speeds in the top part of the soil, the till underlying the clay and the bedrock. The estimated properties of the uppermost soil are found to have a profound influence on the vertical surface response in a narrow frequency band related to the fundamental resonance frequency of the upper soil layer for vertically propagating P-waves, especially with an increasing source-receiver distance. This is caused by the large P-wave speed contrast between the topmost part of the soil and the underlying fully saturated clay. Model investigations demonstrate that the observed resonance peak is caused by the critically refracted P-waves along the interfaces of the underlying layers of soil and the elastic bedrock, resulting in a slow attenuation with distance due to the long wavelengths involved. The observed resonance effect is found, however, to be of varying magnitude when measured during different seasons, suggesting that seasonal variations can have an influence on the properties of the topmost soil and therefore also on the soil's dynamic surface response.

Author statement

The experimental and numerical works as well as the writing of the paper have been performed by the first author. The other authors contributed in the planning of the work, the discussion about the results and the reviewing of the paper.

Declaration of competing interest

The authors declare that they have no known competing financial interests or personal relationships that could have appeared to influence the work reported in this paper.

Acknowledgements

This work was supported by the Swedish Building, Development and Research fund (SBUF). The funding for experiments and site investigations was received from Vinnova, the Richertska foundation and Trafikverket. The financial support is gratefully acknowledged. The authors would like to thank the Swedish Geotechnical Institute (SGI) and Martin Holmén for providing the laboratory analysis of the soil samples. Freddie Theland would like to acknowledge the help of Lola Martínez-Rodrigo, Stefan Trillkott, Abbas Zangeneh and Andréas Andersson in conducting the dynamic site measurements. Finally, the authors would like to extend their gratitude towards Ragnvald Andersson for granting unlimited access to the test site used in this work.

References

[1] Lombaert G, Degrande G, Clouteau D. The influence of the soil stratification on free field traffic-induced vibrations. Arch Appl Mech 2001;71:661–78.
[2] Kouroussis G, Conti C, Verlinden O. Investigating the influence of soil properties on railway traffic vibration using a numerical model. Veh Syst Dyn 2013;51:421–42.
[3] ISO 14837-1:2005. Mechanical vibration – ground-borne noise and vibration arising from rail systems – Part 1: general guidance, Standard. Geneva, CH: International Organization for Standardization; 2005.
[4] Hanson CE, Ross JC, Towers DA. High-speed ground transportation noise and vibration impact assessment, technical report. Federal Railroad Administration; 2012.

[5] Connolly D, Marecki GP, Kouroussis G, Thalassinakis I, Woodward P. The growth of railway ground vibration problems - a review. Sci Total Environ 2016;568:1276–82.

[6] Lombaert G, Degrande G, Kogut J, François S. The experimental validation of a numerical model for the prediction of railway induced vibrations. J Sound Vib 2006;297:512–35.

[7] Kouroussis G, Verlinden O, Conti C. Free field vibrations caused by high-speed lines: measurement and time domain simulation. Soil Dynam Earthq Eng 2011;31:692–707.

[8] Connolly D, Alves Costa P, Kouroussis G, Galvin P, Woodward P, Laghrouche O. Large scale international testing of railway ground vibrations across europe. Soil Dynam Earthq Eng 2015;71:1–12.

[9] Bahrekazemi M. Train-induced ground vibration and its prediction. Ph.D. thesis, KTH Royal Institute of Technology; 2004.

[10] Hunaidi O, Tremblay M. Traffic-induced building vibrations in Montréal. Can J Civ Eng 1997;24:736–53.

[11] Svensson M, Möller B. Geophysics in soil mechanics - in situ shear moduli determined by SASW-technique and more traditional geotechnical methods, Technical Report. SGI - Swedish Geotechnical Institute; 2001.

[12] Larsson R, Mulabdić M. Shear moduli in Scandinavian clays. Measurement of initial shear modulus with seismic cones. Empirical correlations for the initial shear modulus in clay,. Swedish Geotechnical Institute; 1991. Technical Report 40.

[13] Wood T. On the small strain stiffness of some scandinavian soft clays and impact on deep excavations. Chalmers University of Technology; 2016. PhD. thesis.

[14] Adolfsson K, Andréasson B, Bengtsson P-E, Bodare A, Madshus C, Massarsch K, Wallmark G, Zackrisson P. High speed lines on soft ground. Evaluation and analyses of measurements from the West Coast Line Part 1-2. Banverket: Technical Report; 1999.

[15] Madshus C, Kaynia A. High-speed railway lines on soft ground: dynamic behaviour at critical train speed. J Sound Vib 2000;231:689–701.

[16] Hall L, Bodare A. Analyses of the cross-hole method for determining shear wave velocities and damping ratios. Soil Dynam Earthq Eng 2000;20:167–75.

[17] Hall L. Simulations and analyses of train-induced ground vibrations in finite element models. Soil Dynam Earthq Eng 2003;23:403–13.

[18] Paolucci R, Maffeis A, Scandella L, Stupazzini M, Vanini M. Numerical prediction of low-frequency ground vibrations induced by high-speed trains at Ledsgaard, Sweden. Soil Dynam Earthq Eng 2003;23:425–33.

[19] Google Earth Pro V.7.3.3.7786. Brottby, Sweden, march 19, 2020. 59°35'24.3"N 18°10'26.0"W, eye alt 383 m. Maxar Technologies. http://www.earth.google.com. [Accessed 21 September 2020].

[20] SGU. Map viewer, 21; 2020. p. 2020. Retrived September.

[21] SGF, Geoteknisk fälthandbok. Technical report. Swedish Geotechnical Society; 2013.

[22] ISO 22476-15:2016. Geotechnical investigation and testing – field testing – Part 15: measuring while drilling. Geneva, CH: Standard, International Organization for Standardization; 2016.

[23] Areias L, Van Impe FW. Effect of travel path in the SCPT test method. In: GeoShanghai International Conference; 2006. p. 236–42.

[24] ISO 22475-1:2006. Geotechnical investigation and testing – sampling methods and groundwater measurements – Part 1: technical principles for execution, Standard. Geneva, CH: International Organization for Standardization; 2006.

[25] ISO 14688-1:2017. Geotechnical investigation and testing – identification and classification of soil – Part 1: identification and description, Standard. Geneva, CH: International Organization for Standardization; 2017.

[26] ISO 14688-2:2017. Geotechnical investigation and testing – identification and classification of soil – Part 2: principles for a classification, Standard. Geneva, CH: International Organization for Standardization; 2017.

[27] Larsson R, Sällfors G, Bengtsson P-E, Alén C, Bergdahl U, Eriksson L. Skjuvhållfasthet - utvärdering i kohesionsjord. Swedish Geotechnical Institute; 2007. Technical Report 3.

[28] Park J, Kaynia AM. Stiffness matrices for fluid and anisotropic soil layers with applications in soil dynamics. Soil Dynam Earthq Eng 2018;115:169–82.

[29] Cheng Z, Leong E. Determination of damping ratios for soils using bender element tests. Soil Dynam Earthq Eng 2018;111:8–13.

[30] ISO 14837-32:2015. Mechanical vibration – ground-borne noise and vibration arising from rail systems – Part 32: measurement of dynamic properties of the ground, Standard. Geneva, CH: International Organization for Standardization; 2015.

[31] Mayne PW, Rix GJ. $G_{max} - q_c$ relationships for clays. Geotech Test J 1993;16:54–60.

[32] Hunaidi O, Rainer JH. Evaluation of measurement limits of transducer mountings in the ground. Canadian Acoustics; 1990.

[33] Degrande G, Van den Broeck P, Clouteau D. A critical appraisal of in situ vibration measurements. 3rd European conference in structural dynamics. Florence: Balkema; 2014. p. 1107–16.

[34] Heylen W, Lammens S, Sas P. Modal analysis theory and testing, division of production engineering, machine design and automation. Katholieke Universiteit Leuven; 1994.

[35] Bendat J. Statistical errors in measurement of coherence functions and input/output quantities. J Sound Vib 1978;59:405–21.

[36] Forbriger T. Inversion of shallow-seismic wavefields: I. Wavefield transformation. Geophys J Int 2003;153:719–34.

[37] Frazer LN, Gettrust JF. On a generalization of Filon's method and the computation of the oscillatory integrals of seismology. Geophys J Roy Astron Soc 1984;76:461–81.

[38] Schevenels M, François Stijn, Degrande G. EDT: an ElastoDynamics toolbox for MATLAB. Comput Geosci 2009;35:1752–4.

[39] Park CB, Miller RD, Xia J. Multichannel analysis of surface waves. Geophysics 1999;64:800–8.

[40] Badsar SA, Schevenels M, Haegeman W, Degrande G. Determination of the damping ratio in the soil from sasw tests using the half-power bandwidth method. Geophys J Int 2010;182:1493–508.

[41] Verachtert R, Lombaert G, Degrande G. Multimodal determination of Rayleigh dispersion and attenuation curves using the circle fit method. Geophys J Int 2017;212:2143–58.

[42] Kausel E, Roësset JM. Stiffness matrices for layered soils. Bull Seismol Soc Am 1981;71:1743–61.

[43] Thomson WT. Transmission of elastic waves through a stratified solid medium. J Appl Phys 1950;21:89–93.

[44] Haskell NA. The dispersion of surface waves on multilayered media. Bull Seismol Soc Am 1953;43:17–34.

[45] Verachtert R. Deterministic and probabilistic determination of dynamic soil characteristics. KU Leuven, Department of Civil Engineering; 2017. PhD. thesis.

[46] MATLAB optimization toolbox, Matlab optimization toolbox. Natick, MA, USA: The MathWorks; 2019.

[47] Abbiss CP. Shear wave measurements of the elasticity of the ground. Geotechnique 1981;31:91–104.

[48] Karl L, Haegeman W, Degrande G. Determination of the material damping ratio and the shear wave velocity with the seismic cone penetration test. Soil Dynam Earthq Eng 2006;26:1111–26.

[49] Schevenels M, Degrande G, Lombaert G. The influence of the depth of the ground water table on free field road traffic-induced vibrations. Int J Numer Anal Methods GeoMech 2004;28:395–419.

Paper II

Engineering Structures 267 (2022) 114629

Contents lists available at ScienceDirect

Engineering Structures

journal homepage: www.elsevier.com/locate/engstruct

Dynamic response of driven end-bearing piles and a pile group in soft clay: an experimental validation study

Freddie Theland [a,*], Geert Lombaert [b], Stijn François [b], Costin Pacoste [a,c], Fanny Deckner [d], Peter Blom [e], Jean-Marc Battini [a]

[a] KTH Royal Institute of Technology, Division of Structural Engineering and Bridges, Brinellvägen 23, 100 44 Stockholm, Sweden
[b] KU Leuven, Department of Civil Engineering, Kasteelpark Arenberg 40, 3001 Leuven, Belgium
[c] ELU Konsult AB, Valhallavägen 117, 115 31 Stockholm, Sweden
[d] GeoMind KB, Hesselmans Torg 5, 131 54 Nacka, Sweden
[e] ACAD International AB, Sveavägen 151, 113 46 Stockholm, Sweden

ARTICLE INFO

Keywords:
End-bearing piles
Dynamic impedance
Soil–structure interaction
Pile group
Environmental vibration
Pile–soil–pile interaction

ABSTRACT

This paper presents novel measurement data on the dynamic soil–structure interaction of an end-bearing pile foundation. The purpose is to assess the ability to predict the foundation impedances based on the small-strain properties of the soil obtained from site investigations. Measurements were performed in two stages of construction, allowing to assess interaction between the piles through the soil. First, single pile impedances and interaction factors between the piles were experimentally obtained for the four piles when they were free to move at the surface. Second, the impedances of the square pile group were measured after casting a concrete pile cap. The piles were additionally instrumented with accelerometers at depth along the centerline of each pile, allowing to illustrate the global behaviour of the piles within the soil. Numerical predictions based solely on information of the small-strain soil properties obtained from extensive site investigations are compared to the experimental results. The impedances of the individual piles are overestimated compared to the measurements, while the interaction factors show a better agreement. The pile group impedances are better captured than the individual ones, using the same soil model. The pile–soil–pile interaction is clearly manifested in the experimental results by pronounced peaks in the pile group vertical impedance, validating results from previous numerical studies.

1. Introduction

Dynamic soil–structure interaction can have an important influence on the dynamic structural response for applications in earthquake engineering, railway bridge dynamics, machine foundation design and environmental vibration assessment. In Sweden, the geological conditions generally consist of clay, silt or sand overlaying a densely compacted moraine (till) and crystalline bedrock. Formations of cohesive soils are often found in the more densely populated regions and major cities. These site conditions motivate the use of driven end-bearing piles for foundation design, where prefabricated concrete piles are predominantly used [1,2].

Under the assumption of small deformations in the soil, soil–structure interaction can be modelled using a linear elastic model, which allows for separation of the soil-foundation system from the overlying structure in a substructuring scheme [3]. The interaction between the foundation and the soil can be condensed into dynamic impedance functions, characterising the effective stiffness and damping of the soil-foundation system that can subsequently be coupled to an overlying structure. The computation of the dynamic impedance functions of pile foundations from analytical and numerical models have been extensively treated in the literature, showing the significant influence of the interaction between piles through the soil. However, there is lack of experimental evidence of the validity of models of end-bearing piles and pile groups in shallow formations of soils over bedrock, where the distribution of pile displacements differ from the case of floating piles and layer resonances can influence the dynamic response. Existing modelling strategies to obtain the impedances of pile foundations include simplified models providing approximate pile group impedances by superposition of pile–soil–pile interaction factors [4–8], hidden

* Corresponding author.
E-mail addresses: freddie.theland@byv.kth.se (F. Theland), geert.lombaert@kuleven.be (G. Lombaert), stijn.francois@kuleven.be (S. François), costin.pacoste@elu.se (C. Pacoste), fanny.deckner@geomind.se (F. Deckner), peter.blom@acad.se (P. Blom), jean-marc.battini@byv.kth.se (J.-M. Battini).

https://doi.org/10.1016/j.engstruct.2022.114629
Received 10 December 2021; Received in revised form 9 May 2022; Accepted 30 June 2022
Available online 26 July 2022

state variable models [9], Beam-on-dynamic Winkler foundation approaches [10,11] as well as more rigorous solutions using boundary integral, boundary- and finite element model formulations [12–14]. Models have facilitated the analysis of the dynamic behaviour of piles and pile groups, and led to a deeper understanding of the factors influencing the dynamic impedances of piles and pile groups. Gazetas and Makris [15] demonstrated that the main features of pile–soil–pile interaction that influence the vertical and horizontal [16] impedances of pile groups are governed by the pile-to-pile spacing and the small-strain properties of the soil, resulting in a dramatic increase in group stiffness and damping values at certain frequencies. It was also shown that the variation of soil properties with depth can substantially influence the predicted group impedances as it influences the wave field generated by the excited piles. Therefore, an accurate representation of the soil is crucial for the prediction of the dynamic foundation impedances. Padrón et al. [13] used a coupled finite element-boundary element model to present a set of dynamic impedance functions for end-bearing pile groups and a comparison to their floating counterpart for square foundations with 2×2 and 3×3 vertical and battered piles in homogeneous soil deposits. The presence of bedrock was shown to influence the dynamic vertical and rotational impedances of the pile groups substantially, especially for soft soils, while the horizontal impedance was only significantly affected for configurations where piles were inclined.

To confide in the results derived from models, validation by experiments is necessary. A number of experimental studies have been performed under field conditions to validate numerical predictions of the response of floating single piles [17–21] and pile groups in cohesive [22–27] and non-cohesive soils [28–32]. The majority of the experimental studies in the literature have been focused on the excitation and response in the lateral direction and only a handful of experimental results have been presented for the vertical response of pile groups. Novak and Grigg [33] performed experiments on single piles and 2×2 pile groups driven in a soil consisting of silty sand and till to analyse the response due to both vertical and lateral excitations. Variation of the soil's shear modulus with depth and the floating condition at the pile tip were found to be important factors to take into account when comparing the measurements to results obtained from a numerical model. Manna and Baidya [34] performed an experimental study on the non-linear vertical response of cast in situ piles and a 2×2 pile group and compared the results to numerical simulations using an equivalent linear approach with a weakened boundary zone closest to the piles, finding a reasonable agreement. Capatti et al. [35] performed extensive dynamic testing to characterise the translational and rotational response of a 2×2 pile foundation with inclined steel micropiles in an alluvial silt subjected to different amplitudes of dynamic loading. The piles were instrumented with strain gauges and the natural frequencies of the system and the deformation of the piles were found to be influenced by gapping of the most superficial soil, induced by the high amplitude dynamic loads. In a series of small-scale laboratory experiments in a sand [36–39], lateral pile–soil–pile interaction and pile group impedance were studied, considering the influence of non-linear loading conditions. Interaction factors were established for different load amplitudes and compared to linear theory. Dezi et al. [40] measured the response of three large-diameter steel pipe piles installed at a near-shore location in a marine clay when subjected to controlled impact loading, allowing to characterise the interaction between the piles through the soil under field conditions.

In the aforementioned experiments, interaction effects associated with a group stiffness larger than the sum of the stiffnesses of the individual piles are either expected to occur outside the considered frequency range or were not discussed. Therefore, there is a need to experimentally verify, in a full scale setting, the existence of these interaction phenomena predicted by theory. Moreover, while numerical results for end-bearing piles and pile groups have been presented in the literature [13,41], to the best of the authors' knowledge, no experimental studies have been published where a complete set of dynamic impedance functions is presented for an end-bearing pile foundation.

This paper presents the results from an extensive experimental measurement campaign of the dynamic response and impedances of a full scale concrete foundation supported by pre-cast impact driven end-bearing concrete piles installed in a soft clay deposit. The objectives of this paper are twofold. First, to present measurement data on the small-strain dynamic pile–soil–pile interaction and the impedances of end-bearing impact driven concrete piles and a pile group under typical Swedish soil conditions. The novelty of the experiments consists in the specific foundation and site conditions, where a full scale end-bearing pile foundation in soft clay is considered, and the extensive set of measurements performed during different stages of construction of the pile group, allowing to analyse the interaction between the piles and to verify its influence on the dynamic properties of the pile group experimentally. Second, to assess the ability of a linear elastic soil model to predict the dynamic characteristics of the soil-foundation system, using the small-strain soil properties obtained from site investigations. Here, it should be emphasised that a design condition has been considered. The numerical predictions are obtained from a model based solely on the performed soil investigations. No attempt to update this model to better match the experimental results has been performed. This corresponds to a class A prediction in accordance with the classification of predictions in geotechnical engineering proposed by Lambe [42].

The structure of the paper is as follows. Section 2 gives an overview of the test site and the identified small-strain properties at the site. Section 3 motivates and describes the design of the pile group. Section 4 presents a finite element model of the soil-foundation system. Section 5 presents the equipment, experimental setups and the post-processing of the measurements. Section 6 thereafter presents the dynamic responses and impedances of the free-top piles and the pile group and compares the measurements to numerical predictions. Section 7 concludes the paper.

2. Test site

2.1. Site overview

The test site is located 40 km north of Stockholm, Sweden. The site is a remotely located agricultural field that has not been cultivated for more than ten years prior to the experiments. It was chosen because of its particular stratification, with a soft clay underlain by till and bedrock, the possibility to represent the soil using a horizontally layered soil model and that unlimited access to the site could be granted. The soil conditions are representative for sites where impact driven piles are used. Moreover, as the site is located in a remote location, a minimum of environmental background vibration is present during testing. Fig. 1 presents an overview of the site and two sections of the soil interpreted from the site investigations, where the location of the pile group is indicated.

2.2. Soil conditions and small-strain properties

Extensive geotechnical and geophysical site investigations have been performed at the site. The geotechnical investigations consisted of weight soundings, soil-rock probing, cone penetration tests (CPT) and laboratory analysis of piston samples. The soil conditions at the site consist of 1 m dry crust clay followed by homogeneous gray, slightly varved clay with infusions of sand and silt up to 4.9 m depth where a sandy gravelly till overlays the bedrock to a depth of 7.4 m. The small-strain properties of the soil have been determined from in situ wave speed measurements by seismic cone penetration tests (SCPT) and spectral analysis of surface waves (SASW) performed at the location where the pile group is constructed. In addition, bender element tests have been performed on clay piston samples collected at the location

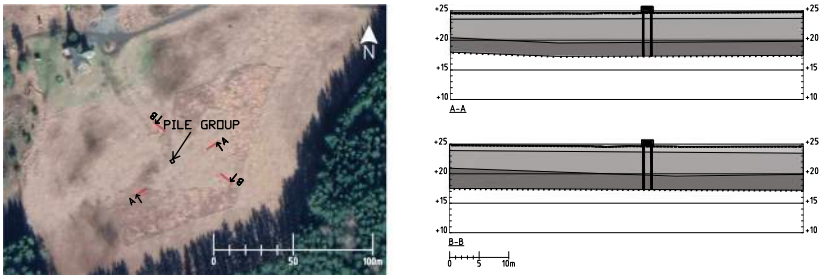

(a) (b)

Fig. 1. Overview of the site with (a) an aerial photography [43] with the location of the pile group indicated and (b) two sections with the stratification interpreted from geotechnical site investigations with a layering of dry crust clay (light gray), saturated soft clay (medium gray) and till (dark gray) on top of a stiff bedrock.

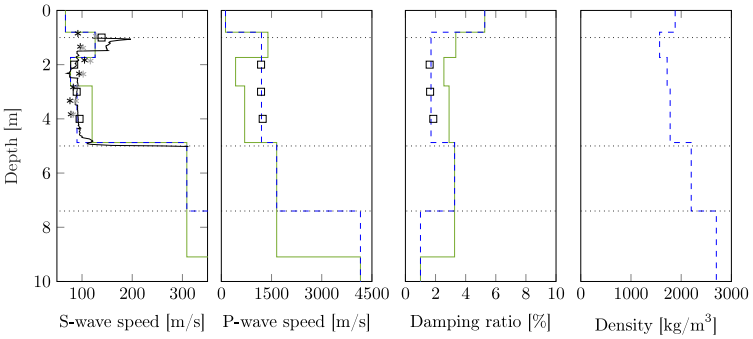

Fig. 2. Small-strain dynamic soil properties estimated from bender element tests (□), SCPT (*), empirical correlation with CPT (black line) and SASW (green line). A representative synthesised soil model (blue dashed line) taking into account the layer boundaries identified from soil/rock probing (dotted lines) is presented. (For interpretation of the references to color in this figure legend, the reader is referred to the web version of this article.)

where the pile group is constructed, to obtain estimates of material wave speeds and damping ratios. Empirical correlation with a CPT performed next to the point where the samples were collected has also been considered. Fig. 2 presents the estimated small-strain soil properties obtained from the different methods. A detailed description of the site investigations and evaluation of the estimated properties was given in Theland et al. [44]. The soil properties estimated using different methods are consistent in the upper three meters, but the deepest layer of clay is estimated to be stiffer by the SASW than by the other methods. Due to the larger body of soil covered by the SASW test, the spatial variability of the soil properties over the test area can affect the estimated soil profile, explaining the observed inconsistency. As the point wise investigations are in close agreement and were performed at the location where the piles were driven, the properties derived from these tests are considered as most reliable at this specific location. Table 1 presents the properties of the profile synthesised from the investigations that are used for modelling the soil.

Table 1
Estimated small-strain soil properties based on dynamic site and laboratory investigations.

Description	Layer	Depth [m]	h [m]	C_s [m/s]	C_p [m/s]	β_s [−]	β_p [−]	ρ [kg/m^3]
Dry crust clay	1	0.80	0.80	67	125	0.053	0.053	1880
Clay	2	1.73	0.93	126	1200	0.017	0.017	1570
Clay	3	2.78	1.05	77	1200	0.017	0.017	1720
Clay	4	4.87	2.09	90	1200	0.017	0.017	1780
Till	5	7.4	2.53	309	1654	0.033	0.033	2200
Bedrock	6	∞	∞	2236	4156	0.010	0.010	2700

3. Pile group design and installation

The pile group was designed to characterise a part of a foundation system for a multi-storey building carrying loads from e.g. a column. Therefore, vertical piles were used. The piles are pre-fabricated and made out of reinforced C50/60 concrete with a square 235 × 235 mm cross-section and equipped with steel toes, transferring the vertical loads to the bedrock in compression. The piles are assumed to have a density of ρ_p = 2400 kg/m^3 and a Poisson's ratio ν_p = 0.2. The modulus of elasticity E_p = 39 MPa was tuned based on the natural frequencies obtained from an experimental modal analysis carried out in the factory, where one of the piles was suspended in springs to simulate free-free boundary conditions. The identified modulus agrees with the tangent modulus specified by the manufacturer.

To allow for installation of sensors within the piles after driving them at site, a cylindrical cavity was introduced along the center of the piles. This was achieved by installing a 76 mm diameter plastic pipe along the center line when casting the piles. The spacing between the piles was chosen to be representative for design solutions while at the same time highlighting the dynamic interaction between the piles,

especially in the vertical and rotational modes of vibration that are most affected by the end-bearing condition [13]. The pile–soil–pile interaction depends on the wavelengths of body waves in the soil relative to the separation distance between the piles [24,45]. In the literature, normalization of the frequency and the pile separation is commonly performed with reference to a pile diameter. The equivalent separation to pile diameter ratio of the pile group with square section piles is $s/d_{eq} = 5.15$, with the equivalent diameter defined as $d_{eq} = 2b/\sqrt{\pi}$ where b is the cross-section side length and the separation distance $s = 1.365$ m. For the soil conditions at the site, this situates the effects of pile–soil–pile interaction within the frequency band 1–80 Hz, covering the band of interest for environmental building vibrations [46].

The piles were installed at the site in February 2020 with a BANUT 550/Volvo EC280 impact pile driver with a fall-weight of 5 ton and a fall-height of 20–30 cm. The piles were driven to a stop, with a stopping criteria of 10 mm/10 impacts and were estimated to have reached bedrock. An apparent inclination of the bedrock surface was observed in the north-west direction as the piles came to a stop at different depths, resulting in the piles reaching a depth of 6.3 m for piles P2 and P3 positioned to the south-east and 5.6 m for P1 and P4 positioned to the north-west. This is either due to the natural variation of the bedrock surface, or an indication of the presence of a boulder where the piles were installed.

After performing measurements on the free-top piles, the pile group was joined in a reinforced $2 \times 2 \times 0.85$ m concrete pile cap. The cap is assumed to have the same material properties as the piles. Contact at the interface between the pile cap and the soil can influence the dynamic response of the pile group [33,34,47]. The contact condition between the cap and the soil can be difficult to model and in the case of end-bearing piles in soft soil the cap can separate from the soil when settlement takes place. Therefore, the pile cap was elevated 120 mm from the soil's surface to eliminate any interaction between the pile cap and the soil.

4. Numerical model

Numerical simulations are performed using the finite element method. The foundation and the soil are assumed to be linear elastic and the problem can therefore be solved in the frequency domain. The material properties of the soil are obtained from Table 1 and material damping is introduced as hysteretic damping by modifying the modulus of elasticity $E^* = E(1 + i2\beta)$, with $i^2 = -1$ defining the imaginary unit and where the damping ratios in deviatoric (β_s) and volumetric (β_p) deformation are implicitly assumed to be equal. Fig. 3 presents the model geometry considered for the simulations. The soil layers, piles and pile cap are modelled as a three dimensional solid body. The pipes in the piles are considered as cylindrical cavities introduced along the center line of the piles. Perfectly matched layers (PML) are adopted in the region closest to the outer boundary of the soil in order to attenuate any outgoing waves, representing the extension to infinity. The thickness of the PML domains is 2 m and the stretch functions proposed by Basu and Chopra [48] are applied to effectively attenuate both evanescent and propagating waves. The attenuation profile in the PML region is linear with scaling factors for evanescent and propagating waves both equal to 10. The PML region is discretized by quadratic hexahedra solid elements while quadratic tetrahedra elements are used for the piles, the concrete cap and the soil within the computational domain. The maximum prescribed element size is determined such that a minimum resolution of five quadratic elements per wavelength in the soil are present in the considered frequency range, resulting in a minimum element size of 0.17 m in the top soil layer. The mesh is verified to yield converged results in the frequency range of interest. In the case where the pile group is joined at the surface by the concrete cap, the symmetry of the problem is exploited to reduce the computational effort.

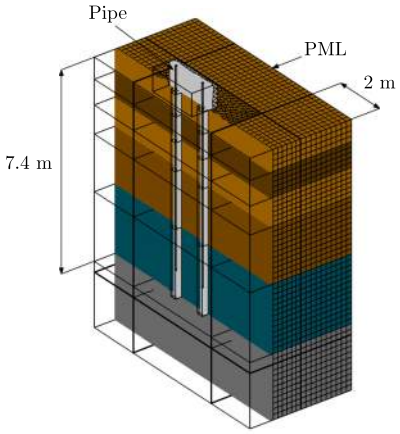

Fig. 3. Section of the finite element model of the pile foundation. The layering of the soil is indicated in colors with the layers of clay (brown), till (blue) and bedrock (gray). (For interpretation of the references to color in this figure legend, the reader is referred to the web version of this article.)

5. Experimental setup

The experimental investigations were performed using two measurement setups. The first setup considers the driven piles alone before casting of the concrete cap. The accelerations of all piles are measured when excitation is applied to each pile top. The measurements were performed five months after the piles had been driven, allowing excess pore pressures due to installation to even out. Measurements of only the pile top's responses were also conducted after two months. The second setup concerns the measurement of translational and rotational responses of the pile group. The tests were performed two months after the pile top measurements and one month after casting of the concrete cap.

5.1. Measurement equipment

The dynamic tests were performed with excitation from an impact hammer of model Dytran 5803A IEPE with a mass of 5.5 kg. Acceleration of the pile tops and the pile cap were measured by means of accelerometers of models PCB 393A01 and PCB 393B31. The response measurements within the piles were performed using a Geotomographie DDS presented in Fig. 4(a), equipped with two stations with PCB 66332APZ1 accelerometers mounted in a triaxial arrangement. The vertical spacing between the two stations is one meter. The equipment was originally designed for down-hole and cross-hole measurements where the coupling of the stations to the borehole is achieved by pneumatic clamping, allowing an arbitrary number of measurement points along each pile.

5.2. Setup 1: Pile tops

Fig. 5 presents an overview of the first setup where only the piles are present. Each pile was instrumented with six accelerometers at the top. Excitation was applied in the two horizontal directions at the same height and on the opposite side to where the sensors were mounted. Applying impacts at the top of the piles in the vertical direction inevitably produces a rotation of the pile cross-section as the piles cannot be excited at the center of the cross-section due to the presence of the

(a) (b) (c)

Fig. 4. Measurement equipment (a) Geotomographie DDS with pneumatic clamping of two triaxial measurement stations, (b) mounted in one of the piles together with PCB 393A01 accelerometers and (c) a Dytran 5803 A impact hammer.

Fig. 5. Measurement setup for the tests on the piles before the casting of the pile cap. The numbering of the piles P1 to P4 are indicated on the side of each pile.

pipe. Therefore, the vertical impacts were applied as close as possible to the center and the signals obtained from the four vertically orientated sensors were averaged, aimed at cancelling the influence of cross-sectional rotations. The setup further allows for obtaining the rotations of the pile cross-sections from the vertical acceleration measurements. In each test, a minimum of fifteen hammer impacts were applied in the vertical and two horizontal directions at each pile. Measurements at depth were performed by mounting the accelerometers within one of the piles at the desired depth and applying impacts in the three directions at the top of each one of the piles. This was repeated with the sensors mounted in each one of the piles for all the depths considered. For piles P1 and P4, two setups were performed at the depths (0.75 m, 1.75 m) and (2.75 m, 3.75 m) whereas for the longer piles P2 and P3 additional measurements at 4.75 m were performed, resulting in a total of ten setups.

5.3. Setup 2: Pile group

Fig. 6 presents the instrumentation for the test performed on the pile group. Seven accelerometers were installed on the pile cap with five mounted in the vertical direction ($a_1 - a_5$) and two in the horizontal directions (a_6 and a_7). The excitation was applied in the vertical direction by hammer impacts at position `Fz1` to characterise the response of the piles and the pile group due to a vertical load. Vertical impacts were additionally applied at positions `Fz2` and `Fz3` to obtain the rotational impedances of the pile cap around the horizontal x- and y-axis, respectively, assuming the pile cap to behave as a rigid block in the frequency range of interest. Horizontal excitations were applied along the two perpendicular horizontal axes, where the excitation and measurement points were positioned at the mid height of the concrete cap.

6. Results

From the impact tests, the frequency response functions are estimated from multiple impacts using the H_1 estimator, assuming the input signal to be free of any noise [49]. The estimated acceleration frequency response functions are integrated to receptances by division with $(\mathrm{i}\omega)^2$. The receptances at the pile tops and the pile cap are subsequently inverted in order to obtain the impedances. The complex valued impedance $Z_{ij}(\omega)$ represents the dynamic stiffness and damping of the foundation in the degree of freedom i related to the displacement or rotation in degree of freedom j where the real part $\mathrm{Re}(Z_{ij}(\omega))$ represents the frequency dependent stiffness and inertia, and the imaginary part $\mathrm{Im}(Z_{ij}(\omega))$ the damping.

6.1. Structural impedances of piles

Fig. 7 compares the experimentally and numerically obtained vertical and horizontal impedances at the top of the individual piles. While the experimentally determined impedances in the horizontal directions are very similar for all the piles in the group, the vertical impedances are different for the sets (`P1,P4`) and (`P2,P3`). This is due to the difference in length of the piles, where the shorter piles P1 and P4 have a higher stiffness than the longer ones. The horizontal impedances, on the other hand, are not affected by the difference in pile lengths. This is explained by the fact that the active length of a pile under lateral excitation is shorter than the total length of the piles, and is therefore almost unaffected by the depth of penetration into the non-cohesive soil [41]. The numerically predicted impedances are overestimated in both the vertical and horizontal direction. It should be noted that the numerical model assumes a pile that extends to a depth of 7.4 m, and therefore an even larger model error should be expected in the vertical impedance if considering the bedrock positioned at the actual pile lengths.

6.2. Pile–soil–pile interaction of free-top piles

The interaction between the piles in the group is illustrated by relating the motion of the excited pile to the motion of the receiving piles at the soil's surface by the pile interaction factor defined as:

$$\alpha_{ij}(\omega) = \frac{\text{displacement/rotation of pile } i \text{ due to a load at pile } j}{\text{displacement/rotation of pile } j \text{ due to a load at pile } j} \quad (1)$$

The real and imaginary parts of the interaction factor describe the amplitude and phase of the receiver pile relative to the displacement or rotation of the loaded pile, which govern the dynamic interaction effects in the pile group when joined together at the surface [4,15,16]. If the interaction factor is a purely positive or negative real number, the receiver pile moves in- or out of phase with the excited pile, respectively. This interaction between the piles gives rise to constructive or destructive interference with the forced motion of each pile when

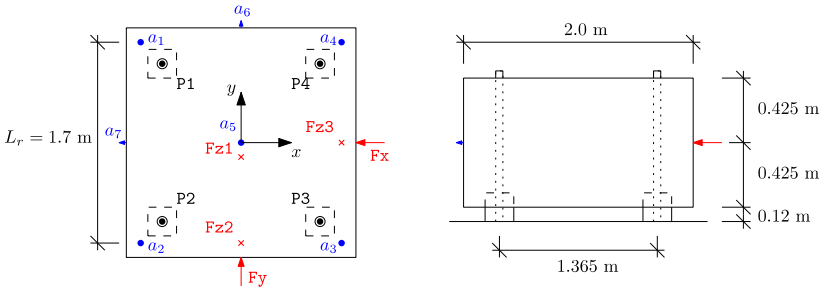

Fig. 6. Measurement setup and dimensions for the 2 × 2 pile group concrete cap with accelerometers indicated by a_j, piles by P1–4 and excitation points by F.

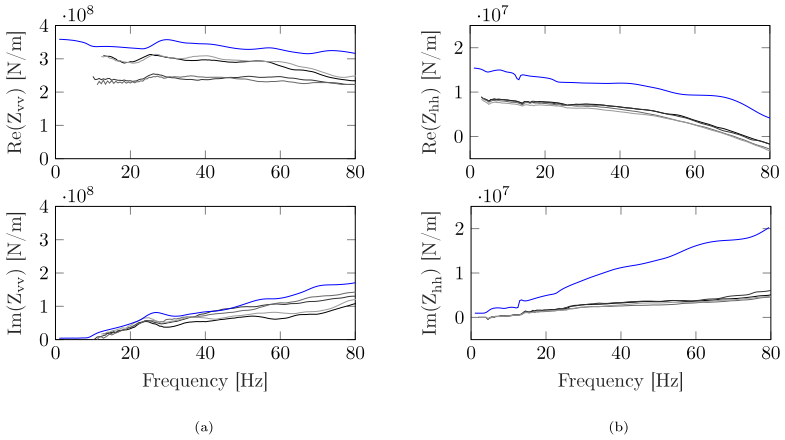

Fig. 7. Real (top) and imaginary part (bottom) of experimental pile top impedances for piles P1 to P4 (black to light gray) compared to the numerically predicted impedances (blue line) in the (a) vertical and (b) horizontal directions. (For interpretation of the references to color in this figure legend, the reader is referred to the web version of this article.)

the group of piles is loaded through e.g. a rigid pile cap, resulting in either a reduction or increase in the dynamic group stiffness.

Fig. 8 presents the interaction factors for horizontal translation due to a horizontal load ($\alpha_{\mathrm{hh},ij}$), cross sectional rotations due to a horizontal load ($\alpha_{\mathrm{h}\theta,ij}$) and vertical translations due to a vertical load ($\alpha_{\mathrm{vv},ij}$). The horizontal interaction factors are presented only considering the load applied to the piles in the x-direction and rotations measured around the y-axis, with reference to Fig. 6. The experimentally obtained interaction factors are compared to the ones obtained from the numerical model. The horizontal interaction factors are influenced by the position of the receiver pile with respect to the direction of excitation, as it governs the type of waves induced in the soil by the motion of the excited pile [16]. Therefore, the piles are categorised based on the angle φ between the line of the two piles considered and the x-direction, which is the direction of horizontal excitation. In Figs. 8(b) and 8(c), it is observed that the piles that are subjected mainly to longitudinal waves, i.e. for which $\varphi = 0°$, move out of phase at about 45 Hz. The piles for which $\varphi = 90°$ are mainly subjected to horizontally polarized S-waves that have a lower wave speed, and move out of phase with the loaded pile at about 30 Hz. The diagonal pile pairs are subjected to a combination of these two wave types and also move out of phase for a frequency of about 30 Hz. Naturally, as the vertical load case is symmetric with respect to the considered values of φ, it should have no significant influence on the vertical interaction factors, which is verified in Figs. 8(b) and 8(c).

The interaction factors obtained from the numerical model agrees fairly well with the experimental results. The amplitudes of α_{hh} and $\alpha_{\mathrm{h}\theta}$ for the pile pairs where $\varphi = 90°$ are overestimated, but the relation between the real and imaginary part, i.e. the phase, is well captured up to about 55 Hz. The interaction factor α_{hh} for the diagonal piles is on the other hand quite well represented in amplitude, but slightly shifted towards lower frequencies in the oscillations of the real and imaginary parts. In all the horizontal and cross horizontal-rotational interaction factors, the first three natural frequencies of the soil deposit can be observed as local peaks at 5, 14 and 26 Hz, which can also be observed as dents in the pile impedances of Fig. 7(b).

The predicted vertical interaction factors α_{vv} are similar in character to the measured ones. However, a shift in frequency from 27 to 30 Hz of the out of phase motion is observed when comparing the measurements to the numerical predictions. For floating piles in a homogeneous soil, this out of phase motion occurs at the frequency where the pile spacing is equal to half the wavelength of horizontally propagating vertically polarized S-waves [15]. This indicates that the effective S-wave speed in the soil between the piles is slightly higher in the model. Measurements performed at depth due to the loads applied at the surface allows to study the global motion of the group of piles in the

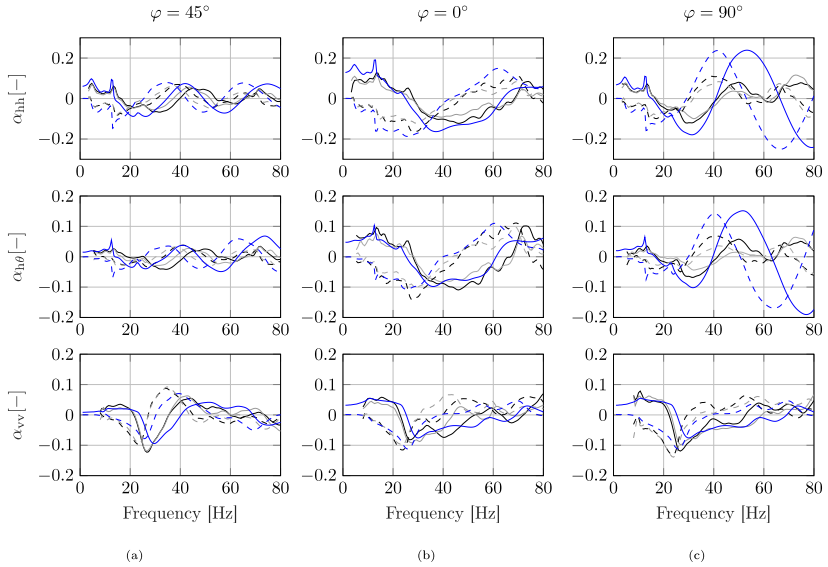

Fig. 8. Real (solid lines) and imaginary parts (dashed lines) of pile interaction factors (black and gray) (a) α_{13} and α_{42}, (b) α_{14} and α_{32} and (c) α_{12} and α_{43} of horizontal displacement due to a horizontal load (top), cross section rotation due to a horizontal load (middle) and vertical displacement due to a vertical load (bottom) obtained from the measurements compared to the numerical predictions (blue). (For interpretation of the references to color in this figure legend, the reader is referred to the web version of this article.)

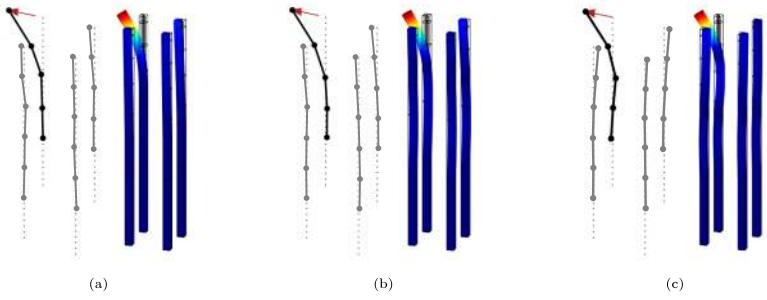

Fig. 9. Measured (left) and predicted (right) deflections of free-top piles due to horizontal pile head excitation at pile P1 at frequencies (a) 5, (b) 14 and (c) 26 Hz in the horizontal direction. The displacements are identically scaled for the measured and computed illustrations.

soil. Fig. 9 presents a comparison between snapshots of the measured and computed harmonic motion of the group of free-top piles due to a force applied in the horizontal direction at the top of pile P1. The wavelengths associated with standing waves in the clay can be observed not only for the excited pile, but also for the three receiving piles.

The deformations are largely concentrated in the upper portion of the soil, agreeing with the numerical predictions, further supporting the observation that the horizontal impedances of the piles are practically unaffected by the total length of the piles due to the active length being smaller than the total depth of the stratum.

6.3. Temporal variations due to environmental conditions

The sensitivity of the horizontal impedance of the single pile to the properties of the soil closest to the surface and the ability of the model to capture the interaction between the piles due to horizontal excitation, as presented in Fig. 8, suggest that the discrepancies between the measured and predicted horizontal pile impedances are due to local effects at the excited pile. This is consistent with findings by other authors [31,41,50]. Consideration of a free length closest to the soil's surface between the pile and the soil, or a weakened zone at the pile–soil interface have been suggested to obtain more accurate predictions of the horizontal impedance of single piles [51]. However,

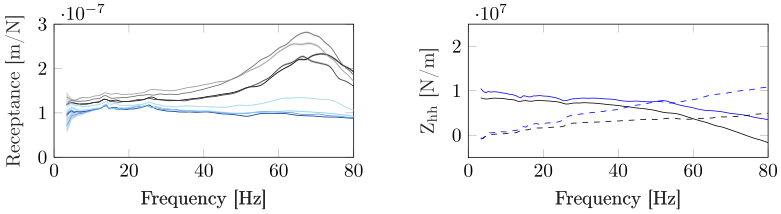

Fig. 10. Comparison between measurement results in spring (blue) and summer (black) of horizontal pile (a) receptances with 95% confidence bounds for piles P1 to P4 (dark to light) and (b) real (solid lines) and imaginary part (dashed lines) impedance of pile P1. (For interpretation of the references to color in this figure legend, the reader is referred to the web version of this article.)

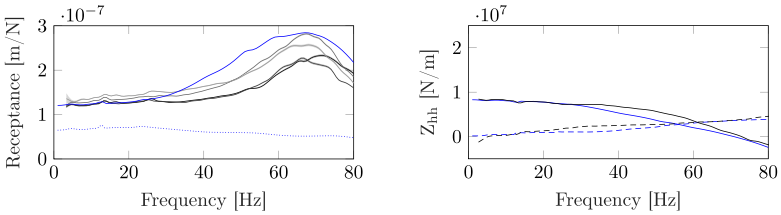

Fig. 11. Numerical results (blue) based on a model of a single pile assuming a loss of contact with the most shallow soil layer extending to a depth of 0.6 m compared to the (a) horizontal receptances obtained from the original model (blue dotted line) and the measurements for piles P1 to P4 in the summer (black to light gray) with 95% confidence bounds and (b) the measured real (black solid lines) and imaginary (black dashed lines) parts of the impedance of pile P1. (For interpretation of the references to color in this figure legend, the reader is referred to the web version of this article.)

an appropriate selection of parameters is required for these model adjustments to obtain accurate results. Moreover, these considerations might not be appropriate for pile groups, which are not as sensitive as single piles to the conditions closest to the surface [52].

At the present site, and under similar soil conditions, the mechanical properties of the layer of soil closest to the surface change over time due to the environmental conditions [44]. Therefore, the change in environmental conditions are expected to influence the horizontal impedances of the piles. Fig. 10(a) compares the horizontal receptances of the four piles measured in summer and in the spring three months before. In both cases, the impacts applied to the piles were of approximately the same magnitude. A pronounced peak is observed around 70 Hz for all the piles during the measurements performed in summer. This peak can only be distinguished for pile P4 in the spring, but with a significantly lower amplitude. The real and imaginary parts of the impedances for pile P1 in spring and in summer are compared in Fig. 10(b). The impedance of the pile is higher over the entire frequency range considered when measured in spring, but especially in the upper part of the band associated with the observed resonance. However, the impedance is still significantly lower compared to the predicted one of Fig. 7(b). This indicates that while environmental conditions might influence the horizontal impedance of the piles, the soil closest to the surface is not accurately enough described by the layered soil model to capture the true horizontal impedance of the individual piles.

In summer, it was observed that drying of the crust had occurred, causing it to crack up at the surface such that stakes set out at the site had become loose. It was therefore investigated whether a loss of contact between the piles and the soil could explain the observed resonance phenomenon. Fig. 11 compares the pile top response of all four piles and the impedance of pile P1 to the numerical results obtained from a model of a single pile with the soil modified by reducing the depth of the uppermost soil layer to 0.6 m and separating this layer from the pile with a spacing of 25 mm. The loss of contact between the pile and the soil dramatically decreases the horizontal stiffness of the pile, making it more flexible and giving rise to a resonance phenomenon in the pile similar to what was observed in the measurements. The correspondence between the simulations and the measurements indicate that the inconsistencies observed in Fig. 10 are indeed caused by a change in the contact conditions between the piles and the soil closest to the surface. This shows not only the difficulty in predicting the horizontal impedance of piles, but also that slight variations in the condition of the topmost soil between april and june can significantly influence the impedance that is measured.

6.4. Response of pile group joined at the surface

Fig. 12 presents a comparison between experimentally and numerically obtained receptances in the vertical and horizontal directions of the concrete pile cap and the responses at depth within the diagonally placed piles P1 and P3. The vertical frequency response is obtained as the average of the recorded signals from accelerometers $a_1 - a_5$ due to the impact test at the position Fz1. The horizontal responses are close to identical for the two perpendicular directions and only the response due to the impact load Fx is presented here.

As for the free-top piles, the resonance frequencies in horizontal motion are identified as peaks in the response spectra. The third natural frequency is not well pronounced in the receptance plots, but is more easily located in the accelerance spectrum not shown here. The responses at depth show slightly different amplitudes in the two diagonally placed piles in the upper 2 m, while the same responses are measured at deeper levels. The model captures the horizontal motion of the foundation well apart from a slight shift in the predicted resonance

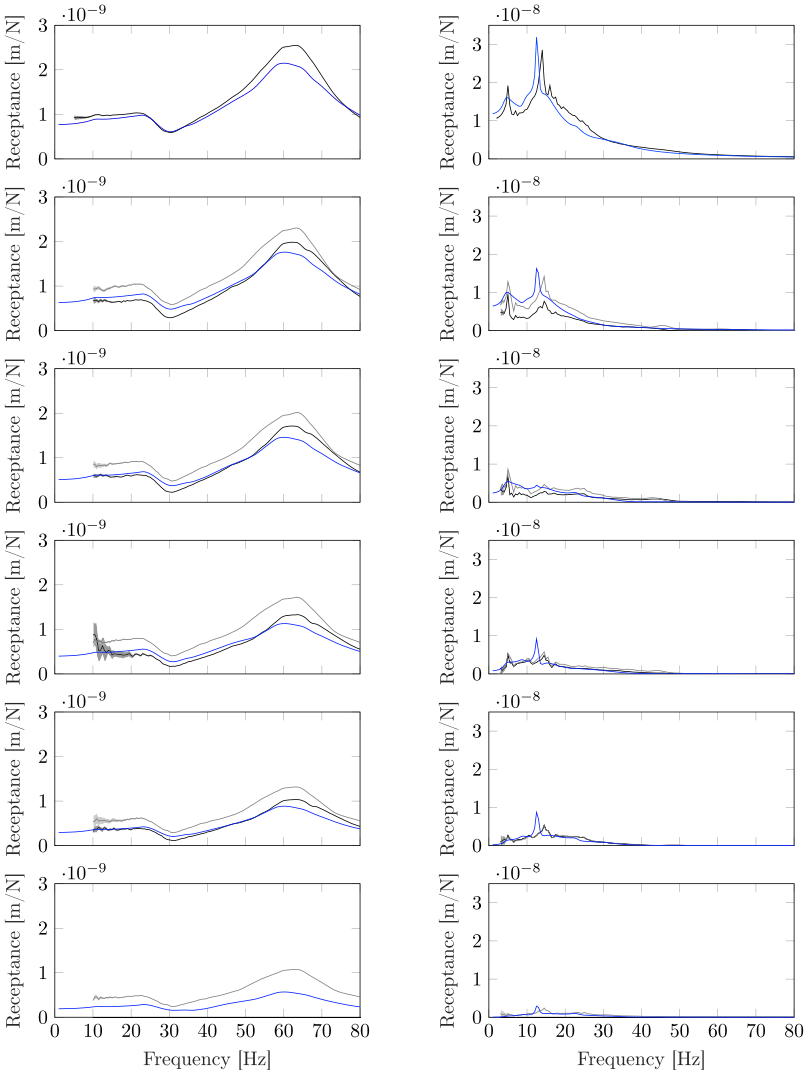

Fig. 12. Receptances in the vertical direction due to the vertical load Fz1 (left) and horizontal direction due to the horizontal load Fx (right). Results are presented for the pile cap (top row) and at the depths 0.75, 1.75, 2.75, 3.75 and 4.75 m within the piles P1 (black line) and P3 (gray line) compared to numerical predictions (blue line). The 95% confidence bounds on measured quantities are indicated by a shaded region. (For interpretation of the references to color in this figure legend, the reader is referred to the web version of this article.)

frequencies. The vertical response shows a modest peak at 23 Hz, a trough at 30 Hz and a more pronounced peak at 63 Hz. As the foundation is not fully symmetric and a small eccentricity is present for the applied impact load, the piles show slightly different amplitudes in the measured responses. The numerical predictions capture the vertical responses, but the amplitude of the response around peak in at 63 Hz is slightly underestimated. The presence of this peak is the result of inertial interaction between the piles and the mass of the pile cap. That is, considering the foundation as massless eliminates this part of the response altogether. Due to a low signal-to-noise ratio at frequencies below 10 Hz, the measurements at depth in the vertical direction show a low coherence in this frequency range and are therefore considered inaccurate.

Fig. 13 presents the measured and computed snapshots of harmonic displacements of the pile foundation at its horizontal resonance frequencies when subjected to horizontal excitation. The wavelengths

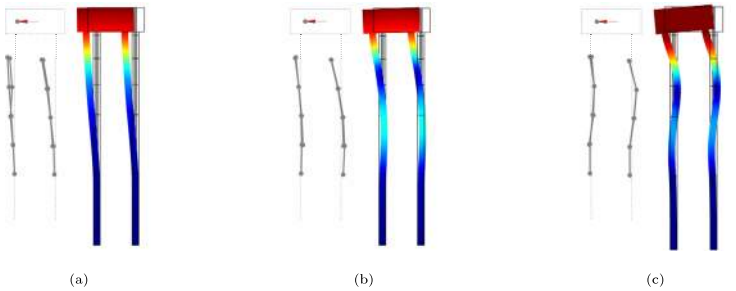

Fig. 13. Measured (left) and computed (right) harmonic displacements at the (a) first (b) second and (c) third resonance frequency of the pile group due to horizontal excitation. The displacements are identically scaled for the measured and computed illustrations.

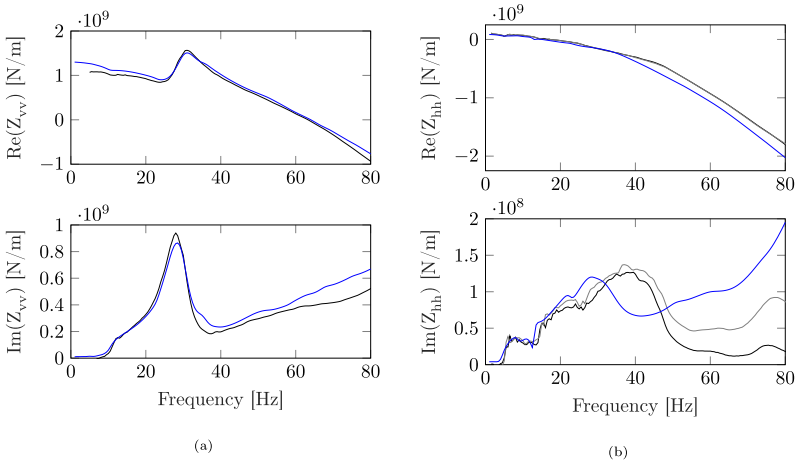

Fig. 14. Real (top) and imaginary part (bottom) of the experimental (black and gray lines) and numerical (blue line) pile group impedance in the (a) vertical and (b) two horizontal directions. (For interpretation of the references to color in this figure legend, the reader is referred to the web version of this article.)

associated with the standing waves in the clay are clearly seen for the three frequencies considered and correspond well with the numerical results.

6.5. Structural impedances of the joined pile group

Fig. 14 presents the measured and predicted structural impedances of the joined pile group in the vertical and horizontal directions. The vertical impedances are obtained from the impact test `Fz1` and the average vertical response of sensors $a_1 - a_5$. The horizontal impedances are obtained in both horizontal directions from the impact tests `Fx` and `Fy`. The impedances of the joined pile group are well predicted in both the vertical and horizontal directions. The peaks observed in the real and imaginary parts of the vertical impedance, caused by pile–soil–pile interaction, are well captured by the model. The measured vertical interaction factors of the piles in Fig. 8 indicate a frequency of 27 Hz where the piles move out of phase, whereas the numerical interaction factors are slightly shifted towards 30 Hz. The dominating interaction frequency highly depends upon the soil properties and the inter-spacing between the piles in the group. A change in soil properties, especially closest to the surface, can therefore have a significant influence on the apparent interaction frequency, which has been demonstrated in the literature using numerical models [14,53]. Consequently, the slight shift in frequency observed between the two measurements indicates that the stiffness of the soil, and therefore the effective wave speed between the piles, have slightly changed after construction of the pile cap. It should be noted that the inertia of the pile cap contributes to the real parts of the vertical and horizontal impedances as the term $-\omega^2 m$, with m the mass of the pile cap. In the vertical direction, this makes the real part of the impedance become zero at 63 Hz, resulting in the resonance peak observed in Fig. 12. The imaginary part of the vertical impedance is slightly overestimated by the model for frequencies over 40 Hz, resulting in under-predicted response amplitudes near the resonance frequency where the response is mostly damping controlled.

The horizontal impedance of the pile group is well captured by the model up to a frequency of 30 Hz and the cut-off frequencies corresponding to the resonance frequencies of the clay are seen in the imaginary part of the horizontal impedance as the onset at 5 Hz and the local minima at 14 and 26 Hz. It is noted that despite the larger differences observed between measured and predicted horizontal impedances of the single piles, the prediction of the horizontal pile group impedance agree reasonably well with the measurements. These

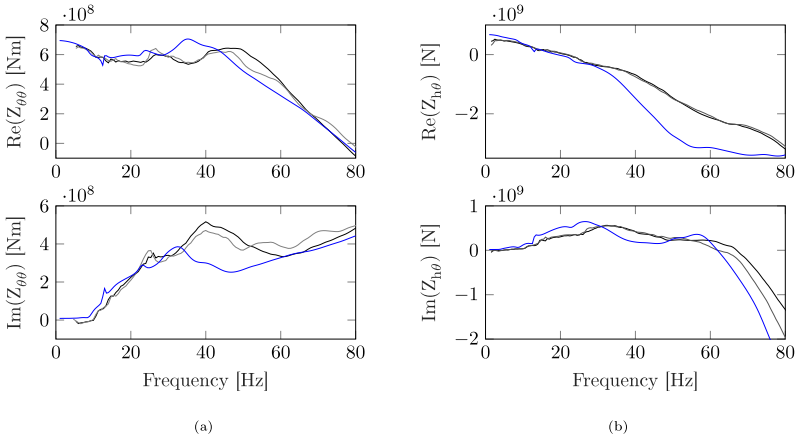

Fig. 15. Real (top) and imaginary part (bottom) of the experimental (black and gray lines) and numerical (blue line) pile group (a) rotational and (b) cross horizontal-rotational impedances. (For interpretation of the references to color in this figure legend, the reader is referred to the web version of this article.)

observations support numerical and previous experimental findings that pile groups are less influenced by the soil conditions closest to the surface than solitary piles [31,52].

The rotational and cross horizontal-rotational impedances are estimated from the impacts tests at positions Fz2 and Fz3. For Fz2 the impedances are calculated with reference to Fig. 6 as:

$$Z_{\theta\theta}(\omega) = -\frac{\omega^2 F_{z2}(\omega) L_r^2}{(a_1 + a_4) - (a_2 + a_3)} \tag{2}$$

$$Z_{h\theta}(\omega) = -\frac{\omega^2 F_{z2}(\omega) L_r}{2a_6(\omega)} \tag{3}$$

Fig. 15 presents a comparison between the measured and predicted rotational and cross horizontal-rotational impedances. Experimental results obtained from the measurements of the rotations around the two horizontal axes are included, which illustrates that the rotational stiffness is almost unaffected by the differences in the length of the piles. The rotational impedance is well predicted by the model, apart from differences in the locations of the peaks in the spectra similar to what is found for the horizontal impedance.

Both horizontal and rotational numerical impedances, which are coupled, start to deviate from the measured ones for frequencies above 30 Hz. While the pile–soil–pile interaction is well captured by the model for the individual piles for both horizontal and cross horizontal-rotational motion, the increase in the pile group impedances due to pile–soil–pile interaction is found at a higher frequency of approximately 45 Hz, corresponding to the peaks in the real and imaginary parts of the impedances. As for the vertical impedance, this further indicates a lengthening of the wavelengths involved in the pile–soil–pile interaction, i.e. a stiffening of the soil. On the other hand, it is noted that the lateral natural frequencies of the clay are essentially the same in the measurements of the free piles and the pile cap. This indicates that the average soil properties are not significantly affected over the whole body of clay, and the variation in small-strain properties is probably localised in the upper part of the soil profile.

7. Conclusion

This paper presents the experimental results of the dynamic response of impact driven concrete piles and a 2 × 2 pile group for the purpose of model validation. The piles were driven at a test site where extensive site investigations have been performed and the small-strain properties required for modelling the soil have been determined by geophysical in situ methods, analysis of laboratory samples and empirical relations. The soil conditions consist of a 4.9 m layer of soft clay on top of a 2.5 m layer of till resting on a stiff bedrock.

Frequency response functions were measured in two stages of construction. First when the piles had been driven and were free at the surface and then after the concrete cap had been cast, joining the piles together at the surface. Excitation was applied to the pile tops and the pile cap by means of an instrumented impact hammer and the acceleration response of the piles and the pile cap were measured. Each pile was prepared in the factory with a central cylindrical cavity, allowing to install sensors in the field and to measure the response within the piles at depth using equipment for down-hole geophysical surveys. The measurements of the free top piles are used to obtain the individual pile impedances and pile-to-pile interaction factors, describing the interaction between the piles through the soil. The measurements of the vertical, horizontal, rotational and horizontal-rotational impedances of the pile group joined by the concrete cap are also presented.

A linear elastic three dimensional finite element model with perfectly matched layers is used to predict the dynamic characteristics of both the free individual piles and the joined pile group foundation, subjected to the same load cases as in the measurements. A design condition is considered for predicting the impedances of the foundation, meaning that the numerical predictions are obtained from a model based solely on the performed soil investigations and no attempt to update the model to better fit the measurement results have been performed. The numerical predictions are compared to the measurements to assess the ability of the model to capture the dynamic interaction between the soil and the foundation. The following conclusions from the study are made:

- The impedances of the pile group foundation on driven end-bearing concrete piles in soft clay are well predicted using a linear elastic three dimensional finite element model. In particular, the predicted variation of the vertical impedance with frequency due to pile–soil–pile interaction is in excellent agreement with the measurements.
- The vertical and horizontal impedances of the free top piles are not as well predicted as the group impedance.

- Horizontal impedances of the free top piles are found to be different between spring and summer. This is caused by a loss of contact between the pile and the topmost soil, showing that even small changes in the environmental conditions can significantly influence the measured pile impedance.
- Measured dynamic pile–soil–pile interaction factors clearly show the out-of-phase motion associated with an increase in foundation impedance within the studied frequency range. The corresponding interaction effects are also found in the measurements of the group impedances, validating previous theoretical findings.
- The horizontal impedances of the piles and the pile group are influenced by the clay layer's first three natural frequencies and are unaffected by the depth of the stiffer non-cohesive soil into which they are driven. The associated modes of the piles obtained from the model are in agreement with the measurements.

CRediT authorship contribution statement

Freddie Theland: Conceptualization, Methodology, Software, Writing– original draft, Investigation, Data curation, Formal analysis. **Geert Lombaert:** Supervision, Conceptualization, Methodology, Writing – review & editing. **Stijn François:** Conceptualization, Methodology, Writing – review & editing. **Costin Pacoste:** Conceptualization. **Fanny Deckner:** Supervision, Conceptualization, Methodology, Writing – review & editing. **Peter Blom:** Conceptualization. **Jean-Marc Battini:** Supervision, Conceptualization, Methodology, Writing – review & editing, Funding acquisition.

Declaration of competing interest

The authors declare that they have no known competing financial interests or personal relationships that could have appeared to influence the work reported in this paper.

Acknowledgments

This work is supported by the Development Fund of the Swedish Construction Industry (SBUF). The funding for experiments and site investigations is received from Vinnova, Trafikverket and the Richertska foundation. The financial support is gratefully acknowledged. The authors would also like to extend their gratitude towards Ragnvald Andersson for granting unlimited access to the test site used for the experiments performed in this work.

References

[1] Axelsson G. Design of piles - Swedish practice. In: ISSMGE - ETC 3 international symposium on design of piles in Europe, Leuven, Belgium. 2016.
[2] Commission on Pile Research. Pile statistics for Sweden 2019. 2020, URL: http://www.palkommissionen.org/web/page.aspx?refid=73.
[3] Kausel E. Advanced structural dynamics. Cambridge University Press; 2017, http://dx.doi.org/10.1017/9781316761403.
[4] Dobry R, Gazetas G. Simple method for dynamic stiffness and damping of floating pile groups. Géotechnique 1988;38(4):557–74.
[5] Makris N, Badoni D. Seismic response of pile groups under oblique-shear and Rayleigh waves. Earthq Eng Struct Dyn 1995;24(4):517–32.
[6] Gazetas G, Fan K, Kaynia A, Kausel E. Dynamic interaction factors for floating pile groups. J Geotech Eng 1991;117(10):1531–48.
[7] Saitoh M, Padrón LA, Aznárez JJ, Maeso O, Goit CS. Expanded superposition method for impedance functions of inclined-pile groups. Int J Numer Anal Methods Geomech 2016;40(2):185–206.
[8] Dai W, Shi C, Tan Y, Rojas F. A numerical solution and evaluation of dynamic stiffness of pile groups and comparison to experimental results. Eng Struct 2017;151:253–60.
[9] Taherzadeh R, Clouteau D, Cottereau R. Simple formulas for the dynamic stiffness of pile groups. Earthq Eng Struct Dyn 2009;38(15):1665–85.
[10] Dezi F, Carbonari S, Leoni G. A model for the 3D kinematic interaction analysis of pile groups in layered soils. Earthq Eng Struct Dyn 2009;38(11):1281–305.
[11] Carbonari S, Morici M, Dezi F, Leoni G. Analytical evaluation of impedances and kinematic response of inclined piles. Eng Struct 2016;117:384–96.
[12] Kaynia AM, Kausel E. Dynamics of piles and pile groups in layered soil media. Soil Dyn Earthq Eng 1991;10(8):386–401.
[13] Padrón L, Aznárez J, Maeso O, Saitoh M. Impedance functions of end-bearing inclined piles. Soil Dyn Earthq Eng 2012;38:97–108.
[14] Álamo GM, Martínez-Castro AE, Padrón LA, Aznárez JJ, Gallego R, Maeso O. Efficient numerical model for the computation of impedance functions of inclined pile groups in layered soils. Eng Struct 2016;126:379–90.
[15] Gazetas G, Makris N. Dynamic pile-soil-pile interaction. Part I: Analysis of axial vibration. Earthq Eng Struct Dyn 1991;20(2):115–32.
[16] Makris N, Gazetas G. Dynamic pile-soil-pile interaction. Part II: Lateral and seismic response. Earthq Eng Struct Dyn 1992;21(2):145–62.
[17] Masoumi HR, Degrande G, Holeyman A. Pile response and free field vibrations due to low strain dynamic loading. Soil Dyn Earthq Eng 2009;29(5):834–44.
[18] Elkasabgy M, El Naggar MH. Dynamic response of vertically loaded helical and driven steel piles. Can Geotech J 2013;50(5):521–35.
[19] Tantayopin K, Thammarak P. Effect of soft soil layer on local dynamic response of floating pile under harmonic lateral loading. Can Geotech J 2017;54(12):1637–46.
[20] Esmaeilzadeh Seylabi E, Kurtuluş A, Stokoe KH, Taciroglu E. Interaction of a pile with layered-soil under vertical excitations: field experiments versus numerical simulations. Bull Earthq Eng 2017;15(9):3529–53.
[21] Capatti MC, Dezi F, Carbonari S, Gara F. Full-scale experimental assessment of the dynamic horizontal behavior of micropiles in alluvial silty soils. Soil Dyn Earthq Eng 2018;113:58–74.
[22] Han Y, Vaziri H. Dynamic response of pile groups under lateral loading. Soil Dyn Earthq Eng 1992;11(2):87–99.
[23] Blaney GW, O'Neill MW. Dynamic lateral response of a pile group in clay. Geotech Test J 1989;12(1):22–9.
[24] Burr JP, Pender MJ, Larkin TJ. Dynamic response of laterally excited pile groups. J Geotech Geoenviron Eng 1997;123(1):1–8.
[25] Biswas S, Manna B. Experimental and theoretical studies on the nonlinear characteristics of soil-pile systems under coupled vibrations. J Geotech Geoenviron Eng 2018;144(3):04018007.
[26] Choudhary SS, Biswas S, Manna B. Effect of pile arrangements on the dynamic coupled response of pile groups. Geotech Geol Eng 2021;39:1573–978.
[27] Cao X, Wang S, Gong W, Wu W, Dai G, Zhou F. Experimental and theoretical study on dynamic stiffness of floating single pile and pile groups in multi-layered soil. Soil Dyn Earthq Eng 2022;157:107282.
[28] El Sharnouby BB, Novak M. Dynamic experiments with group of piles. 1984;110(6):719–737.
[29] Goit CS, Saitoh M. Model tests on horizontal impedance functions of fixed-head inclined pile groups under soil nonlinearity. J Geotech Geoenviron Eng 2014;140(6):04014023.
[30] Kobori T, Miura K, Nakazawa M, Hijikata K, Miyamoto Y, Moroi T, Kobayashi Y. Study on dynamic characteristics of a pile group foundation. 1991;(45).
[31] El-marsafawi H, Han YC, Novak M. Dynamic experiments on two pile groups. J Geotech Eng 1992;118(4):576–92.
[32] Manna B, Baidya DK. Nonlinear dynamic response of piles under horizontal excitation. J Geotech Geoenviron Eng 2010;136(12):1600–9.
[33] Novak M, Grigg FR. Dynamic experiments with small pile foundations. Can Geotech J 1976;13(4):372–85.
[34] Manna B, Baidya DK. Dynamic nonlinear response of pile foundations under vertical vibration-theory versus experiment. Soil Dyn Earthq Eng 2010;30(6):456–69.
[35] Capatti MC, Dezi F, Carbonari S, Gara F. Dynamic performance of a full-scale micropile group: Relevance of nonlinear behaviour of the soil adjacent to micropiles. Soil Dyn Earthq Eng 2020;128:105858.
[36] Goit CS, Saitoh M, Mylonakis G, Kawakami H, Oikawa H. Model tests on horizontal pile-to-pile interaction incorporating local non-linearity and resonance effects. Soil Dyn Earthq Eng 2013;48:175–92.
[37] Goit CS, Saitoh M. Experimental approach on the pile-to-pile interaction factors and impedance functions of inclined piles. Géotechnique 2016;66(11):888–901.
[38] Ullah MS, Yamamoto H, Goit CS, Saitoh M. On the verification of superposition method of kinematic interaction and inertial interaction in dynamic response analysis of soil-pile-structure systems. Soil Dyn Earthq Eng 2018;113:522–33.
[39] Zafar U, Goit C, Saitoh M. Experimental and numerical investigations on vertical dynamic pile-to-pile interactions considering soil and interface nonlinearities. Bull Earthq Eng 2021.
[40] Dezi F, Gara F, Roia D. Linear and nonlinear dynamic response of piles in soft marine clay. J Geotech Geoenviron Eng 2017;143(1):04016085.
[41] Gazetas G. Seismic response of end-bearing single piles. Int J Soil Dyn Earthq Eng 1984;3(2):82–93.
[42] Lambe TW. Predictions in soil engineering. Géotechnique 1973;23(2):151–202.

[43] Google Earth Pro V7337786. Brottby, Sweden. 59°35'24.3"N 18°10'26.0"W, Eye alt 383 m. Maxar technologies 2020. 2020, http://www.earth.google.com [September 21, 2020].
[44] Theland F, Lombaert G, François S, Pacoste C, Deckner F, Battini J-M. Assessment of small-strain characteristics for vibration predictions in a Swedish clay deposit. Soil Dyn Earthq Eng 2021;150:106804.
[45] Nogami T. Dynamic group effect in axial responses of grouped piles. J Geotech Eng 1983;109(2):228–43.
[46] Mechanical vibration and shock – Evaluation of human exposure to whole-body vibration – Part 2: Vibration in buildings (1 Hz to 80 Hz). ISO 2631-2:2003, 2003, Geneva, CH: International Organization for Standardization; 2003.
[47] Emani P, Maheshwari B. Dynamic impedances of pile groups with embedded caps in homogeneous elastic soils using CIFECM. Soil Dyn Earthq Eng 2009;29(6):963–73.
[48] Basu U, Chopra AK. Perfectly matched layers for time-harmonic elastodynamics of unbounded domains: theory and finite-element implementation. Comput Methods Appl Mech Engrg 2003;192(11):1337–75.
[49] Bendat J. Statistical errors in measurement of coherence functions and input/output quantities. J Sound Vib 1978;59(3):405–21.
[50] Wang MC, Liao WP. Active length of laterally loaded piles. J Geotech Eng 1987;113(9):1044–8.
[51] Novak M. Piles under dynamic loads. In: Second international conference on recent advances in geotechnical earthquake engineering and soil dynamics. (12). 1991.
[52] Kaynia AM. Dynamic stiffness and seismic response of pile groups (Ph.D. thesis), Massachusetts institute of technology; 1982.
[53] Kaynia AM, editor. Analysis of pile foundations subject to static and dynamic loading. 1st ed.. CRC Press; 2021, http://dx.doi.org/10.1201/9780429354281.

Paper III

Measurements and predictions of vibration response of end-bearing pile group in soft clay due to vertical ground surface load

Freddie Theland[a,*], Geert Lombaert[b], Stijn François[b], Abbas Zangeneh[a,c], Fanny Deckner[d], Jean-Marc Battini[a]

[a] *KTH Royal Institute of Technology, Department of Civil and Architectural Engineering, Brinellvägen 23, 100 44 Stockholm, Sweden*
[b] *KU Leuven, Department of Civil Engineering, Kasteelpark Arenberg 40, 3001 Leuven, Belgium*
[c] *ELU Konsult AB, Valhallavägen 117, 115 31 Stockholm, Sweden*
[d] *GeoMind KB, Fannys väg 3, 131 54 Nacka, Sweden*

Abstract

Ground-borne vibration from roads or railways is a growing concern in the planning of new buildings in urban environments. Vibration assessment is often based on initial measurements of the free field vibrations to estimate building vibrations by either empirical or numerical procedures. Dynamic interaction between the soil and the foundation has an important influence on the transmitted vibrations, especially for embedded foundations, and should therefore be properly accounted for. This paper presents the results from a series of full-scale field experiments that were performed to characterise the vibration response of an end-bearing pile group foundation in soft clay subjected to a dynamic load applied at the ground surface. Controlled dynamic excitation is applied vertically at the ground surface from 10 and 20 m horizontal distance using an electrodynamic inertial shaker. Accelerations are measured at different construction stages: prior to construction, after driving of the piles and after completion of the pile cap. Predictions from a numerical model and from a hybrid method utilising measurement data acquired in an earlier construction stage are both validated with the data from the field tests. The results indicate that the relationship between the amplitudes of the vertical foundation and free field responses are insensitive to source-receiver distance. It is also found that pile-soil-pile interaction has an important influence on the vertical response of the piles.

Keywords: End-bearing piles, Surface waves, Kinematic interaction, Dynamic soil-structure interaction, Pile group, Ground borne vibration

1. Introduction

Vibrations in buildings originating from roads or railways are a growing concern in the planning of buildings located close to transportation infrastructure. Such vibrations can cause discomfort to residents

*Corresponding author: Tel. +46(0) 70 408 41 97
Email addresses: freddie.theland@byv.kth.se (Freddie Theland), geert.lombaert@kuleven.be (Geert Lombaert), stijn.francois@kuleven.be (Stijn François), abbas.zangeneh@elu.se (Abbas Zangeneh), fanny.deckner@geomind.se (Fanny Deckner), jean-marc.battini@byv.kth.se (Jean-Marc Battini)

or malfunctioning of vibration sensitive equipment and are often both difficult and costly to mitigate. It is therefore important to include vibration assessment as an integral part of the design process for buildings in urban environments. The vibration response in buildings to ground borne vibration is highly influenced by the mechanical properties of the soil and the foundation type [1]. Whenever the shear strains in the soil are sufficiently small, which is usually the case for e.g. traffic induced ground borne vibrations, linear viscoelastic constitutive behaviour can be assumed to model the soil with sufficient accuracy in the frequency range of interest [2]. For such linear systems, dynamic soil-structure interaction can be decomposed into two parts: inertial and kinematic interaction [3]. The inertial interaction characterises the stiffness and energy dissipation properties of the soil-foundation system by taking into account the soil impedance at the foundation-soil boundary, which influences the dynamic properties of the superstructure. The kinematic interaction, on the other hand, refers to the response of the massless structure when subjected to an incident wave field, which for a rigid foundation corresponds to the foundation response without the superstructure present. This response is in the literature often related to the motion at the free ground surface to illustrate the influence of soil-foundation interaction. Decomposing the problem into these two interaction terms allows for a better understanding of how soil-foundation interaction influences the transmission of vibrations into a building. Moreover, it offers a straightforward way for making vibration assessment based on site measurements prior to construction. This is an attractive approach, as site measurements inherently takes into account the influence of local site conditions, such as nearby structures or heterogeneities in the subsoil underneath the building, something which can have a large impact on the transmitted vibrations and is often difficult to fully characterise and to accurately model [4, 5].

For the prediction of ground borne vibrations in buildings, it is common to use only the vertical component of the free field motion as an input for predicting the vertical floor responses in a building, assuming it is the dominant source of excitation. This approach is adopted both in scoping models [6–9] and empirical prediction models [10, 11]. This is in contrast to applications in earthquake engineering, where the horizontal and rocking modes are of major interest. However, in the general case, all components of the foundation response should be considered for the prediction of vibrations in a building. Foundations subjected to incident waves produced by e.g. at-grade railway or road traffic, are in general strongly affected by the dynamic interaction between foundation and soil such that the foundation response differs significantly from the free field motion [12]. Accounting for this influence of soil-structure interaction therefore becomes important for vibration assessment. In the widely used measurement based procedure proposed by the US Federal Rail road Administration [11], building vibrations are estimated from free field vibrations using adjustment factors to account for the soil-foundation and foundation-building interaction. These adjustment factors do not take site specific soil conditions into account, which in many cases is inappropriate since

the mechanical properties of the soil are the most important aspects to consider in case of both shallow foundations [13–15] and pile foundations [16, 17]. The relationship between the foundation and free field responses is in general strongly frequency dependent and is in practice characterised by a large degree of uncertainty [18, 19]. This is especially the case for the vertical response of end-bearing piles in soft soil, where the relationship between the vibration response amplitude of the piles and the vibrations in the free field is governed by the relationship between the pile axial stiffness and the stiffness of the soil. Moreover, in soft soils with a shallow depth to bedrock, surface waves are dispersive, layer resonances exist and body waves are reflected back and forth between the bedrock and the free ground surface. This makes it more challenging to accurately model the wave propagation in the soil and to relate the foundation response to the free field motion at the ground surface, as it becomes more sensitive to the source-receiver distance [20, 21]. Numerical studies have advanced the understanding of such dynamic phenomena, but there is a lack of experimental treatment of this problem in the scientific literature which can be used to validate conclusions drawn from modelling results.

To fill this gap, this paper presents a set of full-scale field experiments conducted to characterise the response of an end-bearing pile foundation subjected to a vertical load at the ground surface. The primary objective of the paper is to experimentally characterise the influence of dynamic soil-structure interaction on the vibration response of an end-bearing pile foundation. The secondary objective is to assess predictions of the foundation response made using a deterministic numerical model. Also, a hybrid prediction method based on measurements made prior to the completion of the foundation is evaluated.

Measurements were performed in a fixed location at three different stages of construction. Figure 1 presents a conceptual overview of the test setup divided in the three different stages. First, the vibrations

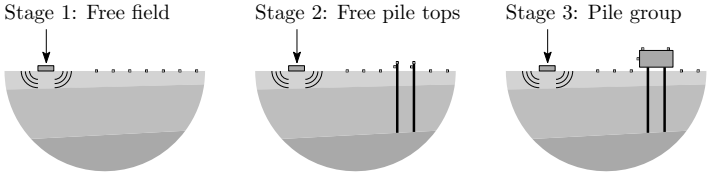

Figure 1: Conceptual experiment layout where dynamic excitation is applied at the ground surface (vertical arrow) in three different stages of construction of the pile group.

at the ground surface before the installation of piles were measured. Then, the vibration responses of four individual piles were recorded. Finally, the vibrations of a concrete pile cap supported by the pile group were measured when subjected to the same load. Performing measurements at these three different stages facilitates not only characterisation of the vibration response by relating it to free field vibrations, but also allows assessing predictions made for each stage and the influence of the construction of the foundation.

Also, it enables the use of measurements taken at a prior stage to make predictions about the next.

The site used in this study has previously been considered for assessment of the small-strain soil characteristics for vibrations predictions at the ground surface using a horizontally stratified soil model [22]. The foundation has also been characterised in terms of its vibration response due to forces applied at the top of the piles and on the pile cap [23]. The present paper addresses the foundation vibration responses caused by an incident wave field, completing a set of experiments conducted to evaluate the dynamic soil-structure interaction of this end-bearing pile foundation.

The structure of the paper is as follows. Section 2 presents the test site used for the experiments and a summary of the small-strain soil properties obtained from site investigations. Section 3 describes the foundation design and installation. Section 4 thereafter describes the experimental setup. Section 5 presents the numerical model used for making predictions based on the identified site properties. Section 6 compares the experimental results to the numerical predictions. Section 7 proceeds with adopting a method to predict the vibrations of the pile cap based on the measured pile top vibrations in the prior construction stage. Section 8 concludes the paper.

2. Test site

2.1. Site overview

The test site used for the experiments is a remote agricultural field located about 40 km north of Stockholm, Sweden. The field has not been used for agricultural purposes for more than ten years prior to the experiments. The site was chosen due to its soil stratification, the fact that unlimited access to the site could be granted and that no other construction activities were performed over the duration of the experiments. This allows to eliminate the influence that other nearby construction activities and foundation elements might have on the results, which is typically a problem when performing consecutive measurements at an actual construction site.

Geotechnical tests performed at the site consist of weight soundings, soil-rock probing, cone penetration tests (CPTu) and laboratory analysis of piston samples of clay. The soil consists of 1 m dry crust clay, a gray slightly varved clay with infusions of sand and silt up to 4.9 m depth followed by a sandy gravelly till which extend to a depth of 7.4 m where it rests on a stiff granite bedrock.

Figure 2 presents an overview of the site and two sections where the interpreted stratification over the test region is illustrated. The positions of two square 500 mm $\times$ 500 mm concrete foundations with a height of 200 mm, used as excitation points in the tests, and the pile group foundation are indicated.

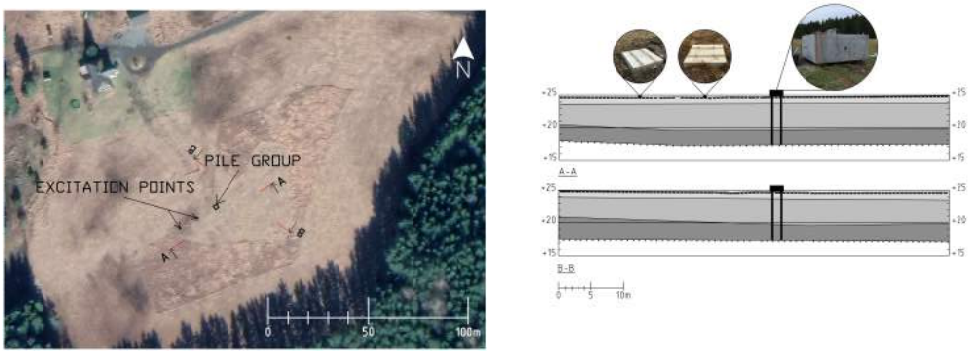

(a) (b)

Figure 2: Overview of the site with (a) an aerial photography [24] with the location of the two excitation points and the pile group indicated and (b) two sections with the stratification interpreted from geotechnical site investigations with a layering of dry crust clay (light gray), saturated soft clay (medium gray) and till (dark gray) on top of a stiff bedrock.

2.2. Small-strain soil properties

The small-strain properties of the soil have been extensively investigated at the site using dynamic measurements including surface wave measurements (SASW/MASW), seismic cone penetration tests (SCPT) and bender element tests of clay samples. The derived soil properties were used to establish a synthesised horizontally stratified viscoelastic soil model. The soil layers are described by the layer thickness h, the wave speeds C_s and C_p of S- and P-waves with their corresponding material hysteretic damping ratios β_s and β_p, and the layer density ρ. The damping ratios β_s and β_p are in the following assumed to be equal and are therefore both denoted by the value β. The estimated small-strain properties at the position of the pile group are summarised in table 1. A more detailed description of the site investigations can be found in [22].

Table 1: Small-strain soil properties at the test site based on dynamic in situ and laboratory tests [22].

Description	Layer	Depth	h	C_s	C_p	β	ρ
		[m]	[m]	[m/s]	[m/s]	[−]	[kg/m^3]
Dry crust clay	1	0.80	0.80	67	125	0.053	1880
Clay	2	1.73	0.93	126	1200	0.017	1570
Clay	3	2.78	1.05	77	1200	0.017	1720
Clay	4	4.87	2.09	90	1200	0.017	1780
Till	5	7.4	2.53	309	1654	0.033	2200
Bedrock	6	∞	∞	2236	4156	0.010	2700

3. Foundation design and installation

The pile foundation was designed to be representative of a full-scale component of a foundation system for a multi-storey building, carrying loads from e.g. a column. Vertical pre-fabricated reinforced concrete piles of strength class C50/60 with a square 235 mm × 235 mm cross-section and steel toes were used. The pile density is assumed as $\rho_{\mathrm{p}} = 2400$ kg/m^3 and the Poisson's ratio $\nu_{\mathrm{p}} = 0.25$. The piles modulus of elasticity $E_{\mathrm{p}} = 39$ MPa was identified from an experimental modal analysis performed in the factory for one of the piles. This value agrees with the tangent modulus specified by the manufacturer. To allow for measurements at depth within the piles, a plastic pipe with a 76 mm diameter was installed along the centre line when they were cast.

(a) (b)

Figure 3: Impact driven concrete piles installed at the site (a) in full length before cutting illustrating the difference in driving depth between the piles and (b) when levelled.

The piles were installed at the site with a BANUT 550/Volvo EC280 impact pile driver with a fall-weight of 5000 kg and a fall-height of 20-30 cm. The piles were driven to a stop, with a stopping criterion of 10 mm/10 impacts and were estimated to have reached the bedrock. Figure 3 shows the full length of the piles when installed at the site. The piles in the north-west direction (`P1` and `P4`), were driven to 5.6 m depth while the south-east piles (`P2` and `P3`) were driven to a depth of 6.3 m. The piles were consecutively levelled before conducting the measurements on the individual piles. Although estimated to have reached the bedrock, the different driving depths of the piles are based on the fulfilled stopping criterion. The stopping criterion does not guarantee that the piles reach the bedrock, but that they are effectively end-bearing. The discrepancy between the depth of the bedrock observed from the site investigations and the driving depth of the piles could be due to various reasons such as local variation of the bedrock surface, the presence of a large boulder or the piles reaching a dense and very stiff layer of till.

After the measurements on the individual piles were performed, the pile group was joined in a 2 m × 2 m × 0.85 m reinforced concrete pile cap. The concrete is assumed to have the same material properties as

the piles. In general, end-bearing pile foundations may have uncertain contact conditions between the soil and the bottom surface of the pile cap, as it may change over time due to settlement. In order to avoid this, the pile cap was elevated 120 mm from the ground.

4. Experimental setup

The measurements were performed at three occasions. Prior to these experiments, two small concrete foundations of dimensions 500 mm $\times$ 500 mm with a height of 200 mm (see fig. 2) were cast in place. These two foundations were the points onto which dynamic excitation was applied at all three occasions.

The measurements at the ground surface were performed in the autumn (October). The piles were installed in the end of winter (February). The measurements on the piles were performed in summer, five months after their installation in the soil, allowing excess pore water pressures to even out. By doing so, the influence of temporary installation effects from the pile driving is assumed to be small [25]. The last set of measurements was performed in the beginning of autumn one month after casting the concrete pile cap. As winter conditions such as freezing of the soil could potentially influence the results, these conditions were intentionally avoided.

4.1. Measurement equipment

The experiments were performed with dynamic excitation applied using sine sweep loading from a Wölfel BD.05 inertial shaker with a moving mass of 27.5 kg. Three minute sine sweeps were used with a force amplitude of approximately 500 N. The shaker was firmly mounted on top of the concrete foundation with screws. The acceleration of the moving mass was measured with an accelerometer of model PCB 308B and the acceleration at the base of the shaker was measured using an accelerometer of model PCB 393A01. The responses in the soil and on the pile foundation were recorded using accelerometers of models PCB 393A01 and PCB 393B31. The sensors were connected to a DAQ system consisting of a single sixteen channel MX1601B and two eight channel MX840B HBM QuantumX modules.

In the case where the response was measured on the ground surface, the accelerometers were mounted on 300 mm long aluminium stakes with a cruciform cross section which were driven into the soil. These stakes have been designed to minimize the influence of soil-structure interaction on the response measurements in the frequency range of interest [26, 27]. Figure 4 shows the instrumented inertial shaker and the accelerometers mounted on the aluminium stakes.

4.2. Instrumentation setup

Figure 5 presents the instrumentation plan for all three stages in which tests were performed:

(a)

(b)

Figure 4: Measurement equipment (a) Wölfel BD.05 inertial shaker mounted on one of the small concrete surface foundations and (b) PCB 939A01 accelerometers mounted both horizontally and vertically on aluminium stakes.

1. The vertical and horizontal acceleration responses of the soil were measured at the positions where the four piles were to be installed and at the center of the pile group footprint. In addition, responses of the soil were measured at eight points over the line between the excitation points and the pile group position.

2. Each pile was instrumented with two horizontal sensors and four vertical sensors. By instrumenting each corner of the piles' cross section in their axial direction, both the vertical and rotational responses of the piles could be obtained.

3. In the final setup, the pile group was instrumented to be able to characterise it's translational and rotational responses caused by the excitation. The vertical sensors were mounted on the top of the foundation whereas the horizontal sensors were placed at half the height of the concrete pile cap.

4.3. Post-processing

The data recorded from the tests are used to estimate frequency response functions for each setup. As the uppermost soil is relatively soft, the mass of the excitation foundations and the body of the shaker can cause local interaction effects which influence the force exerted on the soil. To accurately capture this interaction, detailed knowledge of the uppermost soil's properties is required, which is difficult to obtain. To eliminate the need for modelling this interaction, the reaction forces between the small concrete foundations and the soil are considered as the input forces. Assuming that the small concrete surface foundations can be idealised

Stage 1: Free field

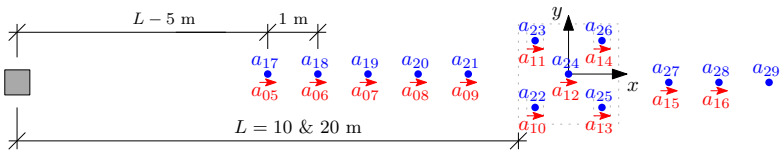

Stage 2: Free pile tops

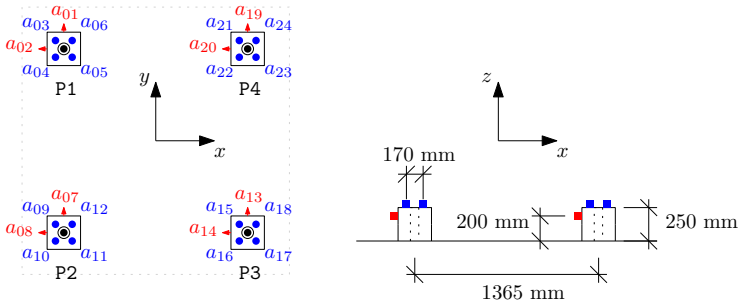

Stage 3: Pile group

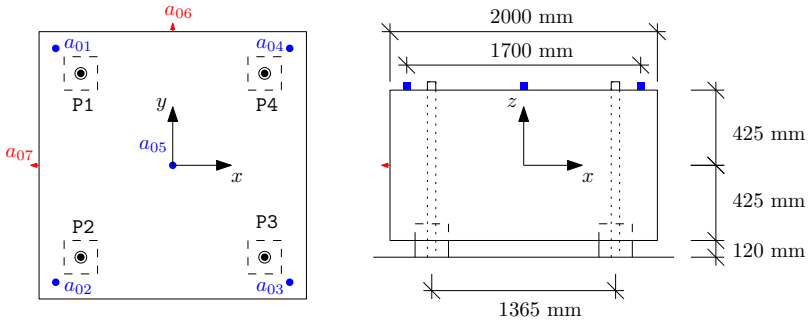

Figure 5: Setup for verically (blue) and horizontally (red) mounted acclerometers in the three stages of construction with reference to the concrete foundation where vertical dynamic excitation is applied (gray square).

as rigid bodies in the frequency range of interest, the forces acting on the soil are obtained from:

$$p(t) = m_{s1} a_{s1}(t) + m_{s2} a_{s2}(t) \tag{1}$$

where $a_{s1}(t)$ is the acceleration of the moving mass m_{s1} and $a_{s2}(t)$ is the acceleration of the mass m_{s2} of the foundation and the body of the shaker.

The calculated forces and the acceleration response signals are transformed to the frequency domain to estimate frequency response functions. The estimated frequency response functions in terms of accelerances are subsequently divided by $\mathrm{i}\omega$ to obtain mobilities, with i being the imaginary unit and ω the circular frequency, which is the format used for presentation of the results in this paper. In all the presented results, a small spike can be seen at 19.7 Hz. This is an artefact due to the natural frequency of the shaker suspension system. This has only a minor influence on the results for excitation frequencies close to this frequency, but it should be kept in mind in the interpretation of the experimental results.

5. Numerical model

The experiments considered in this paper involve loading which causes vibrations in the soil that are in the range of small shear strain. As such, a linear visco-elastic model is used for predicting the responses in the system. In this work, a three dimensional finite element model with perfectly matched layers (PML) is used. The PML elements are used to attenuate any outgoing waves from the model by complex coordinate stretching to artificially model the soil's infinite extent. The problem is solved in the frequency domain and a time-harmonic PML implementation is used, adopting the stretch functions proposed by Basu and Chopra [28], with scaling factors equal to 10 for both propagating and evanescent waves and a parabolic increase in the attenuation profile within the PML domain. The soil in the PML domain is discretised with 20 node solid elements. The soil, the piles and the pile cap in the computational domain are discretised with 10 node tetrahedral elements. The mesh resolution is assigned such that there are at least five elements per shear wavelength λ_s in the soil. A hysteretic damping model for the soil is introduced by assigning a complex modulus of elasticity $E_k^* = E_k(1 + \mathrm{i}2\beta_k)$ for each soil material k. The concrete is not assigned any material damping.

To reduce the computational effort, a substructure approach combined with PMLs proposed by Papadopoulos et al. [5] is adopted to propagate an incident wave field from a separate source model. The incident wave field is computed as equivalent loads at the boundary between the computational and PML domains. The computation of this boundary load requires that the free field displacements and tractions on this boundary are available. These are obtained semi-analytically for the case of a vertical point load at the

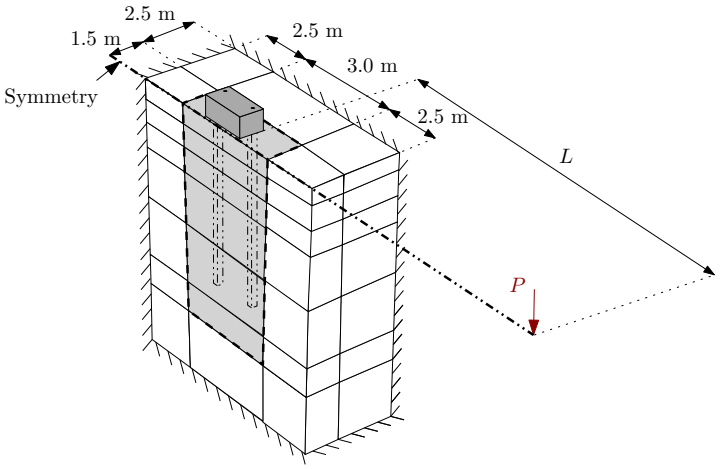

Figure 6: Geometry of the FE-PML model in construction stage 3 indicating the computational domain (gray) which is bounded by PMLs (white). A fixed condition is applied at the outer boundary of the PML domains whereas a free condition is applied at the ground surface. The vertical point load P applied in the source model is indicated by a vertical red arrow outside the model domain and is applied to the model as a load over the boundary between the computational and PML domains (dashed line).

ground surface, using the direct stiffness method implemented in the Matlab toolbox EDT [29].

As mentioned in section 3, the piles were installed to different depths. With regard to the unknown conditions of the bedrock surface and the soil underneath the piles while also taking into consideration that the incident wave field is nearly symmetric in the transverse direction, an average pile length of 5.9 m is adopted for all four piles. The soil is further assumed to be horizontally stratified, which is a reasonable approximation seeing to the interpreted soil profile obtained from the site investigations.

As the model has a plane of symmetry between the load and the center of the pile foundation, a symmetry condition is adopted to reduce the computational effort. Figure 6 presents a schematic overview of the three dimensional model domain adopted for the numerical simulations of the experiments.

6. Experimental results and numerical predictions

6.1. Vertical responses

Figure 7 presents a comparison between the experimental and numerical results for the vertical responses in the free field, on the pile tops and of the pile group foundation due to excitation applied at distances of 10 and 20 m from the edge of the pile cap footprint.

The vertical free field response amplitude is averaged over the footprint of the foundation (sensors $a_{22} - a_{26}$). The free field vibrations at the ground surface depend on the source-receiver distance. Dispersion of

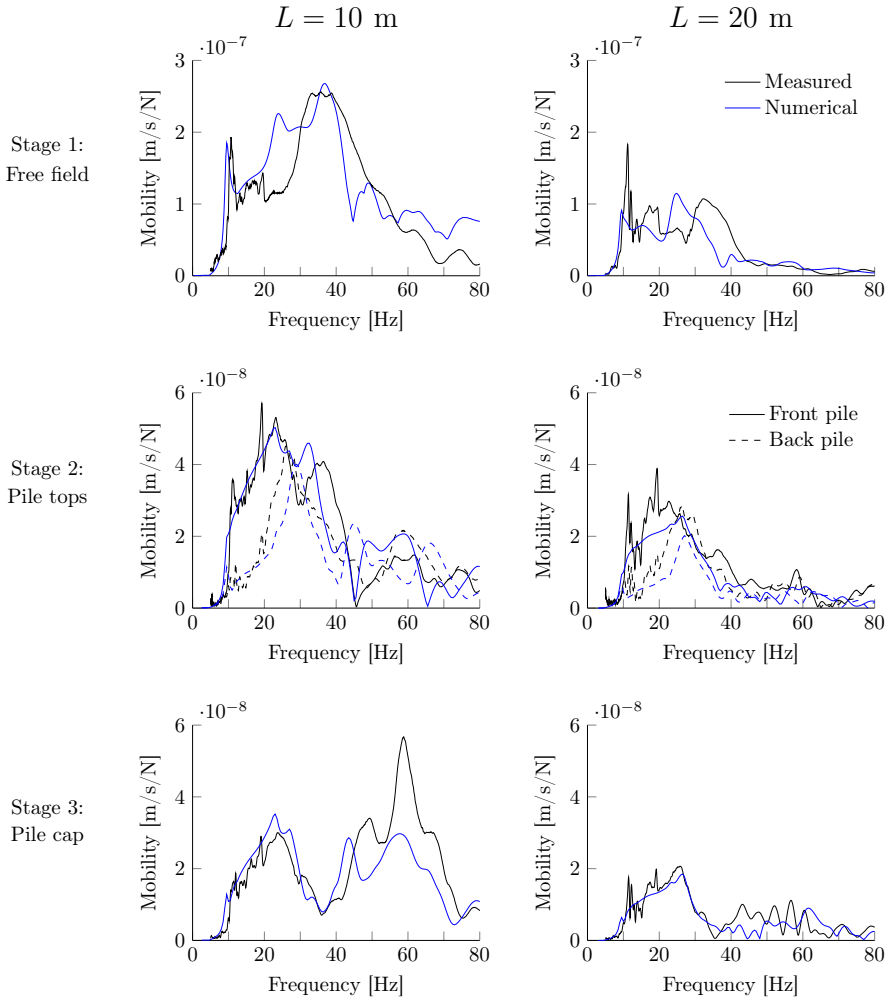

Figure 7: Comparison of the vertical responses obtained from the measurements (black) and from the numerical predictions (blue), at source-receiver distances $L = 10$ and 20 m. The free field responses are evaluated as an amplitude average over the footprint of the foundation (sensors $a_{22} - a_{26}$).

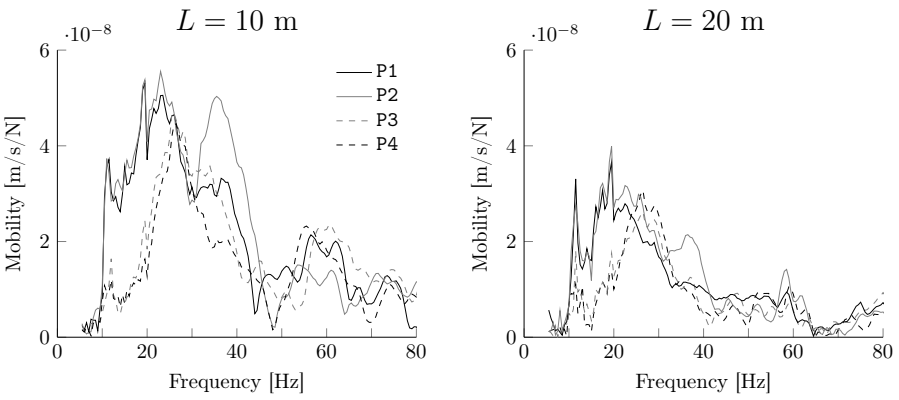

Figure 8: Measured vertical responses of the individual piles P1–P4 for the two source-receiver distances $L = 10$ and 20 m.

surface waves and the conversion, reflection and refraction of body waves at layer interfaces cause interference patterns in the ground surface response, which are difficult to accurately predict due to model uncertainty related to the assumed horizontally layered soil model.

There is a fairly good agreement between the measured and predicted free field vibrations for $L = 10$ m. For $L = 20$ m, the response is underestimated in the frequency range 10–15 Hz, close to the cut-off frequency for wave propagation in the soil. This is also reflected in the responses of the piles and the pile cap for $L = 20$ m.

The averages of the two pile pairs (P1, P2) (sensors $a_{03} - a_{06}$ and $a_{09} - a_{12}$ in stage 2) and (P3, P4) (sensors $a_{15} - a_{18}$ and $a_{21} - a_{24}$ in stage 2) are presented in fig. 7 when compared to the numerical results. Figure 8 show that, despite the piles being of slightly different lengths, the responses of the piles are similar for the two pairs which are farthest and closest to the source points. This is because the piles are symmetrically placed with respect to the source points and the excitation is thereby similar for each pile pair. The largest differences in the vertical responses of the piles occur between 30–40 Hz, where the response amplitudes of the longer piles are higher than for the shorter piles, comparing P1 to P2 and P3 to P4.

The numerically predicted responses in stage 2 agree well with the measurements, especially in the relationship between the response of the piles in the front and in the back. The responses of the pile pairs differ significantly in their amplitudes for frequencies below 25 Hz, where the response of the piles in the front (P1,P2) is much higher than for the pile pair in the back (P3,P4). This indicates the presence of a strong scattered wave field which interferes with the incident wave field, meaning that the responses of the piles are affected by the presence of the other piles in the group. This is in contrast with the influence of pile-soil-pile interaction for floating pile groups in a homogeneous halfspace subjected to Rayleigh waves.

In that case, pile-soil-pile interaction has only a minor influence on the vertical group response [17]. Both the numerical and experimental results presented here show that this is not the case for this type of pile foundation.

The numerically predicted responses in fig. 7 of the pile cap are in equally good agreement with the measured response, obtained as the average of sensors $a_{01} - a_{04}$ in stage 3, as for the pile tops in stage 2. Compared to stage 2, there is a rather pronounced amplification of the response around 60 Hz for the source-receiver distance of $L = 10$ m. This amplification of the response is due to the pile cap inertia, which causes the real part of the vertical pile group impedance to become zero around this frequency, i.e. the natural frequency for the fundamental vertical mode of vibration of the pile group [23]. This amplification is not as pronounced for the distance $L = 20$ m because of the stronger attenuation of waves with shorter wavelength due to soil material damping. Increasing the distance between the source and receiver, more wavelengths are required to cover the travel distance. The attenuation due to material damping is governed by the number of cycles in the hysteresis loop, and higher frequency waves are therefore more strongly attenuated as the source-receiver distance increases.

The vertical response of the pile cap can be analysed in terms of the individual pile responses measured in the previous construction stage. This is further elaborated in section 7, but a few observations on the response characteristics of the pile tops can be made. The peak velocity response is found around 26 Hz for both $L = 10$ m and 20 m. At this frequency, the front and back pile rows' responses are similar in amplitude and fig. 9 shows that the phase differences in their motion are less than $2\pi/3$, indicating that the pile responses add constructively to the vertical response amplitude. At a frequency of 31 Hz, the vertical motions of the front and back rows of piles are out of phase. For a homogeneous soil, this frequency is related to the Rayleigh wave speed of the soil and the pile spacing s as $f_{\mathrm{d}} = C_{\mathrm{R}}/2s$. For the present pile spacing, this frequency corresponds to a Rayleigh wave speed of $C_{\mathrm{R}} \approx 85$ m/s, which agrees with the approximate surface wave speed for the clay layer (no. 4 in table 1) corresponding to the penetration depth of the surface wave.

The amplitude of the free field response should here be considered as a reference level for the evaluated pile responses. As it is the most commonly adopted type of experimental data used for vibration assessment purposes, it is of practical interest to relate the foundation response to the free field motion. Figure 10 presents a comparison between the measured responses of the piles and the pile cap normalised by the free field response amplitude for the two source-receiver distances $L = 10$ m and $L = 20$ m, expressed as a vertical

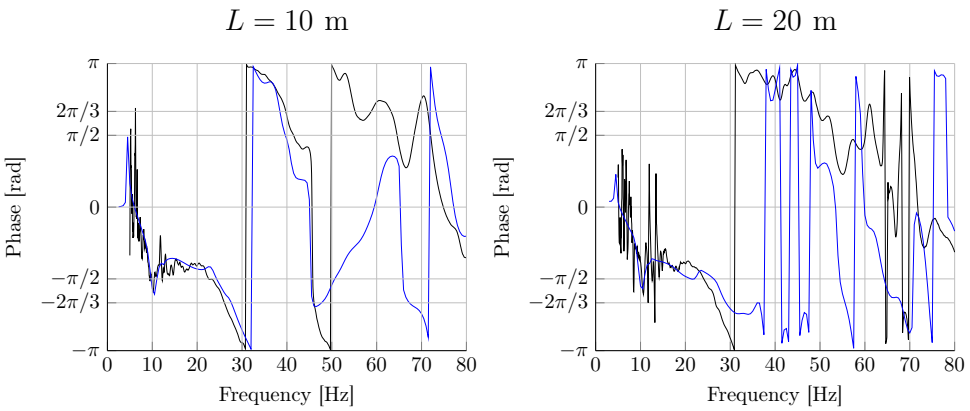

Figure 9: Phase between the vertical response of the back and front row of piles obtained from the measurements (black) compared to the numerical results (blue) for two source-receiver distances $L = 10$ and 20 m.

interaction factor:

$$\mathrm{I_v} = \frac{|v_\mathrm{p}|}{|v_\mathrm{ff}|} \tag{2}$$

where v_p denotes the foundation mobilities in stages 2 and 3 and v_ff the corresponding reference free field mobility in stage 1. In this case, to cancel some of the interference patterns in the vertical free field response, the amplitude of the reference free field vibrations are averaged over a distance corresponding to the length of the piles. This is done using sensors a_{20}, a_{21}, a_{23}, a_{24}, a_{25}, a_{27} and a_{28}, which only has a minor effect on $\mathrm{I_v}$ compared to using sensor a_{24} as reference. For frequencies lower than 20 Hz, this averaging has virtually no effect. It is clear that the relationship between the amplitudes of the foundation and free field responses follows a similar trend for the two distances and there is an almost perfect agreement for frequencies below 23 Hz. The influence of the pile cap inertia, although not as clearly observed in the absolute response for the distance $L = 20$ m in fig. 7, is similar in relation to the free field response compared to the case where $L = 10$ m. This shows that the relative attenuation due to the increase in distance is similar for the free field and pile group responses. These results also suggest that the influence of soil-foundation interaction on the vertical response is not very sensitive to the distance between the source and the foundation when surface waves are the dominant sources of excitation. The practical implication is that the influence of soil-foundation interaction can be taken into account in a relative sense for vibration assessment purposes, where the vertical vibration response of a pile foundation can be estimated from free field vibrations. However, additional test data is required to support the general validity of this conclusion.

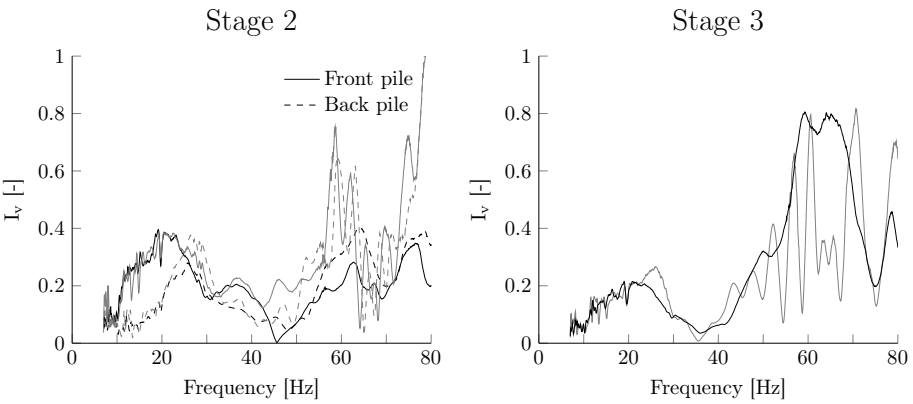

Figure 10: Vertical response factor of the free pile tops in stage 2 (left) and of the pile cap in stage 3 (right) with reference to the average amplitude of the free field response in stage 1 over the measurement line including the sensors a_{20}, a_{21}, a_{23}, a_{24}, a_{25}, a_{27} and a_{28} for $L = 10$ m (black) and $L = 20$ m (gray).

6.2. Horizontal responses

To illustrate the filtering effects of the pile union and pile cap inertia, vibrations in the horizontal x-direction in fig. 5 in the three stages are studied. In the horizontal direction, the responses over the footprint of the pile foundation are very similar and the response measured at the position a_{12} in fig. 5 is therefore presented as the representative free field motion. Figure 11 compares the numerical responses to the measured ones for the three construction stages. Comparing the measurement data between stage 1 and 2, it is clear that, in general, the piles follow the free field motion. The pile group responses in stage 3 closely follow the pile responses in stage 2 up to about 16 Hz. For higher frequencies, the responses in stage 3 are significantly lower due to the connections of the piles and pile cap inertia. Standing waves in soil layers, which occur due to layer stiffness contrasts, may produce peaks in the response spectrum. The peaks in the measured horizontal pile group responses at 14 and 24 Hz observed in fig. 11 correspond to the second and third modes of standing vertically propagating shear waves. These were also identified as peaks in the response from tests were forces were applied at top of the piles in stage 2 and on the pile cap in stage 3 [23]. The corresponding peaks for the model are shifted towards lower frequencies, indicating that the soil model is not entirely accurate.

6.3. Rotational responses

As the wave loading impinges on the piles, cross sectional rotations are induced on the pile tops in Stage 2 and rotation of the pile cap in Stage 3. The rotations are calculated from the vertical acceleration measurements recorded in stage 2 and 3. In stage 3, the rotational velocities around the y-axis are obtained,

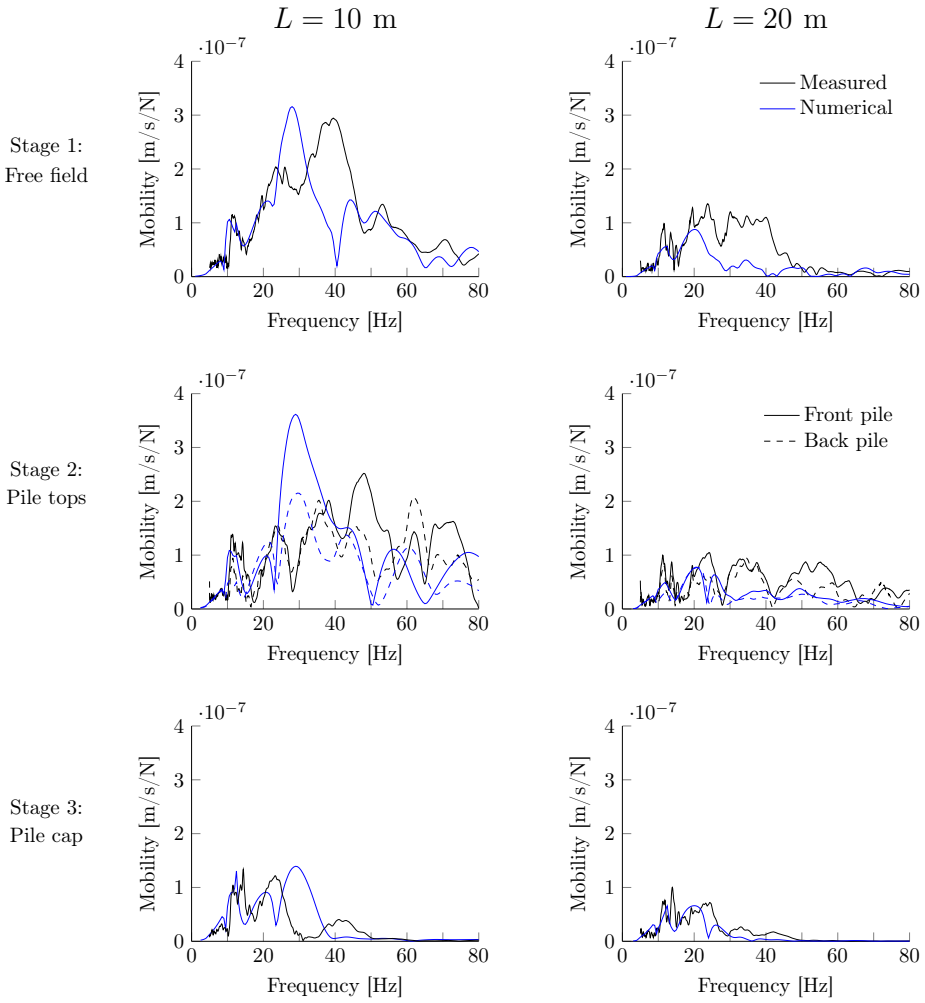

Figure 11: Comparison of the horizontal responses obtained from the measurements (black) and from the numerical predictions (blue), at source-receiver distances $L = 10$ and 20 m.

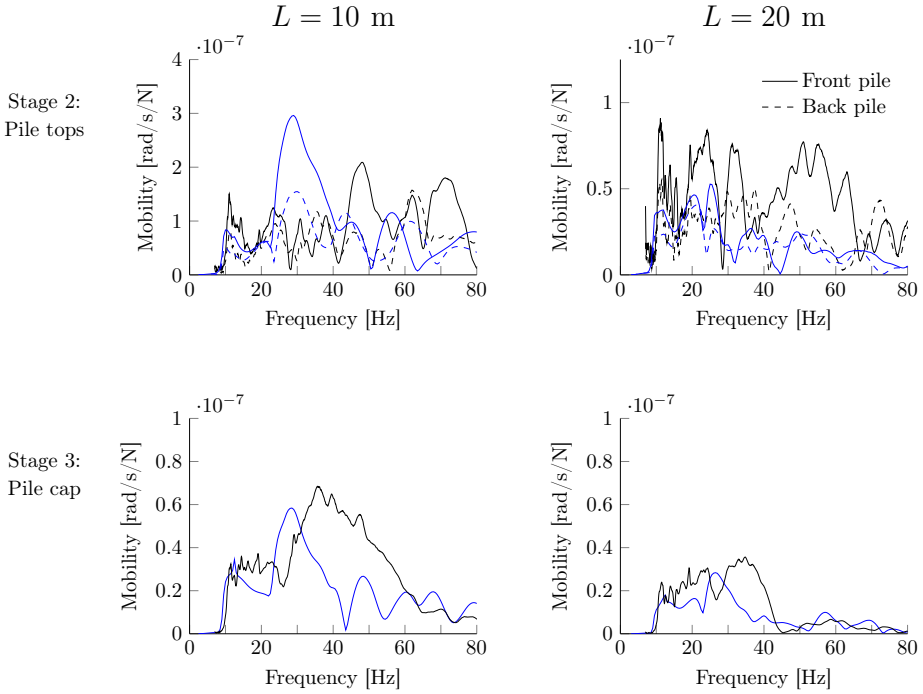

Figure 12: Comparison of the rotational responses around the y-axis obtained from the measurements (black) and from the numerical predictions (blue) for the pile cross sections and of the pile cap, at source-receiver distances $L = 10$ and 20 m.

with reference to fig. 5, from:

$$\theta = \frac{1}{\mathrm{i}\omega} \frac{(a_{01} + a_{02}) - (a_{03} + a_{04})}{2 \cdot 1.7} \tag{3}$$

and the cross sectional rotations of the piles tops in stage 2 are obtained similarly.

Figure 12 presents a comparison between the measured and numerically predicted rotations around the y-axis for the two tests performed. The numerical results in stage 2 compare in a similar way to the measurements as the horizontal vibrations of the piles. This is not very surprising, as the bending of the piles is coupled to their horizontal motion. The pile cap rotational response, on the other hand, is essentially due to the kinematic compatibility of the pile cap and the vertical components of the individual piles [16]. The numerically predicted response for $L = 10$ m shows a maximum around a frequency of 31 Hz, which correspond to the out-of-phase vertical motion of the front and back-row piles, as observed from fig. 9. This is not the case for the measured pile group rotations, where this peak is shifted to a frequency of about

35 Hz, corresponding to the minima in fig. 7 in the vertical responses of the pile cap and where the vertical motions of the sensor pairs ($a_{01},\ a_{02}$) and ($a_{03},\ a_{04}$) in stage 3 are out of phase.

7. Hybrid prediction using the method of mobilities

A drawback of numerical modelling for this type of problem is that it generally requires idealising assumptions about both the surrounding environment and the composition of the soil which generally do not agree with reality. An alternative to numerically simulating the full problem is to make use of measurements taken at an intermediate construction stage. By doing so, the numerical solution of the source problem (i.e. the excitation by the incident wave field) is replaced by measured foundation responses. These are subsequently used as input to a numerical model to make predictions of the response of the overlying structure. François et al. [30] implemented such a hybrid approach for a floating pile foundation through the use of the method of mobilities first introduced in acoustics by Mondot and Petersson [31] and later adopted for application to ground-borne vibration by Ropars [32]. This method aims to compute the response of a coupled source-receiver system where only the motion of the uncoupled source system is known.

In the present application, the source system consists of the soil domain and the piles whereas the receiver system is the pile cap. The method is formulated in the frequency domain and thus requires that the systems can be considered linear and time invariant. It also assumes that the surface areas of contact between the source and receiver can be considered rigid. Figure 13 gives an overview of the decomposition of the source-receiver problem.

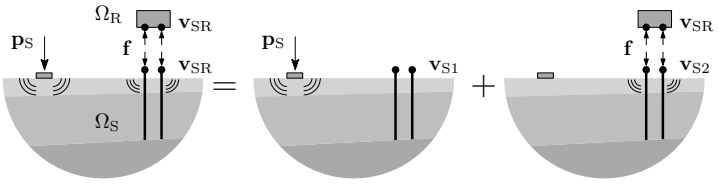

Figure 13: Decomposition of the pile group source-receiver system for the method of mobilities.

The excitation force $\mathbf{p}_S$ applied to the source domain Ω_S gives rise to the velocity responses $\mathbf{v}_{SR}$ and the corresponding interaction forces $\mathbf{f}$ at the contact points at the interface $\Omega_S \cap \Omega_R$ between the source and receiver domains. The velocities $\mathbf{v}_{SR}$ of the coupled source-receiver system differ from the velocities $\mathbf{v}_{S1}$ where the receiver system is absent. Similarly, applying the interaction forces $\mathbf{f}$ at the contact points of the source system results in the velocities $\mathbf{v}_{S2}$ on the source side, which is due to the interaction with the receiver system. The total velocity response of the coupled source-receiver system can thus be obtained by

superposition of the states 1 and 2 on the source side as:

$$\mathbf{v}_{\mathrm{SR}} = \mathbf{v}_{\mathrm{S1}} + \mathbf{v}_{\mathrm{S2}} \tag{4}$$

For state 2, the contact point velocities of the source and receiver systems can be written as:

$$\mathbf{v}_{\mathrm{S2}} = \mathbf{Y}_{\mathrm{S}}\mathbf{f} \tag{5}$$

$$\mathbf{v}_{\mathrm{SR}} = -\mathbf{Y}_{\mathrm{R}}\mathbf{f} \tag{6}$$

where $\mathbf{Y}_{\mathrm{S}}$ and $\mathbf{Y}_{\mathrm{R}}$ contain the contact point mobilities of the source and receiver, respectively. Combining eqs. (4) to (6), $\mathbf{v}_{\mathrm{S2}}$ can be eliminated to obtain:

$$\mathbf{v}_{\mathrm{SR}} = \mathbf{Y}_{\mathrm{R}}\Big(\mathbf{Y}_{\mathrm{S}} + \mathbf{Y}_{\mathrm{R}}\Big)^{-1}\mathbf{v}_{\mathrm{S1}} \tag{7}$$

It should be noted that the transformation of the velocities $\mathbf{v}_{\mathrm{S1}}$ to the velocities $\mathbf{v}_{\mathrm{SR}}$ is achieved through a matrix which is dimensionless. Examining eq. (7), it is clear that this matrix can also be written in terms of the systems' impedances, receptances, accelerances or any other term which relates the contact points' motions to contact point forces.

7.1. Pile cap mobility matrix

In the present application, a pile cap is added on top of the piles. As the pile cap is massive, it can be coupled to the piles using rigid body kinematics.

The relation between the translational and rotational velocities and the forces and moments applied at the center of mass of the pile cap is obtained from the force equilibrium of the free pile cap:

$$\mathbf{v}_0 = \begin{Bmatrix} v_{0x} \\ v_{0y} \\ v_{0z} \\ \vartheta_{0x} \\ \vartheta_{0y} \\ \vartheta_{0z} \end{Bmatrix} = \frac{1}{\mathrm{i}\omega} \begin{bmatrix} m & 0 & 0 & 0 & 0 & 0 \\ 0 & m & 0 & 0 & 0 & 0 \\ 0 & 0 & m & 0 & 0 & 0 \\ 0 & 0 & 0 & I_x & 0 & 0 \\ 0 & 0 & 0 & 0 & I_y & 0 \\ 0 & 0 & 0 & 0 & 0 & I_z \end{bmatrix}^{-1} \begin{Bmatrix} N_{0x} \\ N_{0y} \\ N_{0z} \\ M_{0x} \\ M_{0y} \\ M_{0z} \end{Bmatrix} = \mathbf{Y}_0\mathbf{f}_0 \tag{8}$$

where m denotes the mass of the pile cap and I_x, I_y and I_z it's rotational inertia. The contact point velocities

$\mathbf{v}_{\mathrm{SR}}$ at the positions of the pile tops are subsequently written in terms of the pile cap velocities $\mathbf{v}_0$ as:

$$\mathbf{v}_{\mathrm{SR}} = \mathbf{T}^{\mathrm{T}}\mathbf{v}_0 \tag{9}$$

with

$$\mathbf{T} = \begin{bmatrix} \mathbf{t}_1 & \mathbf{t}_2 & \mathbf{t}_3 & \mathbf{t}_4 \end{bmatrix} \tag{10}$$

$$\mathbf{t}_k^{\mathrm{T}} = \begin{bmatrix} 1 & 0 & 0 & 0 & z_{\mathrm{p}k} & -y_{\mathrm{p}k} \\ 0 & 1 & 0 & -z_{\mathrm{p}k} & 0 & x_{\mathrm{p}k} \\ 0 & 0 & 1 & y_{\mathrm{p}k} & -x_{\mathrm{p}k} & 0 \\ 0 & 0 & 0 & 1 & 0 & 0 \\ 0 & 0 & 0 & 0 & 1 & 0 \end{bmatrix} \tag{11}$$

where $x_{\mathrm{p}k}$, $y_{\mathrm{p}k}$ and $z_{\mathrm{p}k}$ are the coordinates of the pile tops with respect to the center of mass of the pile cap. The forces acting on the pile cap are related to the contact point forces by:

$$\mathbf{f}_0 = -\mathbf{T}\mathbf{f} \tag{12}$$

It then follows from eqs. (6), (8), (9) and (12) that:

$$\mathbf{Y}_{\mathrm{R}} = \mathbf{T}^{\mathrm{T}}\mathbf{Y}_0\mathbf{T} \tag{13}$$

which can be used in eq. (7) to account for the effects of pile cap inertia.

Finally, the velocities of the pile cap are obtained from the contact point velocities as:

$$\mathbf{v}_0 = \left(\mathbf{T}\mathbf{T}^{\mathrm{T}}\right)^{-1}\mathbf{T}\mathbf{v}_{\mathrm{SR}} \tag{14}$$

7.2. Experimental mobility matrix

The mobilities at the pile tops were determined by local excitation on the top of the piles in the vertical and horizontal directions in stage 2. An in-depth analysis of the local responses of the piles and the pile group can be found in [23].

The measurements of the pile mobilities are gathered in the matrix $\mathbf{Y}_{\mathrm{S}} \in \mathbb{C}^{20\times 20}$:

$$\mathbf{Y}_{\mathrm{S}} = \begin{bmatrix} \mathbf{Y}_{xx} & \mathbf{Y}_{xy} & \mathbf{Y}_{xz} & \mathbf{Y}_{x\varphi} & \mathbf{Y}_{x\theta} \\ \mathbf{Y}_{yx} & \mathbf{Y}_{yy} & \mathbf{Y}_{yz} & \mathbf{Y}_{y\varphi} & \mathbf{Y}_{y\theta} \\ \mathbf{Y}_{zx} & \mathbf{Y}_{zy} & \mathbf{Y}_{zz} & \mathbf{Y}_{z\varphi} & \mathbf{Y}_{z\theta} \\ \mathbf{Y}_{\varphi x} & \mathbf{Y}_{\varphi y} & \mathbf{Y}_{\varphi z} & \mathbf{Y}_{\varphi\varphi} & \mathbf{Y}_{\varphi\theta} \\ \mathbf{Y}_{\theta x} & \mathbf{Y}_{\theta y} & \mathbf{Y}_{\theta z} & \mathbf{Y}_{\theta\varphi} & \mathbf{Y}_{\theta\theta} \end{bmatrix} \tag{15}$$

where the sub-matrices $\mathbf{Y}_{ij} \in \mathbb{C}^{4\times 4}$ are evaluated for each frequency ω. The coupling terms between the rotational degrees of freedom, φ around the x-axis and θ around the y-axis, and the translational degrees of freedom, are evaluated for the case of rotational response due to the translational load. Assuming that the system is linear, reciprocity holds and the submatrices $\mathbf{Y}_{ij}$ are consequently symmetric (i.e. $\mathbf{Y}_{ji} = \mathbf{Y}_{ij}^{\mathrm{T}}$). Thereby, the submatrices corresponding to responses in translational degrees of freedom due to rotations are obtained by transposing the corresponding reciprocal submatrix. The rotational mobilities for each pile were obtained by applying an eccentric vertical load on the pile cross section to generate a moment. This allows estimating the moment induced rotations at each pile head, but as the other piles are subjected to the wave field also induced by the vertical pile motion, the cross-terms cannot be accurately captured and are therefore disregarded, which means that $\mathbf{Y}_{\theta\theta}$ and $\mathbf{Y}_{\varphi\varphi}$ are diagonal and $\mathbf{Y}_{\varphi\theta}$ and $\mathbf{Y}_{\theta\varphi}$ are both zero. It is further assumed that the vertical-horizontal and vertical-rotational coupling terms can be disregarded. The validity of these simplifications has been confirmed by application of the method of mobilities on the numerical model used in this work.

7.3. Hybrid prediction of the vertical pile cap response

Figure 14 compares vertical mobilities obtained from the hybrid prediction to the measured pile cap mobilities. As discussed in section 6, the amplification of the response observed around 60 Hz is due to the inertia of the pile cap. This is also predicted using the hybrid method and is indeed dependent on the relationship between the pile top mobilities and the mass of the pile cap. It is also observed that the peaks and troughs in the responses are slightly shifted in frequency compared to the measured pile cap responses. This was also observed locally, i.e in the evaluation of the vertical pile-to-pile interaction terms and the vertical pile group impedance [23]. A possible explanation could be that the construction of the pile cap might have had an influence on the soil directly underneath the pile cap in terms of the soil stiffness or modification of the contact conditions between the soil and the piles.

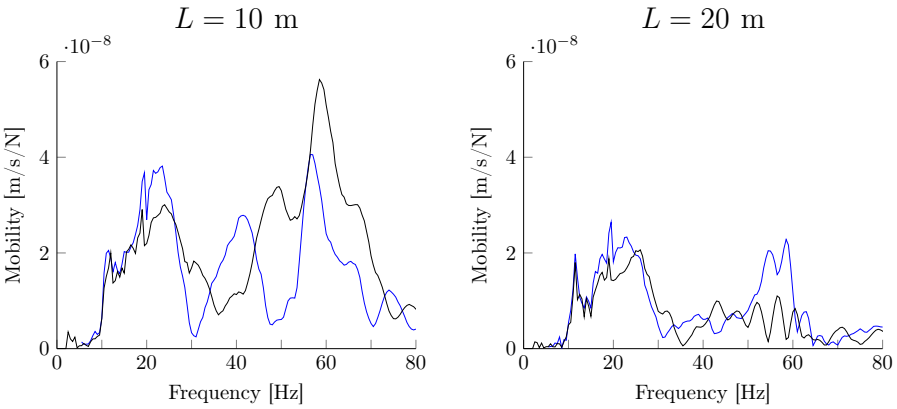

Figure 14: Hybrid prediction (blue) compared to measurements (black) of the vertical pile group response due to a vertical load applied at a $L = 10$ m and $L = 20$ m horizontal distance.

7.4. Hybrid prediction of the horizontal pile cap response

While the vertical response of the pile cap is mainly dependent on the vertical pile responses, the horizontal response is coupled to the cross sectional rotations of the piles through the matrix $\mathbf{Y}_{\mathrm{S}}$. Therefore, prediction of the horizontal and rotational pile group responses is more sensitive to the relationships described by $\mathbf{Y}_{\mathrm{S}}$. Figure 15 compares the horizontal pile group response in stage 3 to the hybrid prediction obtained using the method of mobilities. Generally, the horizontal pile group response follows the free field motion (see

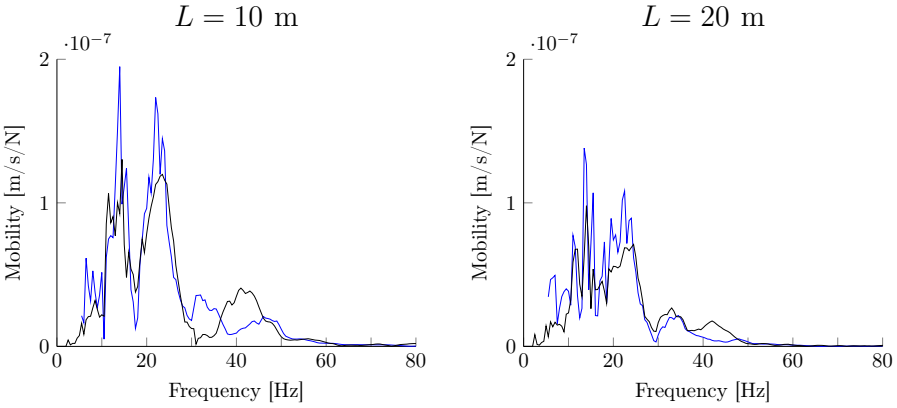

Figure 15: Hybrid prediction (blue solid line) compared to the measurements (black) of the horizontal pile group response due to a vertical load applied at a $L = 10$ m and $L = 20$ m horizontal distance.

fig. 11) up to a frequency of 14 Hz, which coincides with the second natural frequency of the soil layer in horizontal motion [23], for which the response is amplified, while it is attenuated for higher frequencies. This

amplification around 14 Hz and the attenuation of the response with frequency is captured in the hybrid prediction, but the amplification of the response for frequencies up to 25 Hz is slightly overestimated.

7.5. Hybrid prediction of the rotational pile cap response

Figure 16 indicates that the influence of the pile cap on the rotational response of the pile group is somewhat overestimated using the method of mobilities, especially for frequencies higher than 40 Hz. However, the predicted response is closer to the measured response when compared to the numerically predicted responses in fig. 12.

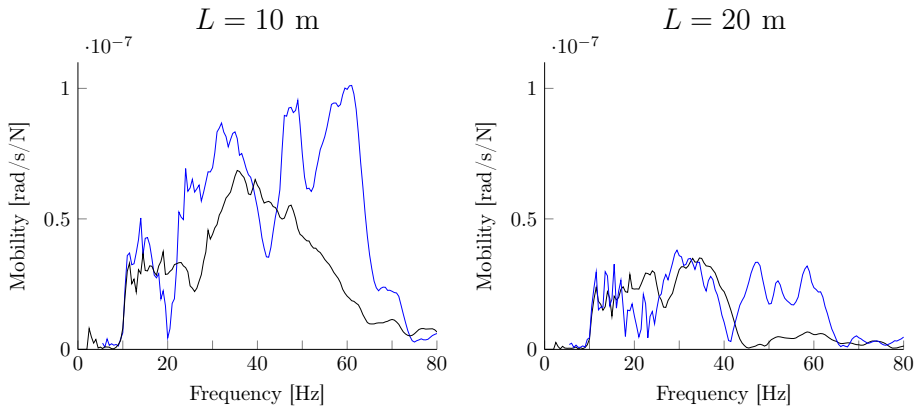

Figure 16: Hybrid prediction (blue) and measurement (black) results of the rotational pile group response due to a vertical load applied at a $L = 10$ m and $L = 20$ m horizontal distance from the pile group.

The fairly good agreement between the measurements and the predictions obtained for this rather simple problem is a promising step for extending the application of hybrid substructuring methods for larger foundation systems.

8. Conclusion

This paper aims to provide experimental data from full-scale field experiments on the vibration response of an end-bearing pile foundation subjected to a vertical ground surface load and to assess predictions from both a numerical model and from measurements performed prior to the completion of the foundation.

To experimentally characterise the dynamic response of an end-bearing pile group in soft clay, measurements have been performed at a designated test site in three stages of construction of a 2×2 concrete pile group when subjected to vertical excitation applied at the ground surface at two horizontal source-receiver distances of 10 and 20 m. The measurements were performed (1) in the free field before construction, (2) on

the free pile tops after driving of the piles and (3) after the casting of the concrete pile cap joining the piles together. Performing measurements in these three stages allow to experimentally establish the connection between free field vibrations and the vibrations of the foundation.

The measurements are subsequently used to validate a numerical model of the experiment. In addition, a hybrid method to estimate the response of the pile cap from measurements of the pile top responses and mobilities performed in stage 2 is evaluated. The following conclusions are made:

1. In the context of ground borne vibration, the numerical predictions of the vertical responses in all three stages of construction are in fairly good agreement with the measurements. This motivates the use of numerical models of end-bearing pile foundations for practical vibration assessment where the vertical floor vibrations in a building are estimated from the vertical vibration of the foundation.

2. The horizontal and rotational responses of the pile group are less accurately captured by the numerical model, whilst the over-all amplitude of the responses are reasonably well represented.

3. The vertical responses of the free pile tops for frequencies below 25 Hz are substantially different when comparing the pile pair closest and farthest from the source point. This shows that, in contrast to floating pile groups in homogeneous soil, pile-soil-pile interaction has an important influence on the vertical response of end-bearing piles.

4. The ratio between the vertical amplitude of the piles and the free field vibrations are similar for the two considered source-receiver distances. This suggests that the amplitude of the foundation response can be estimated from measured free field vibrations.

5. Hybrid predictions of the pile group response capture the influence of the pile union and pile cap inertia. The hybrid predictions are equally good compared to the numerical ones for the vertical response and offers an improvement in the prediction of the horizontal and rotational pile group responses. This shows that measurements performed on piles at an early construction stage can potentially improve predictions of ground-borne vibration.

9. Acknowledgements

This work is supported by the Development Fund of the Swedish Construction Industry (SBUF) and the Swedish Transport Administration (Trafikverket). The financial support is gratefully acknowledged. The authors would also like to extend their gratitude towards Ragnvald Andersson for providing free access to the site used for the experiments performed in this work.

References

[1] S. François, L. Pyl, H. Masoumi, G. Degrande, The influence of dynamic soilstructure interaction on traffic induced vibrations in buildings, Soil Dynamics and Earthquake Engineering 27 (2007) 655–674.

[2] M. Schevenels, G. Degrande, G. Lombaert, The influence of the depth of the ground water table on free field road traffic-induced vibrations, International Journal for Numerical and Analytical Methods in Geomechanics 28 (2004) 395–419.

[3] E. Kausel, Advanced Structural Dynamics, Cambridge University Press, 2017. doi:10.1017/9781316761403.

[4] P. Persson, K. Persson, G. Sandberg, Numerical study on reducing building vibrations by foundation improvement, Engineering Structures 124 (2016) 361–375.

[5] M. Papadopoulos, S. François, G. Degrande, G. Lombaert, The influence of uncertain local subsoil conditions on the response of buildings to ground vibration, Journal of Sound and Vibration 418 (2018) 200–220.

[6] L. Auersch, Wave propagation in the elastic half-space due to an interior load and its application to ground vibration problems and buildings on pile foundations, Soil Dynamics and Earthquake Engineering 30 (2010) 925–936.

[7] D. Connolly, G. Kouroussis, P. Woodward, A. Giannopoulos, O. Verlinden, M. Forde, Scoping prediction of re-radiated ground-borne noise and vibration near high speed rail lines with variable soils, Soil Dynamics and Earthquake Engineering 66 (2014) 78–88.

[8] D. López-Mendoza, A. Romero, D. Connolly, P. Galvń, Scoping assessment of building vibration induced by railway traffic, Soil Dynamics and Earthquake Engineering 93 (2017) 147–161.

[9] L. Auersch, Simple and fast prediction of train-induced track forces, ground and building vibrations, Railway Engineering Science 28 (2020) 1–19.

[10] C. Madshus, B. Bessason, L. Hårvik, Prediction model for low frequency vibration from high speed railways on soft ground, Journal of Sound and Vibration 193 (1996) 195–203.

[11] C. E. Hanson, J. C. Ross, D. A. Towers, High-Speed Ground Transportation Noise and Vibration Impact Assessment, Technical Report DOT/FRA/ORD-12/15, U.S. Department of Transportation, Federal Railroad Administration, Office of Railroad Policy and Development, 2012.

[12] E. Kausel, R. V. Whitman, J. P. Morray, F. Elsabee, The spring method for embedded foundations, Nuclear Engineering and Design 48 (1978) 377–392.

[13] J. E. Luco, H. L. Wong, Dynamic response of rectangular foundations for Rayleigh wave excitation, in: Proc. 6th World Conf. on Earthquake Eng., volume 2, 1977, pp. 1542–1548.

[14] L. Tham, J. Qian, Y. Cheung, Dynamic response of a group of flexible foundations to incident seismic waves, Soil Dynamics and Earthquake Engineering 17 (1998) 127–137.

[15] L. Auersch, Response to harmonic wave excitation of finite or infinite elastic plates on a homogeneous or layered half-space, Computers and Geotechnics 51 (2013) 50–59.

[16] A. M. Kaynia, M. Novak, Response of pile foundations to Rayleigh waves and obliquely incident body waves, Earthquake Engineering & Structural Dynamics 21 (1992) 303–318.

[17] N. Makris, D. Badoni, Seismic response of pile groups under oblique-shear and Rayleigh waves, Earthquake Engineering & Structural Dynamics 24 (1995) 517–532.

[18] K. Kuo, M. Papadopoulos, G. Lombaert, G. Degrande, The coupling loss of a building subject to railway induced vibrations: Numerical modelling and experimental measurements, Journal of Sound and Vibration 442 (2019) 459–481.

[19] G. Sanitate, J. Talbot, Foundation vibration and the added-building effect: Experimental evidence from a ground-borne vibration measurement campaign, Journal of Sound and Vibration 544 (2023) 117390.

[20] N. Chouw, R. Le, G. Schmid, Propagation of vibration in a soil layer over bedrock, Engineering Analysis with Boundary Elements 8 (1991) 125–131.

[21] G. Lombaert, G. Degrande, D. Clouteau, The influence of the soil stratification on free field traffic-induced vibrations, Archive of Applied Mechanics 71 (2001) 661–678.

[22] F. Theland, G. Lombaert, S. François, C. Pacoste, F. Deckner, J.-M. Battini, Assessment of small-strain characteristics for vibration predictions in a Swedish clay deposit, Soil Dynamics and Earthquake Engineering 150 (2021) 106804.

[23] F. Theland, G. Lombaert, S. Franois, C. Pacoste, F. Deckner, P. Blom, J.-M. Battini, Dynamic response of driven end-bearing piles and a pile group in soft clay: an experimental validation study, Engineering Structures 267 (2022) 114629.

[24] Google Earth Pro V.7.3.3.7786, Brottby, Sweden, March 19, 2020. 59°35'24.3"N 18°10'26.0"W, Eye alt 383 m. Maxar Technologies 2020. http://www.earth.google.com [September 21, 2020].

[25] P. Eriksson, L. Jendeby, T. Olsson, T. Svensson, Kohesionspålar, Technical Report 100, Commission of Pile Research, 2004.

[26] O. Hunaidi, J. H. Rainer, Evaluation of measurement limits of transducer mountings in the ground, Canadian Acoustics (1990).

[27] G. Degrande, P. Van den Broeck, D. Clouteau, A critical appraisal of in situ vibration measurements, in: 3rd European conference in Structural Dynamics, Balkema, Florence, 2014, pp. 1107–1116.

[28] U. Basu, A. K. Chopra, Perfectly matched layers for time-harmonic elastodynamics of unbounded domains: theory and finite-element implementation, Computer Methods in Applied Mechanics and Engineering 192 (2003) 1337 – 1375.

[29] M. Schevenels, S. François, G. Degrande, EDT: An ElastoDynamics Toolbox for MATLAB, Computers & Geosciences 35 (2009) 1752 – 1754.

[30] S. François, M. Schevenels, G. Lombaert, G. Degrande, Numerical modeling and in situ vibration measurements during the design and construction of low vibration floors at the corelab 1b research facility, in: Proceedings of ISMA 2014, International Conference on Noise and Vibration Engineering, Leuven, Belgium, 2014.

[31] J. Mondot, B. Petersson, Characterization of structure-borne sound sources: The source descriptor and the coupling function, Journal of Sound and Vibration 114 (1987) 507–518.

[32] P. Ropars, Modélisation des vibrations d'origine ferroviaire transmises aux bâtiments par le sol, Theses, Université Paris-Est, 2011. URL: `https://theses.hal.science/tel-00681780`.

Paper IV

Design procedure for estimating the vertical response of end-bearing piles from free field vibrations produced by a nearby surface load

Freddie Theland[a,*], Geert Lombaert[b], Stijn François[b], Abbas Zangeneh[a,c], Fanny Deckner[d], Jean-Marc Battini[a]

[a] *KTH Royal Institute of Technology, Department of Civil and Architectural Engineering, Brinellvägen 23, 100 44 Stockholm, Sweden*
[b] *KU Leuven, Department of Civil Engineering, Kasteelpark Arenberg 40, 3001 Leuven, Belgium*
[c] *ELU Konsult AB, Valhallavägen 117, 115 31 Stockholm, Sweden*
[d] *GeoMind KB, Fannys väg 3, 131 54 Nacka, Sweden*

Abstract

This paper investigates the vertical response of end-bearing piles in a homogeneous isotropic linear elastic soil on a rigid bedrock subjected to a vertical harmonic point load at the soil's surface. A numerical model is used to compute vibration responses. A novel system of dimensionless parameters is established to bring insight into the influence of the relationships between soil and pile properties on the dynamic pile-soil interaction and to allow for general conclusions to be drawn. The results show the conditions under which the relationship between the axial stiffness of the pile and the stiffness of the soil has a significant influence on the end-bearing pile response. Different pile group configurations are considered where the vertical response is found to be bounded by the single pile response, justifying its use as a conservative estimate for the group response. Finally, an expression including only two dimensionless parameters, the pile slenderness ratio and the pile-soil stiffness ratio, is proposed for calculating an estimation of the vertical response of an end-bearing pile from the free field vibrations.

Keywords: End-bearing piles, Floating piles, Surface waves, Kinematic interaction, Dynamic soil-structure interaction, Pile group, Ground-borne vibration

1. Introduction

In the urban environment, industrial or construction activities, major roads or railway traffic can give rise to significant levels of ground-borne vibration, potentially causing annoyance for residents or disruption of vibration sensitive equipment when transmitted through the soil into nearby buildings. In the planning of new buildings in the vicinity of such vibration sources, it is important to be able to estimate the risk of exceeding vibration threshold criteria. The prediction of ground-borne vibration in buildings requires an

*Corresponding author: Tel. +46(0) 70 408 41 97
Email addresses: freddie.theland@byv.kth.se (Freddie Theland), geert.lombaert@kuleven.be (Geert Lombaert), stijn.francois@kuleven.be (Stijn François), abbas.zangeneh@elu.se (Abbas Zangeneh), fanny.deckner@geomind.se (Fanny Deckner), jean-marc.battini@byv.kth.se (Jean-Marc Battini)

accurate representation of the vibration source, the wave propagation through the soil and the receiving structure. This is a challenging task, as each of these terms is subject to model bias, parametric uncertainty and, in practice, a limited knowledge of the spatial distribution of the subsoil conditions. For this reason, it is of interest to predict the vibration response of a building from vibrations measured at the soil's surface prior to construction, as adopted in both simplified parametric models and empirical prediction schemes [1–5]. Still, these models require that soil-foundation-structure interaction is properly taken into account, as it has a significant influence on the transmission of vibrations [6–8]. The interaction between soil and foundations can be subdivided into kinematic and inertial interaction. The kinematic interaction concerns the foundations influence on the dynamic excitation of a building caused by an incident wave field, whereas the inertial interaction concerns the modification of the dynamic characteristics of the building due to soil-structure interaction [9].

For pile foundations, kinematic interaction can have a significant impact on the vibration transmission characteristics. The kinematic interaction depends not only on the foundation and the properties of the soil, but also on the incident wave type. The kinematic interaction of piles has been extensively covered in the literature in the context of earthquake engineering, primarily for body waves of vertical incidence [10, 11]. Less attention has been directed towards the kinematic interaction between the pile and the soil in case of surface waves.

For homogeneous soils, the response of piles in a halfspace have been considered. Kaynia and Novak [12] used a rigorous boundary integral model to obtain the horizontal and rocking responses of piles and square pile groups subjected to obliquely incident body waves and Rayleigh waves. Pile-soil-pile interaction was found to be insignificant to the response and, while the horizontal motion due to Rayleigh waves was bounded by the soil free field response, significant rotational motion was produced in the pile groups considered. Makris [13] developed closed-form expressions for vertical and horizontal displacements of a single pile subjected to Rayleigh waves based on a dynamic Winkler foundation model. Vertical displacements were found to be sensitive to the total length of the pile and to differ considerably from the vertical displacements of the soil. Makris and Badoni [14] further developed the model to study the response of square pile groups subjected to inclined shear and Rayleigh waves. For Rayleigh waves, the vertical response of the pile groups was primarily affected by the phase differences in the response of the individual piles. The influence of pile-soil-pile interaction was found to be negligible, as for both rocking and horizontal translation [12]. Similar observations have been made for the response of pile foundations subjected to a nearby vertical point load at the soil's surface [15, 16].

While the response of pile foundations subjected to surface waves has been studied for homogeneous halfspace conditions, the influence of soil stratification has not been systematically treated. Soft soils on

very stiff bedrock are soil conditions often encountered in Sweden and other parts of Scandinavia, which are prone to problems related to ground-borne vibration. Under such conditions, end-bearing piles become attractive for foundation design, which can show significant differences in their vertical response compared to their floating counterpart, as for the case of vertically propagating P-waves [11, 17]. These differences occur due to the change in the dynamic behaviour of the soil and the fixation of the pile to the underlying stiffer layer.

The aim of this paper is to show how the presence of a shallow bedrock influence the vertical vibration response of piles when subjected to a load acting at the soil's surface and to propose engineering approximations to estimate the response of end-bearing pile foundations from vibrations measured in the free field. The novel contributions of this paper are:

1. General results provided by the dimensionless representation of the soil-on-bedrock problem.
2. Assessment of the influence of bedrock on the vertical responses of end-bearing piles in shallow formations of soft soil.
3. Development of a practical procedure for estimating the vertical response of end-bearing piles from free field vibrations.

A numerical model of end-bearing pile foundations in a homogeneous soil on rigid bedrock is considered. The piles are subjected to an incident wave field generated by a nearby vertical point load applied at the soil's surface. The idealisation of a homogeneous layer on bedrock allows for a dimensionless representation of the problem which provides a better understanding of the influence of the soil and pile properties on the dynamic soil-pile interaction. Floating and end-bearing piles in the same soil profile are considered to investigate the influence of fixating the pile to the bedrock, and pile groups with different pile-to-pile spacing are studied to address the influence of group effects.

This paper focuses on the vertical vibrations of pile foundations. The reason is that for ground-borne vibration in buildings, which is the application focus of this paper, it has been shown that the vertical vibrations of floors in buildings are mainly due to the vertical vibrations of the foundation [4, 18]. However, horizontal and rotational responses of pile foundations may also be of interest and some results are therefore presented in appendix A.

The paper is structured as follows. Section 2 defines the considered geometry, the dimensionless representation of the data and the numerical model. Section 3 presents the responses of single piles and sensitivity analyses of problem parameters. Section 4 extends the analysis to square pile groups. Section 5 presents an expression for an approximate vertical interaction factor for end-bearing piles derived from the results

of the single pile analyses. A procedure with a summary of the equations required to estimate the vertical vibration response of end-bearing piles from free field vibrations is outlined. Section 6 concludes the paper.

2. Problem definition

The vertical response of a vertical pile in a homogeneous soil layer over a rigid bedrock is considered. This idealisation is representative for shallow deposits, where the stiffness variation with depth is not very pronounced.

Figure 1 presents an illustration of the problem geometry. The pile is of circular cross section with diameter d and is of linear elastic material with a modulus of elasticity E_p, Poisson's ratio ν_p and density ρ_p. The thickness of the soil layer is H and the distance between the pile tip and the bedrock is δ, so that the length of pile becomes $H-\delta$. The soil is of linear viscoelastic material with the material properties defined in terms of the S and P-wave speeds C_s and C_p, their corresponding hysteretic damping ratios β_s and β_p, and the soil density ρ. A linear hysteretic material damping model is adopted, modifying the soil material wave speeds as $C_\mathrm{p}^* = C_\mathrm{p}\sqrt{1+\mathrm{i}2\beta_\mathrm{p}}$ and $C_\mathrm{s}^* = C_\mathrm{s}\sqrt{1+\mathrm{i}2\beta_\mathrm{s}}$. The pile is assumed perfectly bonded to the soil.

A unit harmonic point load $P=\exp(\mathrm{i}\omega t)$ is applied at the soil's surface at a horizontal distance L from the pile, with ω the circular frequency. The vertical displacement of the pile is denoted u_z.

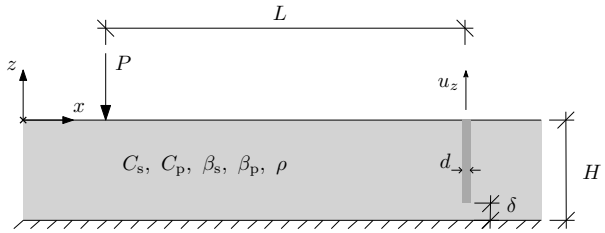

Figure 1: Definition of the problem geometry for a single pile.

To illustrate the influence of the relationships between the properties of the soil and the properties of the pile, a system of dimensionless parameters is established to analyse the problem. The responses are in the following presented in terms of dimensionless translational vertical velocities:

$$\tilde{v} = \mathrm{i}\omega u_z C_\mathrm{s}\rho H L/P \tag{1}$$

as functions of the ratio between the layer depth and the S-wavelength H/λ_s, which can alternatively be interpreted as a dimensionless frequency fH/C_s, where f is the cyclic frequency. This representation of the data provides results that are valid for a wide range of different conditions based on the internal relations

between soil and pile parameters. It should be emphasised that the dimensionless free field velocity $\tilde{v}_{\mathrm{ff}}$ obtained by replacing u_z with the free field displacement at the soil's surface $u_{z,\mathrm{ff}}$ in eq. (1), is uniquely determined as a function of H/λ_{s} for a given dimensionless distance L/H, provided that the dimensionless properties of the soil $C_{\mathrm{p}}/C_{\mathrm{s}}$, β_{s}, β_{p} are unchanged.

For all the analyses presented in this paper, the following dimensionless parameters for the soil are assumed:

- Soil wave speed ratio $C_{\mathrm{p}}/C_{\mathrm{s}} = 15$ ($\nu = 0.4978$) which is intended to represent a fully saturated soil. For the analysis of ground-borne vibration, the frequency is sufficiently low for the saturated soil to behave as a frozen mixture and can thus be modelled as a single phase material [19].
- Damping ratios β_{p} and β_{s} for dilatational and shear waves are both assumed equal to 0.03. This is within the range of values typically encountered for clays or sands [20].

As for the free field response, the dimensionless response of the pile is uniquely determined for a given Poisson's ratio of the pile ν_{p}, depth to diameter ratio H/d, pile-soil stiffness ratio $E_{\mathrm{p}}/E_{\mathrm{s}}$, soil-pile density ratio ρ/ρ_{p} and pile-bedrock separation ratio δ/H. Variations of these parameters are studied to highlight the influence of the relationship between soil and pile properties. The following values of dimensionless parameters are considered:

- Source-pile distance to depth ratio $L/H = 1, 2, 10$
- Depth to diameter ratio $H/d = 50, 25, 12.5$
- Pile-soil stiffness ratio $E_{\mathrm{p}}/E_{\mathrm{s}} = 500, 1000, 2000$
- Soil-pile density ratios $\rho/\rho_{\mathrm{p}} = 0.75, 0.5, 0.25$ for the specific analysis of it's influence on the response. In all other cases, a value of $\rho/\rho_{\mathrm{p}} = 0.75$ is adopted.

Pile-bedrock separation ratios $\delta/H = 0$ and $\delta/H = 0.05$ are considered, corresponding to end-bearing and floating piles, where the separation effectively makes the rigid body motion of the piles the dominating part of the response. Poisson's ratio of the piles is for all cases assumed to be $\nu_{\mathrm{p}} = 0.25$.

All results are presented for ratios H/λ_{s} ranging from 0 to 10, corresponding to a frequency range up to 80 Hz for a soft soil with $C_{\mathrm{s}} = 60$ m/s with a stratum depth of $H = 7.5$ m or for a stiffer soil with $C_{\mathrm{s}} = 120$ m/s and a stratum depth of $H = 15$ m. The focus in this paper is on environmental ground-borne vibration where the shear strains in the soil are sufficiently low to allow for the use of linear elastic material models. In this case, the upper and lower bounds of the range of the pile-soil stiffness ratio correspond to concrete piles for the soft and stiff soil example profiles, respectively. The density ratios considered herein

are set to represent the variation of soil density for concrete and concrete filled steel pipe piles, and the lower bound $\rho/\rho_{\mathrm{p}} = 0.25$ corresponds to a steel core pile in a soil with a density around 2000 kg/m^3.

To study group effects of end-bearing pile groups, square 2×2 arrangements of piles with the separation ratios $s/d = 3,\ 5$ and 10 for piles with $E_{\mathrm{p}}/E_{\mathrm{s}} = 1000$ are considered. Figure 2 presents an overview of the geometry for the pile group problem. The piles are connected to form a group through a massless rigid pile cap at the soil's surface. For the purpose of model verification (in section 2.2), horizontal translation u_x and the rotation θ_y of the rigid pile cap, defined in fig. 2, are also considered.

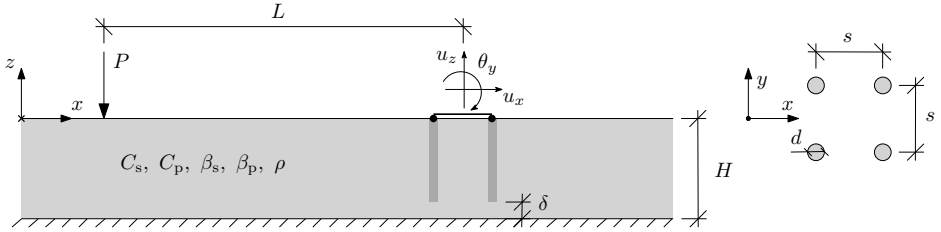

Figure 2: Definition of 2×2 pile group geometry in section (left) and planar (right) view.

2.1. Numerical model

In this work, a three-dimensional finite element model with perfectly matched layers (FE-PML) is used. The pile-soil interface is assumed fully bonded and a linear elastic material model is adopted. The modulus of elasticity and the Poisson's ratio are defined in terms of the material wave speeds according to:

$$C_{\mathrm{s}} = \sqrt{\frac{G}{\rho}} \tag{2}$$

$$C_{\mathrm{p}} = \sqrt{\frac{\lambda + 2G}{\rho}} \tag{3}$$

$$\lambda = \frac{\nu E_{\mathrm{s}}}{(1+\nu)(1-2\nu)}, \quad G = \frac{E_{\mathrm{s}}}{2(1+\nu)} \tag{4}$$

Since the hysteretic damping ratios β_{p} and β_{s} are assumed equal, material damping is incorporated by assigning a complex modulus of elasticity $E_{\mathrm{s}}^* = E_{\mathrm{s}}(1 + \mathrm{i}2\beta)$ for the soil material. Due to the cubic increase of the number of elements with domain size, a subdomain formulation for FE-PML models presented by Papadopoulos et al. [21] is adopted to reduce the domain size and computational effort. The formulation allows for the use of a separate source model. Assuming decoupling between the source and receiver, an equivalent traction field is computed at the inwards PML boundary which is connected to the interior computational soil domain to propagate the incident wave field to the FE-PML model. The computation of the tractions propagating the incident wave field requires the displacement and traction fields in the soil at

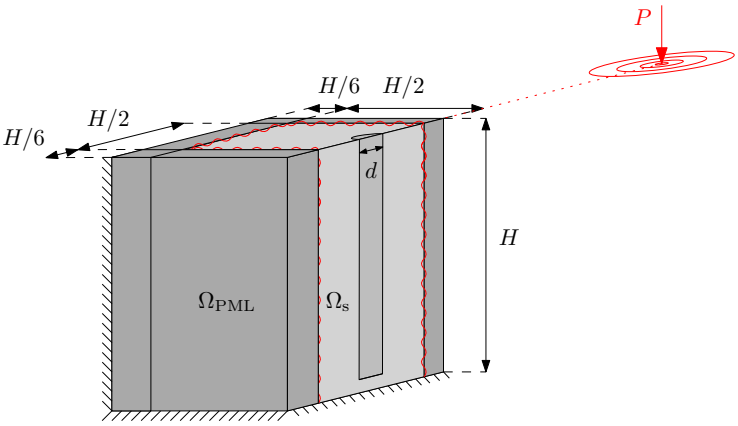

Figure 3: Geometry and conceptual layout of the FE-PML model with equivalent tractions applied at the boundary $\Omega_{\mathrm{PML}} \cap \Omega_{\mathrm{s}}$ between the PML and interior soil domain, representing an incident wave field computed with a separate source model.

the FE-PML boundary to be obtained from the source model. In the present case, the direct stiffness method is used to obtain these for a unit vertical point load applied at the soil's surface [22]. Figure 3 presents the three-dimensional geometry of the problem where the respective domains of the soil Ω_{s} and PML Ω_{PML} are indicated. The domain size is specified in relation to the total depth H. The width of the PML domains is $H/6$ and the computational domain of the soil is $H/2 \times H/2 \times H$. The model is discretized such that there are at least five elements per shear wavelength λ_{s}, using 20 node solid elements for both soil and piles. As the problem has a plane of symmetry along the radial path between the source point and the center of the symmetric pile foundation, symmetry conditions are applied to further reduce the computational effort.

2.2. Model verification

The model is verified for the present application by comparison to kinematic interaction factors available in the literature for a 3×3 pile group in a homogeneous half space [12, 13]. The soil and pile properties for the problem are $\rho/\rho_{\mathrm{p}} = 2/3$, $\nu = 1/3$, $\nu_{\mathrm{p}} = 1/4$, $\beta_{\mathrm{p}} = 0$, $\beta_{\mathrm{s}} = 0.05$, $E_{\mathrm{p}}/E_{\mathrm{s}} = 1000$ and $L_{\mathrm{p}}/d = 20$, where L_{p} is the length of the pile. The responses are presented relative to the free field motions $u_{x,\mathrm{ff}}$ and $u_{z,\mathrm{ff}}$ at the center of the pile group and expressed as functions of the dimensionless frequency $a_0 = \omega d/C_{\mathrm{s}}$.

In the aforementioned studies, plane waves were considered for the excitation of the pile group. As a vertical point load at the soil's surface is considered in this work, the wave front is instead cylindrical and does not only contain the Rayleigh wave, but also P and S-waves. By considering a distance of $25L_{\mathrm{p}}$ between the source point and the center of the pile group, the incident wave front becomes approximately of plane incidence with respect to the dimensions of the foundation. The influence of the body waves is limited due to their faster attenuation with distance compared to the Rayleigh wave. As a hysteretic material damping

model is incorporated in the source model, the surface waves become dispersive [22]. In this verification example, material damping ratios β_{s} and β_{p} are therefore both set to 0.01 to render any effects arising from dispersion to become insignificant.

Figure 4 verifies the translational and rotational responses of the pile group $u_x,\ u_z$ and θ_y to Rayleigh waves. The results of the FE-PML model are in agreement with previously published results, in particular those which correspond to horizontal translation and rotational motion which were obtained from a rigorous boundary integral model [12, 23].

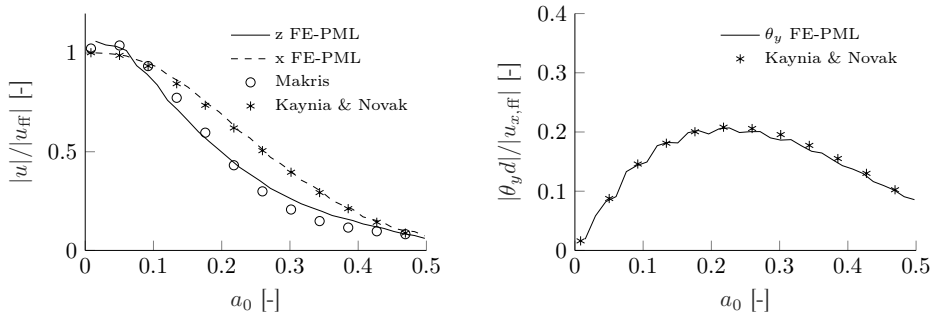

Figure 4: Kinematic response of a 3×3 pile group subjected to Rayleigh waves obtained from the FE-PML model and comparison to previously published results for the vertical response by Makris [13] (∘) and for the horizontal and rotational response by Kaynia and Novak [12] (∗).

2.3. Spatial averaging of free field vibrations

A more complicated wave pattern arises in the layer-on-bedrock profile than in the halfspace [24, 25]. The combination of reflected body waves and dispersive surface waves propagating in the layer gives rise to interference patterns, which depend on both receiver location and frequency. To relate pile foundation and free field responses is therefore not as straightforward as for the case of Rayleigh waves in a homogeneous halfspace.

Piles are generally much stiffer in their axial direction than the soil into which they are installed. When subjected to incident wave loading, the pile therefore acts as a spatial filter for the component of the incident wave field aligning with the axial direction of the pile. Due to the low bending stiffness of piles, they are able to more closely follow the motion of the soil in the lateral direction. The horizontal pile top response can therefore be directly related to the horizontal free field motion at the surface of the soil in the same point.

To establish meaningful relative measures for the vertical response of end-bearing piles resembling those obtained for the homogeneous halfspace, the vertical free field motion amplitude along the soil's surface at

the distance L is averaged over one pile length:

$$\bar{u}_{z,\mathrm{ff}}(L,\omega) = \frac{1}{H}\int_{L-H/2}^{L+H/2} |u_{z,\mathrm{ff}}(r,\omega)|\ \mathrm{d}r \tag{5}$$

The averaging reduces the influence of wave interference over a distance corresponding to the depth of the pile foundation, making the comparison less dependent on the chosen reference point.

This way, kinematic response factors $\mathrm{I_v} = |u_z|/\bar{u}_{z,\mathrm{ff}}$ can be computed relating the average vertical free field vibrations to the response of pile foundations which are not overly sensitive to the relative position of the piles with respect to the vibration source. Figure 5 compares the dimensionless averaged vertical response using eqs. (1) and (5) to the response in the reference point for the two distances $L/H = 2$ and 3. The spatial average provides a smoother variation with H/λ_s and cancels the most severe oscillations with

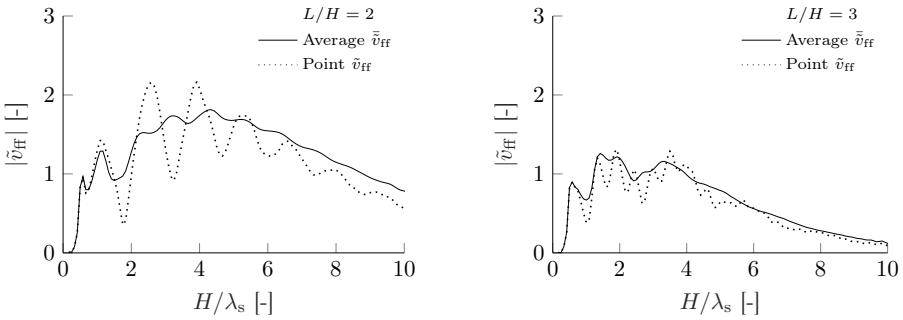

Figure 5: Amplitude of the dimensionless vertical velocity free field response spatially averaged over a distance H compared to point response at the reference distances $L/H = 2$ and 3.

frequency due to wave interference while representing the average response amplitude reasonably well.

3. Single pile response

3.1. The influence of source-receiver distance

To assess the influence of the source-receiver distance L/H, the vertical averaged free field responses at distances $L/H = 1, 2$ and 3, the corresponding pile responses and the resulting estimates of $\mathrm{I_v}$ are presented in fig. 6. To illustrate the influence of source-receiver distance more clearly, the attenuation due to geometrical and material damping is adjusted such that it becomes approximately equal for a reference distance, assuming that the response is mainly due to the fundamental surface wave with a wavelength $\lambda_\mathrm{R} \approx \lambda_\mathrm{s}$. For a point source at the soil's surface, the attenuation of displacement amplitude at a distance r is, for both surface waves and guided body waves, due to the expansion of the wave front and is proportional

to $1/\sqrt{r}$ [26]. The relative attenuation due to geometrical damping between two points on the soil's surface at the distances L and r is thereby $\sqrt{r/L}$. For small values of the material damping ratio, say $\beta \leq 0.1$, which is often applicable for soils subjected to small-strain loading, the attenuation of a plane surface wave due to material damping is approximately $\exp(-r\beta_s\omega/C_s)$, considering that the speed of the surface wave is close to the S-wave speed ($C_R \approx C_s$). Assuming that the vertical response is dominated by the fundamental surface wave, the difference in attenuation between the points at the distances L and r due to material damping can be adjusted for by the factor $\exp\left(\beta_s \frac{\omega}{C_s}(r-L)\right)$. Consequently, an adjustment factor for the dimensionless response $\tilde{v}$ that approximately compensates for wave attenuation can be written as:

$$\varsigma = \left(\frac{L}{H}\Big/\left(\frac{L}{H}\right)_{\text{ref}}\right)^{-0.5} \exp\left(\beta_s 2\pi \frac{H}{\lambda_s}\left(\frac{L}{H} - \left(\frac{L}{H}\right)_{\text{ref}}\right)\right) \tag{6}$$

where the first term is related to the attenuation due to geometrical spreading whereas the second term is due to material damping of the surface wave.

Equation (6) is used in fig. 6 to match the attenuation at the dimensionless reference distance $(L/H)_{\text{ref}} = 2$. The response factor I_v based on the spatial averaging of free field responses is sensitive to the distance in the range $H/\lambda_s \leq 3$ and exhibits significant variation for the different values of L/H considered. This is mainly a consequence of variations in the reference free field response which are not entirely averaged out by the use of eq. (5). The vertical pile responses are on the other hand only mildly affected by the L/H ratio in this range of H/λ_s, and thereby less sensitive to the distance when subjected to surface wave loading. These effects are cancelled out if an average value for I_v is considered.

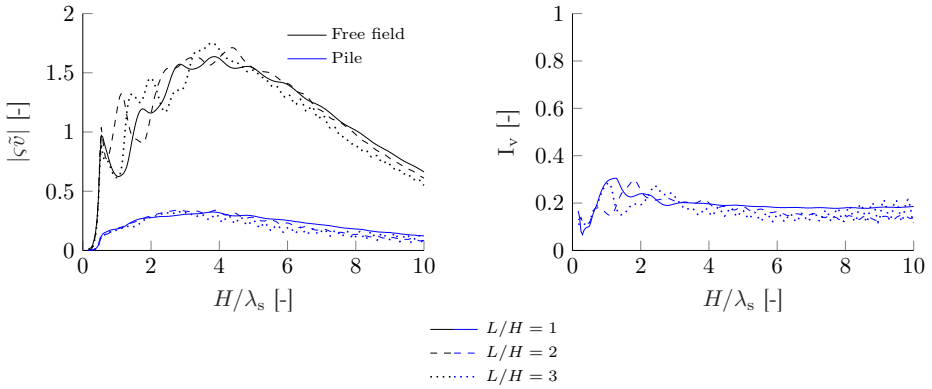

Figure 6: Scaled average free field and end-bearing pile vertical dimensionless velocity responses (left) at different dimensionless distances with a reference distance $(L/H)_{\text{ref}} = 2$ with their corresponding kinematic response factors (right) for pile properties $H/d = 25$ and $E_p/E_s = 1000$.

3.2. The influence of guided P-waves

Due to the presence of bedrock at the depth H, the homogeneous soil layer acts as a waveguide for the propagating S- and P-waves and the attenuation of the body waves due to geometrical spreading is limited to two dimensions as for surface waves [26]. In saturated soils, and especially in soft clays, the P-wave speed is significantly higher than the S-wave speed. As a consequence, the guided P-waves are subjected to less material damping compared to S-waves and surface waves, as the attenuation with distance due to material damping increases as the wavelength becomes shorter [27].

Figure 7 presents the responses of piles at the distance $L/H = 10$ from the excitation point. At $H/\lambda_s = 3.75$, a second peak in the vertical response is observed, which corresponds to the first layer resonance (cut-off frequency) of vertically propagating P-waves $(H/\lambda_s)_{pn} = (2n-1)C_p/C_s/4$ for a profile with $C_p/C_s = 15$. The vertical response of piles is more sensitive to this type of incident wave, as the relative response I_v increases about a factor of two at the cut-off for P-wave propagation and thereafter increases with H/λ_s. However, in absolute terms, the velocity amplitude due to the incident P-waves is the highest around the cut-off frequency.

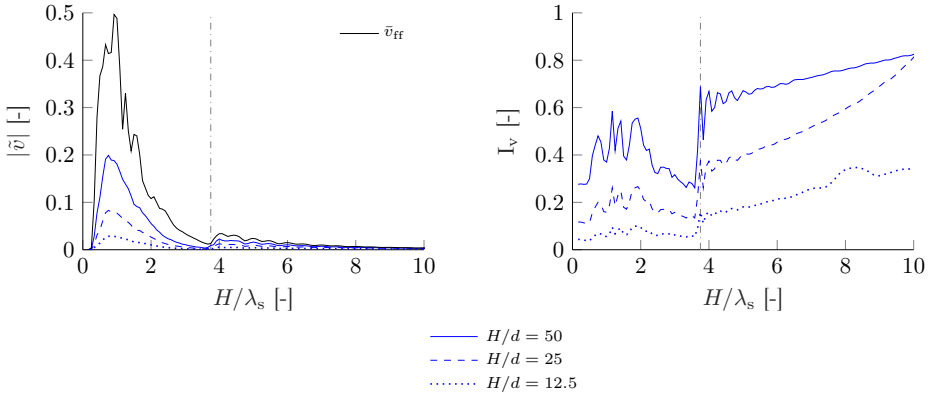

Figure 7: Dimensionless vertical velocity response for a source-pile distance to depth ratio $L/H = 10$ for piles with $E_p/E_s = 1000$ and different values of the H/d ratio (left) and the corresponding kinematic response factors I_v based on the average free field response $\bar{v}_{ff}$ (right). The cut-off H/λ_s for P-wave propagation is indicated by a vertical dashdotted line.

For the considered conditions, the vertical velocity response due to surface wave excitation is significantly higher than the response due to P-wave excitation. However, the ratio between the amplitudes depends both on the distance L/H and on the values of the damping ratios β_s and β_p which control the attenuation of the two wave types. Moreover, a low-velocity unsaturated layer closest to the surface and critically refracted waves propagating along an elastic underlying stiff bedrock can cause amplification of the response due to P-waves, making it a significant part of the vertical velocity response at certain source-receiver distances

[28]. Under such conditions, pile group responses might exceed the response of a single pile when excited by guided P-waves [29]. Therefore, the dominating wave type, which depends on the distance between the vibration source and the foundations, should be considered for values $H/\lambda_s \geq (H/\lambda_s)_{p1}$.

As the rate of attenuation due to geometrical spreading is equal for the surface waves and the guided body waves, only the material damping ratios, β_s and β_p, and their corresponding wave speeds influence the different wave types' relative rate of attenuation. As discussed in section 3.1, for small values of the damping ratio β, the attenuation factor of a plane wave due to material damping is $a = \exp(-\beta 2\pi L/\lambda)$. Based on this attenuation law, an expression for the maximum dimensionless distance $(L/H)_{max}$ up to which the fundamental surface wave dominates the response over the full range of H/λ_s is obtained. By taking the ratio between the attenuation factors of the the P-waves (a_p) and the surface waves (a_R), considering that the surface wavelength $\lambda_R \approx \lambda_s$ and that the cut-off value for P-wave propagation in the layer is $(H/\lambda_s)_{p1} = C_p/C_s/4$, this distance is obtained by:

$$\left(\frac{L}{H}\right)_{max} = \frac{2}{\pi}\log\left(\frac{a_p}{a_R}\right)\left(\beta_s\frac{C_p}{C_s} - \beta_p\right)^{-1} \tag{7}$$

where the ratio a_p/a_R between the attenuation factors of the two different wave types is imposed at the cut-off frequency for P-wave propagation. From simulation experiments, it is found that for a value of $a_p/a_R = 15$, which yields $2\log(a_p/a_R)/\pi \approx 1.7$, the increase in I_v for values of $H/\lambda_s \geq C_p/C_s/4$ seen in fig. 7 is starting to form. This simple relation can be used to indicate whether the influence of guided P-waves should be accounted for or not, based on the properties of the soil.

3.3. Influence of soil-pile density ratio on the vertical response of end-bearing piles

To illustrate the sensitivity of the vertical pile response to the soil-pile density ratio, the response due to a load applied at $L/H = 2$ for piles with different combinations of ρ/ρ_p, H/d and E_p/E_s is presented in fig. 8. For the considered values of ρ/ρ_p, amplification of the response is observed for the lower values of ρ/ρ_p compared to the reference case where $\rho/\rho_p = 0.75$. The H/λ_s range where the response is amplified for ρ/ρ_p is essentially the same for $H/d = 25$ and 12.5, but depends on the pile-soil stiffness ratio E_p/E_s. This amplification of the response occurs around the fundamental resonance frequency of a bar with one end fixed $f_p = \sqrt{E_p/\rho_p}/4H$. This resonance frequency can be written as $H/\lambda_s = \sqrt{(E_p/E_s)(\rho/\rho_p)(1+\nu)/8}$, with $\nu = -(2-(C_p/C_s)^2)/(2-2(2-(C_p/C_s)^2))$. The values of H/λ_s where resonance occur for a density ratio of $\rho/\rho_p = 0.25$ are indicated in fig. 8. These values correspond well to the locations of the peaks of the amplification compared to the response with $\rho/\rho_p = 0.75$. This effect is not as clearly manifested for $\rho/\rho_p = 0.5$.

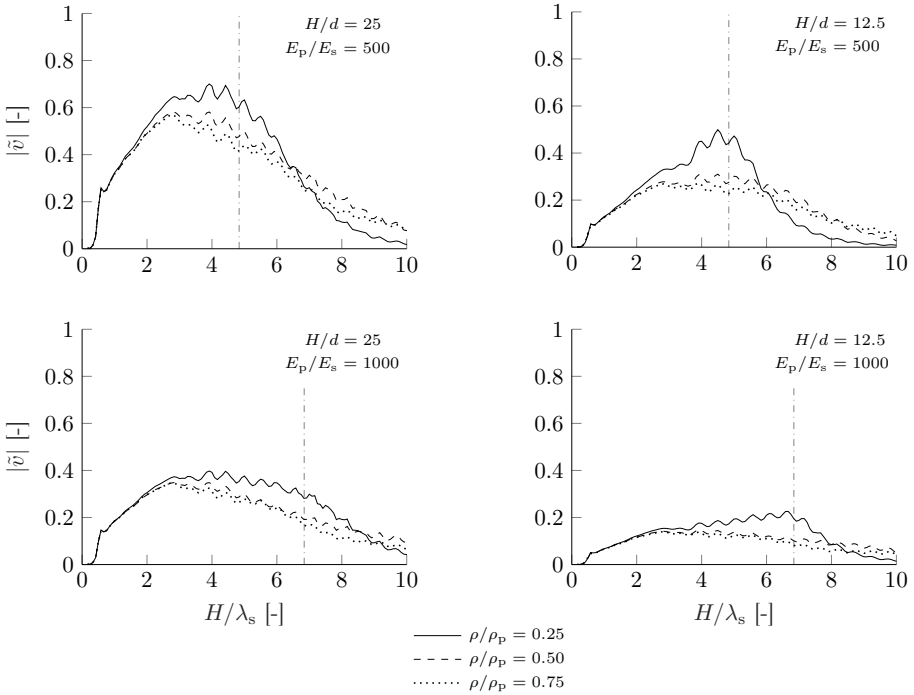

Figure 8: Vertical response of end-bearing piles at $L/H = 2$ for different values of the soil-pile density ratio ρ/ρ_p with soil-pile stiffness ratios $E_p/E_s = 500$ and 1000. The natural frequencies of a bar with one end fixed for $\rho/\rho_p = 0.25$ are indicated by vertical dashdotted lines.

For the range of parameters studied herein, only the density ratio of 0.25 has a significant influence on the response. In a practical context, this value of the density ratio situates the axial pile resonance frequency outside of the frequency range of interest for ground-borne vibration (1-80 Hz) for most practically relevant problems. Thereby, for most problems related to ground-borne vibration, the influence of the pile density on the response of end-bearing piles is limited. However, for applications related to re-radiated sound (16–250 Hz), this effect may become relevant.

3.4. Influence of the end-bearing condition

Figure 9 compares the dimensionless vertical velocity response of floating and end-bearing piles excited from a distance $L/H = 2$ for different values of the dimensionless parameters H/d and E_p/E_s. The response of the floating piles is significantly higher than the response of the end-bearing piles for wavelengths longer than $H/4$ for all the combinations considered, except for the case where $E_p/E_s = 500$ and $H/d = 50$, where the responses of the floating and end-bearing pile are similar. For shorter wavelengths ($\lambda_s < H/4$),

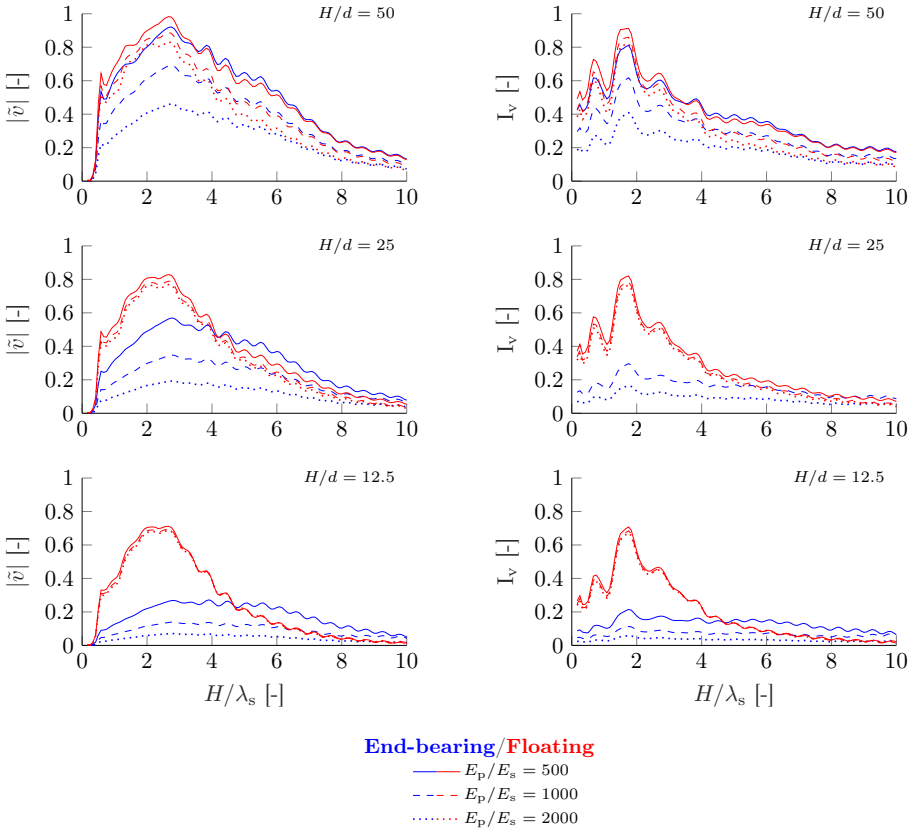

Figure 9: Vertical dimensionless pile velocities response (left) and the corresponding kinematic response factors (right) for end-bearing (blue) and floating (red) piles with source-pile distance to depth ratio $L/H = 2$ and different combinations of depth to diameter ratios H/d and pile-soil stiffness ratios E_p/E_s.

the configuration with the highest response depends on the pile-soil stiffness ratio and the end-bearing pile response can exceed the floating pile response.

The end condition of the pile generally becomes more important for a higher axial stiffness of the pile. As the ratio H/d decreases, the vertical response of the piles is reduced. This influence is much more pronounced for the end-bearing pile than for the floating pile. A similar observation can be made regarding the pile-soil stiffness ratio E_p/E_s. As the pile stiffness increases, or the stiffness of the soil decreases, the vertical response of the end-bearing pile is drastically reduced while the response of the floating pile is in comparison almost unaffected by the change in pile-soil stiffness ratio. This is because the vertical motion of stiff floating piles is mainly due to rigid body motion within the softer soil medium. This is an important distinction between

floating and (vertically oriented) end-bearing piles, which instead deform vertically only by axial straining. On the contrary, horizontal and rotational motions of the individual pile are virtually unaffected by the end-bearing condition (see appendix A).

For soft soils with a relatively shallow depth to bedrock, the influence of the end-bearing condition on the vertical response becomes significant and should therefore be taken into account in vibration assessment. The response of the end-bearing pile relative to the free field response $\mathrm{I_v}$ is tending towards a value which is constant throughout the studied range of H/λ_s as the relative axial stiffness of the pile increases. This allows for a conservative estimate of the interaction factor $\mathrm{I_v}$ based on the relationship between the axial stiffness of the pile and the stiffness of the soil, which is further elaborated in section 5.

4. Pile group response

The study of single piles gives insight into the fundamental influence of soil-pile interaction for the kinematic response of floating and end-bearing piles. However, piles are often arranged in smaller groups to carry loads from e.g. columns or walls, and can exhibit significant group effects due to both pile-soil-pile interaction and from phase differences in the motion of the piles due to passing waves. Pile-soil-pile interaction has an important influence on foundation impedances of pile groups, but has an insignificant influence on the kinematic response due to surface waves for floating pile groups in homogeneous soil [12, 14]. For soil conditions other than a homogeneous halfspace, the influence of the interaction between the piles on the group response has not previously been documented.

The response of square 2×2 end-bearing pile groups are presented herein to facilitate analysis of these group effects and to assess the influence of the end-bearing condition. Pile groups with pile-to-pile spacing of $s/d = 3,\ 5\ 10$ are considered for the three dimensionless depths $H/d = 50,\ 25,\ 12.5$. In this paper, the focus is set on the vertical responses of pile foundations. However, it should be noted that while the horizontal and rotational responses of a single pile are virtually unaffected by the end-condition of the pile, this is not the case for groups of piles. This is because the rocking response of pile groups is primarily due to the individual vertical motions of the piles [12]. For further details the reader is referred to appendix A.

Figure 10 compares the vertical single pile responses for $E_\mathrm{p}/E_\mathrm{s} = 1000$ and $L/H = 2$ to the responses of end-bearing and floating pile groups. Destructive interference occurs whenever the motion of the individual piles are out of phase. This results in pronounced minima in the pile group responses in the neighbourhood of the parameter values $(H/\lambda_\mathrm{s})_n^* = (2n-1)(H/d)/(2(s/d))$ where the pile spacing becomes equal to $n - 1/2$ wavelengths of the surface wave. This out-of-phase motion of the individual piles has a major influence on both floating and end-bearing pile groups.

Comparing the single pile response to the pile group responses for end-bearing and floating piles illustrates the influence of pile-soil-pile interaction. This is most clearly illustrated for the groups with the most closely spaced piles ($s/d = 3$) in fig. 10, which exhibit different characteristics depending on the end-condition, when compared to the single pile response. For the end-bearing pile group with $H/d = 50$ and $s/d = 3$, the group response compared to the single pile response is much lower for values $H/\lambda_s < 4$ than for the case of floating piles, whereas the opposite is true for values $H/\lambda_s \geq 4$. Moreover, the floating pile group responses are lower compared to that of the single pile for values $H/\lambda_s < 1$. This is not the case for piles in a homogeneous half space, where the group response follow the free field motion whenever the footprint of the pile group is small compared to the incident wavelength (see fig. 4). These results suggests that pile-soil-pile interaction can become important for pile groups in layered soil, where the soil stiffness varies along the depth of the pile. This is in contrast to the case of piles in a homogeneous halfspace, for which it has been emphasised that such effects can safely be neglected [12, 14].

The vertical group responses of both end-bearing and floating piles are practically bounded by the responses of the single piles, apart from a few values of H/λ_s where the group response only slightly exceeds the single pile response. This is of practical relevance, as it allows for conservative estimation of a kinematic response factor based on the single pile response whenever surface waves dominate the excitation.

5. Estimation of vertical kinematic response factor $\mathbf{I_v}$ for end-bearing piles

As the kinematic response of a single end-bearing pile gives a representative indication of the response also for groups of piles, it is of practical interest to provide an estimate of the vertical response factor I_v based on the set of dimensionless parameters that influence the vertical response. As discussed in section 3, the axial stiffness of piles influence the vertical response when the piles are end-bearing. This relationship is non-linear in terms of (H/d) and (E_p/E_s). Anoyatis et al. [17] observed that pile-soil systems with the same values of a mechanical slenderness:

$$\ell = \Big(\frac{H}{d}\Big)\Big(\frac{E_p}{E_s}\Big)^{\alpha} \tag{8}$$

with $\alpha = -1/2$, behaved in a similar way for the case of end-bearing piles subjected to vertically propagating P-waves. For the problem studied in this paper, a value of $\alpha = -0.6$ yields vertical pile responses for piles with the same value of ℓ that are of similar amplitude.

As the mechanical slenderness of a pile decreases, the factor I_v for the response dominated by surface waves tends to become approximately constant in terms of H/λ_s (see fig. 9). On the other hand, for a high value of mechanical slenderness, the response varies considerably with H/λ_s compared to the stiffer

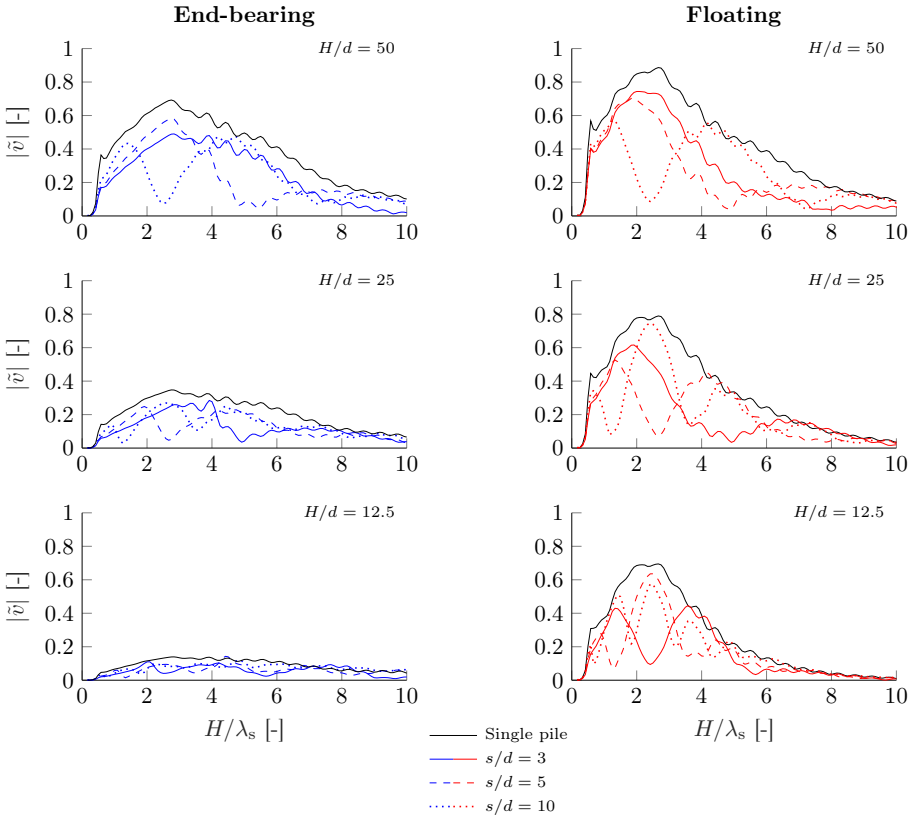

Figure 10: Comparison between the dimensionless vertical velocity response of a single pile and 2×2 square pile groups for end-bearing and floating piles with different depth to diameter ratios H/d and pile spacings s/d for the case where $E_p/E_s = 1000$ and $L/H = 2$.

piles. However, an average constant factor may be considered in the range $H/\lambda_s \leq 4$. As an engineering approximation, a constant factor $\bar{I}_v$ can therefore be used to represent the average amplitude reduction in this range, which then becomes a conservative estimate for $H/\lambda_s > 4$. Using eq. (8) with $\alpha = -0.6$, weighted average values of I_v for $H/\lambda_s \leq 4$ obtained from the results in fig. 9 can be fitted by a line:

$$\bar{I}_v = 0.578\ell - 0.034 \tag{9}$$

or expressed in terms of the geometrical slenderness and the pile-soil stiffness ratio:

$$\bar{I}_v = 0.578\left(\frac{H}{d}\right)\left(\frac{E_p}{E_s}\right)^{-0.6} - 0.034 \tag{10}$$

which is valid in the studied parameter ranges of $500 \leq E_p/E_s \leq 2000$ and $12.5 \leq H/d \leq 50$, covering a range of cases encountered in practice. As noted in section 3, the upper bound for the values of I_v for an end-bearing pile converges towards the floating pile response. Therefore, for cases where the mechanical slenderness is higher than $\ell^* = 50/500^{0.6} \approx 1.2$, the solution for a floating pile may be used instead.

To verify the approximation, fig. 11 presents a comparison between the estimated pile response $\bar{I}_v \bar{\tilde{v}}_{ff}$ using eq. (10) to the single pile response for values of H/d and E_p/E_s and at distances L/H which were not used for calibration. The general amplitude reduction is captured, verifying the ability of this simple relation to estimate the vertical response of end-bearing piles.

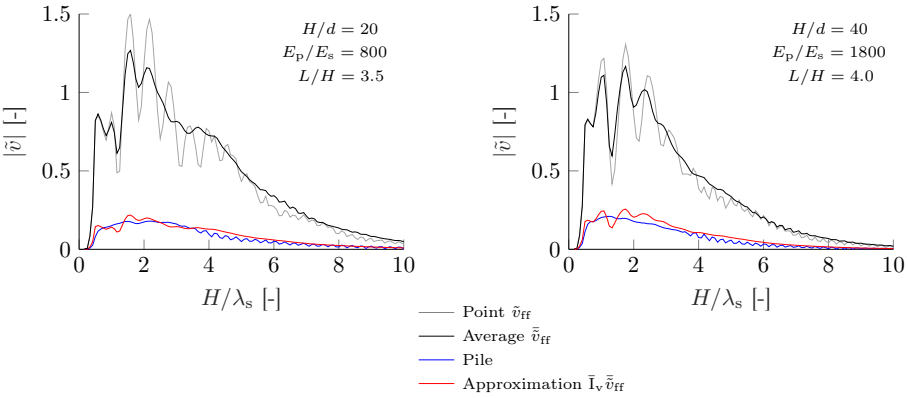

Figure 11: Verification of the approximation $\bar{I}_v \bar{\tilde{v}}_{ff}$ by comparison to the end-bearing pile response obtained for two sets of parameters not included in the curve fitting to obtain expression for the approximate interaction factor $\bar{I}_v$. The average and point wise free field responses $\bar{\tilde{v}}_{ff}$ and $\tilde{v}_{ff}$ are also presented.

Figure 12 presents an overview of the function values of eq. (10) expressed in decibels, providing a tool for quick assessment of the kinematic foundation response of end-bearing piles. This approximation can potentially be used for preliminary assessment or for use with simplified models where the vertical free field vibration is assumed to be the principal mode of excitation (see e.g. [2, 3, 30]).

From eq. (10), it is seen that an increase in pile dimension has a larger impact on $\bar{I}_v$ than increasing the pile stiffness. This is convenient from a practical point of view, as the major freedom in design lies in the choice of pile dimension while options of material properties are often limited and the value of E_p/E_s is mostly governed by the soil material.

To provide an overview of the results derived from the presented analysis, a procedure to estimate the vertical response of vertically oriented end-bearing piles from free field vibrations is presented in table 1. It should be stressed that the analysis procedure presented herein requires that the soil can be properly idealised as a homogeneous soil layer on bedrock. When this is not the case, the variation of soil properties

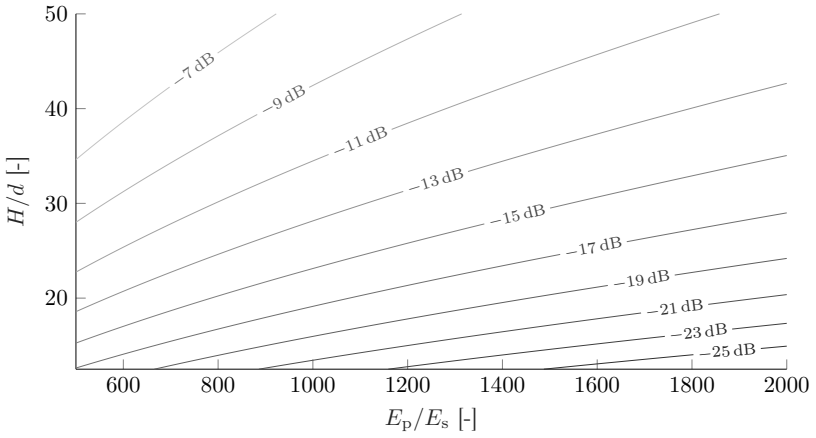

Figure 12: Contour lines of the vertical kinematic interaction factor approximation $\bar{\mathrm{I}}_{\mathrm{v}}$ for end-bearing piles expressed in decibels.

with depth should be taken into account. It is also pointed out that only the general behaviour of the foundation response is considered here. Predicting responses within a building requires, in a next step, an appropriate model which can capture the dynamic behaviour of the building.

6. Conclusion

In this paper, the vertical response of end-bearing piles in a homogeneous soil on a rigid bedrock subjected to a vertical harmonic point load at the soil's surface is studied. A dimensionless set of parameters is established to numerically analyse the influence of relationships between pile and soil properties.

The influence of the fixation to the bedrock is assessed by comparing the responses of floating and end-bearing piles and pile groups. The vibrations of the pile foundations are related to the vibrations in the free field measured at the soil's surface to allow for assessing the foundation response from free field measurements using an interaction factor. The following conclusions are made:

1. The influence of wave interference is much less pronounced in the vertical response of a pile compared to the vertical free field motion at the soil's surface.

2. The vertical response of an end-bearing pile is strongly influenced by the relationship between the pile's axial stiffness and the stiffness of the soil. This is in contrast to a floating pile which is only mildly affected by a change in the axial stiffness. However, for situations where the pile slenderness ratio $H/d \geq 50$ and the pile-soil stiffness ratio $E_{\mathrm{p}}/E_{\mathrm{s}} \leq 500$, the influence of the end-bearing condition has no significant influence on the vertical pile response and is essentially the same as for a floating pile.

Table 1: Summary of a procedure to estimate the vertical response of end-bearing piles subjected to nearby surface loading.

Procedure to estimate the vertical response of end-bearing piles due to a nearby surface load

1. Obtain vertical free field vibrations by prediction or measurements.
2. Estimate soil and geometrical site properties to establish the dimensionless quantities: $H/d,\ E_\mathrm{p}/E_\mathrm{s},\ \rho/\rho_\mathrm{p},\ C_\mathrm{p}/C_\mathrm{s},\ \beta_\mathrm{s}$ and β_p.
3. If $\rho/\rho_\mathrm{p} < 0.5$, check if the first pile resonance frequency $f_{\mathrm{p}1} = \sqrt{E_\mathrm{p}/\rho_\mathrm{p}}/4H$ is within the frequency range of interest. If so, the proposed procedure cannot be used.
4. Estimate the maximum distance $(L/H)_\mathrm{max} \approx 1.7(\beta_\mathrm{s}C_\mathrm{p}/C_\mathrm{s} - \beta_\mathrm{p})^{-1}$ up to which the contribution from the fundamental surface wave dominates the response and the contribution from guided P-waves can be neglected.
   - If $L/H \leq (L/H)_\mathrm{max}$, reduction of the free field response can be considered for the full frequency range.
   - If $L/H > (L/H)_\mathrm{max}$, a reduction of the free field response can only be considered for frequencies below the P-wave cut-off frequency $f_\mathrm{cp} = C_\mathrm{p}/4H$.
5. Compute $\bar{\mathrm{I}}_\mathrm{v} = 0.578(H/d)(E_\mathrm{p}/E_\mathrm{s})^{-0.6} - 0.034$ or use fig. 12 to obtain an approximation of the vertical foundation response based on the predicted or measured free field vibrations.

3. At a certain distance from the source point and for frequencies higher than the cut-off frequency for propagation of P-waves, guided P-waves start to dominate the excitation. The vertical pile response is more sensitive to this mode of excitation than to surface waves.

4. The axial resonance frequency of end-bearing piles can contribute to a higher response at certain frequencies. However, this is found to be outside of the frequency range of interest for ground-borne vibration (1-80 Hz) for most practically relevant cases.

5. The vertical responses of 2×2 pile groups with different spacing between the piles are all bounded by the single pile response whenever surface waves are the predominant source of excitation.

6. Pile-soil-pile interaction becomes more important for pile groups in soil on bedrock than for pile groups in deep homogeneous soil, and end-bearing pile groups are more strongly affected than floating pile groups. Future research should address this further to better understand the phenomena and experimentally confirm the results.

The dimensionless representation allows also to propose an approximate relation for a constant vertical interaction factor for end-bearing piles based on the pile slenderness and pile-soil stiffness ratio. This factor is applied as a reduction factor to the free field response, providing a simple tool to estimate vertical vibrations of end-bearing pile foundations.

7. Acknowledgements

This work is supported by the Development Fund of the Swedish Construction Industry (SBUF) and the Swedish Transport Administration (Trafikverket). The financial support is gratefully acknowledged.

References

[1] D. Connolly, G. Kouroussis, P. Woodward, A. Giannopoulos, O. Verlinden, M. Forde, Scoping prediction of re-radiated ground-borne noise and vibration near high speed rail lines with variable soils, Soil Dynamics and Earthquake Engineering 66 (2014) 78–88.

[2] D. López-Mendoza, A. Romero, D. Connolly, P. Galvń, Scoping assessment of building vibration induced by railway traffic, Soil Dynamics and Earthquake Engineering 93 (2017) 147–161.

[3] L. Auersch, Simple and fast prediction of train-induced track forces, ground and building vibrations, Railway Engineering Science 28 (2020) 1–19.

[4] C. E. Hanson, J. C. Ross, D. A. Towers, High-Speed Ground Transportation Noise and Vibration Impact Assessment, Technical Report DOT/FRA/ORD-12/15, U.S. Department of Transportation, Federal Railroad Administration, Office of Railroad Policy and Development, 2012.

[5] J. T. Nelson, H. J. Saurenman, A prediction procedure for rail transportation groundborne noise and vibration, Transportation Research Record (1987).

[6] P. Jean, M. Villot, Study of the vibrational power injected to a wall excited by a ground surface wave, Journal of Sound and Vibration 231 (2000) 721–726.

[7] K. Kuo, M. Papadopoulos, G. Lombaert, G. Degrande, The coupling loss of a building subject to railway induced vibrations: Numerical modelling and experimental measurements, Journal of Sound and Vibration 442 (2019) 459–481.

[8] G. Sanitate, J. Talbot, Foundation vibration and the added-building effect: Experimental evidence from a ground-borne vibration measurement campaign, Journal of Sound and Vibration 544 (2023) 117390.

[9] E. Kausel, Advanced Structural Dynamics, Cambridge University Press, 2017. doi:https://doi.org/10.1017/9781316761403.

[10] A. M. Kaynia (Ed.), Analysis of Pile Foundations Subject to Static and Dynamic Loading, 1st ed., CRC Press, 2021. doi:https://doi.org/10.1201/9780429354281.

[11] G. Mylonakis, G. Gazetas, Kinematic pile response to vertical P-wave seismic excitation, Journal of Geotechnical and Geoenvironmental Engineering 128 (2002) 860–867.

[12] A. M. Kaynia, M. Novak, Response of pile foundations to Rayleigh waves and obliquely incident body waves, Earthquake Engineering & Structural Dynamics 21 (1992) 303–318.

[13] N. Makris, Soil-pile interaction during the passage of Rayleigh waves: An analytical solution, Earthquake Engineering & Structural Dynamics 23 (1994) 153–167.

[14] N. Makris, D. Badoni, Seismic response of pile groups under oblique-shear and Rayleigh waves, Earthquake Engineering & Structural Dynamics 24 (1995) 517–532.

[15] L. Auersch, Wave propagation in the elastic half-space due to an interior load and its application to ground vibration problems and buildings on pile foundations, Soil Dynamics and Earthquake Engineering 30 (2010) 925–936.

[16] G. Efthymiou, C. Vrettos, Kinematic response of pile groups and piled rafts to a distant stationary or moving harmonic load via the FEM, Soil Dynamics and Earthquake Engineering 176 (2024) 108264.

[17] G. Anoyatis, R. Di Laora, G. Mylonakis, Axial kinematic response of end-bearing piles to P waves, International Journal for Numerical and Analytical Methods in Geomechanics 37 (2013) 2877–2896.

[18] ISO 14837-1:2005, Mechanical vibration - Ground-borne noise and vibration arising from rail systems - Part 1: General guidance, Standard, International Organization for Standardization, Geneva, CH, 2005.

[19] M. Schevenels, G. Degrande, G. Lombaert, The influence of the depth of the ground water table on free field road traffic-induced vibrations, International Journal for Numerical and Analytical Methods in Geomechanics 28 (2004) 395–419.

[20] ISO 14837-32:2015, Mechanical vibration – Ground-borne noise and vibration arising from rail systems – Part 32: Measurement of dynamic properties of the ground, Standard, International Organization for Standardization, Geneva, CH, 2015.

[21] M. Papadopoulos, S. François, G. Degrande, G. Lombaert, The influence of uncertain local subsoil conditions on the response of buildings to ground vibration, Journal of Sound and Vibration 418 (2018) 200–220.

[22] M. Schevenels, S. François, G. Degrande, EDT: An ElastoDynamics Toolbox for MATLAB, Computers & Geosciences 35 (2009) 1752 – 1754.

[23] A. M. Kaynia, E. Kausel, Dynamics of piles and pile groups in layered soil media, Soil Dynamics and Earthquake Engineering 10 (1991) 386 – 401.

[24] G. Lombaert, G. Degrande, D. Clouteau, The influence of the soil stratification on free field traffic-induced vibrations, Archive of Applied Mechanics 71 (2001) 661–678.

[25] N. Chouw, R. Le, G. Schmid, Propagation of vibration in a soil layer over bedrock, Engineering Analysis with Boundary Elements 8 (1991) 125–131.

[26] J. Li, S. Hanafy, G. Schuster, Wave-equation dispersion inversion of guided P waves in a waveguide of arbitrary geometry, Journal of Geophysical Research: Solid Earth 123 (2018) 7760–7774.

[27] S. L. Kramer, Geotechnical Earthquake Engineering, Prentice Hall, Upper Saddle River New Jersey, 1996.

[28] F. Theland, G. Lombaert, S. François, C. Pacoste, F. Deckner, J.-M. Battini, Assessment of small-strain characteristics for vibration predictions in a Swedish clay deposit, Soil Dynamics and Earthquake Engineering 150 (2021) 106804.

[29] F. Theland, C. Pacoste, J.-M. Battini, G. Lombaert, S. François, F. Deckner, The influence of near-surface soil layer resonance on vibrations in pile foundations, in: Current Perspectives and New Directions in Mechanics, Modelling and Design of Structural Systems, 2022, p. 84. doi:10.1201/9781003348450-13.

[30] A. Clot, R. Arcos, J. Romeu, Efficient three-dimensional building-soil model for the prediction of ground-borne vibrations in buildings, Journal of Structural Engineering 143 (2017) 04017098.

A. Horizontal and rotational responses of piles and pile groups

As it is the component in the axial direction of the pile which is mostly affected by the end-condition at the soil-bedrock interface, the horizontal and rocking components for a single pile subjected to a point load at the soil's surface are almost unaffected by the end-condition. Figure 13 illustrates this for the cases studied in section 3.4, where the dimensionless horizontal velocity response is obtained from considering u_x instead of u_z in eq. (1) and the dimensionless rotational velocity is defined as:

$$\tilde{\vartheta} = \mathrm{i}\omega\theta_y C_\mathrm{s} HLd/P \tag{11}$$

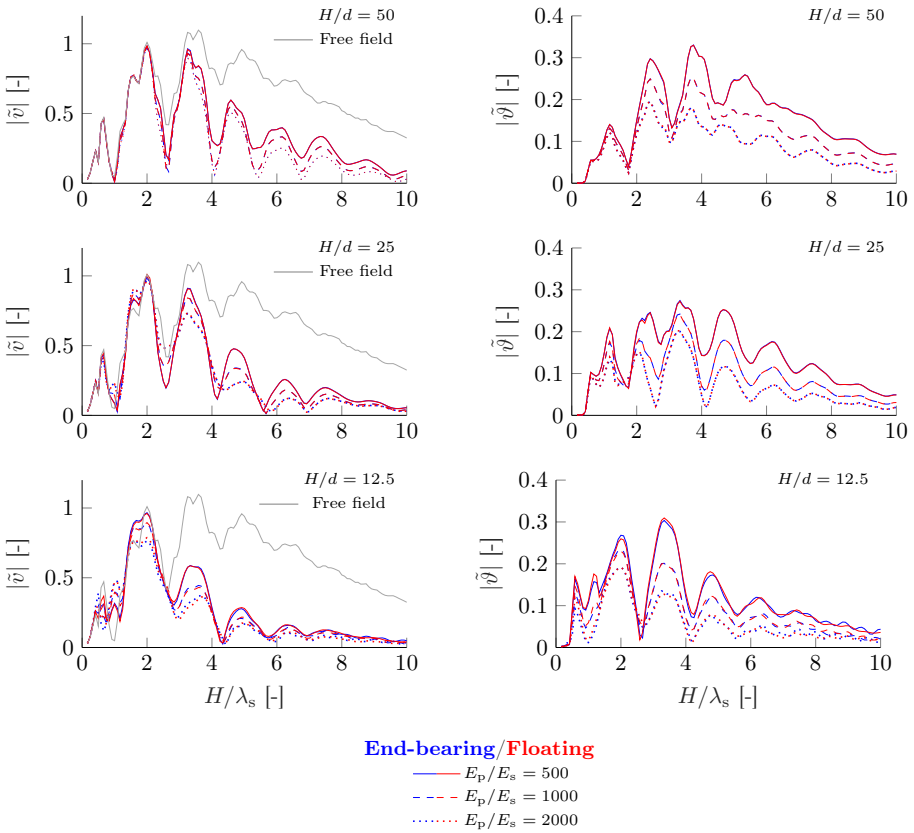

Figure 13: Horizontal dimensionless velocity response (left) compared to the free field response and the corresponding dimensionless cross sectional rotations (right) for end-bearing and floating piles for different combinations of depth to diameter ratios H/d and pile-soil stiffness ratios E_p/E_s for a source-pile distance to depth ratio $L/H = 2$.

where θ_y is the cross sectional rotation at the tip of the pile at the soil's surface.

The rocking vibrations of pile groups are, on the other hand, governed by the vertical responses of the piles [12]. The rocking response of the pile cap is therefore affected by the end-condition. Figure 14 show the influence of the end-condition on the rocking response of the pile cap foundation for the 2×2 pile foundations considered in section 4. As expected, with an increasing axial stiffness of the piles, the difference in the rocking responses between the floating and end-bearing pile groups increases.

Due to the coupling between rocking and horizontal motion of the piles, the horizontal group response is also affected by the end-condition. Figure 15 compares the horizontal group responses of the floating and end-bearing 2×2 pile groups. In general, the group response is lower for the end-bearing pile group and the

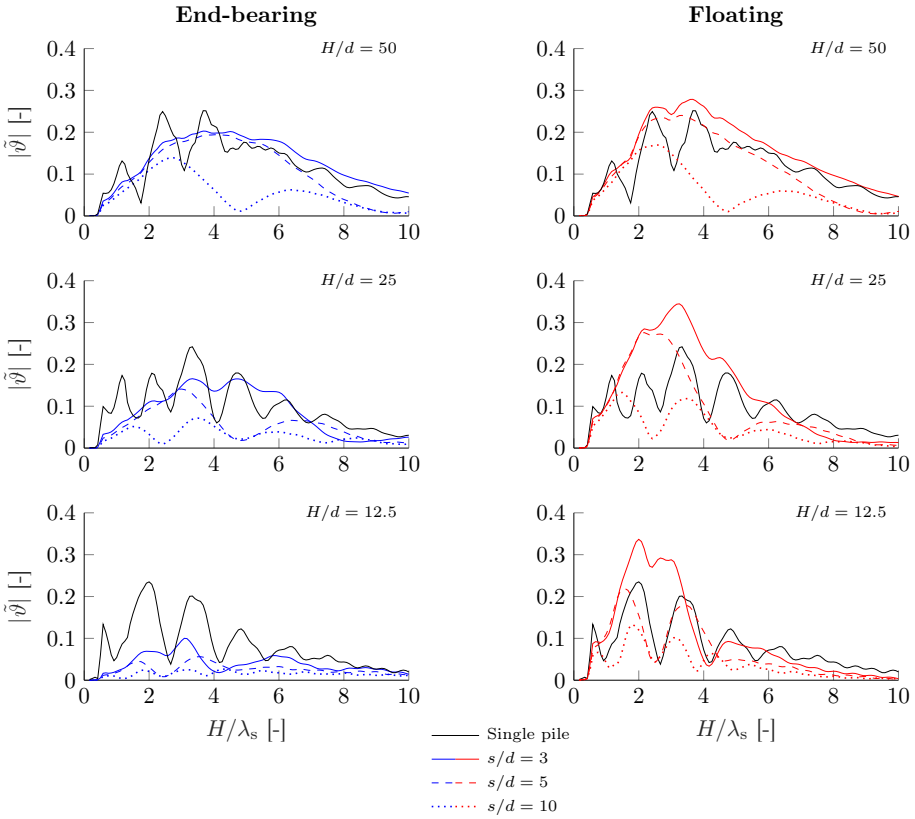

Figure 14: Comparison between the dimensionless rotational velocity response of a single pile and 2×2 square pile groups for end-bearing and floating piles with different depth to diameter ratios H/d and pile spacings s/d for the case where $E_p/E_s = 1000$ and $L/H = 2$.

influence of the end-condition increases with an increased axial stiffness of the piles.

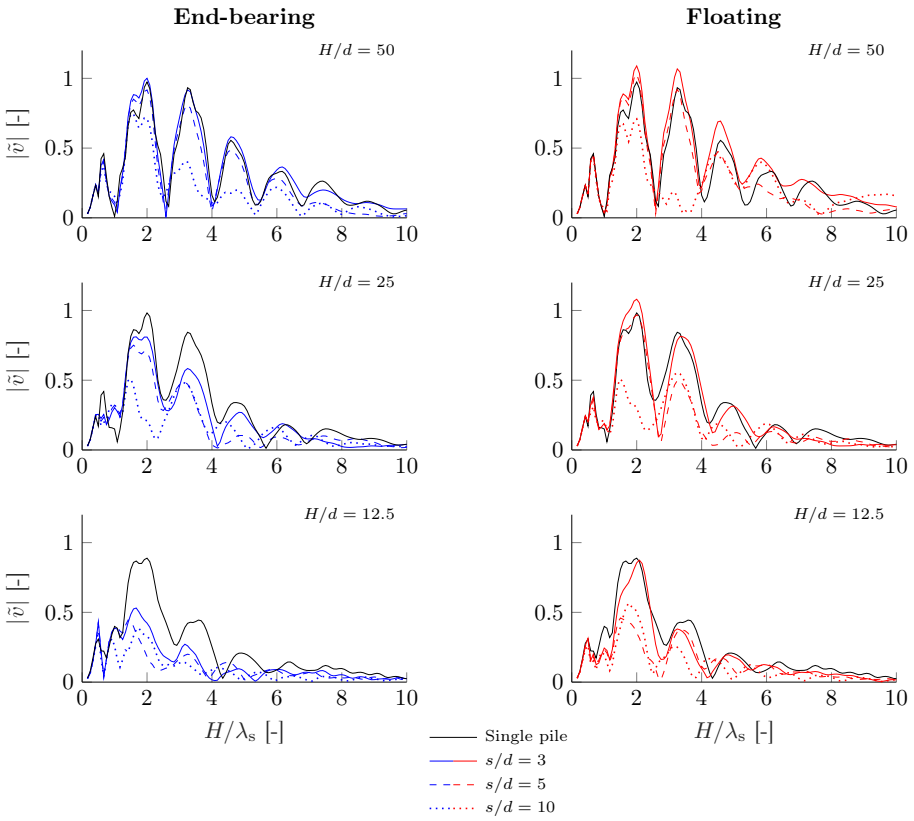

Figure 15: Comparison between the dimensionless horizontal velocity response of a single pile and 2×2 square pile groups for end-bearing and floating piles with different depth to diameter ratios H/d and pile spacings s/d for the case where $E_p/E_s = 1000$ and $L/H = 2$.

Paper V

The influence of pile-soil-pile interaction on the vertical response of end-bearing pile groups in soil on bedrock subjected to a vertical load at the soil's surface

Freddie Theland[a,*], Geert Lombaert[b], Stijn François[b], Abbas Zangeneh[a,c], Fanny Deckner[d], Jean-Marc Battini[a]

[a] *KTH Royal Institute of Technology, Department of Civil and Architectural Engineering, Brinellvägen 23, 100 44 Stockholm, Sweden*
[b] *KU Leuven, Department of Civil Engineering, Kasteelpark Arenberg 40, 3001 Leuven, Belgium*
[c] *ELU Konsult AB, Valhallavägen 117, 115 31 Stockholm, Sweden*
[d] *GeoMind KB, Fannys väg 3, 131 54 Nacka, Sweden*

Abstract

The influence of pile-soil-pile interaction on the vertical response of end-bearing pile groups when subjected to an incident wave field generated from a vertical load at the soil's surface is investigated. A numerical model which allows for considering or disregarding the influence of pile-soil-pile interaction is adopted. Vertical end-bearing pile groups with different pile axial stiffness and pile-to-pile spacing are considered. This study shows that in contrast to floating piles in homogeneous soil, the interaction effects caused by wave scattering between the piles are important for end-bearing piles. These may either reduce or amplify the group response, depending on the wavelength in the soil, the spacing between the piles, the pile slenderness and the pile-soil stiffness ratio. The interaction between the piles which are aligned in the direction transverse to the propagation direction of the incident wave field is found to amplify the group response at certain frequencies. Reducing the pile spacing in this direction is found to influence the vertical vibration response of end-bearing pile group foundations considerably by shifting the amplification effects due to pile-soil-pile interaction to higher frequencies.

Keywords: End-bearing piles, Surface waves, Kinematic interaction, Dynamic soil-structure interaction, Pile group, Ground borne vibration, Pile-soil-pile interaction

1. Introduction

Ground borne vibration arising from transportation infrastructure is a growing concern for the design of new buildings in urban environments. Soil-structure interaction has a considerable influence on the vibration transmission to buildings and should therefore be accounted for in vibration assessment [1]. Transmission

*Corresponding author: Tel. +46(0) 70 408 41 97
Email addresses: freddie.theland@byv.kth.se (Freddie Theland), geert.lombaert@kuleven.be (Geert Lombaert), stijn.francois@kuleven.be (Stijn François), abbas.zangeneh@elu.se (Abbas Zangeneh), fanny.deckner@geomind.se (Fanny Deckner), jean-marc.battini@byv.kth.se (Jean-Marc Battini)

of ground borne vibrations from foundations into buildings can be divided into two parts. The first part concerns the influence of soil-structure interaction on the dynamic properties of the soil-structure system. This can be accounted for by including the soil-foundation system impedance in a building model. The second part concerns the response of the foundation, without the structure present, when subjected to an incident wave field. The solution to the transmission problem can be obtained by combining these two interaction phenomena using a substructure formulation [2]. This serves as a theoretical framework that can be used for the development of simplified models [3, 4], or for combining site measurements with a numerical model for the purpose of vibration assessment [5, 6].

Pile group foundations are strongly affected by the dynamic interactions that occur between each individual pile and the soil, but also by the interaction between the piles through the soil. Pile-soil-pile interaction (PSPI) is well understood for the case where the foundation cap is subjected to external loads or when the piles are subjected to vertically propagating waves, which have been extensively studied in earthquake engineering. Dobry and Gazetas [7] developed physically motivated approximations for dynamic interaction factors for modelling dynamic pile-soil-pile interaction based on the scattered wave field emanating from an oscillating pile in homogeneous soil. A striking agreement with more rigorous solutions provided a sound understanding of the phenomenon and the method has successfully been used or extended to develop analytical models which account for pile-soil-pile interaction in both homogeneous and inhomogeneous soils [8–11]. Adopting this approximation for pile-soil-pile interaction, Makris and Badoni [12] developed an analytical model to study the dynamic responses of pile groups in homogeneous soil due to excitation caused by Rayleigh waves and oblique S-waves. The results were found to be in excellent agreement with a subset of results obtained from a more rigorous numerical model [13]. For floating piles in homogeneous soil, the wave-passage, i.e. phase differences in the excitation of the individual piles, was found to have an important influence on the group response due to incident wave loading, especially for horizontally propagating body waves and Rayleigh waves. The influence of pile-soil-pile interaction was, on the other hand, insignificant.

The influence of pile-soil-pile interaction on the response of end-bearing pile groups subjected to surface waves have not been thoroughly studied. For end-bearing piles in layered soil, Theland et al. [14] indicated that pile-soil-pile interaction can amplify the vertical response of pile groups at certain frequencies. Moreover, field measurements conducted by the authors on the end-bearing pile foundation in reference [15], have also indicated that pile-soil-pile interaction can have an important influence on the vertical pile group response. These observations stand in direct contrast with the case of floating piles in homogeneous soil. As the interaction may cause amplification of the group response, it is important to understand under which circumstances pile-soil-pile interaction should be accounted for or can safely be disregarded for applications of estimating the vibration response of structures, such as vibration assessment in buildings.

This paper aims to explain how pile-soil-pile interaction influences the vertical response of end-bearing pile groups in soft soils on bedrock subjected to an incident wave field primarily consisting of surface waves. The problem is addressed using a numerical model for which the influence of pile-soil-pile interaction is accounted for through a pile-soil coupling matrix, which can easily be modified to disregard the interaction between the piles through the soil. In this model, the total response in the surrounding soil is obtained as a superposition of the incident and the scattered wave fields. This allows analysing the influence of the relationships between the two wave fields to investigate how they affect the total response of pile group foundations.

The structure of the paper is as follows. Section 2 presents the cases studied and the system of dimensionless parameters established to present the results. Section 3 presents the numerical model used in this work. Section 4 compares the influence of pile-soil-pile interaction on the vertical response of floating and end-bearing piles. Section 5 analyses the influence of pile axial stiffness, pile-to-pile spacing and the direction of the incident wave field on the vertical group response. Section 6 presents the conclusions.

2. Problem outline

Figure 1 presents an overview of the studied problem for the case of a 2×2 pile group arrangement. To aid the understanding of how pile-soil-pile interaction effects are influenced by the pile and soil properties, the problem is expressed in terms of dimensionless parameters. Vertical circular piles with diameter d are

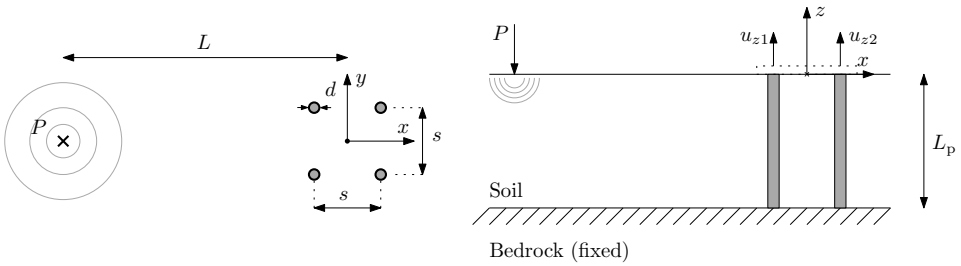

Figure 1: Problem geometry for a uniformly spaced 2×2 pile group in soil on bedrock subjected to a vertical point load applied at the soil's surface.

considered and the length of the piles is expressed in terms of the pile slenderness ratio L_p/d, the pile-to-pile spacing s/d and the distance between the center of the pile group and the excitation point L/L_p. The results presented in this paper assume a dimensionless distance $L/L_p = 5$. Numerical simulations performed for this problem have indicated that the influence of pile-soil-pile interaction on the vertical response of rigidly connected pile groups is practically unaffected by this distance.

The material properties of the piles and the soil are assigned to be representative for concrete piles in relatively soft cohesive soil. The material properties of the piles and the soil are defined by:

- The pile-soil stiffness ratio $E_\mathrm{p}/E_\mathrm{s} = 1000$ between the pile and soil material elastic moduli. In section 5, the values $E_\mathrm{p}/E_\mathrm{s} = 500$ and $E_\mathrm{p}/E_\mathrm{s} = 2000$ are also considered.
- The soil-pile density ratio $\rho/\rho_\mathrm{p} = 0.75$.
- Soil hysteretic material damping ratios $\beta_\mathrm{s} = 0.03$ and $\beta_\mathrm{p} = 0.03$ in shear and dilatation, respectively.
- Poisson's ratio for the soil $\nu = 0.33$.
- Poisson's ratio for the piles $\nu_\mathrm{p} = 0.25$.

The vibration responses of the pile foundations are expressed in terms of a dimensionless velocity:

$$\tilde{v} = \mathrm{i}\omega u_z C_\mathrm{s} \rho L_\mathrm{p} L/P \tag{1}$$

as a function of the dimensionless frequency $a_0 = \omega d/C_\mathrm{s}$, with ω the circular frequency, i the imaginary unit and C_s the S-wave speed of the soil.

3. Numerical model

To address the pile-soil-pile interaction problem, a numerical model proposed by Álamo et al. [16] based on beam elements and numerical integration of Green's functions for a layered halfspace, hereafter referred to as the beam-integral model (BI), is adopted. The model is formulated in the frequency domain and thus assumes the system to be linear. A brief description of the model is presented in the following. For further details, the reader is referred to the PhD thesis of Álamo [17].

The soil is assumed to consist of horizontal viscoelastic isotropic layers which are either fixed at the base or overlying a homogeneous halfspace. Piles are modelled by Timoshenko beam elements subjected to distributed loads which represent the pile-soil interaction tractions in the lateral and axial directions of the piles. Torsion of the piles is neglected. The linear system of equations for the pile elements can be expressed by:

$$\mathbf{Z}\mathbf{u}_\mathrm{p} - \mathbf{Q}\mathbf{q}_\mathrm{p} = \mathbf{p}_\mathrm{p} \tag{2}$$

where $\mathbf{Z} = \mathbf{K}(1 + 2\mathrm{i}\beta) - \omega^2\mathbf{M}$, with $\mathbf{K}$ the pile stiffness matrix, β the hysteretic damping ratio for the piles, ω the circular frequency, $\mathbf{M}$ the pile mass matrix, $\mathbf{u}_\mathrm{p}$ the pile displacements, $\mathbf{Q}$ the transformation matrix

of equivalent nodal loads, $\mathbf{q}_\mathrm{p}$ the nodal values of distributed tractions and $\mathbf{p}_\mathrm{p}$ the external loads applied to the piles.

In the soil, the piles are considered as line loads and the relationship between tractions and displacements at the pile coordinates are established through Green's functions for a layered soil, allowing to express the displacements in the soil as:

$$\mathbf{u}^\kappa = \sum_{m=1}^{N_\mathrm{p}} \int_{\Gamma_m} \mathbf{u}_m^* \, \mathbf{q}_m \mathrm{d}\Gamma_m + \sum_{n=1}^{N_\mathrm{e}} \mathbf{u}_n^* \mathbf{p}_n \tag{3}$$

where $\mathbf{u}^\kappa$ is the vector of soil displacements at the collocation point κ, Γ_m is the load line of pile m, N_p is the total number of piles, $\mathbf{u}_m^*$ is a tensor containing the Green's functions for displacements between the load line m and the collocation point κ, $\mathbf{q}_m$ are the tractions acting over the load line m, $\mathbf{u}_n^*$ is the tensor containing the Green's functions for displacements between a point source n in the soil domain and the collocation point κ, $\mathbf{p}_n$ is the corresponding load vector and N_e is the total number of sources in the exterior soil domain. Assuming linear shape functions for the interaction tractions $\mathbf{q}_m$, the integral in eq. (3) is evaluated numerically using Gaussian quadrature. Applying eq. (3) to all pile nodes, a system of equations for the soil domain can be written as:

$$\boldsymbol{\Upsilon}\mathbf{u} - \mathbf{G}\mathbf{q} = \mathbf{u}_\mathrm{ff} \tag{4}$$

where $\mathbf{u}$ and $\mathbf{q}$ contain the soil displacements and tractions at the nodes of the piles, $\boldsymbol{\Upsilon}$ is a collocation matrix which in the case of vertical piles is a selection matrix for the translational degrees of freedom of the piles, $\mathbf{G}$ is the pile-soil coupling matrix obtained from integration of the Green's functions multiplied with the shape functions for the tractions along each pile element and $\mathbf{u}_\mathrm{ff}$ is the vector of free field displacements due to the point sources $\mathbf{p}_n$. The Green's functions are in the present work computed for the layered halfspace using the direct stiffness method implemented in the Matlab toolbox EDT [18].

By imposing the compatibility and equilibrium conditions $\mathbf{u}_\mathrm{p} = \mathbf{u}$ and $\mathbf{q}_\mathrm{p} = -\mathbf{q}$, eqs. (2) and (4) can be combined to obtain a system of equations expressed only in terms of the the pile displacements $\mathbf{u}_\mathrm{p}$ and the interaction tractions $\mathbf{q}_\mathrm{p}$:

$$\begin{bmatrix} \mathbf{Z} & -\mathbf{Q} \\ \boldsymbol{\Upsilon} & \mathbf{G} \end{bmatrix} \begin{Bmatrix} \mathbf{u}_\mathrm{p} \\ \mathbf{q}_\mathrm{p} \end{Bmatrix} = \begin{Bmatrix} \mathbf{p}_\mathrm{p} \\ \mathbf{u}_\mathrm{ff} \end{Bmatrix} \tag{5}$$

A rigid pile cap union can subsequently be implemented by including kinematic constraints and equilibrium equations in eq. (5), or the piles can be directly coupled to a deformable foundation modelled with finite

elements [19].

In a post-processing step, the total displacement field in the soil can be obtained as:

$$\mathbf{u}_{\mathrm{t}} = \mathbf{u}_{\mathrm{s}} + \mathbf{u}_{\mathrm{ff}} \tag{6}$$

$$\mathbf{u}_{\mathrm{s}} = -\mathbf{G}_{\mathrm{e}}\mathbf{q}_{\mathrm{p}} \tag{7}$$

where the total wave field is expressed as a superposition of the incident wave field $\mathbf{u}_{\mathrm{ff}}$ and the scattered wave field $\mathbf{u}_{\mathrm{s}}$ which is obtained from the soil influence matrix $\mathbf{G}_{\mathrm{e}}$ between the pile nodes and points in the exterior soil domain, and the pile-soil interaction tractions $\mathbf{q}_{\mathrm{p}}$.

This formulation is not only computationally efficient but offers the following advantages for analysing the problem addressed in this paper:

1. It decomposes the problem in an incident and a scattered wave field, as seen from eq. (6), making it straightforward to illustrate the influence of wave scattering.

2. The matrix $\mathbf{G}$ in eq. (5) accounts for the interaction between the piles and the soil. By disregarding the cross-coupling terms between the individual piles in $\mathbf{G}$, the influence of pile-soil-pile interaction on the response of the piles can be removed. Comparison between the cases where pile-soil-pile interaction is accounted for and when it is disregarded allows to analyse its influence on the group response.

3.1. Verification

To verify the BI model for the analysis of end-bearing pile groups, results computed for a 3×3 pile group are compared to the ones obtained from a finite element model. This allows to assess the influence of modelling the piles as line loads in the soil. As a reference model, a finite element model with perfectly matched layers (FE-PML) is adopted, where the incident wave field is obtained through a subdomain formulation [20]. In this case, both the piles and the soil are modelled using solid elements with a discretisation that ensures that there are at least five elements per S-wavelength in the soil.

Figure 2 presents the results for square 3×3 pile groups with pile-to-pile spacings $s/d = 3$ and $s/d = 5$. The results from the two models agree well in the studied range of dimensionless frequencies for the group with $s/d = 5$ and the solutions start to deviate at about $a_0 = 0.8$ for the group with more closely spaced piles, which is due to the lack of geometrical diffraction effects in the BI model [21]. The results verify the ability of the model to capture the essential features of pile-soil-pile interaction which are of interest in this study.

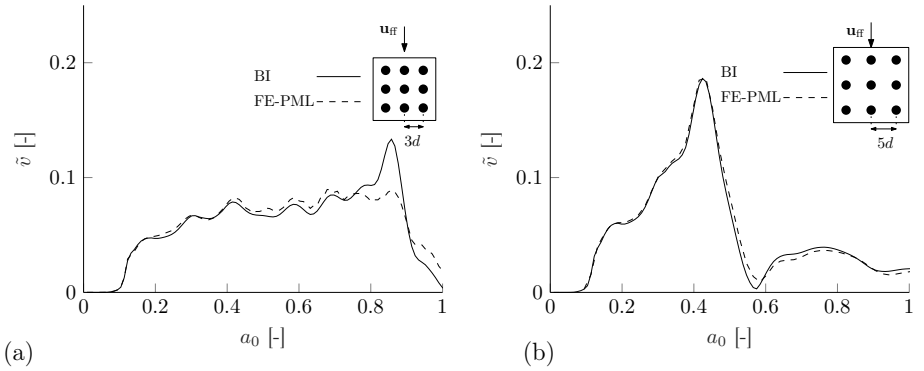

Figure 2: Comparison of the vertical response of a 3×3 pile group ($E_\mathrm{p}/E_\mathrm{s} = 1000$, $L_\mathrm{p}/d = 25$) obtained from the FE-PML model (dashed lines) and the beam-integral (BI) model (solid lines) for a pile spacing (a) $s/d = 3$ and (b) $s/d = 5$.

4. The significance of the end-bearing condition

4.1. The influence of the end-condition on the vertical response of pile groups

In the following, two different soil conditions are considered to illustrate the influence of the end-bearing condition on the vertical response of the piles. The vertical responses of square 2×2 pile groups with floating piles in a homogeneous halfspace and end-bearing piles in homogeneous soil with pile spacing $s/d = 5$, pile slenderness $L_\mathrm{p}/d = 25$ and pile-soil stiffness ratio $E_\mathrm{p}/E_\mathrm{s} = 1000$ are considered. Figures 3 and 4 illustrate the influence of pile-soil-pile interaction on the vertical group response for the two cases of different soil conditions by comparing the vertical responses of the pile groups and of the individual piles without a rigid connection between the piles, with and without pile-soil-pile interaction. Pile-soil-pile interaction indeed

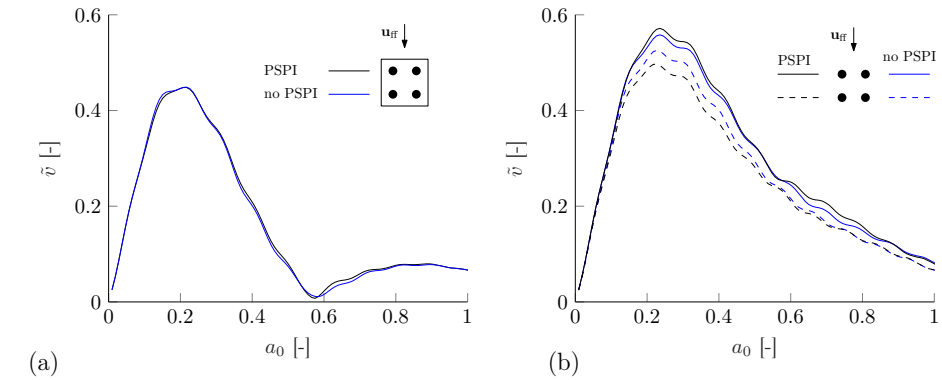

Figure 3: Amplitude of the vertical response of (a) a rigid pile cap and (b) individual piles without a rigid connection between the piles with (black) and without (blue) consideration of pile-soil-pile interaction for a 2×2pile group in a **homogeneous halfspace** with a pile spacing of $s/d = 5$, pile-soil stiffness ratio $E_\mathrm{p}/E_\mathrm{s} = 1000$ and slenderness ratio $L_\mathrm{p}/d = 25$.

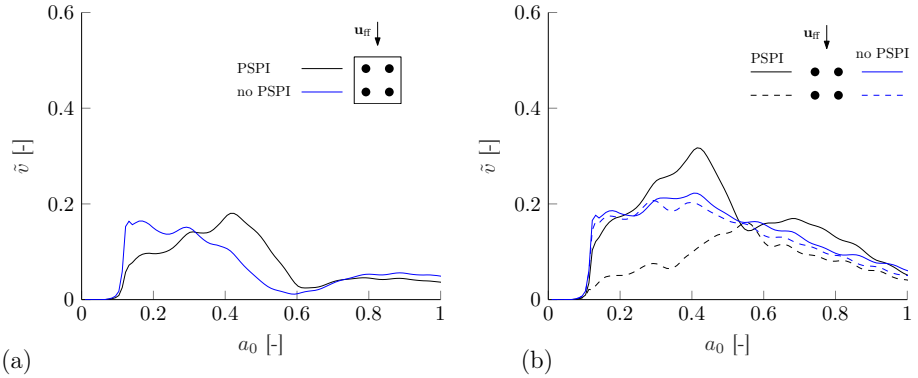

Figure 4: Amplitude of the vertical response of (a) a rigid pile cap and (b) individual piles without a rigid connection between the piles with (black) and without (blue) consideration of pile-soil-pile interaction for a 2×2 end-bearing pile group in **soil on bedrock** with a pile spacing of $s/d = 5$, pile-soil stiffness ratio $E_{\mathrm{p}}/E_{\mathrm{s}} = 1000$ and slenderness ratio $L_{\mathrm{p}}/d = 25$.

has a negligible influence on the vertical pile group response in fig. 3 (a) for the case of floating piles in a homogeneous halfspace, which is in line with the results of Makris and Badoni [12]. On the other hand, for the end-bearing pile group in the soil layer over rigid bedrock, neglecting through-soil coupling between the piles results in significant errors. Comparing the responses with and without consideration of pile-soil-pile interaction in fig. 4 (a), it is observed that the interaction causes a strong reduction of the group response for dimensionless frequencies $a_0 < 0.3$, but amplification for higher frequencies up to about $a_0 = 0.7$.

For the cases where the piles are not connected at the surface in fig. 3 (b) and fig. 4 (b), the pile-soil-pile interaction generally amplifies the response of the piles which are closest to the excitation point, but reduces the response for the piles farther away along propagation direction of the incident wave field. This is more pronounced for the end-bearing piles when $a_0 \leq 0.5$.

4.2. The scattered wave field

The through-soil interaction between the piles is due to waves emanating from the individual piles as a consequence of their excitation through the soil. This scattered wave field $\mathbf{u}_{\mathrm{s}}$ is due to the difference between the displacements along the pile and the corresponding soil displacements of the incident wave field $\Delta\mathbf{u} = \mathbf{u}_{\mathrm{p}} - \mathbf{u}_{\mathrm{ff}}$, which gives rise to the interaction tractions $\mathbf{q}_{\mathrm{p}}$. To better understand this interaction, the scattered wave field for a single pile is considered for the two different soil conditions.

Figure 5 compares the vertical free field soil displacements at the position of the pile displacements as a function of depth for a single pile in a homogeneous halfspace. The vertical component of the corresponding scattered wave field is also illustrated. For a stiff floating pile, the vertical pile displacement can be approximated as the average of the soil free field displacements over the depth equal to the pile length. For

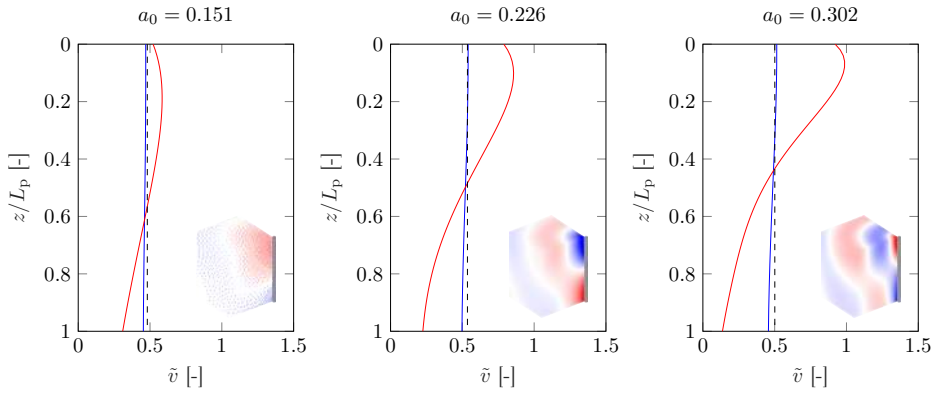

Figure 5: Amplitude of vertical pile (blue) ($E_\mathrm{p}/E_\mathrm{s} = 1000$, $L_\mathrm{p}/d = 25$) and free field (red) velocities due to a vertical point load applied to the soil's surface as a function of depth in a homogeneous half space at three different dimensionless frequencies. The average of the free field response over the depth of the pile is indicated (black dashed line). The real part of the corresponding scattered wave field (+:red , 0:white -:blue) due to the interaction tractions $\mathbf{q}_\mathrm{p}$ is indicated.

sufficiently low frequencies where the wave excitation over the pile length is approximately in phase ($a_0 \leq 0.3$ for the present pile length), this results in a scattered wave field, which propagates cylindrically from the pile, that shifts in polarity over the pile length. The net influence of this wave field on a nearby pile will therefore be small compared to the incident wave field.

Figure 6 presents the same situation for the case of an end-bearing pile in a soil layer over rigid bedrock. Two main differences can be observed compared to the case of a floating pile:

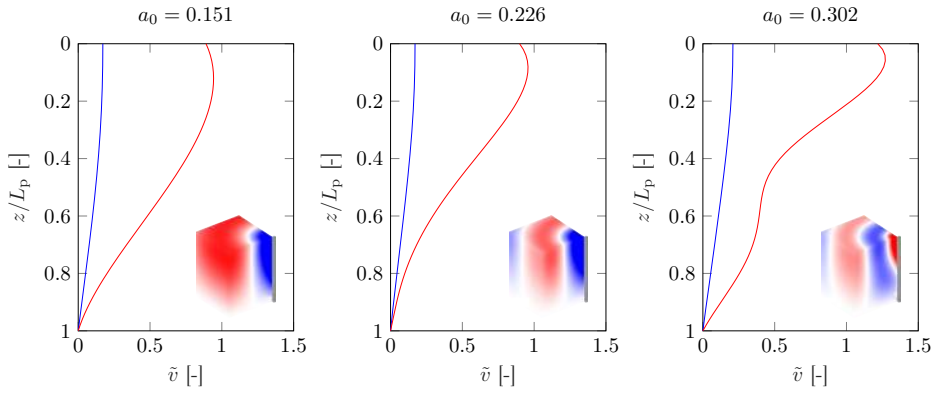

Figure 6: Amplitude of vertical pile (blue) ($E_\mathrm{p}/E_\mathrm{s} = 1000$, $L_\mathrm{p}/d = 25$) and free field (red) velocities due to a vertical point load applied to the soil's surface as a function of depth in soil on rigid bedrock at three different dimensionless frequencies. The real part of the corresponding scattered wave field (+:red, 0:white -:blue) due to the interaction tractions $\mathbf{q}_\mathrm{p}$ is indicated.

1. The difference between the vertical displacements of the pile and the incident wave field are much

larger due to the axial stiffness of the pile. This yields a stronger scattered wave field.

2. The displacement of the pile cannot be described as an average of the free field motion over the depth of the pile and $\Delta\mathbf{u}$ is thereby no longer polarized over the pile length in the same way as for the floating pile in fig. 5.

The influence of the scattered wave field depends not only on the wavelength and the spacing between the piles, but also on the direction of the incident wave field with respect to the positions of the piles. For a group of piles, the excitation of the piles is due to the total wave field of the superimposed free field vibrations $\mathbf{u}_{\mathrm{ff}}$ and the scattered field $\mathbf{u}_{\mathrm{s}}$ emanating from the piles. Whether the excitation of a pile is amplified or suppressed by pile-soil-pile interaction is mainly governed by the phase angle between the two wave fields $\mathbf{u}_{\mathrm{s}}$ and $\mathbf{u}_{\mathrm{ff}}$. At positions where the wave fields are in phase, amplification can be expected whereas positions where the wave fields are out of phase, the motion is suppressed. The phase angle at which the superposition of the two wave fields results in an amplitude equal to the incident wave field depends on the ratio of the amplitudes of the two individual wave fields and can be obtained from:

$$\varphi = \arccos\Big(-\frac{1}{2}\Big|\frac{u_{\mathrm{s}}}{u_{\mathrm{ff}}}\Big|\Big), \qquad \Big|\frac{u_{\mathrm{s}}}{u_{\mathrm{ff}}}\Big| \leq 2 \tag{8}$$

where u_{s} and u_{ff} are the point wise displacements of the scattered and incident wave fields, respectively. For positions where the value of the phase angle is around $\pi/2$, and up to $2\pi/3$ for equally strong fields, the influence of the scattered field $\mathbf{u}_{\mathrm{s}}$ is thereby negligible.

Figure 7 presents the phase field at the soil's surface for the three dimensionless frequencies considered in figs. 5 and 6, with three positions indicated which are separated from the scattering pile by a spacing $s/d = 5$, corresponding to the pile spacing considered in fig. 4. For this pile spacing, the excitation of piles

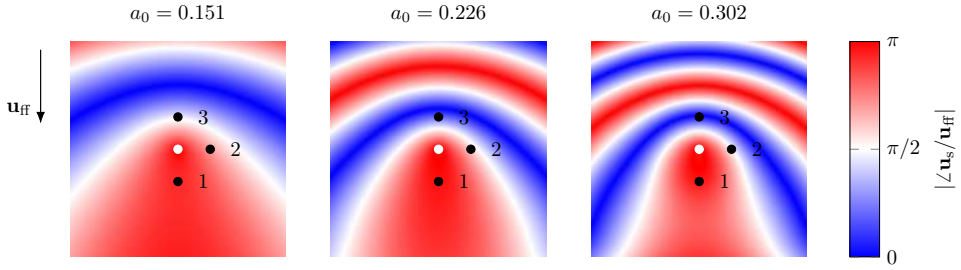

Figure 7: Absolute value of the phase angle at the soil's surface between the vertical components of scattered wave field $\mathbf{u}_{\mathrm{s}}$ and the incident wave field $\mathbf{u}_{\mathrm{ff}}$ for the case of a single end-bearing pile ($E_{\mathrm{p}}/E_{\mathrm{s}} = 1000$, $L_{\mathrm{p}}/d = 25$) in a soil layer over a rigid bedrock. Three points with a distance $s/d = 5$ (black dots) from the pile position (white dot) are indicated corresponding to the relative pile positions in a square pile group.

located in positions 1 and 2 is suppressed by the existence of the scattered wave field. The opposite is true for a pile in position 3, where the scattered wave field is almost in phase with the free field motion. This explains the amplification and reduction of the response due to pile-soil-pile interaction for the individual piles in the square 2×2 group observed in fig. 3 (b) and fig. 4 (b).

5. Pile-soil-pile interaction for end-bearing pile groups

5.1. The influence of pile-soil-pile interaction on the vertical response of a pile pair

Figure 8 compares the vertical responses of 2×1 end-bearing pile groups connected by a rigid pile cap with pile-to-pile spacings $s/d = 10,\ 5$ and 3, with and without consideration of pile-soil-pile interaction, when subjected to an incident wave field with a propagation direction which is either in line with or transverse to the line between the two piles. When the propagation direction of the incident wave field is in line with the pile array, both phase differences in the excitation of the piles and pile-soil-pile interaction affect the vertical group response. At the characteristic troughs around $a_0 = d\pi/s$, the vertical responses of the individual

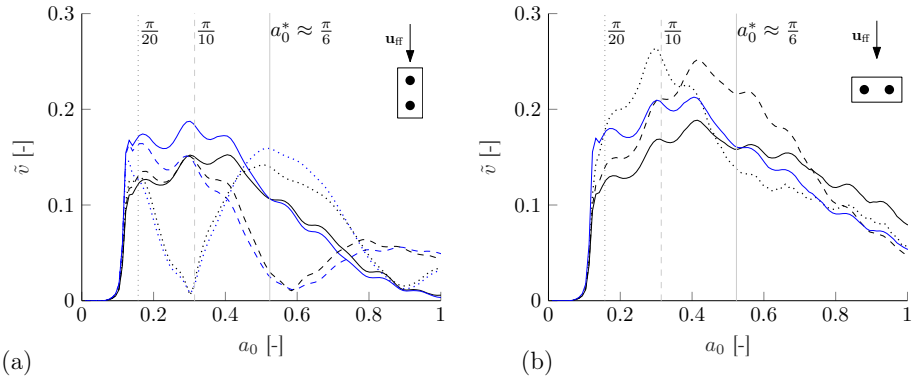

Figure 8: Amplitude of the vertical response for a 2×1 pile group in soil over rigid bedrock with pile-to-pile spacing $s/d = 3$ (solid lines), 5 (dashed lines) and 10 (dotted lines) with (black) and without (blue) pile-soil-pile interaction for piles arranged (a) along and (b) transverse to the direction of the incident wave field. Estimated values for the frequency a_0^* for each pile spacing are indicated (gray vertical lines).

piles are out of phase. For the case where the piles are arranged in the transverse direction to the incident wave field, no such phase differences exist due to symmetry in the excitation of the piles. As the wave front $\mathbf{u}_{\mathrm{ff}}$ is of approximately plane incidence with respect to the positions of the piles, the responses of the pile groups in fig. 8 b) with different spacing are the same if pile-soil-pile interaction is disregarded.

For both cases considered in fig. 8, pile-soil-pile interaction decreases the group response for dimensionless frequencies below a certain frequency a_0^* and amplifies the response in the frequency range $a_0^* \leq a_0 \sim\leq 2.8a_0^*$. The amplification of the response due to pile-soil-pile interaction in this range is much more pronounced for

the case when there are no phase differences in the excitation of the piles. The frequency a_0^* approximately coincides with $a_0 = 0.302$ in fig. 7 for a pile spacing $s/d = 5$. At this frequency, points 1 and 3 in fig. 7 are out of phase, cancelling the effect of the wave scattering in the group response. The phase between the scattered and incident wave fields in point 2 is about $\pi/2$ at the surface. This illustrates that a_0^* strongly depends on the relationship between the incident and the scattered wave fields at the position of the piles. For this case, the frequency a_0^* can be related to the pile spacing as being equal to a fraction of the S-wavelength in the soil:

$$a_0^* = \frac{\pi}{\alpha s/d} \tag{9}$$

For the piles under consideration in fig. 8, the response is unaffected by pile-soil-pile interaction whenever the pile spacing is approximately equal to a quarter of the S-wavelength in the soil, i.e. $\alpha = 2$. The agreement between this simple relation and the results for the 2×1 pile groups with spacings $s/d = 3,\ 5$ and 10 is illustrated in fig. 8. It also gives a good indication in the case of the 2×2 pile group in fig. 4.

5.2. The influence of pile axial stiffness

Equation (9) is based on the assumption that the response at the soil's surface is representative over the depth of the soil layer such that eq. (8) holds for all pile nodes. This is only true if there are no phase differences in neither the incident nor the scattered wave field over the length of the pile. This is generally not the case, as indicated by figs. 5 and 6, and phase differences over the pile depth can therefore influence the value of a_0^*.

Figure 9 illustrates how the pile axial stiffness affects the influence of pile-soil-pile interaction for a 2×1 pile group by considering three different combinations of the pile-soil stiffness ratio $E_\mathrm{p}/E_\mathrm{s}$ and the pile slenderness ratio L_p/d. The value of a_0^* (where the ratio in fig. 9 is equal to 1) is decreased for the case $L/d = 50$ and $E_\mathrm{p}/E_\mathrm{s} = 500$. On the contrary, it is increased above the value for a_0^* with $\alpha = 2$ as the axial stiffness of the pile increases. This is due to an increase in the ratio between the amplitudes of the scattered and the incident wave fields, in line with eq. (8). This also explains the slight differences in a_0^* for different pile spacings in fig. 8, as the amplitude ratio between the wave fields is generally larger closer to the pile for the considered frequencies.

5.3. The influence of pile-to-pile spacing in pile groups

The analysis presented in the preceding section concerns the interaction between only two piles. For larger groups of piles, a combination of interactions between piles with different inter-spacing will come into play. Figure 10 compares the responses of a 2×2 and a 3×3 pile group with two different pile spacings,

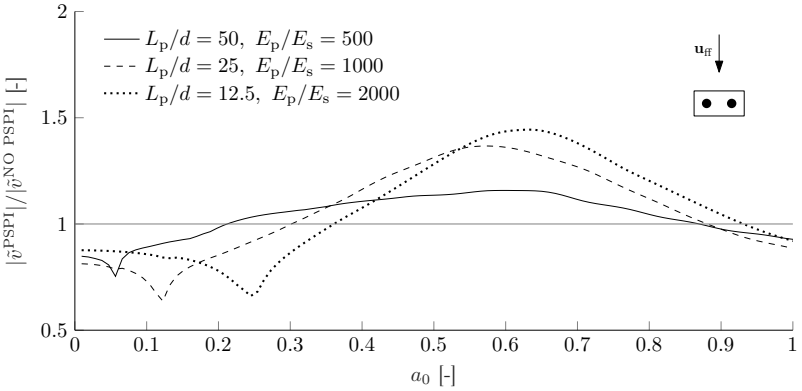

Figure 9: Relative influence of pile-soil-pile interaction on the vertical response of a 2×1 pile group in soil on bedrock with pile-to-pile spacing $s/d = 5$ for three different combinations of the pile slenderness ratio L_p/d and pile-soil stiffness ratios E_p/E_s.

$s_x = 5d$ and $s_y = 3d$, to the case of a pile group with a uniform spacing $s_x = s_y = 5$. Disregarding pile-soil-pile interaction results in the same vertical response for both pile groups, as the same spacing in the propagation direction of the incident wave field is considered.

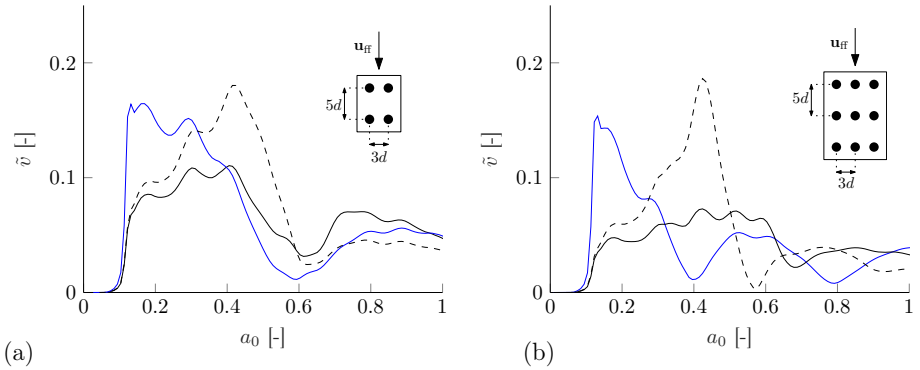

Figure 10: Vertical responses of (a) 2×2 and (b) 3×3 end-bearing pile groups ($E_p/E_s = 1000$ and $L_p/d = 25$) with non-uniform pile spacing (black solid lines) compared to the cases of uniform spacing $s_x = s_y = 5d$ (black dashed lines) and when pile-soil-pile interaction is disregarded (blue solid lines).

The influence of pile-soil-pile interaction is considerable, especially for the 3×3 configuration. As for the case of the pile pairs in fig. 8, reducing the spacing in the transverse direction results in a shift of a_0^* to a higher value. This is the reason for the strong reduction of the distinct peaks that can be observed around $a_0 = 0.42$ for the square pile groups with uniform spacing.

It is important to emphasise that the reduction of the foundation response due to a modification of the pile group layout does not necessarily imply the same amount of reduction in the total response of a structure

supported by the pile foundation. As the layout of the pile group is altered, the vertical impedance of the pile group is also affected, which changes the dynamic properties of the system.

6. Conclusion

The influence of pile-soil-pile interaction on the vertical response of end-bearing pile groups subjected to an incident wave field caused by a vertical load acting at the soil's surface has been considered. A numerical model that considers the coupling between the piles and the soil through pile-soil interaction tractions considered as line loads over the piles and in the soil is adopted. The influence of the soil is accounted for by a soil influence matrix which is based on Green's functions for a layered halfspace. The cases when the coupling between the piles through the soil are considered or disregarded are compared to analyse the influence of pile-soil-pile interaction.

The following conclusions are made:

- In contrast to floating piles in homogeneous soil, groups of end-bearing piles are found to be significantly affected by the wave scattering from the individual piles, which may either reduce or amplify the vertical group response.
- The influence of the interactions between the piles depend mainly on the spacing between the piles and the wavelengths in the soil, but also on the pile slenderness ratio and the relative stiffness of the pile with respect to the stiffness of the soil.
- Amplification caused by pile-soil-pile interaction in pile groups is found to be mostly governed by the interaction between piles which are aligned in the transverse direction with respect to the direction of the incident wave field. This amplification can become significant, especially for larger pile groups.
- It is found that by decreasing the pile spacing in the direction transverse to the incident wave field, the vertical group response can be substantially reduced for lower frequencies by shifting the frequency at which amplification due to pile-soil-pile interaction takes place higher up in the band.

7. Acknowledgements

This work is supported by the Development Fund of the Swedish Construction Industry (SBUF) and the Swedish Transport Administration (Trafikverket). The financial support is gratefully acknowledged.

References

[1] K. Kuo, M. Papadopoulos, G. Lombaert, G. Degrande, The coupling loss of a building subject to railway induced vibrations: Numerical modelling and experimental measurements, Journal of Sound and Vibration 442 (2019) 459–481.

[2] E. Kausel, R. V. Whitman, J. P. Morray, F. Elsabee, The spring method for embedded foundations, Nuclear Engineering and Design 48 (1978) 377–392.

[3] G. Sanitate, A performance-based design framework for base-isolated buildings against ground-borne vibration, Ph.D. thesis, 2020. doi:10.17863/CAM.48986.

[4] L. Auersch, Simple and fast prediction of train-induced track forces, ground and building vibrations, Railway Engineering Science 28 (2020) 1–19.

[5] S. François, M. Schevenels, G. Lombaert, G. Degrande, Numerical modeling and in situ vibration measurements during the design and construction of low vibration floors at the corelab 1b research facility, in: Proceedings of ISMA 2014, International Conference on Noise and Vibration Engineering, Leuven, Belgium, 2014.

[6] A. Colaço, D. Barbosa, P. Alves Costa, Hybrid soil-structure interaction approach for the assessment of vibrations in buildings due to railway traffic, Transportation Geotechnics 32 (2022) 100691.

[7] R. Dobry, G. Gazetas, Simple method for dynamic stiffness and damping of floating pile groups, Géotechnique 38 (1988) 557–574.

[8] G. Gazetas, N. Makris, Dynamic pile-soil-pile interaction. Part I: Analysis of axial vibration, Earthquake Engineering & Structural Dynamics 20 (1991) 115–132.

[9] N. Makris, G. Gazetas, Dynamic pile-soil-pile interaction. Part II: Lateral and seismic response, Earthquake Engineering & Structural Dynamics 21 (1992) 145–162.

[10] G. Mylonakis, G. Gazetas, Vertical vibration and additional distress of grouped piles in layered soil, Soils and Foundations 38 (1998) 1–14.

[11] G. Mylonakis, G. Gazetas, Kinematic pile response to vertical P-wave seismic excitation, Journal of Geotechnical and Geoenvironmental Engineering 128 (2002) 860–867.

[12] N. Makris, D. Badoni, Seismic response of pile groups under oblique-shear and Rayleigh waves, Earthquake Engineering & Structural Dynamics 24 (1995) 517–532.

[13] A. M. Kaynia, M. Novak, Response of pile foundations to Rayleigh waves and obliquely incident body waves, Earthquake Engineering & Structural Dynamics 21 (1992) 303–318.

[14] F. Theland, C. Pacoste, J.-M. Battini, G. Lombaert, S. François, F. Deckner, The influence of near-surface soil layer resonance on vibrations in pile foundations, in: Current Perspectives and New Directions in Mechanics, Modelling and Design of Structural Systems, 2022, p. 84. doi:10.1201/9781003348450-13.

[15] F. Theland, G. Lombaert, S. Franois, C. Pacoste, F. Deckner, P. Blom, J.-M. Battini, Dynamic response of driven end-bearing piles and a pile group in soft clay: an experimental validation study, Engineering Structures 267 (2022) 114629.

[16] G. M. Álamo, A. E. Martínez-Castro, L. A. Padrón, J. J. Aznárez, R. Gallego, O. Maeso, Efficient numerical model for the computation of impedance functions of inclined pile groups in layered soils, Engineering Structures 126 (2016) 379–390.

[17] G. M. Álamo, Dynamic response of piled structures : Implementation of a model based on the integral formulation of the problem and the use of a fundamental solution for the layered half space, Ph.D. thesis, Instituto Universitario de Sistemas Inteligentes y Aplicaciones Numéricas en Ingeniera (SIANI), 2018.

[18] M. Schevenels, S. François, G. Degrande, EDT: An ElastoDynamics Toolbox for MATLAB, Computers & Geosciences 35 (2009) 1752 – 1754.

[19] G. M. Álamo, L. Padrón, J. Aznárez, Numerical model for the dynamic and seismic analysis of pile-supported structures with a meshless integral representation of the layered soil, Bulletin of Earthquake Engineering (2022) 3215–3238.

[20] M. Papadopoulos, S. François, G. Degrande, G. Lombaert, The influence of uncertain local subsoil conditions on the response of buildings to ground vibration, Journal of Sound and Vibration 418 (2018) 200–220.

[21] G. M. Álamo, J. D. Bordón, J. J. Aznárez, G. Lombaert, The effectiveness of a pile barrier for vibration transmission in a soil stratum over a rigid bedrock, Computers and Geotechnics 110 (2019) 274–286.